DISSERTATION

ENGINEERING COMPLEX LIVER MODELS FOR DRUG SCREENING AND INFECTIOUS DISEASES: A BIOMATERIALS AND CO-CULTURE PERSPECTIVE

Submitted by

Christine Lin

Graduate Degree Program in Bioengineering

In partial fulfillment of the requirements

For the Degree of Doctor of Philosophy

Colorado State University

Fort Collins, Colorado

Spring 2018

Doctoral Committee:

Advisor: Salman R. Khetani

Daniel Gustafson
Matthew Kipper
Michael Pagliassotti

ABSTRACT

ENGINEERING COMPLEX LIVER MODELS FOR DRUG SCREENING AND INFECTIOUS DISEASES: A BIOMATERIALS AND CO-CULTURE PERSPECTIVE

In vitro liver models have many applications in disease modeling and drug screening. Micropatterned cocultures (MPCCs) of primary human hepatocytes (PHHs) and supportive stromal cells have been shown to display high hepatic functions for long-term drug and disease studies. However, MPCCs lack liver non-parenchymal cells (NPCs) and the proper microenvironmental cues that can play important roles in conditions such as drug-induced liver injury (DILI), which is the leading cause of the prelaunch attrition and post-market withdrawal of pharmaceuticals, or diseases such as viral hepatitis. Hepatitis B virus (HBV) and hepatitis C virus (HCV) infection are major health problems that affect >250 million and ~130-170 million people worldwide, respectively, and the development of therapeutics has been hindered due to the lack of models in which to study human response to virus and drugs. Thus, long-term *in vitro* models that can be used to study the progression of viral infection and drug pharmacodynamics are required to develop safe and efficacious therapeutics. These models must also be human-relevant due to the narrow host tropism of hepatitis B and C and differences in liver pathways across species. Thus, the goal of this dissertation is to augment the MPCC model to include the relevant substrates and cell types for the study of cell-cell interactions in diseases such as hepatitis and DILI. Biomaterials can present important microenvironmental factors that interact with cells. Chitosan and heparin polyelectrolyte multilayers (PEMs) were utilized as a substrate to present extracellular matrix (ECM) proteins and growth factors (GF) to hepatocyte cultures.

Liver biomatrix (LBM) derived from human and porcine sources were also assessed as substrates since LBM contains both soluble and insoluble cues that are usually found in the liver *in vivo*. In addition to improving the MPCC substrate, liver NPCs, such as primary human Kupffer cells (KCs), were incorporated into the MPCC model since KCs play key roles in immune responses and inflammation. This work will be used to establish models that integrate multiple liver cell types on a physiologically-relevant substrate to study disease states such as hepatitis and DILI towards creating effective therapeutics.

ACKNOWLEDGEMENTS

I would first and foremost like to thank my advisor, Dr. Salman Khetani, for your guidance and patience. I would also like to thank my committee members Drs. Daniel Gustafson, Matt Kipper, and Michael Pagliassotti, for your knowledge, guidance, and thoughtful questions.

I would like to thank all of the current and past members of the Microfabricated Tissue Models lab with whom I have worked alongside. Each and every one of you has enriched my time in the lab in one way or another. I would particularly like to thank Kim Ballinger, Dustin Berger, Matt Davidson, and Brent Ware for being there for me from the very beginning and always being so kind and generous with your time and providing thoughtful feedback and advice. I would like to acknowledge my funding sources, without which none of this would be possible, Colorado State University and the University of Illinois at Chicago.

I would like to thank all of my collaborators in both academia and industry: Julianne Shi, Amanda Moore, Dr. Raimundo Romero, Mila Sorokina, Dr. Laura Place, Dr. Matt Kipper, Dr. Stephen Badylak, Dr. Denver Faulk, Dr. Michelle Scarritt, Dr. Scott Heyward, Caitlin Brown, Dr. Hugo Rosen, Dr. Silvia Giugliano, Dr. Lucy Golden, Linling Cheng, Dr. Jacinta Holmes, Dr. Raymond Chung, and Dr. Jisu Li for your assistance with my projects. Thank you to the support staff at both Colorado State University and the University of Illinois at Chicago: Mrs. Sara Mattern, Mrs. Ellen Brennan-Pierce, and Mr. Lukasz Zientara for technical support, training, equipment use, and experimental assistance.

Finally, I would like to thank my family and friends for their continuous and unwavering support throughout this endeavor. Thank you for believing in me when I doubted myself. Special thanks to my boyfriend, David Heleniak, for always being there for me.

TABLE OF CONTENTS

Chapter 1

Introduction[1]

1.1 Liver composition and functions

The liver is composed of approximately a million functional units (lobules), which consist of hepatocyte plates radiating from a central vein[3]. Hepatocytes in the plate are exposed to capillaries on either side, which comprise the sinusoid. The sinusoid is composed of parenchymal hepatocytes (60%) and non-parenchymal stromal cells (40%), including Kupffer cells (KCs), hepatic stellate cells (HSCs), liver sinusoidal endothelial cells (LSECs), and cholangiocytes, that interact with the extracellular matrix (ECM) and soluble factors to perform over 500 functions (**Figure 1.1**). Although the liver is not as abundant in ECM as other organs, the ECM plays an important role in maintaining the phenotype and functionality of hepatocytes and the NPCs[3]. During liver fibrosis and cirrhosis, the ECM can stiffen and affect hepatocyte functionality, which is critical because the liver carries out many functions[4]. Some of the functions, including protein synthesis, drug detoxification, lipid storage, and glucose metabolism, are zonated along the liver sinusoid. For example, drug metabolism and lipid storage occur in the perivenous zone, whereas protein and glucose production occur in the periportal zone. The metabolism of drugs and xenobiotics involves the cytochrome P450

[1] Sections of this chapter have been adapted from: Lin, C. and Khetani, S.R. Advances in engineered liver models for investigating drug-induced liver injury. BioMed Research International: 1829148 (2016) and Lin, C. et al, The application of engineered liver tissues for novel drug discovery. Expert Opinion on Drug Discovery 10(5):519-540 (2015).

(CYP450) enzymes. In Phase I of metabolism, drugs are oxidized or reduced by CYP450 enzymes, with CYP3A4 metabolizing about half of the clinically-relevant drugs[5]. Phase II of metabolism involves the conjugation of the reactive metabolites with charged species, such as sulfate or glucuronic acid, to facilitate excretion. Phase III involves transporters through which drugs and metabolites are excreted.

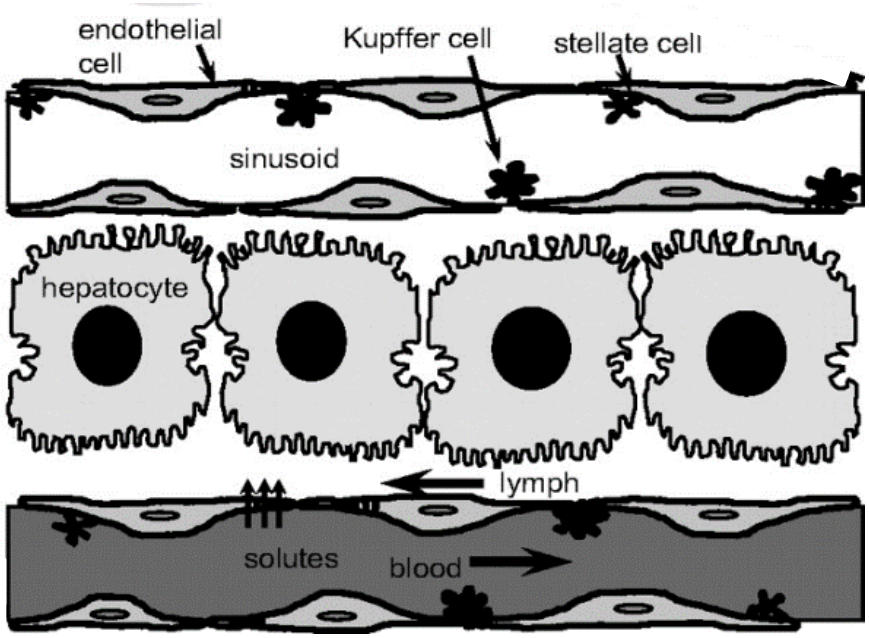

Figure 1.1 The liver is composed of multiple cell types within the sinusoid that all work together to perform over 500 functions. Adapted from [1]. Used with permission by Oxford University Press.

1.2 Current *in vitro* liver models

Several different model systems have been developed to provide human-specific data on drug behavior[6]. These include microsomes, cancerous/immortalized cell lines, isolated primary human liver cells, liver slices and humanized rodents. Several advantages and disadvantages of each of these systems are described in **Table 1.1**. While these models have already been used in some instances to mitigate the risk of DILI during drug development, there remains a need for model systems that are better predictive of clinical outcomes with respect to the type and severity of DILI, and can be used to elucidate inter-individual variability in drug outcomes. Furthermore,

how metabolism in the liver affects toxicity in other tissue types needs to be investigated further using newer culture platforms that link tissue types together through the exchange of culture medium[7]. Primary human hepatocytes (PHHs) are considered to be the gold standard for *in vitro* liver models, but they rapidly decline in function so multiple engineering tools (i.e. micropatterning, microfluidics, and biomaterials) have been utilized to maintain their phenotype for long-term studies[8]. Sandwich cultures utilizing several types of ECM substrates and overlays have been demonstrated to better stabilize the phenotype of hepatocytes *in vitro*, highlighting the importance of liver-relevant substrates. However, PHHs in this format still decline in functions. Three-dimensional cultures in which PHHs and supporting cell types are cultured in spheroids have also been utilized[8]. However, there are limitations with analyzing these cultures since imaging spheroids is not trivial and the low cell number results in undetectable amounts proteins in the media supernatant. Thus, optimization of protocols is necessary for 3D spheroids to become a high-throughput drug screening platform.

Coculture of hepatocytes and stromal cells have been shown to extend hepatocyte lifetime and improve functions[9]. However, randomly-distributed cells in cocultures make consistency and data analysis difficult[10]. Thus, Bhatia et al have implemented soft-lithographic techniques to micropattern proteins in order to control the placement of multiple cell types and therefore, allow for the control of homotypic and heterotypic cell-cell interactions (**Figure 1.2**)[11,12]. Hepatocyte islands 500-μm in diameter with 1200-μm center-to-center spacing has been determined to be optimal[13]. This technique allows for control over the number of hepatocytes that can attach to the substrate and the homotypic and heterotypic cell interactions in these cocultures. Khetani and Bhatia have demonstrated that MPCCs comprised of PHHs and 3T3-J2 mouse embryonic fibroblasts display high levels of sustained (~1 month) hepatic functions[12,13].

Table 1.1 Benefits, limitations and applications of various types of liver models available for drug development.

Model	Benefits	Limitations	Applications
Microsomes	High throughput; Easy to use; Pooling of multiple donors possible	Batch-to-batch variability; Low reaction rates; Do not contain full complement of liver enzymes	Metabolic stability; Metabolite identification
Recombinant enzymes (i.e. CYPs)	High-throughput; Amenable to fluorescent- and luminescent-based assays; Greater stability than microsomes	Limited availability; Not present in a physiological context	Metabolic stability; Metabolite identification and production
Suspension hepatocytes	High-throughput; More complete repertoire of enzymes/co-factors than microsomes; Pooling of multiple donors possible	Limited lifetime (hours); Transporters not properly localized	Metabolic stability; Metabolite identification
2D Liver Cultures / Co-cultures (including micropatterned)	Easy to use; Medium-to-high throughput; Compatible with standard imaging readouts	Often lack all relevant cell types of liver; Lack 3D liver architecture; No bile collection	Metabolic stability; Metabolite identification; Drug-transporter interactions; Drug toxicity; Disease modeling
3D Spheroidal Cultures / Co-cultures	Medium throughput; Interactions of multiple cell types in spheroids	Can suffer from cellular necrosis in aggregate cores; Variability in size of spheroids; Not always compatible with standard high content imaging; No bile collection	Metabolic stability; Metabolite identification; Drug toxicity; Disease modeling
Liver slices	Retain intact and native tissue architecture; Contain all cell types of liver; Microfluidic culture improves lifetime	Heterogeneous distribution of drugs in different layers; Low-throughput; Lack bile/portal flow; Rapid (hours to days) decline in liver functionality	Metabolic stability; Metabolite identification; Disease modeling (e.g. fibrosis, tumors)
Humanized rodents	*In vivo* pharmacokinetics and pharmacodynamics with human-relevant metabolites; Interaction of human liver cells with other organs to study organ-organ crosstalk	Variability in human hepatocyte engraftment efficiency; Low throughput; Residual mouse hepatocytes can metabolize drugs; Interaction of human liver cells with non-human organs may produce confounding results	Metabolite identification; Disease modeling

Our lab has assessed other types of supportive cells, including human liver NPCs, but the 3T3-J2 fibroblasts have been found to support hepatocytes at levels significantly higher than any of the other cell types. Additionally, Khetani et al have demonstrated that the model can maintain hepatocyte transporters, polarity, CYP450 activity, and metabolism capabilities for drug applications[14,15]. Thus, the MPCC provides the field with a highly stable (3-4 weeks) and functional model, but there is still room for improvement. For example, the substrate utilized (rat tail type I collagen) is not human-relevant and the model lacks liver NPCs which can play important roles during normal liver physiology as well as diseased states.

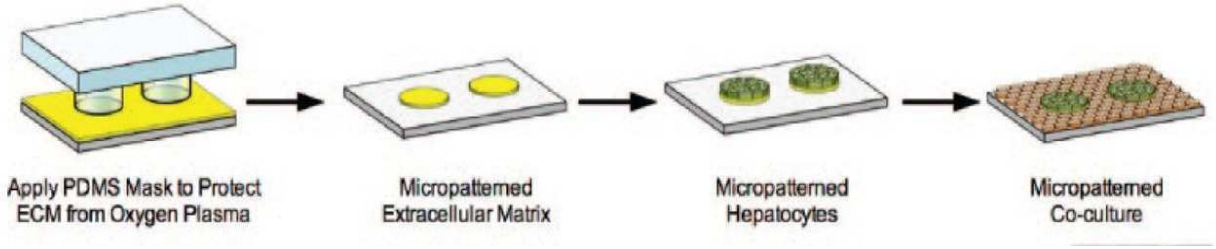

Figure 1.2 To create MPCCs, polydimethylsiloxane (PDMS) stencils are first used to pattern ECM proteins (i.e., collagen) onto tissue culture polystyrene. Hepatocytes attach to the ECM domains, and 24 hours later, supporting 3T3-J2 murine embryonic are seeded and attach to the areas surrounding the hepatocytes. Adapted from [2]. Used with permission by Wiley.

1.3 Polyelectrolyte multilayer substrates

Cell adhesion and functionality *in vitro* is dependent on the physical and chemical properties of the underlying substrate. Biomaterial substrates that present important microenvironmental factors, such as ECM proteins and growth factors, may help stabilize and modulate PHH functions by better mimicking *in vivo* cellular environments. Polyelectrolyte multilayers (PEMs) allow for the layer-by-layer assembly of synthetic (poly-allylamine hydrochloride, poly-acrylic acid, etc.) as well as natural polymers (polypeptides, polysaccharides, DNA, and proteins) to create highly-tunable coatings[16-25]. PEMs self-assemble due to electrostatic interactions between the cationic and anionic polymers, allowing for the

modulation of properties such as thickness, surface composition, topography, and stiffness. Control of these properties can be used to promote or prevent cell adhesion, direct or maintain cell phenotype, and deliver drugs[26]. In order to recapitulate the *in vivo* microenvironment for tissue engineering applications, PEMs can be tailored for the attachment of functional moieties. Various types of PEMs have been used to facilitate hepatocyte attachment, but these studies utilize cancerous/immortalized cell lines or rat/mouse hepatocytes rather than PHHs[27-32]. For example, Chen et al used PEMs to modulate substrate thickness and found that hepatocyte adhesion was optimal on low compliance PEMs whereas on high compliance PEMs, less cell attachment was observed[33]. Primary rat hepatocytes have also been encapsulated in ECM protein and polyelectrolyte microcapsules for use in bioartificial liver devices[34,35]. Although PEMs have been used to modulate the stiffness and surface charge that hepatocytes sense, they have not been used to bind and deliver growth factors to PHHs.

1.4 Liver extracellular matrix substrates

In addition to synthetic polymers, natural substrates such as decellularized tissues have also been used for tissue engineering applications. The native liver ECM represents an ideal substrate for hepatocytes to help maintain their phenotype and functionality because it represents the secreted product of *in vivo* liver cells[36]. The use of complex ECM substrates for hepatocyte culture began more than two decades ago with the use of Matrigel[36]. Multiple protocols exist for decellularizing tissues, leaving behind a complex mixture of proteins that constitute the ECM. This can include physical (snap freezing, mechanical force, mechanical agitation), chemical (acids and detergents), and enzymatic (trypsin, endonucleases, exonucleases) methods[37]. These protocols can be applied to tissues from various organs and species, but must be able to efficiently remove all cellular material while conserving the biochemical composition, biological

activity, and mechanical integrity of the ECM scaffold[37]. For the liver specifically, the most effective protocol for decellularization will depend on the species, age, and lipid content of the liver. To characterize the decellularized ECM, collagen, GAG, and elastin content are assessed in addition to fiber network analysis[36]. Sellaro et al cultured PHHs in sandwich-culture configuration with porcine-liver ECM or Matrigel and observed similar functions between the two substrates[38]. However, the sandwich-culture configuration only allowed for a short-term (10-day) study, whereas if the model were to be applied to long-term drug or disease studies, it would need to function at a high level for a longer period of time. In another study, Lin et al cultured rat hepatocytes on porcine-liver ECM or collagen and found enhanced hepatocyte functions for up to 45 days on the porcine-liver ECM compared to the collagen substrate[39]. However, the molecular mechanisms by which decellularized liver ECM supports hepatocellular function was not studied and the use of human LBM for the culture of PHHs has not yet been assessed.

1.5 Drug metabolism

Prediction of drug clearance rates is important for the pharmaceutical industry since it allows for proper dose selection in animal studies and human clinical trials[40,41]. However, current models used for clearance rate prediction, such as suspension and conventional monolayer cultures, decline so quickly that some drugs are not metabolized at all and low-turnover compounds cannot be assessed[14]. It is important to be able to identify low-turnover compounds because pharmaceutical companies are increasingly developing such drugs for one pill/day dosing regimens, and rank ordering of candidate compounds by clearance rates is necessary to progress with drug development. Models utilizing animal cells are problematic since there are species differences in drug metabolism pathways. Thus, human-relevant models that allow for

long-term assessment of drug clearance rates are necessary. Recently, Pfizer developed a relay method in which suspension PHHs are used sequentially and the cell supernatant with the drug is transferred and incubated across multiple thawed cell vials in order to predict clearance rate of low-turnover drugs[42,43]. However, this method utilizes multiple PHH lots, which must be tested and banked, and even with the use of 5 hepatocyte vials which each allow for a 4-hour incubation, drug incubations are still limited to 20 hours. Cocultures of hepatocytes and supportive stromal cells have been used successfully to predict clearance rates for drugs, but drugs with high clearance rates were not tested, nor was the model compared to conventional models (suspension and monolayer cultures) using the same donor[14]. Furthermore, CYP450 activity levels for multiple donors should be assessed for longer-term studies.

1.6 Drug-induced liver injury

Drug-induced liver injury (DILI) is a leading cause of both the pre-launch attrition and post-market withdrawal of pharmaceuticals[44]. It currently takes approximately $3 billion and 12-15 years to bring a drug to market[45]. Even with the amount of time and money dedicated to drug development, DILI is the cause of ~40% of drug failures in the clinical trial stage of drug development[45] and has been linked to almost 1000 marketed drugs[46]. DILI can mimic many forms of acute or chronic liver diseases, such as necrosis, hepatitis, cholestasis, fibrosis, or a combination of different injury types through multiple mechanisms, including the production of toxic metabolites, dissipation of mitochondrial membrane potential, and inhibition of bile salt export protein[47,48]. While DILI affects the population in a predictable dose-dependent manner, idiosyncratic DILI (iDILI) only affects a small percentage of the population in which a unique set of genetic and environmental factors may be involved and is more difficult to anticipate[44]. Idiosyncratic DILI can be mediated by the innate and adaptive immune systems that are triggered

by injury to hepatocytes or other cell types of the liver. For example, inflammatory cells in the liver such as KCs may modulate hepatic response to drugs to cause toxicity[1]. Such reactions can result in the presence of fever, rash, eosinophilia, a short (1 month) latency period, the presence of autoantibodies, and the rapid recurrence of toxicity on re-exposure of the drug[49]. Ultimately, the interplay between hazardous and adaptive cellular responses can determine whether the liver of a particular patient adapts following a mild injury or proceeds to severe injury due to a drug. However, animal testing is only 50% predictive of human DILI, likely due to the significant differences in drug metabolism pathways between the livers of animals and humans[50]. In addition, use of young animals with limited genetic diversity under well-defined nutritional conditions for drug safety assessment does not capture the aforementioned host risk factors present in humans. Thus, it is important for *in vitro* liver models to be human-relevant and more comprehensive by including factors such as KCs, in order to better predict whether a candidate compound will induce adverse drug reactions in subsets of the population.

1.7 Kupffer cells

The liver is constantly exposed to antigens since 80% of the blood entering the liver through the portal vein is carrying nutrients and bacterial endotoxin, such as lipopolysaccharides (LPS), from the gastrointestinal tract[51]. The immune system in the liver is comprised of monocytes, macrophages, granulocytes, natural killer cells, and dendritic cells that work in unison to respond to pathogens. Kupffer cells (KCs) are liver resident macrophages that originate either through local self-renewal and proliferation or from circulating bone-marrow-derived monocytes. They play important roles in maintaining normal liver physiology and homeostasis as well as participating in immune responses. KCs are able to recognize pathogen-associated

molecular patterns (PAMPs) and endogenous ligands via pattern-recognition receptors (PRRs), which include receptors for bacterial carbohydrates and toll-like receptors (TLRs). When PAMPs bind to PRRs, an immune response is initiated, and pathways are activated to destroy the activating agent by phagocytosis or through the release of inflammatory mediators, growth factors, and reactive oxygen species. Factors such as tumor necrosis factor α (TNF-α) and interleukin 6 (IL-6) can initiate the acute-phase response, which is characterized by an increase in acute-phase proteins (APPs), which serve hemostatic, microbicidal, phagocytic, antithrombotic, and antiproteolytic functions[51]. However, overproduction of these factors can also lead to liver injury. KC phenotype can be classified along a spectrum ranging from pro-inflammatory (M1 or "classically-activated") to anti-inflammatory (M2 or "alternatively-activated"). The resultant phenotype will induce the release of different factors that can cause varying subsequent events.

For example, in HCV infection, the specific roles and pathways that KCs are involved in and the downstream effects they have on HCV infection are still unknown. The intrinsic innate immune response is critical because it is the first immune defense that senses HCV infection, leading to interferon (IFN) production and induction of interferon-stimulated genes (ISGs)[52]. PRRs sense the virus and induce antiviral defenses, but evolutionarily, HCV has acquired strategies to modulate and escape immune recognition by the host, which contributes to HCV persistence. For example, HCV can interfere with innate immunity in infected cells via NS3/4A-mediated cleavage of critical signaling molecules, such as IPS-1, TRIF, and IRF3[53]. HCV may also target DC-SIGN receptors, which are found on both LSECs and KCs, to escape lysosomal degradation[54]. The mechanisms that underlie the different outcomes of viral infection are still not fully understood, but likely involve a complex interaction between the virus and host during the

immune response. Understanding how HCV activates or evades the immune response is critical to the development of more effective therapeutics.

1.8 Induced pluripotent stem cells

Ultimately, PHHs are a limited resource for screening large drug libraries and the lack of donor diversity restricts our understanding of how genetics affect liver-drug interactions. Given their ability to be derived from adult somatic cells, induced pluripotent stem cells (iPSCs) are an unlimited cell source, and thus, have revolutionized the availability of pluripotent stem cells for multiple applications, including drug screening for personalized medicine. iPSCs were first generated from adult dermal fibroblasts through the expression of four genes: Oct3/4, Sox2, c-Myc, and Klf4[55]. iPSCs maintain pluripotency and allow for the creation of genetically-diverse donor panels that can be used to assess interindividual variations in disease progression and drug responses. iPSCs have also been utilized for regenerative medicine applications[56]. Most of the current techniques used to differentiate iPSCs into iPSC-derived human hepatocytes (iPSC-HHs) involve a series of soluble factors that replicate those seen during embryonic development (i.e. FGF-2, HGF, and OsM), with several groups successfully generating iPSC-HHs[57,58]. However, most of these iPSC-HHs remain fetal-like, lose hepatic functionality, and rapidly de-differentiate *in vitro*. Our group has recently demonstrated that iPSC-HHs in an MPCC format (iMPCC) leads to higher functional maturity and culture longevity compared to conventional culture formats[2]. Additionally, the use of soluble small molecules (SM) can help maintain iPSC-HH maturation and functionality[59]. However, studies so far have been limited to drug-dosing studies and short-term infectious disease studies[60,61]. iPSC-HHs have been shown to be permissive to both HBV and HCV and can replicate the entire viral life cycle[62-66]. However, the utility of iPSC-HHs generated from different donors for the study of inter-individual differences in viral progression

and response to therapeutics has not been demonstrated. Additionally, conventional monolayers of iPSC-HHs are not able to sustain high levels of CYP450 enzyme activities for the screening of hepatitis drugs. Since iMPCCs have demonstrated sustained CYP450 activity, they may be used as a sustainable cell source to screen for drugs in various donors.

1.9 Hepatitis B

Hepatitis B virus (HBV) affects 400 million people worldwide[67]. While prophylactic options are available and chronic HBV can be treated with nucleoside/nucleotide inhibitors, lifelong treatment is required due to the stable nature of the HBV episomal DNA. Additionally, these treatments only prevent the HBV from replicating; the inflammation present in the liver can still lead to advanced liver diseases such as fibrosis, cirrhosis, and hepatocellular carcinoma. Thus, *in vitro* models that are permissive to HBV and demonstrate robust HBV replication are required in order to study host-viral interactions towards the creation of better HBV therapeutics.

Although cancerous cell lines are capable of supporting the entire lifecycle of HBV, they display uncontrolled proliferation and altered host responses to infection[68,69]. Conventional culture formats have been shown to support long-term HBV infection, but CYP450 activity levels rapidly decline, making routine implementation for drug screening difficult[70,71]. Although the Bhatia group has demonstrated chronic HBV infection in MPCCs, the use of a broad-spectrum Janus kinase inhibitor was required to attenuate the innate immune response in PHHs[64]. HBV studies with iPSC-HHs now open up the possibility of studying the effects of donor genotype and host genes on infection efficiency, propagation, and resistance to drug therapies. Humanized murine models have been shown to be permissive to HBV and lamivudine was able to reduce the level of viremia[72]. Hallmarks of HBV infection, such as macrophage activation,

leukocyte infiltration, and collagen deposition, can be recapitulated in humanized mice[73]. Finally, Ohashi et al created mice with PHHs embedded in Matrigel that were transplanted in the kidney capsule. These mice were susceptible to HBV infection and completed the viral lifecycle[74].

1.10 Hepatitis C

Hepatitis C virus (HCV) affects 130-170 million people globally[67]. While 20%-30% of infected individuals clear the virus without any therapy, 70%-80% become persistently infected[52]. In chronically-infected individuals, HCV can lead to additional complications such as liver fibrosis, cirrhosis, and hepatocellular carcinoma. Prophylactic treatments are not currently available and current HCV therapies, including pegylated interferon-α plus ribavirin and direct acting antivirals (DAAs), are expensive and have serious side effects. Therefore, robust human-relevant HCV model systems are necessary for the development of better therapeutics. Chimpanzees are the only animal model susceptible to HCV infection, but even though this model exhibits hepatitis progression similar to as it occurs in humans, there are ethical considerations, limited availability and high cost issues[75]. Although cell lines have been demonstrated to support the entire HCV life cycle, they display altered host responses to infection[76]. Conventional culture formats have been shown to support HCV infection, but at low infection efficiencies with PHH functions, such as CYP450 activity levels, declining rapidly[77]. Thus, it is difficult to implement conventional cultures for routine drug screening. iPSC-HHs show promise for personalized HCV drug screening as they serve as an unlimited cell source with genetic variability.

1.11 Scope of this dissertation

There is a clear need for microengineered *in vitro* models that allow for the study of liver diseases and preclinical testing of drugs. These models can be built upon for specific scientific inquires, particularly for studying cell-cell interactions. Thus, we have modified our existing MPCC model to make it more physiologically relevant. Various substrates such as PEMs and LBM were used to present growth factors to hepatocytes in a controlled manner to mimic the liver microenvironment *in vivo*. Additionally, in order to study liver conditions in which the immune response can play a role, such as idiosyncratic DILI and viral infection, KCs were incorporated into this model. Nguyen et al have created cocultures of PHHs and KCs to assess the effects of pro-inflammatory cytokines on CYP450 enzymes and drug transporters, but changes in drug metabolism and toxicity due to the presence of these KCs were not assessed[78]. Thus, we assessed DILI and drug clearance using "normal" MPCC cultures and "inflamed" MPCC-KC cultures. Finally, MPCCs created using various donors of PHHs as well as iPSC-HHs were infected with HBV and HCV to assess inter-individual differences in viral progression, resolution, and patient-specific responses to current therapies. This has not been possible previously using *in vitro* models due to declining hepatic functional levels. In order to study viral hepatitis progression, this model should be permissive to the virus, display robust infection for multiple days, and demonstrate sustained liver functions for the testing of potential therapeutics. Additionally, the model must be able to test for the efficacy, clearance, and toxicity of candidate compounds, since DILI remains a leading cause of pharmaceutical attrition and acute liver failures. Thus, this dissertation has been dedicated to creating more relevant *in vitro* liver models to further our understanding of viral hepatitis towards the creation of more effective therapeutics.

References

1. Roberts RA, Ganey PE, Ju C, Kamendulis LM, Rusyn I, Klaunig JE. Role of the Kupffer cell in mediating hepatic toxicity and carcinogenesis. Toxicol Sci 2007;96(1):2-15.

2. Berger DR, Ware BR, Davidson MD, Allsup SR, Khetani SR. Enhancing the functional maturity of induced pluripotent stem cell-derived human hepatocytes by controlled presentation of cell-cell interactions in vitro. Hepatology (Baltimore, Md) 2015;61(4):1370-1381.

3. Godoy P, Hewitt NJ, Albrecht U, Andersen ME, Ansari N, Bhattacharya S, Bode JG, Bolleyn J, Borner C, Böttger J and others. Recent advances in 2D and 3D in vitro systems using primary hepatocytes, alternative hepatocyte sources and non-parenchymal liver cells and their use in investigating mechanisms of hepatotoxicity, cell signaling and ADME. Archives of toxicology 2013;87(8):1315-1530.

4. Wells RG. Cellular sources of extracellular matrix in hepatic fibrosis. Clin Liver Dis 2008;12(4):759-68, viii.

5. Corsini A, Ganey P, Ju C, Kaplowitz N, Pessayre D, Roth R, Watkins PB, Albassam M, Liu B, Stancic S and others. Current challenges and controversies in drug-induced liver injury. Drug safety : an international journal of medical toxicology and drug experience 2012;35(12):1099-1117.

6. Guillouzo A. Liver cell models in in vitro toxicology. Environmental health perspectives 1998;106 Suppl 2:511-532.

7. Yum K, Hong SG, Healy KE, Lee LP. Physiologically relevant organs on chips. Biotechnology journal 2014;9(1):16-27.

8. Khetani SR, Berger DR, Ballinger KR, Davidson MD, Lin C, Ware BR. Microengineered liver tissues for drug testing. Journal of laboratory automation 2015;20(3):216-250.

9. Begue JM, Guguen-Guillouzo C, Pasdeloup N, Guillouzo A. Prolonged maintenance of active cytochrome P-450 in adult rat hepatocytes co-cultured with another liver cell type. Hepatology 1984;4(5):839-42.

10. March S, Ramanan V, Trehan K, Ng S, Galstian A, Gural N, Scull MA, Shlomai A, Mota MM, Fleming HE and others. Micropatterned coculture of primary human hepatocytes and supportive cells for the study of hepatotropic pathogens. Nature protocols 2015;10(12):2027-2053.

11. Bhatia SN, Yarmush ML, Toner M. Controlling cell interactions by micropatterning in co-cultures: hepatocytes and 3T3 fibroblasts. Journal of biomedical materials research 1997;34(2):189-199.

12. Khetani SR, Szulgit G, Del Rio JA, Barlow C, Bhatia SN. Exploring interactions between rat hepatocytes and nonparenchymal cells using gene expression profiling. Hepatology (Baltimore, Md) 2004;40(3):545-554.

13. Khetani SR, Bhatia SN. Microscale culture of human liver cells for drug development. Nature biotechnology 2008;26(1):120-126.

14. Chan TS, Yu H, Moore A, Khetani SR, Tweedie D. Meeting the challenge of predicting hepatic clearance of compounds slowly metabolized by cytochrome P450 using a novel hepatocyte model, HepatoPac. Drug Metab Dispos 2013;41(12):2024-32.

15. Khetani SR, Kanchagar C, Ukairo O, Krzyzewski S, Moore A, Shi J, Aoyama S, Aleo M, Will Y. Use of micropatterned cocultures to detect compounds that cause drug-induced liver injury in humans. Toxicological sciences : an official journal of the Society of Toxicology 2013;132(1):107-117.

16. Shiratori SS, Rubner MF. pH-dependent thickness behavior of sequentially adsorbed layers of weak polyelectrolytes. Macromolecules 2000;33(11):4213-4219.

17. Mendelsohn JD, Yang SY, Hiller J, Hochbaum AI, Rubner MF. Rational design of cytophilic and cytophobic polyelectrolyte multilayer thin films. Biomacromolecules 2003;4(1):96-106.

18. Thierry B, Winnik FM, Merhi Y, Silver J, Tabrizian M. Bioactive coatings of endovascular stents based on polyelectrolyte multilayers. Biomacromolecules 2003;4(6):1564-71.

19. Zhang J, Senger B, Vautier D, Picart C, Schaaf P, Voegel JC, Lavalle P. Natural polyelectrolyte films based on layer-by layer deposition of collagen and hyaluronic acid. Biomaterials 2005;26(16):3353-61.

20. Rajagopalan P, Shen CJ, Berthiaume F, Tilles AW, Toner M, Yarmush ML. Polyelectrolyte Nano-scaffolds for the Design of Layered Cellular Architectures. Tissue engineering 2006;12(6):1553-1563.

21. Elbert DL, Herbert CB, Hubbell JA. Thin polymer layers formed by polyelectrolyte multilayer techniques on biological surfaces. Langmuir 1999;15(16):5355-5362.

22. Richert L, Lavalle P, Payan E, Shu XZ, Prestwich GD, Stoltz JF, Schaaf P, Voegel JC, Picart C. Layer by layer buildup of polysaccharide films: Physical chemistry and cellular adhesion aspects. Langmuir 2004;20(2):448-458.

23. Antipov AA, Sukhorukov GB, Donath E, Mohwald H. Sustained release properties of polyelectrolyte multilayer capsules. Journal of Physical Chemistry B 2001;105(12):2281-2284.

24. Caruso F, Mohwald H. Protein multilayer formation on colloids through a stepwise self-assembly technique. Journal of the American Chemical Society 1999;121(25):6039-6046.

25. Lvov YM, Lu ZQ, Schenkman JB, Zu XL, Rusling JF. Direct electrochemistry of myoglobin and cytochrome p450(cam) in alternate layer-by-layer films with DNA and other polyions. Journal of the American Chemical Society 1998;120(17):4073-4080.

26. Detzel CJ, Larkin AL, Rajagopalan P. Polyelectrolyte multilayers in tissue engineering. Tissue engineering. Part B, Reviews 2011;17(2):101-113.

27. Park IK, Yang J, Jeong HJ, Bom HS, Harada I, Akaike T, Kim S, Cho CS. Galactosylated chitosan as a synthetic extracellular matrix for hepatocytes attachment. Biomaterials 2003;24(13):2331-2337.

28. Kidambi S, Lee I, Chan C. Controlling primary hepatocyte adhesion and spreading on protein-free polyelectrolyte multilayer films. Journal of the American Chemical Society 2004;126(50):16286-16287.

29. Janorkar AV, Rajagopalan P, Yarmush ML, Megeed Z. The use of elastin-like polypeptide-polyelectrolyte complexes to control hepatocyte morphology and function in vitro. Biomaterials 2008;29(6):625-632.

30. Kidambi S, Udpa N, Schroeder SA, Findlan R, Lee I, Chan C. Cell adhesion on polyelectrolyte multilayer coated polydimethylsiloxane surfaces with varying topographies. Tissue Engineering 2007;13(8):2105-2117.

31. Gwon K, Kim M, Tae G. A biocompatible method of controlled retrieval of cell-encapsulating microgels from a culture plate. Integrative biology : quantitative biosciences from nano to macro 2014;6(6):596-602.

32. Huang X, Lin N, Hang R, Wang X, Zhang X, Tang B. Modulating the behaviors of C3A cells via surface charges of polyelectrolyte multilayers. Carbohydrate polymers 2013;92(2):1064-1070.

33. Chen AA, Khetani SR, Lee S, Bhatia SN, Van Vliet KJ. Modulation of hepatocyte phenotype in vitro via chemomechanical tuning of polyelectrolyte multilayers. Biomaterials 2009;30(6):1113-1120.

34. Quek CH, Li J, Sun T, Ling M, Chan H, Mao HQ, Gan LM, Leong KW, Yu H. Photo-crosslinkable microcapsules formed by polyelectrolyte copolymer and modified collagen for rat hepatocyte encapsulation. Biomaterials 2004;25(17):3531-3540.

35. Zhou Y, Sun T, Chan M, Zhang J, Han ZY, Wang XW, Toh Y, Chen JP, Yu H. Scalable encapsulation of hepatocytes by electrostatic spraying. Journal of Biotechnology 2005;117(1):99-109.

36. Faulk DM, Wildemann JD, Badylak SF. Decellularization and cell seeding of whole liver biologic scaffolds composed of extracellular matrix. J Clin Exp Hepatol 2015;5(1):69-80.

37. Gilbert TW, Sellaro TL, Badylak SF. Decellularization of tissues and organs. Biomaterials 2006;27(19):3675-83.

38. Sellaro TL, Ranade A, Faulk DM, McCabe GP, Dorko K, Badylak SF, Strom SC. Maintenance of human hepatocyte function in vitro by liver-derived extracellular matrix gels. Tissue Eng Part A 2010;16(3):1075-82.

39. Lin P, Chan WC, Badylak SF, Bhatia SN. Assessing porcine liver-derived biomatrix for hepatic tissue engineering. Tissue Eng 2004;10(7-8):1046-53.

40. Ulrich RG. Idiosyncratic toxicity: a convergence of risk factors. Annual review of medicine 2007;58:17-34.

41. Obach RS. Prediction of human clearance of twenty-nine drugs from hepatic microsomal intrinsic clearance data: An examination of in vitro half-life approach and nonspecific binding to microsomes. Drug Metabolism and Disposition 1999;27(11):1350-1359.

42. Di L, Hsu IC, Trapa P, Tokiwa T, Obach RS, Bennett W, Atkinson K, Metcalf RA, Bi Y-A, Welsh JA and others. A novel relay method for determining low-clearance values. Drug metabolism and disposition: the biological fate of chemicals 2012;40(9):1860-1865.

43. Di L, Atkinson K, Orozco CC, Funk C, Zhang H, McDonald TS, Tan B, Lin J, Chang C, Obach RS. In vitro-in vivo correlation for low-clearance compounds using hepatocyte relay method. Drug Metab Dispos 2013;41(12):2018-23.

44. Kaplowitz N. Idiosyncratic drug hepatotoxicity. Nature reviews Drug discovery 2005;4(6):489-499.

45. Ray A. Beyond debacle and debate: developing solutions in drug safety. Nature reviews Drug discovery 2009.

46. Abboud G, Kaplowitz N. Drug-induced liver injury. Drug safety : an international journal of medical toxicology and drug experience 2007;30(4):277-294.

47. Grattagliano I, Bonfrate L, Diogo CV, Wang HH, Wang DQ, Portincasa P. Biochemical mechanisms in drug-induced liver injury: certainties and doubts. World J Gastroenterol 2009;15(39):4865-76.

48. Yuan L, Kaplowitz N. Mechanisms of drug-induced liver injury. Clinics in liver disease 2013;17(4):507-18- vii.

49. Gunawan B, Kaplowitz N. Clinical perspectives on xenobiotic-induced hepatotoxicity. Drug Metab Rev 2004;36(2):301-12.

50. Olson H, Betton G, Robinson D, Thomas K, Monro A, Kolaja G, Lilly P, Sanders J, Sipes G, Bracken W and others. Concordance of the toxicity of pharmaceuticals in humans and in animals. Regulatory toxicology and pharmacology : RTP 2000;32(1):56-67.

51. Liaskou E, Wilson DV, Oo YH. Innate immune cells in liver inflammation. Mediators Inflamm 2012;2012:949157.

52. Yang DR, Zhu HZ. Hepatitis C virus and antiviral innate immunity: who wins at tug-of-war? World J Gastroenterol 2015;21(13):3786-800.

53. Gale M, Jr., Foy EM. Evasion of intracellular host defence by hepatitis C virus. Nature 2005;436(7053):939-45.

54. Ludwig IS, Lekkerkerker AN, Depla E, Bosman F, Musters RJ, Depraetere S, van Kooyk Y, Geijtenbeek TB. Hepatitis C virus targets DC-SIGN and L-SIGN to escape lysosomal degradation. J Virol 2004;78(15):8322-32.

55. Takahashi K, Tanabe K, Ohnuki M, Narita M, Ichisaka T, Tomoda K, Yamanaka S. Induction of pluripotent stem cells from adult human fibroblasts by defined factors. Cell 2007;131(5):861-872.

56. Yu J, Hu K, Smuga-Otto K, Tian S, Stewart R, Slukvin II, Thomson JA. Human induced pluripotent stem cells free of vector and transgene sequences. Science (New York, NY) 2009;324(5928):797-801.

57. Hannan NRF, Segeritz CP, Touboul T, Vallier L. Production of hepatocyte-like cells from human pluripotent stem cells. Nature Protocols 2013;8(2):430-437.

58. Schwartz RE, Fleming HE, Khetani SR, Bhatia SN. Pluripotent stem cell-derived hepatocyte-like cells. Biotechnology advances 2014;32(2):504-513.

59. Shan J, Schwartz RE, Ross NT, Logan DJ, Thomas D, Duncan SA, North TE, Goessling W, Carpenter AE, Bhatia SN. Identification of small molecules for human hepatocyte expansion and iPS differentiation. Nature chemical biology 2013;9(8):514-520.

60. Ware BR, Berger DR, Khetani SR. Prediction of Drug-Induced Liver Injury in Micropatterned Co-cultures Containing iPSC-Derived Human Hepatocytes. Toxicological sciences : an official journal of the Society of Toxicology 2015;145(2):252-262.

61. Davidson MD, Ware BR, Khetani SR. Stem cell-derived liver cells for drug testing and disease modeling. Discovery medicine 2015;19(106):349-358.

62. Sa-Ngiamsuntorn K, Wongkajornsilp A, Phanthong P, Borwornpinyo S, Kitiyanant N, Chantratita W, Hongeng S. A robust model of natural hepatitis C infection using

hepatocyte-like cells derived from human induced pluripotent stem cells as a long-term host. Virol J 2016;13:59.

63. Yoshida T, Takayama K, Kondoh M, Sakurai F, Tani H, Sakamoto N, Matsuura Y, Mizuguchi H, Yagi K. Use of human hepatocyte-like cells derived from induced pluripotent stem cells as a model for hepatocytes in hepatitis C virus infection. Biochem Biophys Res Commun 2011;416(1-2):119-24.

64. Shlomai A, Schwartz RE, Ramanan V, Bhatta A, de Jong YP, Bhatia SN, Rice CM. Modeling host interactions with hepatitis B virus using primary and induced pluripotent stem cell-derived hepatocellular systems. Proc Natl Acad Sci U S A 2014;111(33):12193-8.

65. Sakurai F, Mitani S, Yamamoto T, Takayama K, Tachibana M, Watashi K, Wakita T, Iijima S, Tanaka Y, Mizuguchi H. Human induced-pluripotent stem cell-derived hepatocyte-like cells as an in vitro model of human hepatitis B virus infection. Sci Rep 2017;7:45698.

66. Xia Y, Carpentier A, Cheng XM, Block PD, Zhao Y, Zhang ZS, Protzer U, Liang TJ. Human stem cell-derived hepatocytes as a model for hepatitis B virus infection, spreading and virus-host interactions. Journal of Hepatology 2017;66(3):494-503.

67. Lin C, Ballinger KR, Khetani SR. The application of engineered liver tissues for novel drug discovery. Expert opinion on drug discovery 2015;10(5):519-540.

68. Gerets HHJ, Tilmant K, Gerin B, Chanteux H, Depelchin BO, Dhalluin S, Atienzar FA. Characterization of primary human hepatocytes, HepG2 cells, and HepaRG cells at the mRNA level and CYP activity in response to inducers and their predictivity for the detection of human hepatotoxins. Cell biology and toxicology 2012;28(2):69-87.

69. Wilkening S, Stahl F, Bader A. Comparison of primary human hepatocytes and hepatoma cell line Hepg2 with regard to their biotransformation properties. Drug Metabolism and Disposition 2003;31(8):1035-1042.

70. Gripon P, Diot C, Guguen-Guillouzo C. Reproducible high level infection of cultured adult human hepatocytes by hepatitis B virus: effect of polyethylene glycol on adsorption and penetration. Virology 1993;192(2):534-540.

71. Gripon P, Diot C, Thézé N, Fourel I, Loreal O, Brechot C, Guguen-Guillouzo C. Hepatitis B virus infection of adult human hepatocytes cultured in the presence of dimethyl sulfoxide. Journal of virology 1988;62(11):4136-4143.

72. Yoshizato K, Tateno C. A mouse with humanized liver as an animal model for predicting drug effects and for studying hepatic viral infection: where to next? Expert opinion on drug metabolism & toxicology 2013;9(11):1419-1435.

73. Kleiner DE, Brunt EM, Van Natta M, Behling C, Contos MJ, Cummings OW, Ferrell LD, Liu Y-C, Torbenson MS, Unalp-Arida A and others. Design and validation of a histological scoring system for nonalcoholic fatty liver disease. Hepatology (Baltimore, Md) 2005;41(6):1313-1321.

74. Ohashi K, Marion PL, Nakai H, Meuse L, Cullen JM, Bordier BB, Schwall R, Greenberg HB, Glenn JS, Kay MA. Sustained survival of human hepatocytes in mice: A model for in vivo infection with human hepatitis B and hepatitis delta viruses. Nature medicine 2000;6(3):327-331.

75. Moriishi K, Matsuura Y. Evaluation systems for anti-HCV drugs. Advanced Drug Delivery Reviews 2007;59(12):1213-1221.

76. Pietschmann T, Bartenschlager R. Tissue culture and animal models for hepatitis C virus. Clinics in liver disease 2003;7(1):23-43.

77. Ploss A, Khetani SR, Jones CT, Syder AJ, Trehan K, Gaysinskaya VA, Mu K, Ritola K, Rice CM, Bhatia SN. Persistent hepatitis C virus infection in microscale primary human hepatocyte cultures. Proc Natl Acad Sci U S A 2010;107(7):3141-5.

78. Nguyen TV, Ukairo O, Khetani SR, McVay M, Kanchagar C, Seghezzi W, Ayanoglu G, Irrechukwu O, Evers R. Establishment of a hepatocyte-kupffer cell coculture model for assessment of proinflammatory cytokine effects on metabolizing enzymes and drug transporters. Drug Metab Dispos 2015;43(5):774-85.

Chapter 2

A polyelectrolyte multilayer platform for investigating growth factor delivery modes in human liver cultures[2]

Summary

Polyelectrolyte multilayers (PEMs) of chitosan and heparin are useful for mimicking growth factor (GF) binding to extracellular matrix (ECM) as *in vivo*. Here, we developed a PEM platform for delivering bound/adsorbed GFs to monocultures of primary human hepatocytes (PHHs) and PHH/non-parenchymal cell (NPC) co-cultures, which are useful for drug development and regenerative medicine. The effects of ECM protein coating (collagen I, fibronectin, and Matrigel) and terminal PEM layer on PHH attachment/functions were determined. Then, heparin-terminated and fibronectin-coated PEMs were used to deliver varying concentrations of an adsorbed model GF, transforming growth factor β (TGFβ), to PHH monocultures while using soluble TGFβ delivery via culture medium as the conventional control. Soluble TGFβ delivery caused a severe and monotonic downregulation of PHH functions, whereas adsorbed TGFβ delivery caused an upregulation of 3 out of the 4 measured hepatic functions for 1-3 weeks. Finally, functionally stable co-cultures of PHHs and 3T3-J2 murine embryonic fibroblasts were created on the heparin-terminated and fibronectin-coated PEMs that were further modified with adsorbed TGFβ to elucidate similarities and differences in functional

[2] This chapter has been adapted from Lin, C. et al. 2017. A polyelectrolyte multilayer platform for investigating growth factor delivery modes in human liver cultures. Journal of Biomedical Materials Research-Part A. (in press) With permission from Wiley, which does not require authors of the content being used to obtain a license for their personal reuse.

response relative to the monocultures. In conclusion, chitosan-heparin PEMs constitute a robust platform for investigating the effects of GF delivery modes on PHH monocultures and PHH/NPC co-cultures.

2.1 Introduction

In vivo, many growth factors (GFs) are bound to the glycosaminoglycan (GAG) side chains on proteoglycans in the extracellular matrix (ECM) and such binding can be regulated in a spatiotemporal manner by cell-secreted enzymes towards modulating cell functions[1]. In contrast, GFs are typically delivered to cells in soluble form via culture medium exchanges *in vitro*; however, such a protocol requires high concentrations of costly GFs to elicit a cellular response and frequent dosing due to the very short half-lives of GFs in an aqueous milieu. Furthermore, delivering GFs through culture medium may have non-physiologic effects on the cells as it does not mimic *in vivo*-like regulated presentation of bound GFs from the ECM[2,3]. On the other hand, polyelectrolyte multilayers (PEMs) containing ionically crosslinked layers of chitosan and heparin can be used to mimic GF binding to heparin and thus provide cells with a more *in vivo*-like signaling microenvironment[4]. Such chitosan-heparin PEMs have been successfully used to present heparin-bound fibroblast growth factor 2 (FGF-2) to bone marrow-derived ovine mesenchymal stem cells towards modulating their proliferation *in vitro*[5].

Understanding how GFs affect isolated primary human hepatocytes (PHHs) in physiological and pathophysiological contexts is important for developing robust human liver platforms for applications such as drug toxicity screening, discovery of novel therapeutics, and regenerative medicine (i.e. cell-based therapies)[6]. PHHs are a particularly attractive cell source for the above-mentioned applications because they are closer to human liver physiology than

abnormal cancerous cell lines and animal hepatocytes, and are relatively straight-forward to use in medium- to high-throughput culture formats[7]. Compatibility of PEMs of various compositions with rat hepatocyte cultures has been shown, including poly(diallyldimethylammonium chloride)/sulfonated poly(styrene) (PDAC/SPS)[8], poly(acrylic acid)/poly(allylamine hydrochloride)[9], polyacrylic acid/polyethyleneimine[10], and chitosan/DNA[11]. However, these studies did not culture PHHs on PEMs nor did they determine the effects of bound and soluble GFs on liver functions. Therefore, in this study, we developed a platform using chitosan/heparin PEMs that can be used for investigating GF signaling in short-term and long-term PHH cultures in an *in vivo*-like bound/adsorbed context. Protocols were first developed to enable optimal adhesion and functionality of PHHs on PEMs modified with ECM proteins (collagen I, fibronectin, and Matrigel®). Then, heparin-terminated PEMs coated with ECM protein were used to deliver a model GF, transforming growth factor β (TGFβ), to PHH monocultures and the effects on diverse PHH functions were determined over several weeks relative to conventional delivery of soluble TGFβ via culture medium exchanges. Finally, functionally stable co-cultures of PHHs and 3T3-J2 murine embryonic fibroblasts were created on the heparin-terminated PEMs coated with ECM protein and the effects of adsorbed TGFβ delivery were determined on the co-culture phenotype and compared to results in monocultures.

2.2 Methods

2.2.1 Preparation of polyelectrolyte (PEM) substrates

Chitosan was purchased from Novamatrix (Protasan UP B 90/20, 5% acetylated determined by 1H NMR, MW = 80 kDa; PDI = 1.52; Sandvika, Norway) and heparin sodium was purchased from Celsus Laboratories (from porcine intestinal mucosa, 12.5% sulfur, MW =

14.4 kDa; PDI = 1.14; Cincinnati, OH). Aqueous solutions were prepared at 0.01 M on a saccharide basis in acetate buffer (0.2 M, pH 5.0) and filtered through 0.22 μm polyvinylidene fluoride syringe filters (Thermo Fisher Scientific, Pittsburgh, PA) as previously described[5,12]. An acidified water rinse solution (acetic acid, pH 4.0) was also prepared and filtered. Layer-by-layer assembly of the polyelectrolyte solutions was employed by alternating 5-minute adsorption steps with 5-minute acidified water rinses in standard 24-well or 96-well tissue culture-treated polystyrene plates (TCPS, Corning Life Sciences, Tewksbury, MA). A 300-μL or 50-μL solution for 24-well and 96-well plates, respectively, was added to each well and adsorbed under gentle agitation. Due to TCPS being negatively charged, the first layer adsorbed to TCPS was always chitosan, which is positively charged. Heparin-terminated PEMs were constructed with six polyelectrolyte layers, whereas chitosan-terminated PEMs were constructed with seven layers for complete surface coverage. The PEMs-coated wells were washed three times with double-distilled water (ddH_2O) prior to sterilization with 70% ethanol for 1 hour. The sterilized PEMs-coated wells were then washed three times with ddH_2O prior to TGFβ adsorption. Recombinant human TGFβ1 (R&D Systems, Minneapolis, MN) was diluted to 100, 1000, and 10000 pg/mL, and allowed to adsorb in the PEM-coated wells for 2 hours under gentle agitation, followed by two ddH_2O rinses. ECM proteins including rat tail collagen I, fibronectin, or Matrigel (Corning Life Sciences) were adsorbed at concentrations ranging from 10-100 μg/mL by exposing the wells to the protein solutions for 2 hours at 37°C, followed by two ddH_2O rinses. The plates were then stored at 4°C prior to cell seeding.

2.2.2 Atomic force microscopy (AFM) and X-ray photoelectron spectroscopy (XPS) substrate surface characterization

AFM was used to image the surface topographies of TCPS, heparin-terminated PEM-coated TCPS as well as PEM-coated TCPS with TGFβ (300 pg/ml) only, fibronectin (100 μg/ml) only, or both TGFβ and fibronectin. TCPS and coated TCPS samples were cut out and adhered onto 50 mm glass-bottomed petri dishes for imaging. A Bruker BioScope Resolve BioAFM (Bruker AFM, Santa Barbara, CA) was used to obtain images. The microscope was located on a vibration isolation table (Technical Manufacturing Corporation, Peabody, MA) and housed within an acoustic enclosure (Herzan LLC, Laguna Hills, CA). All images were acquired using Bruker's Nanoscope software version 9.3 (Bruker AFM, Santa Barbara, CA) in the ScanAsyst® mode in air and at room temperature. A Bruker silicon nitride SNL probe was used and the cantilever used had a nominal spring constant of 0.35 N/m, resonance frequency of 65 kHz, and tip radius of 2 nm. An automated thermal tune was performed before each imaging session. The Peakforce setpoint, amplitude, and frequency were manually adjusted to obtain stable imaging conditions and to minimize noise. The typical line scan rate was 1-1.5 Hz. Square images (4 μm × 4 μm and 800 nm × 800 nm) were acquired at a resolution of 256 × 256 pixels. To obtain representative images, 2 samples of each treatment group were imaged with different areas imaged on each sample. Nanoscope Analysis version 1.8 (Bruker AFM, Santa Barbara, CA) was used for image analysis. AFM images were corrected with a plane fit before 3D images were made.

All sample surfaces were analyzed by XPS using a Physical Electronics 5800 spectrometer (Chanhassen, MN). Spectra were obtained using a monochromatic Al Kα X-ray source ($h\nu$ = 1486.6 eV), a hemispherical analyzer, and multichannel detector. High-resolution

spectra of O1s, N1s, C1s, and S2p envelopes were acquired at a pass energy of 23.5 eV, with 0.1 eV steps, a spot size of 800 μm, and a takeoff angle of 45°. A low-energy electron gun was used for charge neutralization. Aliphatic carbon at 284.8 eV in the C1s envelope was used to align spectra. High-resolution spectra curve fits were performed using Phi Electronics Multipak version 9.3.0.3 (Chanhassen, MN).

2.2.3 Assessment of TGFβ adsorption and release on heparin-terminated PEMs via ELISA

Triplicate wells of a 96-well TCPS plate were prepared with heparin-terminated PEMs, TGFβ, and fibronectin as mentioned previously. 100 μg/ml of fibronectin and various concentrations of TGFβ (100, 1000, and 10000 pg/ml) were used. The TCPS microtiter plate was stored at 37°C during the experiment. TGF-β1 Duoset ELISA (R&D Systems, Minneapolis, MN) was used to determine TGFβ adsorption to the PEMs following the manufacturer's instructions. Triplicate whole sample supernatants were immediately assayed and replenished with fresh PBS at D0 (0 hours), D0 (2 hours), D1, and D3. The amount of TGFβ adsorbed to samples was calculated via the difference between the adsorbed values and the observed ELISA values, and cumulative mass of TGFβ retained at each timepoint was calculated.

2.2.4 Cell culture

Cryopreserved PHH vials (BioreclamationIVT, Baltimore, MD; Triangle Research Laboratories, Research Triangle Park, NC) were processed as previously described[13]. Cell viability was assessed using trypan blue exclusion and was found to be >80%. Liver-derived non-parenchymal cells were found to be < 1% of all the cells. Cells were resuspended in serum-free hepatocyte maintenance medium and seeded at 33,000 cells per well in a 96-well plate

format or 200,000 cells per well in a 24-well plate format and left overnight for attachment. The culture supernatant was collected and replaced with fresh medium every other day for assessment of cell functionality (50 µL/well for 96-well format and 300 µL/well for 24-well format). For co-cultures, 3T3-J2 murine embryonic fibroblasts were resuspended in serum-containing hepatocyte maintenance medium and seeded ~24 hours post hepatocyte seeding (1:1 fibroblast:hepatocyte).

2.2.5 Quantification of hepatocyte adhesion and functionality

Cell adhesion was assessed via double-stranded DNA (dsDNA) content in adherent cells. DNA concentration was measured using an AccuBlue dsDNA quantitation kit (Biotium, Hayward, CA) or a Quant-iT PicoGreen dsDNA assay kit (Molecular Probes, Eugene, OR). Culture supernatants were assayed for albumin levels using a competitive enzyme-linked immunosorbent assay (ELISA, MP Biomedicals, Santa Ana, CA) with horseradish peroxidase detection and 3,3',5,5'-tetramethylbenzidine (TMB, Rockland Immunochemicals, Boyertown, PA) as the substrate, as previously described[13]. Urea concentration in culture supernatants was assayed using a colorimetric endpoint assay utilizing diacetyl monoxime with acid and heat (Stanbio Labs, Boerne, TX).[13] CYP3A4 enzyme activity was measured by first incubating the cultures with substrate (luciferin-IPA from Promega Life Sciences, Madison, WI) for 1 hour at 37°C and then detecting the luminescence of the produced metabolite (luciferin) according to manufacturer's protocols. CYP2A6 enzyme activity was measured by incubating the cultures with coumarin for 1 hour at 37°C and measuring the fluorescent metabolite 7-hydroxy-coumarin (Sigma-Aldrich, St. Louis, MO). Absorbance and luminescence for the aforementioned assays were measured using a BioTek (Winooski, VT) Synergy H1 multi-mode plate reader.

2.2.6 Data analysis

Experiments were repeated 2+ times with 3+ wells per condition. Data from representative experiments are presented. Error bars on graphs represent standard deviations. Microsoft Excel and GraphPad Prism 7.0 (La Jolla, CA) were used for data analysis and graphing. Statistical significance was determined using the two-tailed Student's t-test assuming unequal variances or one-way ANOVA with *post-hoc* Tukey test.

2.3 Results

2.3.1 Effects of PEM terminal layer and ECM protein type on PHH attachment and functions

Chitosan and heparin PEMs were constructed on industry-standard TCPS plates. **Figure 2.1A** shows the chemical structures for both polyelectrolytes and **Figure 2.1B** depicts the process of preparing heparin-terminated PEMs modified with ECM protein and GF for cell culture. To create chitosan-terminated PEMs, 7 layers of polyelectrolytes were deposited instead of 6. Surface characterization demonstrated that our PEM construction process resulted in PEMs on the nanometer scale (**Supplemental Figure 2.5.1**). For nanometer-scale PEMs, biological responses have been shown to depend on the terminal layer[14]. Therefore, we sought to assess the effects of either a chitosan or heparin terminal layer on PHH attachment and functions on adsorbed ECM proteins (100 μg/mL in solution). The ECM proteins selected were rat tail collagen type I, human fibronectin, and Matrigel, which have been previously used for hepatocyte culture[7,13]. PHHs were cultured on these surfaces for up to 9 days and culture medium was collected every 2 days for quantification of liver functions that included albumin secretion (a surrogate for protein synthesis) and urea synthesis (a marker of nitrogen metabolism). Finally, at the end of the culture period (day 9), cells were lysed for dsDNA quantification as a measure of

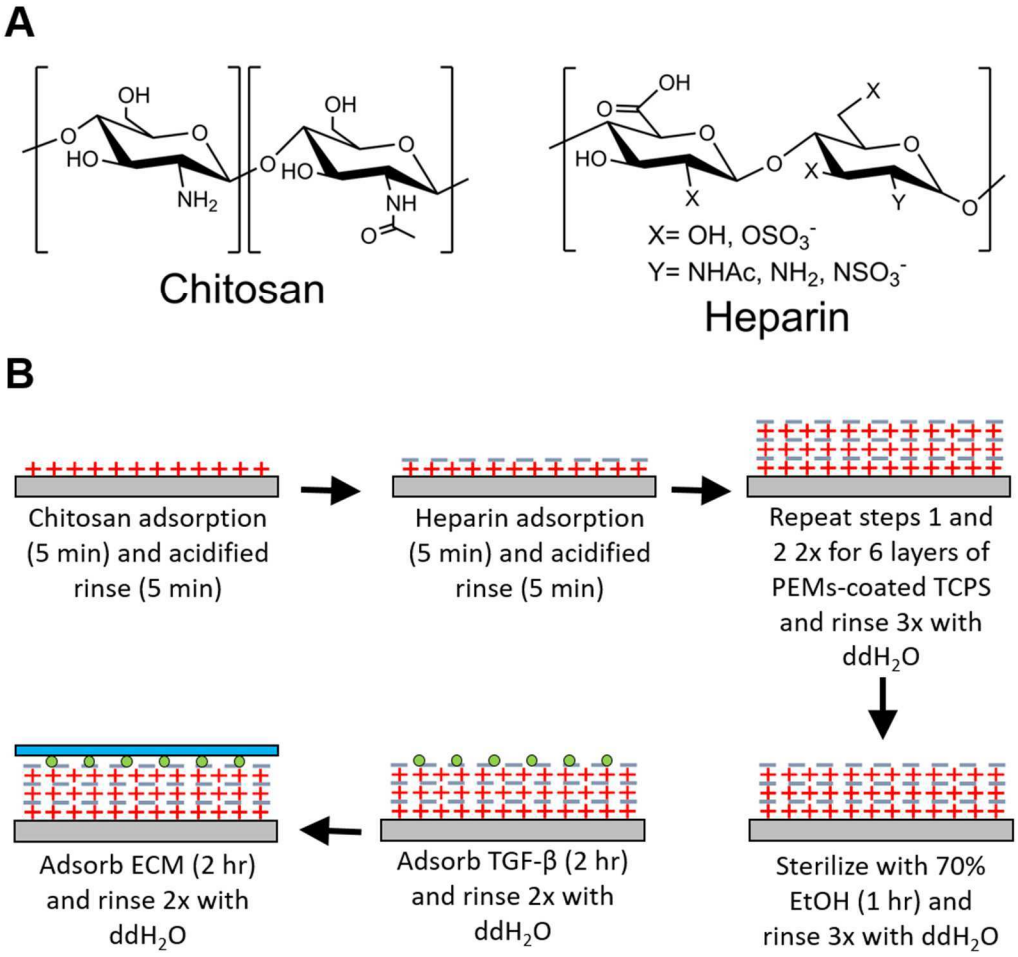

Figure 2.1 Fabrication of polyelectrolyte multilayers (PEMs) containing layers of chitosan and heparin on tissue culture polystyrene (TCPS) for cell attachment and growth factor delivery. (A) Chemical structures of the chitosan (left) and heparin (right) used to assemble PEMs. **(B)** Process steps for first fabricating PEMs on TCPS (top row). The PEM-adsorbed TCPS plates are then sterilized using 70% vol/vol ethanol (EtOH) prior to modifying the PEMs with a growth factor such as transforming growth factor beta (TGFβ) and extracellular matrix (ECM) proteins such as collagen, fibronectin, or Matrigel (bottom row).

the differences in retention of adherent PHHs on the various surfaces. Since hepatocytes do not proliferate *in vitro* in the absence of GFs such as hepatocyte growth factor and epidermal growth factor[15], dsDNA can serve as a measure of differences in the number of adherent cells.

We observed via phase contrast imaging that more PHHs attached to heparin-terminated PEMs coated with collagen (rat tail type I) as compared to chitosan-terminated PEMs (**Figure**

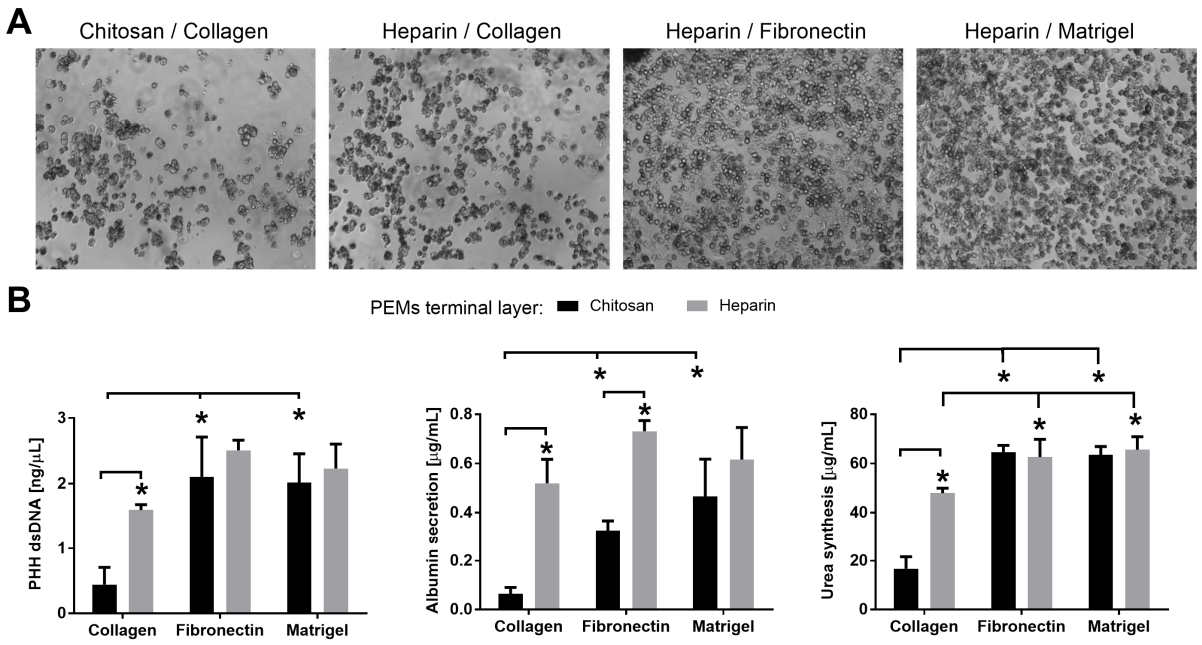

Figure 2.2 Effects of polyelectrolyte terminal layer and extracellular matrix (ECM) protein on adhesion and functions of primary human hepatocytes (PHHs). (A) Phase contrast images (1 day after cell seeding) of PHHs adhered to polyelectrolyte multilayers (PEMs) of the indicated terminal layer (chitosan or heparin) and adsorbed ECM (rat tail type I collagen, fibronectin, and Matrigel at 100 μg/mL density in solution). **(B)** Left: Quantification of double-stranded DNA (dsDNA) from adherent PHHs (9 days after cell seeding) on either chitosan- or heparin-terminated PEMs modified with different ECM proteins. Middle: Cultures as in those created for dsDNA quantification except albumin secretion after 4 days is shown. Right: Same cultures as those used for albumin secretion analysis except urea levels were quantified from the same cell culture supernatants. *P<0.05.

2.2A). The images also revealed that more cells attached to PEMs coated with fibronectin or Matrigel as compared to collagen. Quantification of dsDNA confirmed the phase contrast observations in that ~3.6-fold more dsDNA was measured on heparin-terminated PEMs versus chitosan-terminated PEMs coated with collagen (**Figure 2.2B left**). In contrast to collagen, the terminal layer did not significantly affect PHH retention when either fibronectin or Matrigel was used as the ECM coating. Across the various ECM coatings, chitosan-terminated PEMs modified with collagen had ~21% and ~22% of the dsDNA on chitosan-terminated PEMs modified with fibronectin or Matrigel, respectively. Heparin-terminated PEMs modified with collagen had

~64% and ~72% of the dsDNA on heparin-terminated PEMs modified with fibronectin or Matrigel, respectively. Most of the aforementioned dsDNA trends were also observed with PHH albumin secretion (**Figure 2.2B middle**) and urea synthesis (**Figure 2.2B right**), except heparin-terminated PEMs coated with fibronectin led to ~ 2.2-fold higher albumin secretion from PHHs relative to secretion from chitosan-terminated PEMs coated with fibronectin.

For all subsequent studies described below, we selected heparin-terminated PEMs coated with fibronectin since such a configuration a) allows for high levels of PHH attachment/retention and functions as compared to collagen, b) can be used to present heparin-bound GFs to the cells, and c) is not confounded by the many components present in a complex ECM like Matrigel that may interact differentially and in an unknown way with GFs with each lot/batch. The fibronectin concentration to coat heparin-terminated PEMs for all subsequent studies was chosen to be 100 μg/mL since it led to highest hepatocyte attachment and functions as compared to lower fibronectin concentrations (**Supplemental Figure 2.5.2**).

2.3.2 Surface characterization of substrates via AFM and XPS

Surface morphology characterization of heparin-terminated PEMs coated with fibronectin was performed with AFM. Representative AFM images and average root mean square roughness (Rq) values are shown in **Figure 2.3** with scan sizes of 4 μm × 4 μm (top row) and 800 nm × 800 nm (bottom row). Neat TCPS images are seen in **Figure 2.3A and 2.3F**. Subsequent surface modification with heparin-terminated PEMs are in **Figure 2.3B and 2.3G**. Proteins, TGFβ and fibronectin, adsorbed separately or combined, are seen in **Figure 2.3C-E** and **2.3H-J**. Generally, surfaces coated with either TGFβ or fibronectin separately or combined showed increased

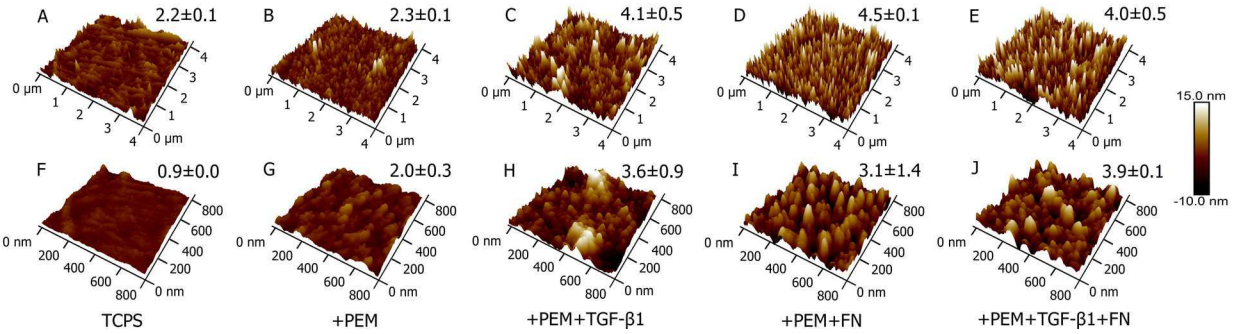

Figure 2.3 Atomic force microscopy (AFM) micrographs of tissue culture polystyrene (TCPS) modified with heparin-terminated polyelectrolyte multilayers (PEMs), transforming growth factor beta (TGFβ), and fibronectin. (A-E, top row) 4 μm × 4 μm and **(F-J, bottom row)** 800 nm × 800 nm scan size micrographs with subsequent TCPS modification steps. Subsequent surface modifications show increased surface features and increased average root mean square roughness (Rq).

roughness and surface features compared to heparin-terminated PEM surfaces and neat TCPS, as also confirmed via increased average Rq values of modified TCPS.

XPS was used to characterize surface chemistry. Since XPS is a surface sensitive technique, it is capable of discerning differences in surface chemistry due to protein adsorption. The atomic percent compositions of the TCPS, chitosan-heparin PEMs, TGFβ-modified PEMs, fibronectin-modified PEMs, and fibronectin- and TGFβ-modified PEMs are shown in **Table 2.1**.

Table 2.1 X-ray photoelectron spectroscopy (XPS) Average Atomic Percentages. Polyelectrolyte multilayers (PEMs) of chitosan and heparin (terminal layer) were created on tissue culture polystyrene (TCPS). Then, transforming growth factor β (TGFβ) or fibronectin (FN, 100 μg/mL) or both were adsorbed on the PEMs as shown in Figure 1. XPS was performed on the samples as described in the Methods section. n.d.-not detected.

Treatment Group	O1s	N1s	C1s	S2p	C/O	N/S
TCPS	13.0 ± 1.3	n.d.	76.8 ± 2.2	n.d.	5.9 ± 0.8	n.d.
+PEM	34.6 ± 0.9	4.5 ± 0.4	54.7 ± 0.5	2.9 ± 0.3	1.6 ± 0.1	1.6 ± 0.0
+PEM+TGFβ	28.8 ± 1.2	3.7 ± 1.5	55.4 ± 2.6	1.5 ± 0.4	1.9 ± 0.0	2.4 ± 0.4
+PEM+FN	25.1 ± 1.9	6.3 ± 3.5	56.9 ± 2.7	0.7 ± 0.3	2.3 ± 0.3	10.4 ± 8.8
+PEM+TGFβ+FN	24.5 ± 0.0	6.2 ± 1.4	56.5 ± 2.2	1.2 ± 0.4	2.3 ± 0.1	5.8 ± 3.1

As expected, TCPS only has detectable carbon and oxygen. Upon PEM addition, the carbon-to-oxygen ratio is reduced, and the nitrogen and sulfur content both increase, in line with the chemical structures of chitosan and heparin. Subsequent addition of TGFβ and fibronectin resulted in the reduction of detectable sulfur compared to PEM-modified TCPS. An increased nitrogen to sulfur ratio was observed in all protein-coated surfaces compared to protein-free surfaces, which further supports TGFβ and fibronectin adsorption on heparin-terminated PEMs. High resolution XPS spectra of the O1s, N1s, C1s, and S2p envelopes are shown in **Figure 2.4**.

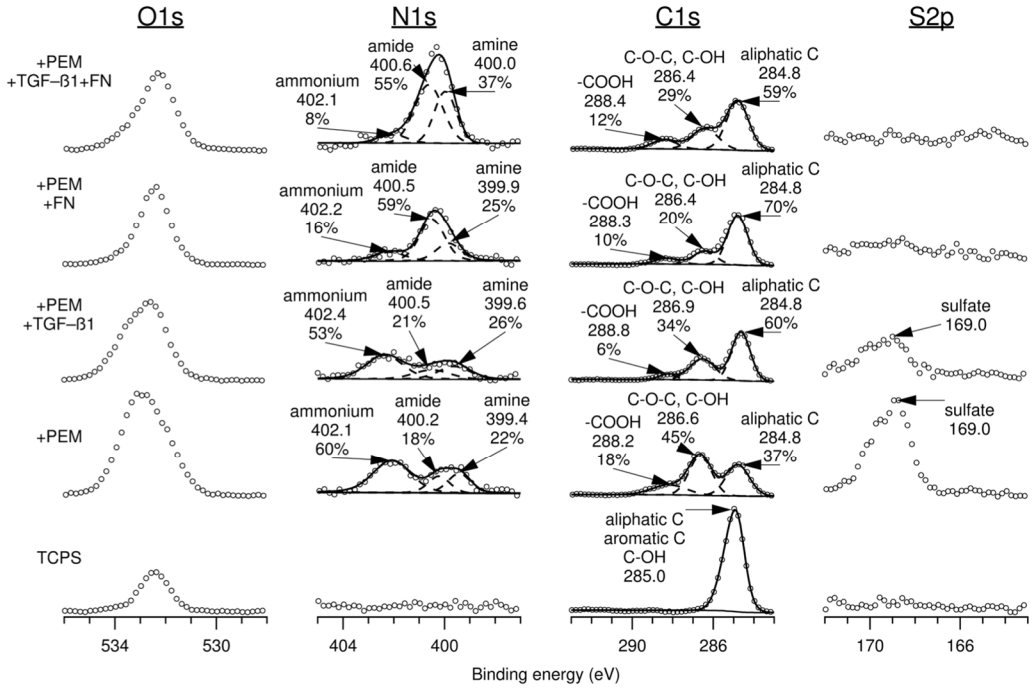

Figure 2.4 X-ray photoelectron spectroscopy (XPS) high resolution spectra of O1s, N1s, C1s, and S2p envelopes of tissue culture polystyrene (TCPS) modified with heparin-terminated polyelectrolyte multilayers (PEMs), transforming growth factor beta (TGFβ), and fibronectin. Attenuation of the sulfate peak (169.0 eV) and changes in the N1s envelope in protein-coated PEMs compared to protein-free PEMs supports protein adsorption onto heparin-terminated PEMs on TCPS.

2.3.3 TGFβ retention on heparin-terminated PEMs with and without fibronectin

TGFβ adsorbed onto heparin-terminated PEMs with and without fibronectin was assessed using ELISA. Amounts of TGFβ adsorbed on samples as well as TGFβ cumulative retention over 3 days are seen in **Table 2.2**. In sample preparation, TGFβ was always adsorbed before fibronectin adsorption, which resulted in samples with and without fibronectin adsorbing similar amounts of TGFβ for all TGFβ concentrations tested. Increased TGFβ solution concentrations resulted in increased amounts of TGFβ adsorption. Overall, we found that >70+% of the TGFβ was adsorbed and subsequently retained over several days on the heparin-terminated PEMs, although fibronectin-coated samples retained less TGFβ compared to fibronectin-free samples.

Table 2.2 Average TGFβ percent cumulative release and retention over 3 days. Polyelectrolyte multilayers (PEMs) of chitosan and heparin (terminal layer) were created on tissue culture polystyrene (TCPS). Then, transforming growth factor β (TGFβ) or fibronectin (FN, 100 μg/mL) or both were adsorbed on the PEMs as shown in Figure 1. TGFβ was quantified in the supernatant to determine potential release following adsorption to the heparin-terminated PEMs. Estimates are given when ELISA response of samples was below the lower limit of detection. 'N.D.' indicates that TGFβ concentration could not be determined in the supernatant, suggesting that the majority of the TGFβ was still retained on the heparin-terminated PEMs.

			% Cumulative TGFβ release			**% Cumulative TGFβ retention**		
TGFβ (pg/ml)	Fibronectin	Average TGFβ mass bound to PEMs (pg)	D0 (2 h)	D1	D3	D0 (2 h)	D1	D3
10,000	-	545.2	9.8	11.4	11.4 - 13.2	90.2	88.6	86.8 - 88.6
1000	-	42.7	15.1	15.1 - 22.6	N.D.	84.9	77.4 - 84.9	N.D.
100	-	1.8 - 5.2	N.D.	N.D.	N.D.	N.D.	N.D.	N.D.
10,000	+	542.3	13.4	15.7	15.7 - 17.5	86.6	84.3	82.5 - 84.3
1000	+	42.9	21.5	29.5	29.5 - 52.6	78.5	70.5	47.4 - 70.5
100	+	1.8 - 5.2	N.D.	N.D.	N.D.	N.D.	N.D.	N.D.

2.3.4 Modulation of PHH functions by TGFβ adsorbed to heparin-terminated PEMs

PHHs were seeded onto heparin-terminated PEMs with or without fibronectin coating, while PEMs-free TCPS coated with fibronectin served as the control substrate. A fibronectin coating on PEMs led to significantly higher PHH attachment relative to fibronectin-free PEMs as assessed by dsDNA levels of adherent cells 1 day after seeding (~4 fold more dsDNA). Furthermore, there were no significant differences in PHH attachment, morphology, albumin secretion, or urea synthesis on PEMs and TCPS coated with fibronectin (**Figure 2.5A-D**). Some minor, but statistically significant, differences were observed in CYP3A4 and CYP2A6 enzyme activities of PHHs across the two substrates (**Figure 2.5E-F**). Nonetheless, both PEMs and TCPS coated with fibronectin supported PHH functions for 3+ weeks, albeit functions were declining after ~1 week as expected from previous literature on PHH monocultures[13].

On heparin-terminated PEM substrates coated with both TGFβ and fibronectin (no further TGFβ was added to the culture medium after the initial adsorption to PEMs), PHH albumin secretion over 21 days was statistically similar at 100 pg/mL TGFβ to secretion from cultures on TGFβ-free PEMs (**Figure 2.6A left**). In contrast, 1000 and 10000 pg/mL of adsorbed TGFβ caused a downregulation of albumin secretion to ~51-66% of secretion from cultures on TGFβ-free PEMs after 7 days; however, such effects were not observed after 15 and 21 days of culture. Urea synthesis from PHH cultures with 100 pg/mL or 10000 pg/mL of adsorbed TGFβ was statistically similar to synthesis from cultures on TGFβ-free PEMs (**Figure 2.6B left**); in contrast, 1000 pg/mL of adsorbed TGFβ increased urea synthesis by ~1.2-fold, ~1.3-fold, and ~1.1-fold after 7, 15, and 21 days of culture, respectively.

CYP3A4 activity in PHH cultures increased transiently ~1.4-fold after 7 days on 1000 pg/mL of adsorbed TGFβ; however, across other timepoints and TGFβ concentrations, CYP3A4

activity in cultures was statistically similar on adsorbed TGFβ to activity in cultures on TGFβ-free PEMs (**Figure 2.6C left)**. Finally, CYP2A6 activity in PHH cultures increased transiently ~1.5-1.6-fold after 7 days on 100 pg/mL and 1000 pg/mL of adsorbed TGFβ, while after 21 days, cultures on 1000 pg/mL and 10000 pg/mL of adsorbed TGFβ had higher CYP2A6 activity than activity in cultures on TGFβ-free PEMs (**Figure 2.6D left**).

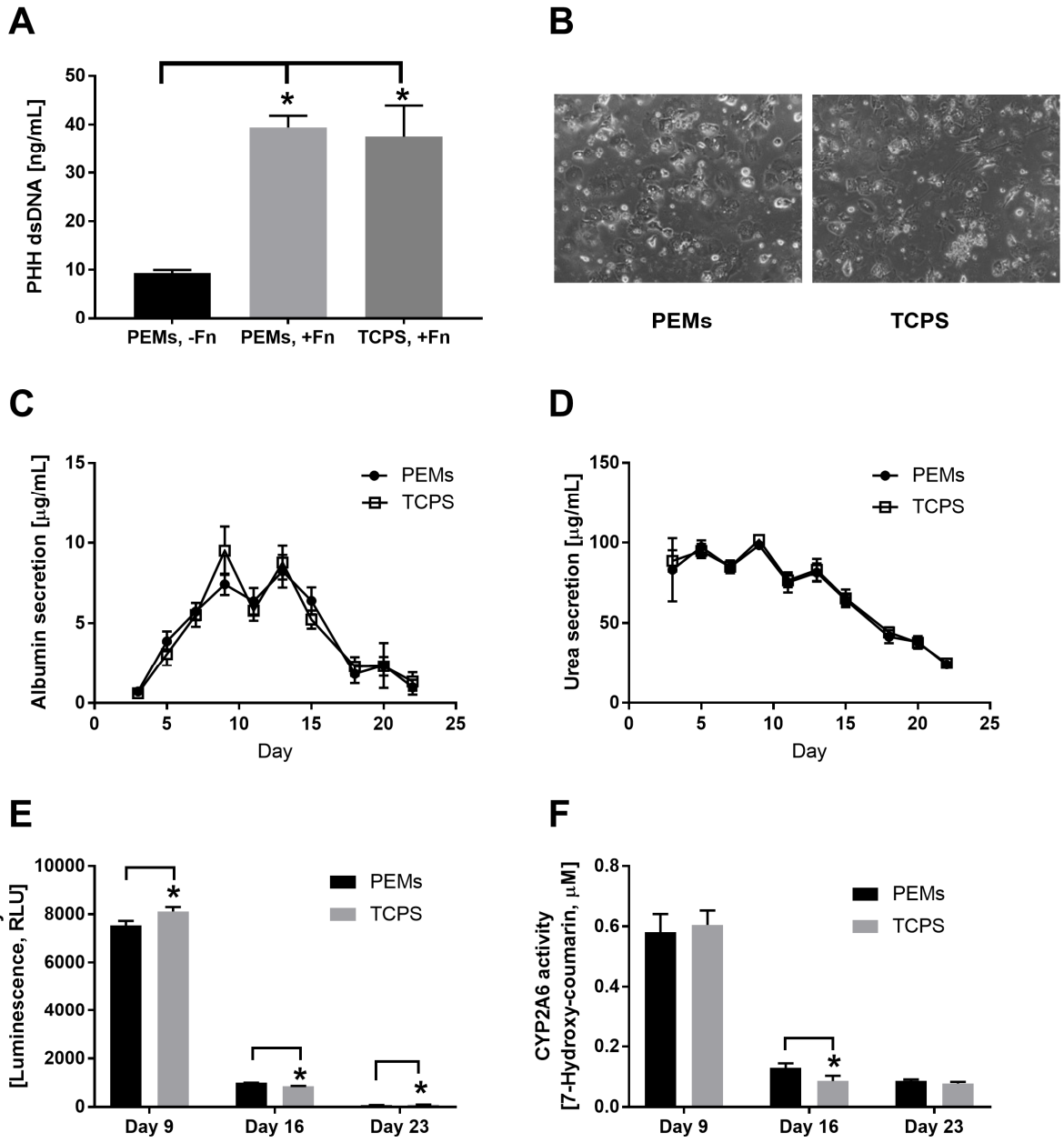

Figure 2.5 Comparison of primary human hepatocyte (PHH) functions on polyelectrolyte multilayers (PEMs) and tissue culture polystyrene (TCPS) substrates. (A) Quantification of double-stranded DNA (dsDNA) from adherent PHHs (1 day after cell seeding) on heparin-terminated PEMs without fibronectin (-Fn), heparin-terminated PEMs modified with 100 μg/mL of fibronectin (+Fn) or TCPS with 100 μg/mL of fibronectin. **(B)** Phase contrast images (from day 5 of culture) of PHHs adhered to heparin-terminated PEMs or TCPS modified with 100 μg/mL of fibronectin. **(C)** Albumin secretion over 3 weeks on heparin-terminated PEMs or TCPS, both modified with 100 μg/mL of fibronectin. **(D)** Urea secretion over time from the same cultures used in panel C. **(E)** Cytochrome P450 3A4 (CYP3A4) enzyme activity in the same cultures used in panel C. **(F)** CYP2A6 enzyme activity in the same cultures used in panel C. *P<0.05.

2.3.5 Modulation of PHH functions by soluble TGFβ in culture medium

For comparison with PHH functions on TGFβ-modified PEMs, we also created PHH cultures on fibronectin-coated TCPS and dosed cultures with soluble TGFβ in culture medium (conventional methodology). One set of such cultures was treated with TGFβ once over 2 days (1 soluble TGFβ), while another set of cultures was treated repeatedly with fresh TGFβ every 2 days over several weeks (continuous). Both the single treatment (**Figure 2.6A middle**) and continuous treatment (**Figure 2.6A right**) with soluble TGFβ led to downregulation of albumin secretion from cultures across all timepoints and all TGFβ concentrations, albeit quantitative differences were observed across the two soluble delivery profiles after 15 and 21 days in culture. Specifically, after 15 days, continuous treatment with soluble TGFβ at 100 pg/mL, 1000 pg/mL, and 10000 pg/mL downregulated albumin secretion from cultures to ~23%, ~1%, and ~4% of secretion from cultures on the TGFβ-free TCPS, respectively; in contrast, a single treatment with soluble TGFβ at 100 pg/mL, 1000 pg/mL, and 10000 pg/mL downregulated albumin secretion to ~56%, 37%, and ~2%, respectively. After 21 days, continuous treatment with soluble TGFβ at 100 pg/mL, 1000 pg/mL, and 10000 pg/mL downregulated albumin secretion to ~24%, ~5%, and ~15% of secretion from cultures on the TGFβ-free TCPS, respectively, whereas a single treatment with soluble TGFβ at 100 pg/mL, 1000 pg/mL, and 10000 pg/mL downregulated albumin secretion from cultures to ~56%, ~45%, and ~55%, respectively.

Urea synthesis showed similar trends as albumin for PHH cultures treated a single time (**Figure 2.6B middle**) or continuously (**Figure 2.6B right**) with soluble TGFβ. After 15 days, continuous treatment with soluble TGFβ at 100 pg/mL, 1000 pg/mL, and 10000 pg/mL downregulated urea synthesis in cultures to ~42%, ~14%, and ~18%, of the synthesis in cultures

on TGFβ-free TCPS, respectively; in contrast, a single treatment with soluble TGFβ at 100 pg/mL, 1000 pg/mL, and 10000 pg/mL downregulated urea synthesis in cultures to ~72%, 63%, and ~15%, respectively. After 21 days, continuous treatment with soluble TGFβ at 100 pg/mL, 1000 pg/mL, and 10000 pg/mL downregulated urea synthesis in cultures to ~26%, ~8%, and ~11% of synthesis in cultures on TGFβ-free TCPS, respectively, whereas a single treatment with soluble TGFβ at 100 pg/mL, 1000 pg/mL, and 10000 pg/mL downregulated urea synthesis in cultures to ~60%, ~36%, and ~13%, respectively.

As with albumin and urea, CYP450 enzyme activities displayed a more severe downregulation in cultures treated continuously with soluble TGFβ as compared to cultures treated a single time with soluble TGFβ. After 13 days, continuous treatment with soluble TGFβ (**Figure 2.6C right**) at 100 pg/mL, 1000 pg/mL, and 10000 pg/mL downregulated CYP3A4 activity in cultures to ~28%, <1%, and <1% of the activity in cultures on TGFβ-free TCPS, respectively; in contrast, a single treatment with soluble TGFβ (**Figure 2.6C middle**) at 100 pg/mL, 1000 pg/mL, and 10000 pg/mL downregulated CYP3A4 activity in cultures to ~67%, 51%, and <1%, respectively. After 21 days, continuous treatment with soluble TGFβ at 100 pg/mL, 1000 pg/mL, and 10000 pg/mL downregulated CYP3A4 activity in cultures to ~5%, ~1%, and ~2% of activity in cultures on TGFβ-free TCPS, respectively, whereas a single treatment with soluble TGFβ at 100 pg/mL and 1000 pg/mL upregulated activity in cultures to ~1.3 fold and ~1.7 fold, respectively. At 10000 pg/mL of soluble TGFβ under a single treatment, CYP3A4 activity in cultures displayed a downregulation to ~16% of activity in cultures on TGFβ-free TCPS. For CYP2A6, after 13 days, continuous treatment with soluble TGFβ (**Figure 2.6D right**) at 100 pg/mL, 1000 pg/mL, and 10000 pg/mL downregulated activity in cultures to ~41%, ~34%, and ~41% of the activity in cultures on TGFβ-free TCPS, respectively; in contrast,

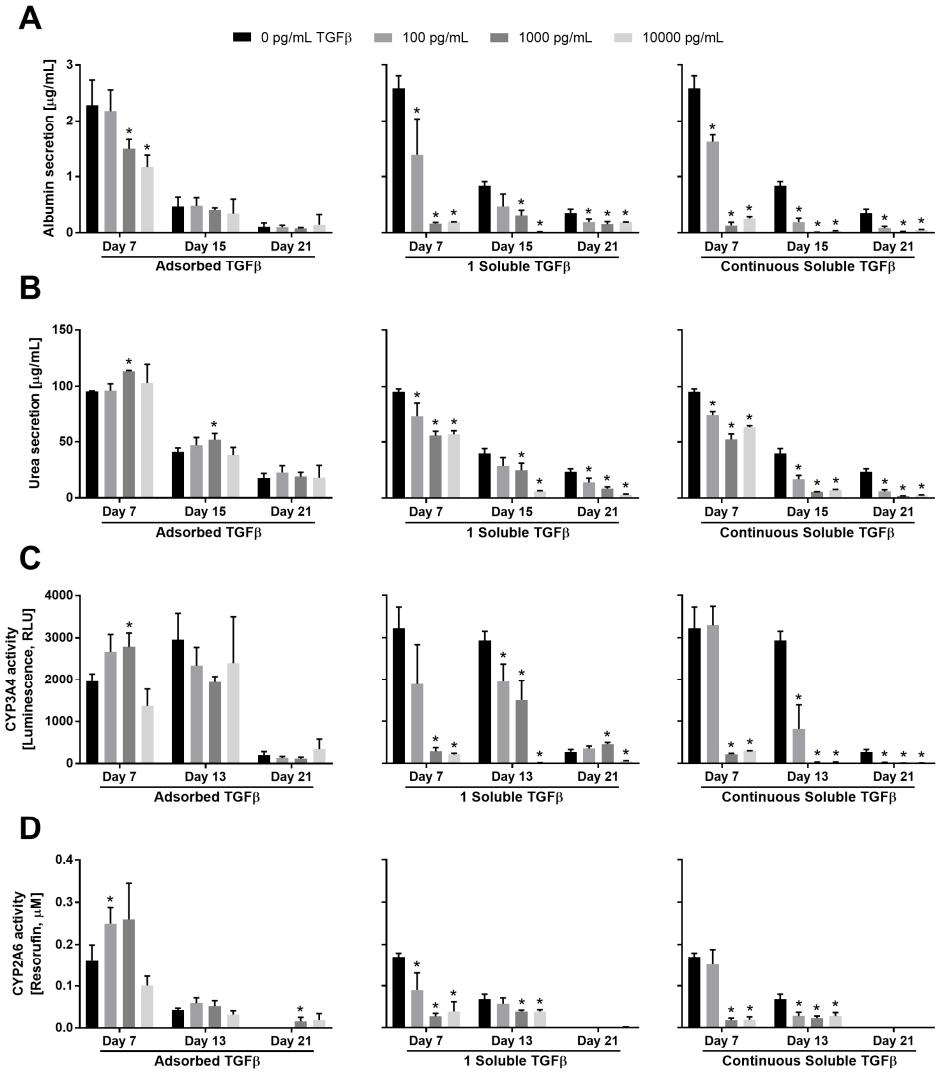

Figure 2.6 Modulation of primary human hepatocyte (PHH) functions by the presentation of transforming growth factor beta (TGFβ) either adsorbed to heparin-terminated polyelectrolyte multilayers (PEMs) or in solution once (1 soluble) or continuously with culture medium changes. For the adsorbed TGFβ conditions, PEMs were created as shown in figure 1B using 100 µg/mL of fibronectin for cell attachment and varying concentrations of TGFβ. For the soluble TGFβ conditions, PHH cultures were established on standard tissue culture polystyrene (TCPS) plates modified with 100 µg/mL of fibronectin. **(A)** Albumin secretion over 3 weeks from PHH cultures at the indicated concentrations of either adsorbed TGFβ (left), soluble TGFβ delivered once over a 2-day media exchange (middle), or soluble TGFβ delivered with every 2-day medium exchanges (right). **(B)** Urea secretion from the same cultures used for panel A. **(C)** Cytochrome P450 3A4 (CYP3A4) enzyme activity in the same cultures used for panel A. **(D)** CYP2A6 enzyme activity in the same cultures used for panel A. Asterisks indicate statistically significant differences ($P<0.05$) between the condition and the TGFβ-free control for that specific timepoint.

a single treatment with soluble TGFβ (**Figure 2.6D middle**) at 100 pg/mL, 1000 pg/mL, and 10000 pg/mL downregulated CYP2A6 activity in cultures to ~84%, ~57%, and ~57%, respectively. After 21 days, CYP2A6 activity in all cultures was very low or undetectable.

2.3.6 Differences between modulation of PHH functions by adsorbed or soluble TGFβ

As discussed above, functions in PHH monocultures displayed significant differences across adsorbed or soluble delivery modes for TGFβ. Specifically, conventional delivery of soluble TGFβ via culture medium exchanges was more detrimental to diverse PHH functions (albumin, urea, CYP3A4/2A6 activities) over the course of 3 weeks than TGFβ adsorbed to heparin-coated PEMs, which instead caused upregulation of all functions at certain timepoints except albumin secretion. Such differences in PHH functions across the TGFβ presentation modes could be due to differential PHH death; however, phase contrast micrographs displayed similar adherent PHH density across conditions over time (**Supplemental Figure 2.5.3**), which suggests downregulation of PHH functions. Lastly, downregulation of PHH functions with soluble TGFβ treatment as compared to adsorbed TGFβ was also confirmed using a coating of 100 μg/mL Matrigel (data not shown), which suggests that the results are not dependent on the ECM protein coating.

2.3.7 Creation of PHH-fibroblast co-cultures on heparin-terminated PEMs

PHH monocultures discussed above, irrespective of substrate type or TGFβ delivery mode, displayed downregulation of all functions over 3 weeks, which is consistent with previous literature showing that neither ECM proteins nor specific soluble factors can fully stabilize the PHH phenotype[6]. In contrast, co-cultures of PHHs and 3T3-J2 murine embryonic fibroblasts on

ECM protein-coated TCPS are known to display high levels of functions over several weeks as compared to pure PHH monocultures[13]. Therefore, here we first sought to determine the compatibility of heparin-terminated and fibronectin-coated PEMs for PHH-fibroblast co-cultures (1:1 PHH:fibroblast ratio). We observed that both cell types were able to attach to and spread on heparin-terminated PEMs coated with 100 μg/mL fibronectin (**Figure 2.7A**). However, in contrast to PHH monocultures, we found that supplementation of the culture media with 10% bovine serum was required to maintain the co-cultures, likely due to the dependency of fibroblast spreading/growth on serum proteins. In serum-supplemented culture medium, PHHs in co-cultures maintained prototypical morphology (i.e. polygonal shape, distinct nuclei/nucleoli, and visible bile canaliculi) on fibronectin-coated PEMs and TCPS control surfaces for 3+ weeks.

Consistent with morphology, PHHs in co-cultures on fibronectin-coated PEMs and TCPS control surfaces displayed relatively stable functions for 3+ weeks, and such functions were significantly higher than those measured in PHH monocultures. Albumin secretion (**Figure 2.7B**) and urea synthesis (**Figure 2.7C**) from co-cultures on PEMs were statistically similar to functions in co-cultures on TCPS; CYP3A4 activity (**Figure 2.7D**) in co-cultures on TCPS was slightly higher than activity in co-cultures on PEMs across all timepoints (~1.4 fold on day 9 and 1.04 fold on days 16 and 23); and, CYP2A6 activity (**Figure 2.7E**) in co-cultures on TCPS was transiently higher (~1.3 fold on day 9) than activity in co-cultures on PEMs.

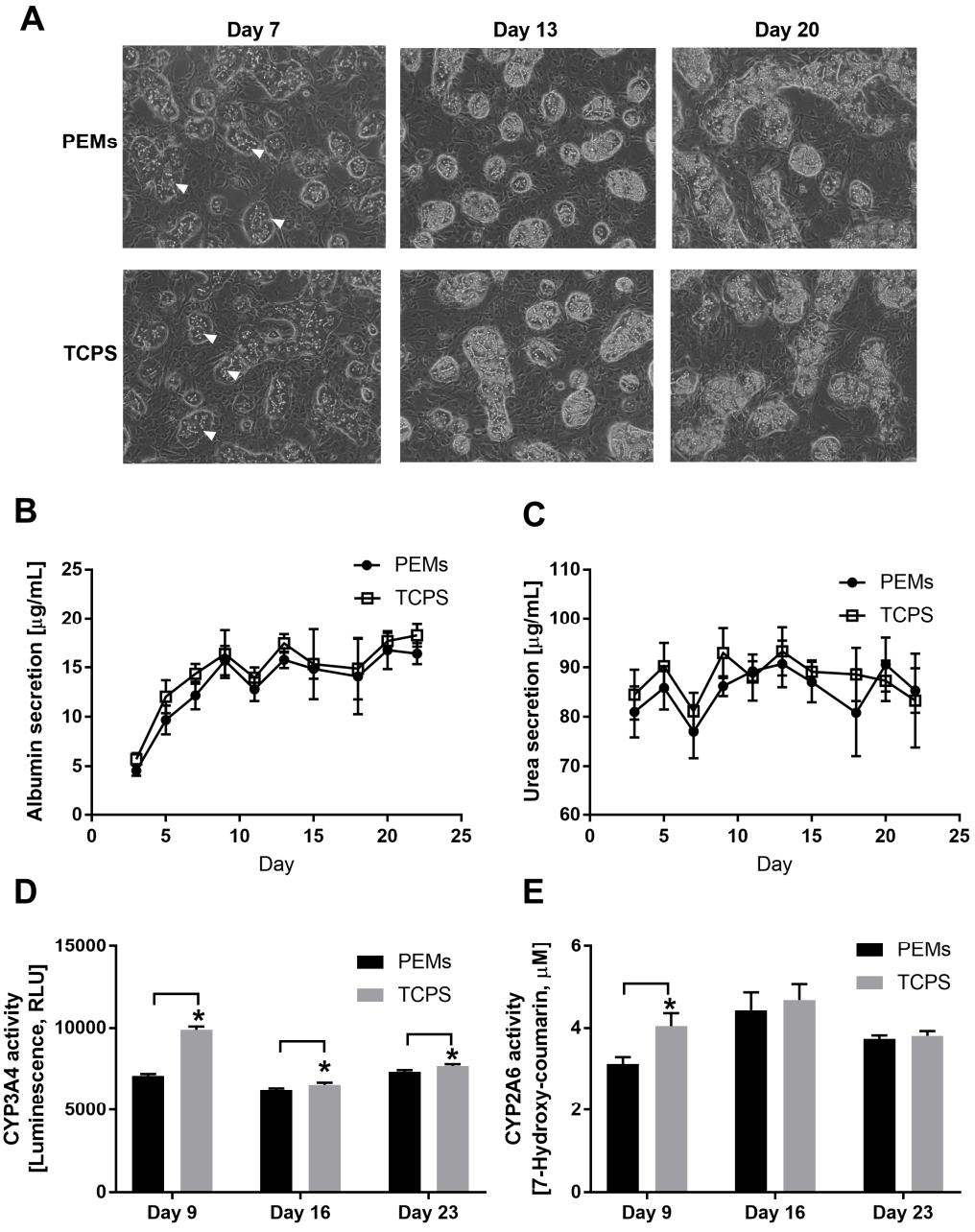

Figure 2.7 Creation of co-cultures of primary human hepatocytes (PHHs) and 3T3-J2 murine embryonic fibroblasts on polyelectrolyte multilayers (PEMs) and assessment of long-term morphology and liver functions. (A) Phase contrast images of co-cultures on heparin-terminated PEMs or TCPS modified with fibronectin for cell attachment. White arrowheads indicate PHHs. **(B)** Albumin secretion from co-cultures created as in panel A. **(C)** Urea secretion over time in the same cultures as those used for panel A. **(D)** Cytochrome P450 3A4 (CYP3A4) enzyme activity in the same cultures as those used for panel A. **(E)** CYP2A6 enzyme activity in the same cultures as those used for panel A. *P<0.05.

2.3.8 Modulation of co-culture functions by TGFβ adsorbed to heparin-terminated PEMs

Next, we determined the effects of TGFβ adsorbed to heparin-terminated and fibronectin-coated PEMs on PHH functions in stable co-cultures using the same TGFβ concentrations as those used for PHH monocultures. Albumin secretion (**Figure 2.8A**) from co-cultures on PEMs was slightly downregulated by adsorbed TGFβ at 100 pg/mL and 1000 pg/mL to ~84-98% of secretion from co-cultures on TGFβ-free PEMs; however, statistical significance was only achieved for 1000 pg/mL of TGFβ after 21 days. Interestingly, at 10000 pg/mL of TGFβ, albumin secretion from co-cultures on PEMs was similar to secretion from co-cultures on TGFβ-free PEMs. In contrast to albumin secretion, adsorbed TGFβ caused downregulation of urea synthesis (**Figure 2.8B**) from co-cultures on PEMs as compared to co-cultures on TGFβ-free PEMs. After 15 days, adsorbed TGFβ at 100 pg/mL, 1000 pg/mL, and 10000 pg/mL downregulated urea synthesis in co-cultures to ~82%, ~63%, and ~72%, of the synthesis in cultures on TGFβ-free PEMs, respectively, and such downregulation was similar at 21 days.

CYP3A4 activity (**Figure 2.8C**) in co-cultures on TGFβ-modified PEMs was downregulated to ~65-69% and ~88-90% by 7 and 13 days, respectively, at TGFβ concentrations up to 1000 pg/mL relative to activity in co-cultures on TGFβ-free PEMs. However, at 10000 pg/mL TGFβ, CYP3A4 activity was statistically similar to activity in co-cultures on TGFβ-free PEMs after 7 and 13 days, and upregulated ~1.3 fold after 21 days. On the other hand, CYP2A6 activity (**Figure 2.8D**) in co-cultures was consistently enhanced by adsorbed TGFβ over 3 weeks. For instance, after 21 days, CYP2A6 activity in co-cultures on PEMs was upregulated ~1.2-1.3 fold by adsorbed TGFβ at 1000 pg/mL and 10000 pg/mL.

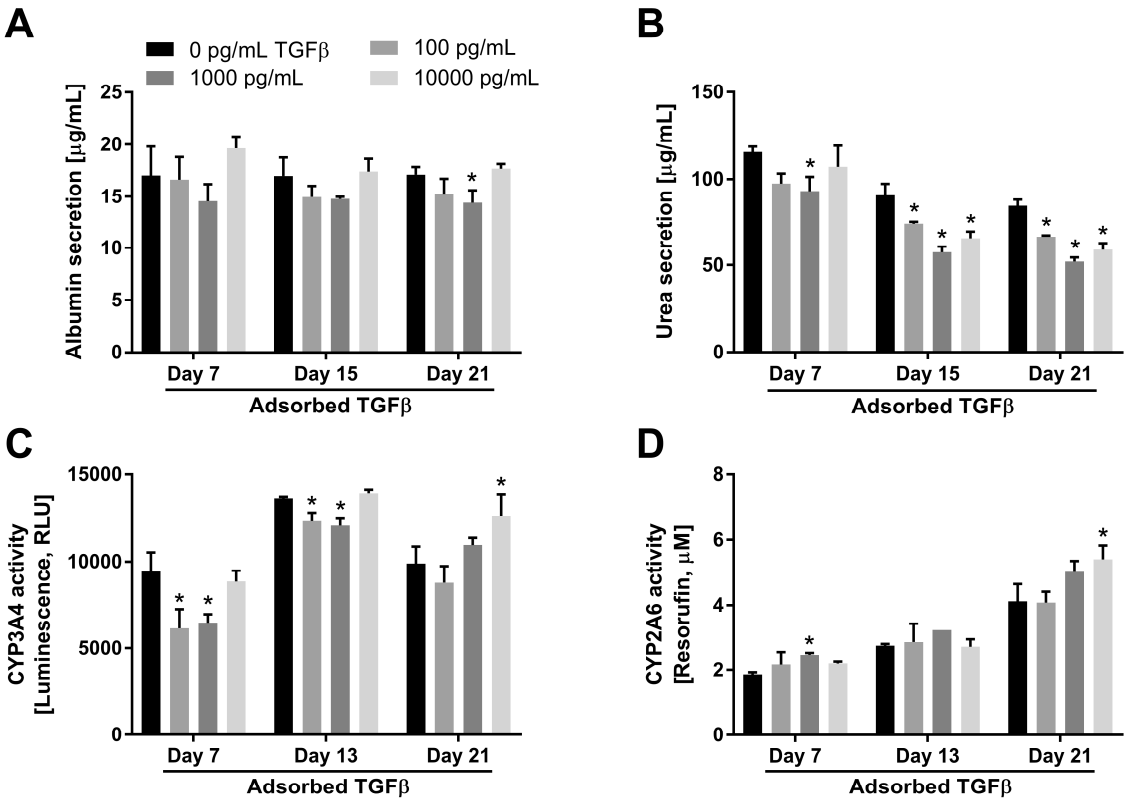

Figure 2.8 Modulation of functions in co-cultures of primary human hepatocytes (PHHs) and 3T3-J2 murine embryonic fibroblasts by the presentation of transforming growth factor beta (TGFβ) adsorbed to heparin-terminated polyelectrolyte multilayers (PEMs). PEMs were created as shown in figure 1B using of 100 μg/mL fibronectin for cell attachment and varying concentrations of adsorbed TGFβ. **(A)** Albumin secretion from co-cultures on PEMs modified with fibronectin and the indicated concentrations of adsorbed TGFβ. **(B)** Urea secretion from the same cultures used for panel A. **(C)** Cytochrome P450 3A4 (CYP3A4) enzyme activity in the same cultures used for panel A. **(D)** CYP2A6 enzyme activity in the same cultures used for panel A. Asterisks indicate statistically significant differences ($P<0.05$) between the condition and the TGFβ-free control for that specific timepoint.

2.4 Discussion

We developed a platform containing chitosan/heparin PEMs to investigate the long-term effects of heparin-bound GFs on PHH functions in monocultures and co-cultures with NPCs. The type of ECM protein coating and the terminal layer for the PEMs (chitosan vs. heparin) were shown to significantly affect PHH attachment and functions. Furthermore, PHH functions were

found to be differentially sensitive to the mode of GF (TGFβ used as a model) delivery, either adsorbed to heparin-terminated PEMs or solubilized in culture medium for either single or continuous treatment (conventional methodology). Finally, similarities and differences were observed in the functional response of co-cultures to adsorbed TGFβ delivery relative to the monocultures.

Fibronectin and Matrigel facilitated PHH attachment/functions on both chitosan- and heparin-terminated PEMs. Fibronectin is negatively-charged at physiological pH (isoelectric point of 5.2), which may facilitate binding to positively-charged chitosan via electrostatic interactions[16]. Additionally, heparin contains binding sites for fibronectin[17]. In contrast to purified fibronectin, Matrigel is an ECM mixture extracted from a mouse sarcoma containing laminin, entactin, collagen, and heparin sulfate proteoglycans[18]. Thus, PEMs can be modified with either purified ECM proteins or complex mixtures to enable cell attachment.

In contrast to fibronectin and Matrigel, rat tail type I collagen, which is widely used for hepatocyte culture[6], facilitated better PHH attachment/functions on heparin-terminated PEMs than on chitosan-terminated PEMs. Heparin can bind to type I collagen independent of collagen's aggregation state[19], and such binding occurs on the N-terminal basic triple helical domain that is represented once within each collagen monomer and at multiple sites within collagen fibrils[20]. Lack of cell retention on chitosan-terminated PEMs coated with collagen suggests that collagen either did not properly adsorb to the chitosan layer and/or formed a non-uniform coating. Chitosan is a weak polycation with pendant amine groups that have pKa ≈ 6.4. At the neutral pH used for the protein adsorption, the free amine groups (not electrostatically bound to heparin in the PEM) are mostly deprotonated, making the surface considerably more hydrophobic, and possibly leading to non-uniform collagen adsorption. However, further

molecular-scale studies would be required to determine the deposition and conformation of collagen on chitosan-terminated PEMs. Others have shown that covalently cross-linking collagen to chitosan layers can aid in cell attachment[21]. We did not execute such a strategy in this study since the effects of the crosslinker on PHH adhesion/functionality would first need to be characterized prior to incorporation into a PEM layer. Furthermore, since both fibronectin and Matrigel promoted sufficient PHH attachment/functions on heparin-terminated PEMs, which are suited for GF delivery, we proceeded with testing GF delivery to PHH cultures/co-cultures using fibronectin as the ECM protein of choice given the batch-to-batch variability inherent in a complex ECM mixture like Matrigel.

Heparin-terminated and fibronectin-coated PEMs adequately supported the attachment and functions of PHH monocultures as compared to the fibronectin-coated TCPS control used by others in the field. Some differences in CYP450 activities were observed over time across the substrate types; however, these differences were minor (<1.4 fold) and the cultures displayed similar kinetics of functions on both substrates. These results show that modification of TCPS with PEMs does not significantly affect PHH ability to attach and function for several weeks.

To demonstrate GF delivery from heparin-terminated PEMs to PHH cultures, we chose TGFβ since it plays a critical role in liver physiology/pathophysiology and has been shown to modulate hepatocyte functions *in vitro*[22]. *In vivo,* TGFβ binds to GAGs such as heparin and heparan sulfate for localized activity and prevention of degradation by enzymes[23]. *In vitro* studies have shown that when TGFβ is bound to heparin, its half-life is tripled, the amount of cell-associated TGFβ is doubled, and TGFβ activity is increased[24,25]. Chitosan is similar to other GAGs and can form ionic complexes with heparin[26]. We confirmed TGFβ adsorption to heparin-terminated PEMs via AFM and XPS. Additionally, the amounts of adsorbed (>70%) and

released TGFβ over several days were assessed using ELISA on supernatants. In previous studies, we have shown FGF-2 delivery from chitosan/heparin PEMs[5] and thus, we anticipate that our platform can be used to deliver different GFs and mixtures to human liver cultures.

Delivery of soluble TGFβ to PHH monocultures on fibronectin-coated TCPS via culture medium exchanges (conventional methodology) caused a monotonic decline in diverse liver functions as a function of time and GF concentration. Surprisingly, even a single treatment with TGFβ over a 2-day medium exchange was generally detrimental to the cultures even after several weeks; continuous treatment with TGFβ with every medium exchange further accelerated the functional decline of the monocultures. On the other hand, adsorbed TGFβ did not lead to sustained downregulation of functions in PHH monocultures, and even caused upregulation of 3 out of 4 measured functions for 1 to 3 weeks. The differences in PHH functions due to TGFβ delivery modes are likely not due to differences in exposure of PHHs to varying amounts of TGFβ since we found that more than 70% of the TGFβ adsorbed to the heparin-terminated and fibronectin-coated PEMs and was retained over several days of measurement. Instead, we anticipate that as *in vivo,* PHHs respond differentially to adsorbed TGFβ as opposed to the solubilized form. Indeed, others have also demonstrated that the mode of GF presentation to cells can make a difference in terms of cell aggregation, spreading, and function[2,3]. Our platform now provides the avenue to study physiologically relevant PHH-GF interactions, while using significantly fewer amounts of costly GFs than required for soluble delivery.

As expected from the previous studies[6,13], ECM protein and GF alone were not sufficient to stabilize PHH phenotype in monocultures. In contrast, co-culture with both liver- and non-liver-derived NPC types has been long known to induce functions in primary hepatocytes from multiple species, including humans, which suggests that the molecular mediators underlying the

'co-culture effect' are relatively well-conserved across species[27,28]. Khetani and Bhatia have demonstrated that 3T3-J2 fibroblasts induce high levels of functions in PHHs[13], which is likely due to the ability of the 3T3-J2 fibroblasts to express diverse hepatocyte-supportive molecules present in the liver, such as decorin[29] and T-cadherin[30]. Furthermore, the use of 3T3-J2 fibroblasts in co-culture with PHHs does not prevent the effective use of the stabilized PHHs for many applications in drug development[31-39]. Therefore, here we created co-cultures of PHHs and 3T3-J2 fibroblasts on heparin-terminated and fibronectin-coated PEMs and compared the long-term morphology and functions to those obtained on fibronectin-coated TCPS (conventional methodology). Overall, PEMs supported a stable PHH morphology and diverse functions for 3+ weeks at comparable levels as those observed in TCPS controls.

Delivering TGFβ to co-cultures at the same concentrations as those used for PHH monocultures revealed some key differences in functional responses between the two culture models. Specifically, adsorbed TGFβ at the higher doses, 1000 and 10000 pg/mL, downregulated albumin secretion in PHH monocultures after 7 days whereas no such downregulation was observed in co-cultures. Furthermore, while urea synthesis and CYP3A4 activity were upregulated in PHH monocultures over 7 to 15 days due to 1000 pg/mL of adsorbed TGFβ, these functions in co-cultures were downregulated at the same timepoints; however, by 21 days, 10000 pg/mL of adsorbed TGFβ caused upregulation of CYP3A4 activity in both PHH monocultures and co-cultures. CYP2A6 activity was upregulated in both PHH monocultures and co-cultures over 3 weeks, albeit at different fold changes. The above-mentioned similarities and differences in functional responses of PHH monocultures and co-cultures to the same concentrations of adsorbed TGFβ on the same substrate could be due to several reasons. First, serum in the culture medium was required for obtaining high functions in co-cultures (due to optimal fibroblast

growth and spreading), whereas PHH monocultures do not need serum to survive and serum can be detrimental to monocultures as shown previously[40]. It may be that serum proteins bind TGFβ and modulate its effects on PHHs in co-cultures relative to monocultures. Second, functionally stable PHHs in co-cultures may have a differential sensitivity to TGFβ than functionally declining PHHs in monocultures. Finally, 3T3-J2s have been shown to express decorin[29], a small leucine-rich proteoglycan that is known to bind to TGFβ and modulate its activity[41]. We plan to investigate these potential differences in TGFβ signaling across monocultures and co-cultures in future detailed studies.

In conclusion, PHH monocultures and PHH-fibroblast co-cultures were successfully established on chitosan-heparin PEMs coated with ECM proteins. Delivering the model GF, TGFβ, to the monocultures in adsorbed form via heparin-terminated PEMs yielded more complex concentration and time effects on PHH functions as compared to a monotonic and severe functional decline with soluble TGFβ delivery. Finally, functional response of co-cultures to adsorbed TGFβ showed similarities and differences across different liver functions to the response of monocultures. In the future, our platform can be extended to investigating the roles of diverse ECM proteins and GFs on human liver models of varying cellular compositions.

2.5 Supplemental Figures

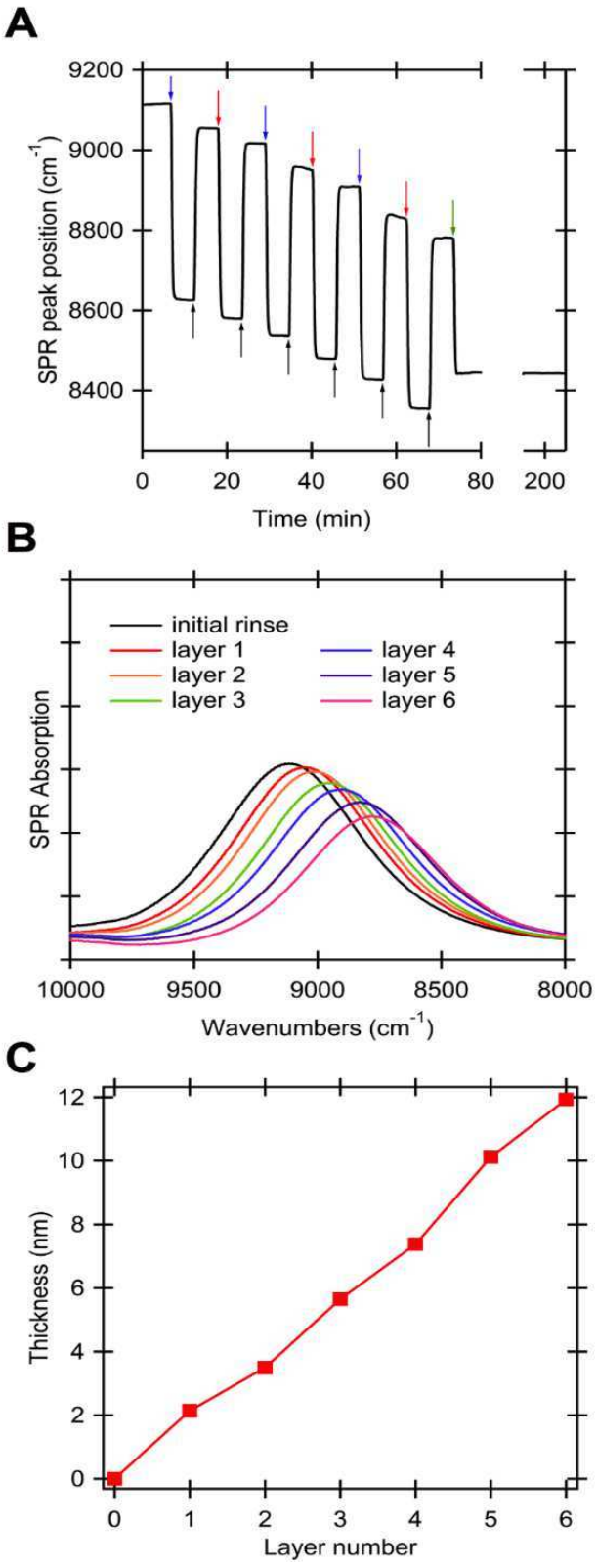

Figure 2.5.1 Characterization of polyelectrolyte multilayer (PEM) substrate via Fourier-transform surface plasmon resonance (FT-SPR). FT-SPR was used to characterize the PEM-modified surfaces. PEMs were prepared on gold-coated glass surfaces. Briefly, gold-coated substrates were first modified with a self-assembled monolayer (SAM) of mercaptoundecanoic acid (MUA). PEMs were constructed on MUA-modified gold films in the flow-cell of an SPR-100 module on a Nicolet 8700 FT-IR spectrometer (Thermo Electron, Madison, WI). The surface was exposed to an acidified water rinse, chitosan solution, acidified water rinse, and heparin solution. Each step was 5-6 minutes, and the sequence was repeated three times, followed by an additional acidified water rinse, to prepare six-layer PEMs (3 bilayers). For subsequent modification with TGFβ, the surfaces were then exposed to either phosphate buffered saline (PBS) without TGFβ, or PBS with TGFβ at concentrations between 100 pg/mL and 300 pg/mL for 2 hours. Each experiment was repeated three times. FT-SPR spectra were collected during the entire surface modification procedure using Omnic 7.3 software (Thermo Electron) at 8 cm^{-1} resolution from 6000 to 12000 cm^{-1}. An FT-SPR spectrum was obtained every 4.7 seconds by co-adding 16 scans at each time point. The SPR peak position as a function of time was computed from the center of gravity, and the film thickness was determined from the rinse following each adsorption step. **(A)** SPR peak position as a function of time during PEM assembly and a 2-hour phosphate buffered saline (PBS) rinse. During the first five minutes, the surface is exposed to an acidified water rinse to establish a baseline peak position. Arrows indicate the introduction of a new solution into the flow cell: blue (chitosan), black (acidified rinse), red (heparin), and green (PBS). Each time a chitosan or heparin solution is introduced, the peak position shifts by nearly 500 cm^{-1}. This shift is due to differences in the refractive index of the rinse and polymer solutions and indicates the adsorption of the polyelectrolyte on the surface. When the subsequent acid rinse is introduced, the peak position does not return to the previous value, because the surface has been modified with adsorbed polyelectrolyte. After the final acidified water rinse, the surface is exposed to PBS. The signal is stable for the subsequent 2 hours, indicating that there are no apparent changes in the optical properties of the film during the PBS rinse. **(B)** Representative FT-SPR spectra during the PEM deposition experiment shown in panel A; each spectrum was taken during an acidified water rinse following the indicated layer. From the relative positions of the center of gravity of these peaks, the film thickness can be calculated. **(C)** PEM thickness determined by the FT-SPR peak shift during the rinse following each of the layer deposition steps, relative to the initial rinse. The chitosan layers (odd-numbered) contribute slightly more incremental thickness than heparin layers (even-numbered) (~2.3 nm compared to ~1.6 nm).

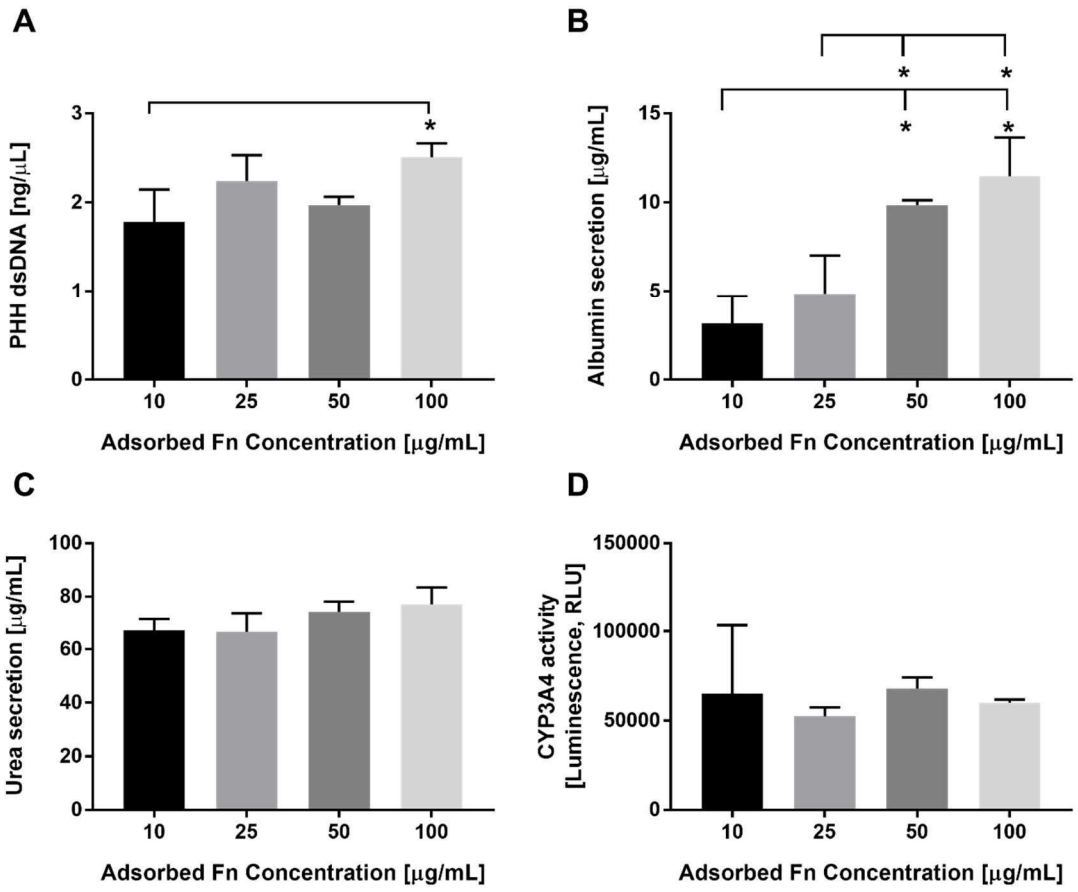

Figure 2.5.2 Comparison of adsorbed fibronectin (Fn) concentrations on heparin-terminated polyelectrolyte multilayers (PEMs) for attachment and functionality of primary human hepatocyte (PHH) monocultures. (A) Double-stranded DNA (dsDNA) quantification from adherent PHHs (9 days after cell seeding) on heparin-terminated PEMs modified with 10, 25, 50, or 100 μg/mL of fibronectin. **(B)** Cultures as in panel 'A' except albumin secretion after 2 days is shown. **(C)** Cultures as in panel 'A' except urea synthesis after 2 days is shown. **(D)** Cultures as in panel 'A' except cytochrome P450 3A4 (CYP3A4) after 6 days is shown. *$P<0.05$ (one-way ANOVA and Tukey's post-hoc test).

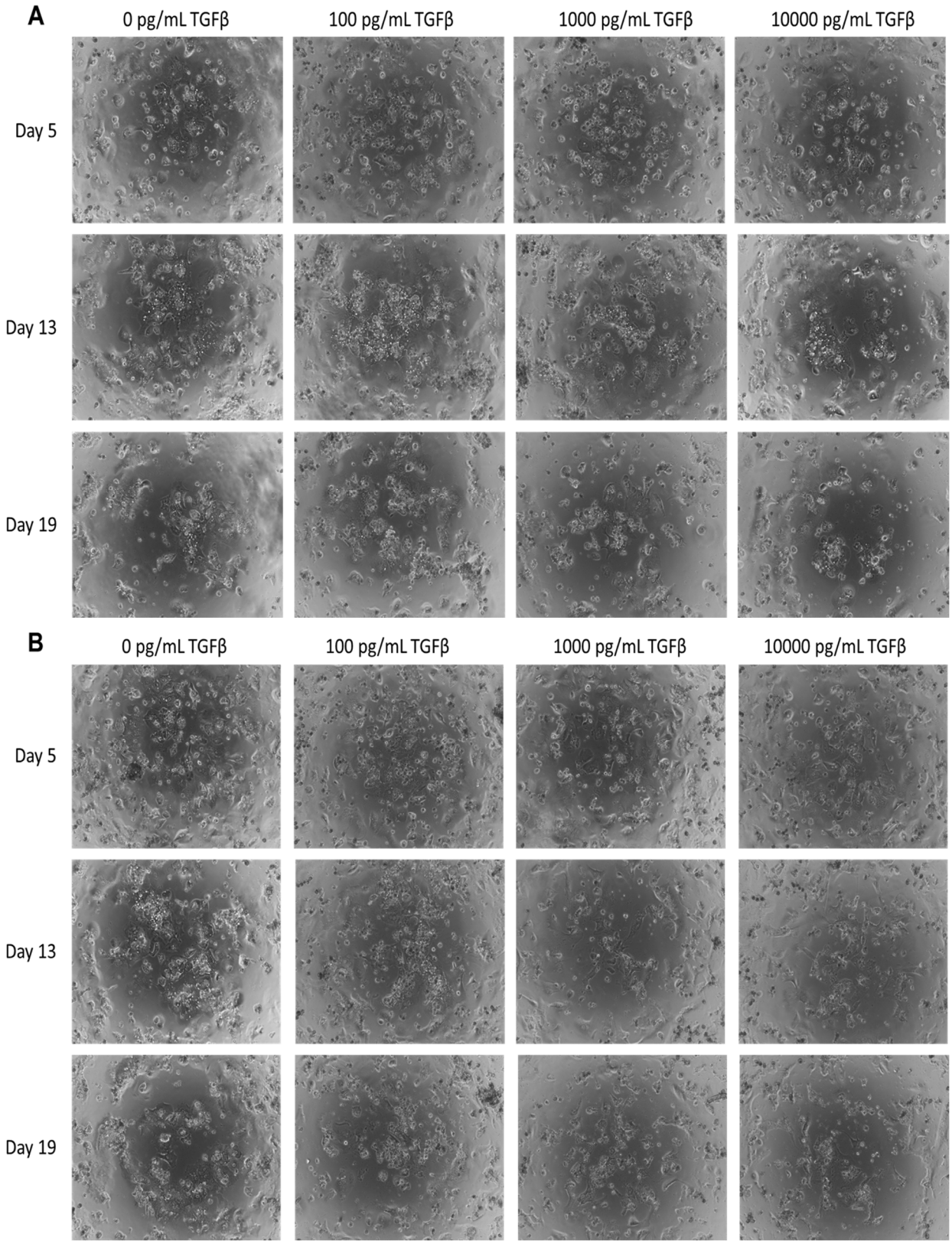
A
0 pg/mL TGFβ
100 pg/mL TGFβ
1000 pg/mL TGFβ
10000 pg/mL TGFβ
Day 5
Day 13
Day 19
B
0 pg/mL TGFβ
100 pg/mL TGFβ
1000 pg/mL TGFβ
10000 pg/mL TGFβ
Day 5
Day 13
Day 19

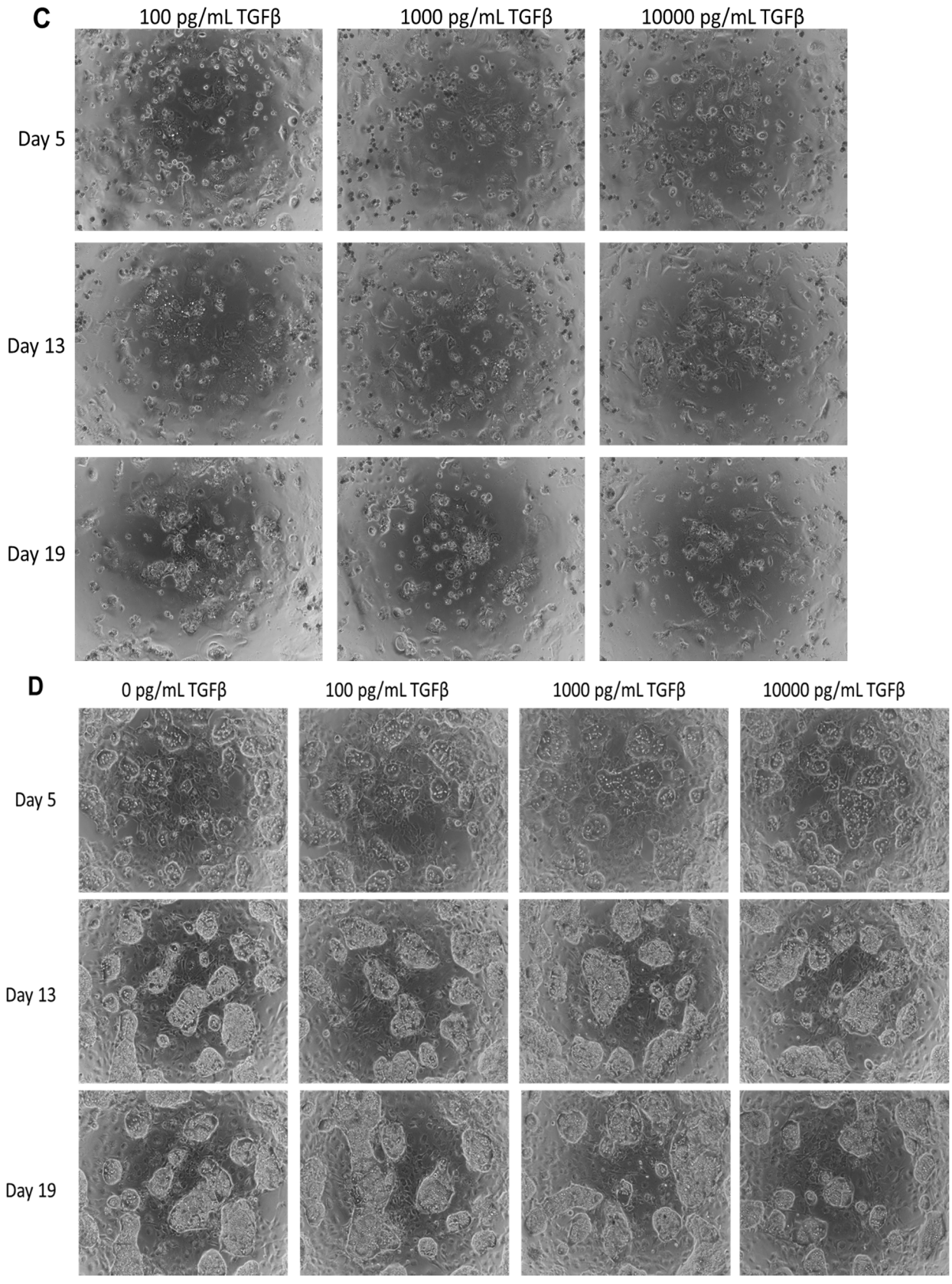
C
100 pg/mL TGFβ
1000 pg/mL TGFβ
10000 pg/mL TGFβ
Day 5
Day 13
Day 19
D
0 pg/mL TGFβ
100 pg/mL TGFβ
1000 pg/mL TGFβ
10000 pg/mL TGFβ
Day 5
Day 13
Day 19

Figure 2.5.3 Phase contrast images over time of primary human hepatocyte (PHH) monocultures and PHH and 3T3-J2 co-cultures treated with varying concentrations of transforming growth factor beta (TGFβ). (A) PHH monocultures were established on heparin-terminated PEMs modified with 100 μg/mL of fibronectin with varying concentrations of adsorbed TGFβ. **(B)** PHH monocultures were established on standard tissue culture polystyrene (TCPS) modified with 100 μg/mL of fibronectin and treated with varying concentrations of soluble TGFβ delivered via culture medium changes every other day in solution starting on day 5 of culture (continuous). **(C)** PHH monocultures were established on TCPS modified with 100 μg/mL of fibronectin and treated with varying concentrations of TGFβ delivered once in solution on day 5 of culture (1 soluble delivery). TGFβ-free controls are not shown since they are the same as those shown in panel B. **(D)** Co-cultures of PHH and 3T3-J2 murine embryonic fibroblasts were established on heparin-terminated PEMs modified with 100 μg/mL of fibronectin with varying concentrations of adsorbed TGFβ.

References

1. Schönherr E, Hausser HJ. Extracellular matrix and cytokines: a functional unit. Developmental immunology 2000;7(2-4):89-101.

2. Kuhl PR, Griffith-Cima LG. Tethered epidermal growth factor as a paradigm for growth factor-induced stimulation from the solid phase. Nat Med 1996;2(9):1022-7.

3. Mehta G, Williams CM, Alvarez L, Lesniewski M, Kamm RD, Griffith LG. Synergistic effects of tethered growth factors and adhesion ligands on DNA synthesis and function of primary hepatocytes cultured on soft synthetic hydrogels. Biomaterials 2010;31(17):4657-71.

4. Boddohi S, Killingsworth CE, Kipper MJ. Polyelectrolyte multilayer assembly as a function of pH and ionic strength using the polysaccharides chitosan and heparin. Biomacromolecules 2008;9(7):2021-2028.

5. Almodóvar J, Bacon S, Gogolski J, Kisiday JD, Kipper MJ. Polysaccharide-based polyelectrolyte multilayer surface coatings can enhance mesenchymal stem cell response to adsorbed growth factors. Biomacromolecules 2010;11(10):2629-2639.

6. Khetani SR, Berger DR, Ballinger KR, Davidson MD, Lin C, Ware BR. Microengineered liver tissues for drug testing. Journal of laboratory automation 2015;20(3):216-250.

7. Godoy P, Hewitt NJ, Albrecht U, Andersen ME, Ansari N, Bhattacharya S, Bode JG, Bolleyn J, Borner C, Böttger J and others. Recent advances in 2D and 3D in vitro systems using primary hepatocytes, alternative hepatocyte sources and non-parenchymal liver cells and their use in investigating mechanisms of hepatotoxicity, cell signaling and ADME. Archives of toxicology 2013;87(8):1315-1530.

8. Kidambi S, Lee I, Chan C. Controlling primary hepatocyte adhesion and spreading on protein-free polyelectrolyte multilayer films. Journal of the American Chemical Society 2004;126(50):16286-16287.

9. Chen AA, Khetani SR, Lee S, Bhatia SN, Van Vliet KJ. Modulation of hepatocyte phenotype in vitro via chemomechanical tuning of polyelectrolyte multilayers. Biomaterials 2009;30(6):1113-1120.

10. Janorkar AV, Rajagopalan P, Yarmush ML, Megeed Z. The use of elastin-like polypeptide-polyelectrolyte complexes to control hepatocyte morphology and function in vitro. Biomaterials 2008;29(6):625-632.

11. Rajagopalan P, Shen CJ, Berthiaume F, Tilles AW, Toner M, Yarmush ML. Polyelectrolyte Nano-scaffolds for the Design of Layered Cellular Architectures. Tissue engineering 2006;12(6):1553-1563.

12. Almodóvar J, Place LW, Gogolski J, Erickson K, Kipper MJ. Layer-by-layer assembly of polysaccharide-based polyelectrolyte multilayers: a spectroscopic study of hydrophilicity, composition, and ion pairing. Biomacromolecules 2011;12(7):2755-2765.

13. Khetani SR, Bhatia SN. Microscale culture of human liver cells for drug development. Nature biotechnology 2008;26(1):120-126.

14. Serizawa T, Yamaguchi M, Akashi M. Alternating bioactivity of polymeric layer-by-layer assemblies: anticoagulation vs procoagulation of human blood. Biomacromolecules 2002;3(4):724-731.

15. Bowen WC, Michalopoulos AW, Orr A, Ding MQ, Stolz DB, Michalopoulos GK. Development of a chemically defined medium and discovery of new mitogenic growth factors for mouse hepatocytes: mitogenic effects of FGF1/2 and PDGF. PLoS ONE 2014;9(4):e95487.

16. Wittmer CR, Phelps JA, Saltzman WM, Van Tassel PR. Fibronectin terminated multilayer films: protein adsorption and cell attachment studies. Biomaterials 2007;28(5):851-860.

17. Kan M, Shi EG. Fibronectin, not laminin, mediates heparin-dependent heparin-binding growth factor type I binding to substrata and stimulation of endothelial cell growth. In vitro cellular & developmental biology : journal of the Tissue Culture Association 1990;26(12):1151-1156.

18. Hughes CS, Postovit LM, Lajoie GA. Matrigel: a complex protein mixture required for optimal growth of cell culture. Proteomics 2010;10(9):1886-90.

19. San Antonio JD, Lander AD, Karnovsky MJ, Slayter HS. Mapping the heparin-binding sites on type I collagen monomers and fibrils. The Journal of cell biology 1994;125(5):1179-1188.

20. Sweeney SM, Guy CA, Fields GB, San Antonio JD. Defining the domains of type I collagen involved in heparin- binding and endothelial tube formation. Proceedings of the National Academy of Sciences of the United States of America 1998;95(13):7275-7280.

21. Wang XH, Li DP, Wang WJ, Feng QL, Cui FZ, Xu YX, Song XH, van der Werf M. Crosslinked collagen/chitosan matrix for artificial livers. Biomaterials 2003;24(19):3213-3220.

22. Chia S-M, Lin P-C, Yu H. TGF-beta1 regulation in hepatocyte-NIH3T3 co-culture is important for the enhanced hepatocyte function in 3D microenvironment. Biotechnology and bioengineering 2005;89(5):565-573.

23. Lee J, Wee S, Gunaratne J, Chua RJE, Smith RAA, Ling L, Fernig DG, Swaminathan K, Nurcombe V, Cool SM. Structural determinants of heparin-transforming growth factor-β1 interactions and their effects on signaling. Glycobiology 2015;25(12):1491-1504.

24. McCaffrey TA, Falcone DJ, Vicente D, Du B, Consigli S, Borth W. Protection of transforming growth factor-beta 1 activity by heparin and fucoidan. Journal of cellular physiology 1994;159(1):51-59.

25. McCaffrey TA, Falcone DJ, Brayton CF, Agarwal LA, Welt FG, Weksler BB. Transforming growth factor-beta activity is potentiated by heparin via dissociation of the transforming growth factor-beta/alpha 2-macroglobulin inactive complex. The Journal of cell biology 1989;109(1):441-448.

26. Bhaskar U, Hickey AM, Li G, Mundra RV, Zhang F, Fu L, Cai C, Ou Z, Dordick JS, Linhardt RJ. A purification process for heparin and precursor polysaccharides using the pH responsive behavior of chitosan. Biotechnology progress 2015;31(5):1348-1359.

27. Bhatia SN, Balis UJ, Yarmush ML, Toner M. Effect of cell-cell interactions in preservation of cellular phenotype: cocultivation of hepatocytes and nonparenchymal cells. The FASEB journal : official publication of the Federation of American Societies for Experimental Biology 1999;13(14):1883-1900.

28. Guillouzo A. Liver cell models in in vitro toxicology. Environmental health perspectives 1998;106 Suppl 2:511-532.

29. Khetani SR, Szulgit G, Del Rio JA, Barlow C, Bhatia SN. Exploring interactions between rat hepatocytes and nonparenchymal cells using gene expression profiling. Hepatology (Baltimore, Md) 2004;40(3):545-554.

30. Khetani SR, Chen AA, Ranscht B, Bhatia SN. T-cadherin modulates hepatocyte functions in vitro. The FASEB journal : official publication of the Federation of American Societies for Experimental Biology 2008;22(11):3768-3775.

31. Lin C, Shi J, Moore A, Khetani SR. Prediction of Drug Clearance and Drug-Drug Interactions in Microscale Cultures of Human Hepatocytes. Drug metabolism and disposition: the biological fate of chemicals 2016;44(1):127-136.

32. Wang WW, Khetani SR, Krzyzewski S, Duignan DB, Obach RS. Assessment of a Micropatterned Hepatocyte Coculture System to Generate Major Human Excretory and Circulating Drug Metabolites. Drug metabolism and disposition: the biological fate of chemicals 2010;38(10):1900-1905.

33. Ramsden D, Tweedie DJ, Chan TS, Taub ME, Li Y. Bridging in vitro and in vivo metabolism and transport of faldaprevir in human using a novel cocultured human hepatocyte system, HepatoPac. Drug metabolism and disposition: the biological fate of chemicals 2014;42(3):394-406.

34. Khetani SR, Kanchagar C, Ukairo O, Krzyzewski S, Moore A, Shi J, Aoyama S, Aleo M, Will Y. Use of micropatterned cocultures to detect compounds that cause drug-induced liver injury in humans. Toxicological sciences : an official journal of the Society of Toxicology 2013;132(1):107-117.

35. Ploss A, Khetani SR, Jones CT, Syder AJ, Trehan K, Gaysinskaya VA, Mu K, Ritola K, Rice CM, Bhatia SN. Persistent hepatitis C virus infection in microscale primary human hepatocyte cultures. Proceedings of the National Academy of Sciences 2010;107(7):3141-3145.

36. Shlomai A, Schwartz RE, Ramanan V, Bhatta A, de Jong YP, Bhatia SN, Rice CM. Modeling host interactions with hepatitis B virus using primary and induced pluripotent stem cell-derived hepatocellular systems. Proceedings of the National Academy of Sciences 2014;111(33):12193-12198.

37. March S, Ng S, Velmurugan S, Galstian A, Shan J, Logan DJ, Carpenter AE, Thomas D, Sim BKL, Mota MM and others. A microscale human liver platform that supports the hepatic stages of Plasmodium falciparum and vivax. Cell host & microbe 2013;14(1):104-115.

38. Davidson MD, Ballinger KR, Khetani SR. Long-term exposure to abnormal glucose levels alters drug metabolism pathways and insulin sensitivity in primary human hepatocytes. Scientific reports 2016;6:28178.

39. Davidson MD, Lehrer M, Khetani SR. Hormone and Drug-Mediated Modulation of Glucose Metabolism in a Microscale Model of the Human Liver. Tissue engineering. Part C, Methods 2015;21(7):716-725.

40. Kidambi S, Yarmush RS, Novik E, Chao P, Yarmush ML, Nahmias Y. Oxygen-mediated enhancement of primary hepatocyte metabolism, functional polarization, gene expression, and drug clearance. Proceedings of the National Academy of Sciences of the United States of America 2009;106(37):15714-15719.

41. Baghy K, Iozzo RV, Kovalszky I. Decorin-TGFβ axis in hepatic fibrosis and cirrhosis. The journal of histochemistry and cytochemistry : official journal of the Histochemistry Society 2012;60(4):262-268.

Chapter 3

Liver extracellular matrix substrates for the long-term culture of primary human hepatocytes[3]

Summary

Given differences between animals and humans in liver pathways, isolated primary human hepatocytes (PHHs) are useful for various applications. However, pure PHH monolayers are difficult to maintain *in vitro* and rapidly lose their phenotype. *In vivo*, PHHs interact with stromal cells and a complex extracellular matrix (ECM) environment that can modulate their functions. Various groups have demonstrated that PHHs can be modulated *in vitro* by co-culturing with stromal cells, controlling the spatial organization of the cells, and optimizing the substrate. We have established and characterized a micropatterned co-culture (MPCC) platform on adsorbed ECM from both porcine and human decellularized livers in comparison to rat tail type I collagen. In addition, we determined whether the organ source of the ECM can modulate PHH functions *in vitro* and found that decellularized ECM from the liver upregulated some hepatic functions compared to using ECM derived from other organs. We also evaluated the effects of solubilized liver ECM on hepatic phenotype in MPCCs. We observed that although dosing with solubilized porcine liver ECM did not lead to significant functional changes, dosing with the human soluble fraction resulted in a dose-dependent increase of CYP450 enzyme activity levels. The findings from the present study suggest that human and porcine liver ECM

[3] A manuscript similar to the work described in this chapter is in preparation and will be submitted for publication shortly.

can be utilized as substrates for the long-term culture of PHHs in the MPCC format and the addition of solubilized human LBM can upregulate some hepatic functions, resulting in a stable *in vitro* hepatocyte model that can be utilized for further cell-ECM biological inquiries.

3.1 Introduction

In vitro human liver models are important for applications such as modeling diseases towards the discovery of novel therapeutics, drug toxicity screening, and regenerative medicine. However, hepatocytes are difficult to maintain *in vitro* as they rapidly dedifferentiate and lose their tissue-specific functions without the proper microenvironmental cues including soluble factors, cell-cell contact, and cell-extracellular matrix interactions[1,2]. Various techniques have been utilized to promote the maintenance of hepatic phenotype *in vitro* including cell culture substrates composed of extracellular matrix (ECM) proteins, coculture of hepatocytes with stromal cells, patterning to control the spatial organization of such cocultures, and supplementation of the cell culture medium with various soluble factors[3-6]. The ECM provides support for the cells and regulates intercellular communication via complex cues. Although individual ECM proteins are commonly used as cell substrates and have been found to modulate cell attachment and functionality, the ECM microenvironment *in vivo* is much more complex as it contains multiple factors, including type I collagen, type IV collagen, fibronectin, laminin, growth factors, and glycosaminoglycans, that all modulate cell attachment, phenotype, and functionality[7]. Ideally, *in vitro* substrates would maintain as much of the native ECM composition and microarchitecture as possible.

Decellularized liver ECM or liver biomatrix (LBM) has been shown to help maintain hepatic functions as well as aid in the differentiation and maintenance of stem cells down the

hepatic lineage *in vitro*[8-11]. Decellularization protocols utilizing enzymes and detergents allow for the retention of ECM and some growth factors which can be then used as scaffolds or substrates for *in vitro* studies[12]. The various ECM components can provide cultured cells with a microenvironment that is more physiologically relevant as compared to individual ECM proteins. However, due to sourcing issues, studies utilizing human liver-derived ECM have been limited. Even fewer studies utilize human-relevant cell sources, such as primary human hepatocytes (PHHs), as most studies use animal cells[8,13] or cell lines[14-16] on animal-derived liver ECM sources. In one such study, Sellaro et al utilized a porcine liver-derived ECM sandwich culture for human hepatocytes and found that multiple functions including albumin secretion, hepatic transporter expression levels, and ammonia metabolism were similar to those observed in hepatocytes cultured between two layers of Matrigel for up to 10 days[17]. Cocultures have also been established in ECM scaffolds. For example, Barakat et al cultured human fetal hepatocytes and stellate cells in a perfused decellularized porcine liver ECM scaffold for up to 13 days and assessed the metabolic and synthetic activities[18]. The authors found that cells differentiated into mature hepatocytes. However, neither of these groups evaluated how PHHs function on human-derived liver ECM.

We hypothesized that decellularized liver ECM may contain factors that can help sustain hepatic functions. Therefore, we assessed the functionality of PHHs, specifically cell morphology, albumin secretion, urea synthesis, and CYP450 enzyme activity levels, on adsorbed human- and porcine-derived LBM and compared them to rat tail type I collagen, the current standard for hepatocyte culture. PHHs were micropatterned and cultured either alone or in a coculture with 3T3-J2 fibroblasts on the liver ECM substrates and hepatic functions were assessed for ~3 weeks. Additionally, to evaluate if the ECM organ source could modulate hepatic

functionality, functionally-stable micropatterned cocultures (MPCCs) were established on porcine ECM from the small intestine and urinary bladder and compared to liver ECM[19]. Finally, both human and porcine-derived liver ECM were separated into insoluble and soluble fractions through centrifugation. The solubilized liver ECM was utilized as a media supplement at various concentrations to evaluate if hepatic functionality could be upregulated.

3.2 Materials and Methods

3.2.1 Liver tissue decellularization and enzymatic digestion

Liver ECM was isolated from human and porcine livers as described previously[17]. Livers were harvested from market weight pigs (110-130 kg). Non-diseased human liver tissue was obtained with Institutional Review Board approval. The tissues were rinsed with water and frozen at -80˚C until processing. Liver tissue from both species was subjected to the same decellularization protocol. The tissues were cut into cubes of approximately 0.5 cm^3 and rinsed with deionized water under mechanical agitation on an orbital shaker at 300 rpm. The sections were then mechanically massaged to aid in cell lysis and soaked in 0.02% trypsin/0.05% EGTA at 37˚C for 2 hours. The tissue was rinsed with water and massaging was repeated followed by mechanical agitation of the liver sections in 3% Triton X-100 for 18-24 hours to induce cell lysis. The sections were rinsed with phosphate buffered saline (PBS) and water until all visible remnants of cellular material were removed. Finally, the sections were disinfected with 0.1% peracetic acid/4% ethanol, followed by repeated rinses in water/PBS at pH 7.4. The resulting decellularized liver ECM was lyophilized overnight, cut into small pieces, and placed in a rotary knife mill to create particulates. The particulates were digested with 1 mg/mL porcine pepsin (Sigma-Aldrich, St. Louis, MO) in 0.01 N HCl and stirred for 72 h at room temperature to form a

10 mg/mL liver ECM digest. The digested ECM was then diluted to 50 µg/mL for adsorption to tissue culture polystyrene (TCPS) plates.

To obtain the soluble fraction, 10 volumes of the digested liver ECM was neutralized with 1.1 volume of 10XPBS, 0.4 volumes of 1XPBS, and 1 volume of 0.1 N NaOH. Neutralized liver ECM was allowed to gelate at 37°C for 45 minutes. The gel was centrifuged at 20000xg for 30 minutes to pellet the insoluble components. The liquid supernatant ("soluble fraction") was collected and brought up to the starting volume with 1XPBS.

3.2.2 Porcine small intestinal submucosa and urinary bladder matrix preparation

The harvest of small intestinal submucosa (SIS) and urinary bladder matrix (UBM) from porcine sources has been described previously[20-25]. Briefly, to prepare SIS, small intestine was obtained from adult market weight (110-130 kg) pigs and the majority of the mucosa and the entire serosa and muscularis externa layers were mechanically delaminated from the intestine. The remaining submucosa, muscularis mucosa, and stratum compactum layers were then washed with water and treated with 0.1% peracetic acid/4% ethanol for 1 hour. The resulting SIS was lyophilized, powdered, and digested with pepsin.

To prepare UBM, urinary bladders were harvested from market weight pigs and the urothelial, serosal, muscular, and submucosal layers were removed by mechanical delamination. The remaining basement membrane and tunica propria was rinsed with deionized water and then treated with 0.1% peracetic acid/4% ethanol on an orbital shaker for 2 hours. The UBM was then rinsed with PBS for 15 minutes twice followed by two 15-minute rinses in deionized water. The resulting UBM was lyophilized, powdered, and digested with pepsin.

3.2.3 Primary human hepatocyte culture

Cryopreserved PHHs were purchased from a vendor permitted to sell products derived from human organs procured in the United States by federally designated Organ Procurement Organizations (Triangle Research Laboratories, Research Triangle Park, NC). PHHs were processed as previously described[26]. Briefly, the cells were thawed at 37°C for 2 minutes and transferred into pre-warmed hepatocyte cell seeding medium, the formulation of which has been described previously[26]. The cells were then spun at 50x*g* for 10 minutes, the supernatant was discarded, and the cells were resuspended in hepatocyte seeding medium prior to assessment of viability using trypan blue exclusion (typically 80-95%). Liver-derived non-parenchymal cells were consistently found to be less than 1% of all the cells.

Micropatterned hepatocytes were established as previously described[27]. Briefly, rat-tail type 1 collagen, human LBM, porcine LBM, porcine SIS, or porcine UBM, were diluted to 50 μg/mL and adsorbed to 24-well TCPS plates for 2 hours at 37°C. After rinsing the plates twice with double-distilled water (ddH_2O), the plates were lithographically patterned using a polydimethylsiloxane mask to create 500-μm diameter circular domains with a center-to-center spacing of 1200-μm. PHHs that were processed as described above selectively attached to the adsorbed ECM domains leaving ~30,000 attached hepatocytes within each well of the TCPS plate. To create MPCCs, 3T3-J2 murine embryonic fibroblasts were seeded 18 to 24 hours later at ~90,000 cells per well. Serum-supplemented culture medium, the formulation of which has been described previously, was replaced on the cultures every 2 days[28].

3.2.4 Biochemical assays

Cell adhesion was assessed via double-stranded DNA (dsDNA) content in adherent cells 1 day after seeding PHHs. DNA was quantified using the Quant-iT PicoGreen dsDNA assay kit (Molecular Probes, Eugene, OR). Albumin levels in cell supernatants were measured using an enzyme-linked immunosorbent assay (MP Biomedicals, Irvine, CA) with horseradish peroxidase detection and 3,3',5,5'-tetramethylbenzidine (TMB, Fitzgerald Industries, Concord, MA) as the substrate. Urea concentration in supernatants was assessed using a colorimetric endpoint assay utilizing diacetyl monoxime with acid and heat (Stanbio Labs, Boerne, TX). Albumin and urea secretion levels were assessed every other day, whereas CYP450 activity levels were assessed approximately once a week. CYP3A4 activity in cultures was measured using a luminescence-based assay by Promega (Madison, WI). Following incubation for 1 hour at 37°C with the CYP3A4-glo substrate, luciferin-IPA, in serum-free dosing culture medium, the luminescence of the produced metabolite (luciferin) was detected according to the manufacturer's protocols. CYP2C9 was measured similarly using a luminescence-based assay by Promega via a 3-hour incubation with the CYP2C9-glo substrate, luciferin-H. CYP2A6 enzyme activity was measured by incubating the cultures with coumarin for 1 hour at 37°C and measuring the fluorescent metabolite 7-hydroxy-coumarin (Sigma-Aldrich, St Louis, MO). CYP1A2 activity was measured by incubating the cultures with ethoxyresorufin for 3 hours and then measuring the fluorescent signal of the metabolite resorufin. Absorbance, luminescence, and fluorescence for the aforementioned assays were measured using a spectrophotometer (BioTek, Winooski, VT).

3.2.5 Statistical Analysis

Each experiment was carried out twice with 2+ wells per condition. Data from one PHH donor is shown in the main figures, while an additional PHH donor was used to verify the observed trends as shown in the supplemental figures. Microsoft Excel and GraphPad Prism 7.0 (La Jolla, CA) were used for data analysis and graphing. Error bars on graphs represent standard deviations. Statistical significance was determined using one-way or two-way ANOVA with *post-hoc* Tukey or Dunnett tests ($p \leq 0.05$).

3.3 Results

3.3.1 Patterning of PHHs on collagen, human LBM, and porcine LBM substrates

In this study, we evaluated whether PHHs could be patterned on human and porcine LBM substrates. LBM and a rat tail collagen control were adsorbed to TCPS and patterned using soft lithography as shown in **Figure 3.1A**. We observed that 1 day after the PHHs were seeded, there were no significant differences in cell morphology or attachment density as assessed via phase contrast imaging (**Figure 3.1B**) and double-stranded DNA quantification (**Figure 3.1C**). Compared to PHHs on collagen, albumin secretion (**Figure 3.1D**) for PHHs on porcine LBM was significantly higher on days 3, 5, 7, and 9 while PHHs on human LBM were significantly higher on days 3, 5, and 7. Urea synthesis (**Figure 3.1E**) was significantly higher in PHHs on LBM from days 3 to 13 and on human LBM on days 7 and 13 as compared to the collagen control. For CYP3A4 enzyme activity (**Figure 3.1F**), human LBM was significantly higher than the collagen control on day 21 while porcine LBM was similar to the collagen control levels. Therefore, although functions were significantly upregulated in cells that were cultured on human or porcine LBM, the effects were transient and hepatic functionality on all three

substrates still declined precipitously over 2 weeks. Similar to the rat tail collagen, neither human LBM nor porcine LBM could stabilize functions in micropatterned PHH cultures.

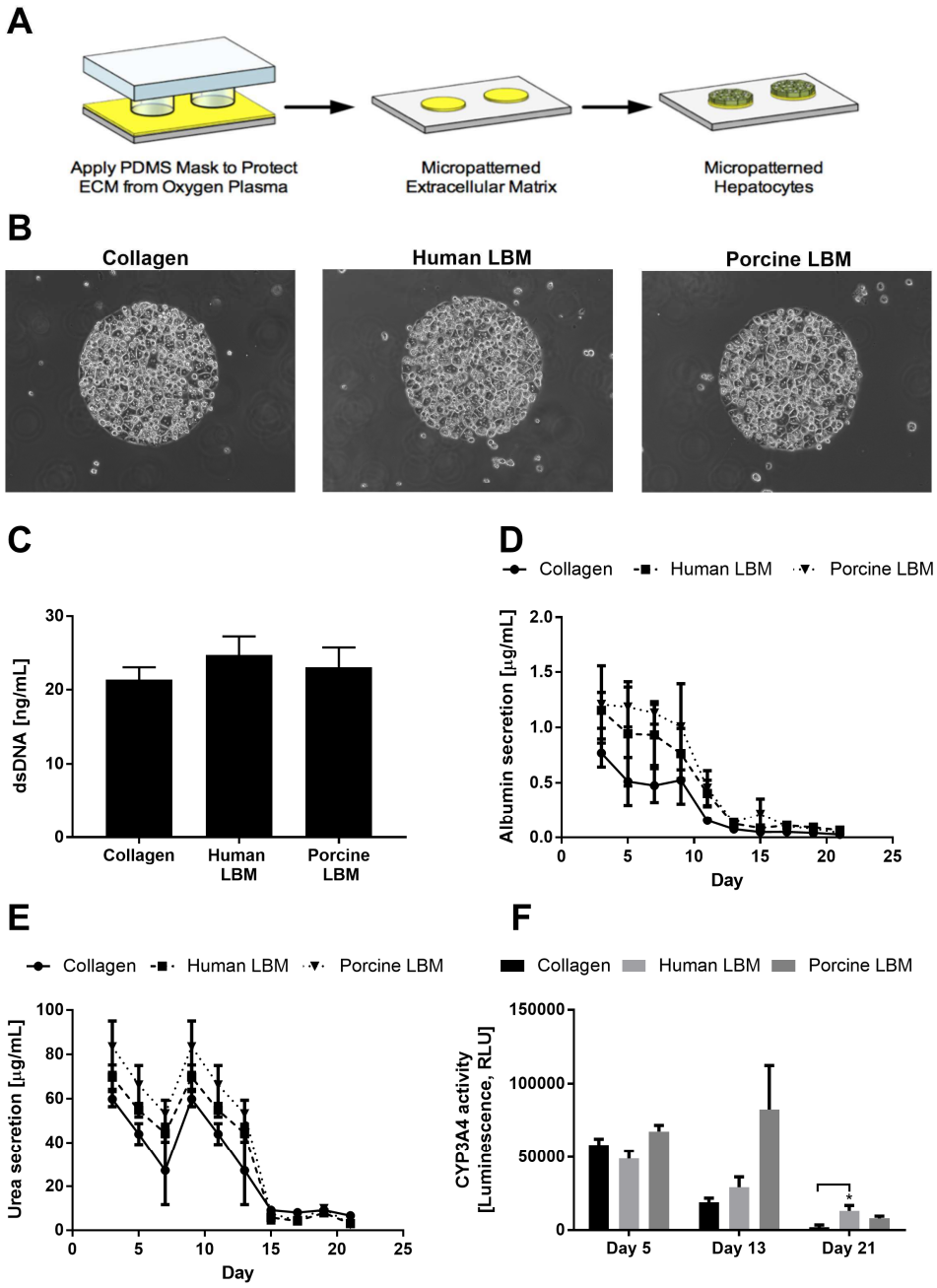

Figure 3.1 Primary human hepatocytes (PHHs) can be patterned on human and porcine liver biomatrix (LBM) substrates. (A) Process steps for patterning extracellular matrix (ECM) substrates for hepatocyte seeding. **(B)** Phase contrast images of micropatterned hepatocytes adhered to the indicated ECM substrate on day 1 of culture. **(C)** Double-stranded DNA (dsDNA) quantified 24 hours post hepatocyte seeding. **(D)** Albumin secretion levels of micropatterned hepatocytes over time. **(E)** Urea secretion levels from the same cultures as those used in panel D. **(F)** CYP3A4 activity levels from the same cultures used in panel D. *P≤0.05 (One-way ANOVA with post-hoc Tukey test). Error bars represent standard deviation.

It has previously been demonstrated that coculture of PHHs with 3T3-J2 fibroblasts can prolong hepatic functions[19]. Thus, MPCCs were established as shown in **Figure 3.2A**. Phase contrast images demonstrate that there were no morphological differences over the course of ~3 weeks between hepatocytes cultured on rat tail collagen type I, human LBM, or porcine LBM (**Figure 3.2B**). MPCCs established on both human and porcine LBM displayed similar albumin and urea secretion levels as compared to MPCCs established on adsorbed rat tail collagen I (**Figure 3.3A**). In comparison to micropatterned cultures of pure hepatocytes, both albumin and urea secretion levels were higher and more stable in MPCCs. Specifically, albumin secretion levels in pure hepatocyte cultures start at ~1 μg/mL and decline while the levels in MPCCs start at ~5 μg/mL and plateau around 10-15 μg/mL by day 10 of culture. While urea secretion levels are similar for pure hepatocyte cultures and MPCCs initially, levels decline in pure cultures whereas MPCC levels remain around 60-90 μg/mL for 3 weeks. CYP1A2, 2A6, 2C9, and 3A4 enzyme activity levels were also stable for at least 3 weeks regardless of which substrate was utilized (**Figure 3.3B**) as compared to the decline in CYP3A4 activity observed with micropatterned cultures of pure hepatocytes. For certain CYP450 enzymes, MPCCs demonstrated higher activity on porcine LBM as compared to on collagen (CYP1A2 on day 7, CYP2A6 on day 21, and CYP3A4 on days 7 and 15). MPCCs created using another PHH donor lot demonstrated similar trends (**Supplemental Figure 3.5.1**). Therefore, PHHs can be patterned on both human and porcine-derived LBM substrates and their functional levels are enhanced/stabilized upon co-cultivation with 3T3-J2 fibroblasts.

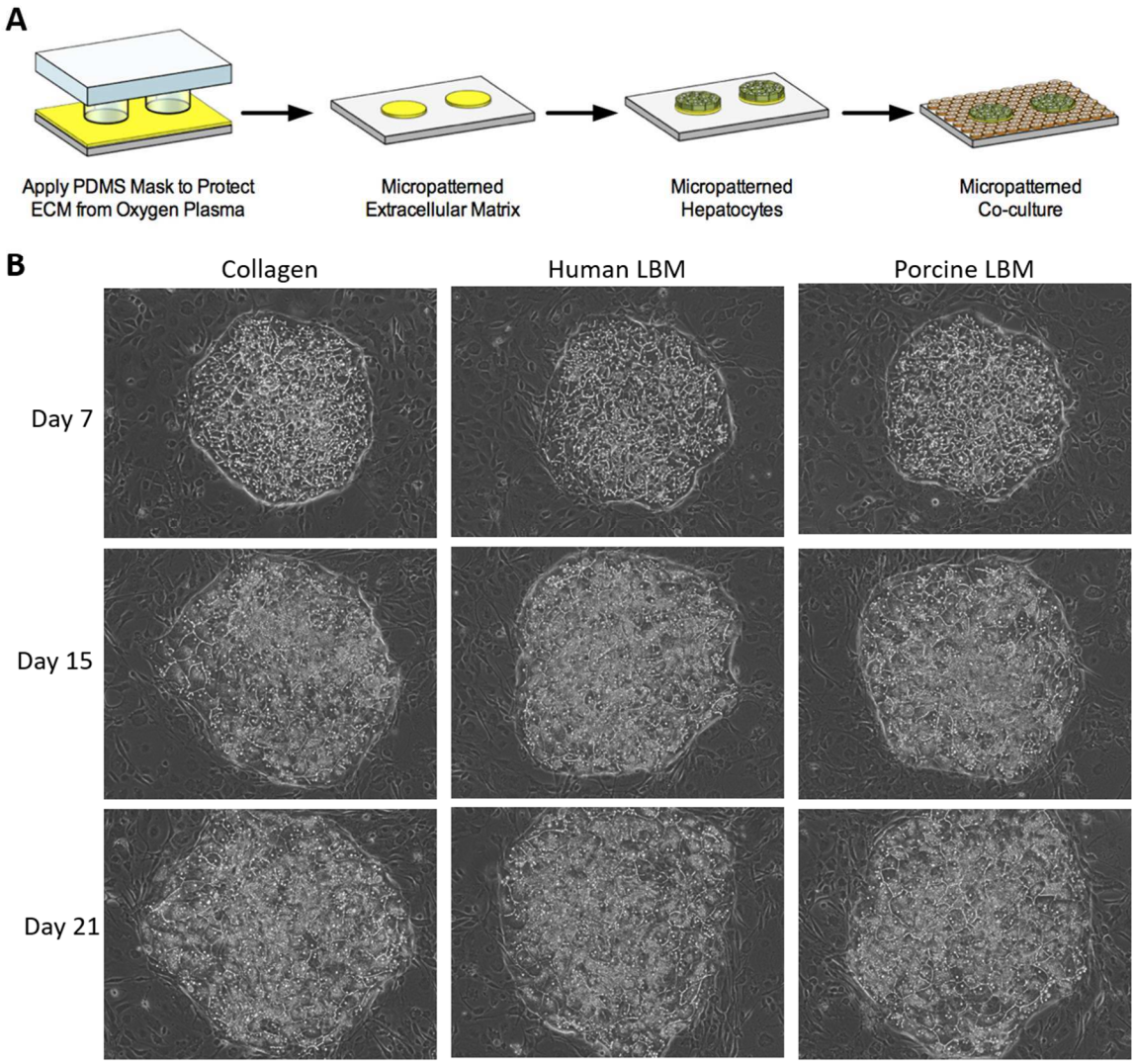

Figure 3.2 Creation of micropatterned cocultures (MPCCs) on liver biomatrix (LBM). (A) Process steps for patterning extracellular matrix (ECM) substrates for hepatocyte seeding. 3T3-J2 fibroblasts are seeded ~24 hours after hepatocyte seeding to create cocultures. **(B)** Phase contrast images of MPCCs adhered to the indicated ECM substrate at the indicated day of culture.

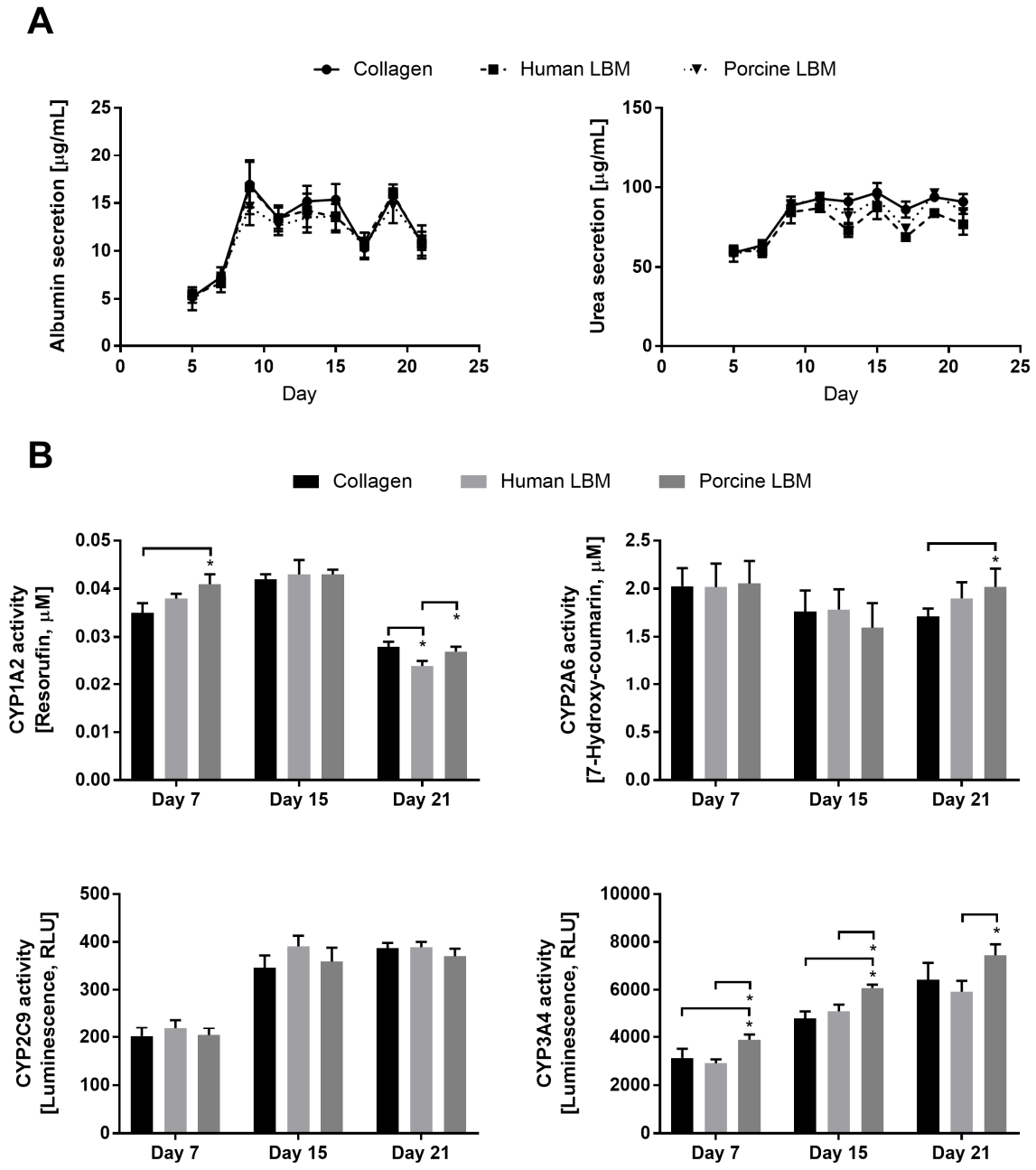

Figure 3.3 Comparison of MPCC functions on adsorbed collagen, human liver biomatrix (LBM), and porcine LBM substrates. (A) Albumin (left) and urea (right) secretion levels over 3 weeks. **(B)** CYP1A2 (top left), CYP2A6 (top right), CYP2C9 (bottom left), and CYP3A4 (bottom right) enzyme activity levels were assessed in the same cultures used in panel A. *P≤0.05 (One-way ANOVA with post-hoc Tukey test). Error bars represent standard deviation.

3.3.2 Effects of ECM from various organ sources on hepatic functionality

MPCCs were established on adsorbed porcine ECM from the small intestine, urinary bladder, and liver. Double-stranded DNA quantification 1 day after PHH seeding demonstrated that there were no significant differences in cell attachment density across the 3 substrates (**Figure 3.4A**). We observed that MPCCs established on LBM or UBM secreted similar levels of albumin, whereas MPCCs on SIS showed significantly lower levels than both LBM and UBM on days 7, 11, 13, 15, 17, 19, and 21 and just LBM on days 5 and 9 (**Figure 3.4B**). Urea synthesis was significantly different among the three substrates except on days 13 and 17. CYP1A2 activity declined over the course of 3 weeks regardless of which substrate was utilized with no significant differences across the three substrates (**Figure 3.4C left**). For both CYP2A6 (**Figure 3.4C middle**) and CYP3A4 (**Figure 3.4C right**), enzyme activity levels for both LBM and UBM were significantly higher than SIS on day 7, but on day 21, SIS was significantly better than UBM. Therefore, although PHHs generally displayed upregulated functions on LBM and UBM as compared to SIS, these effects were transient and not always significant.

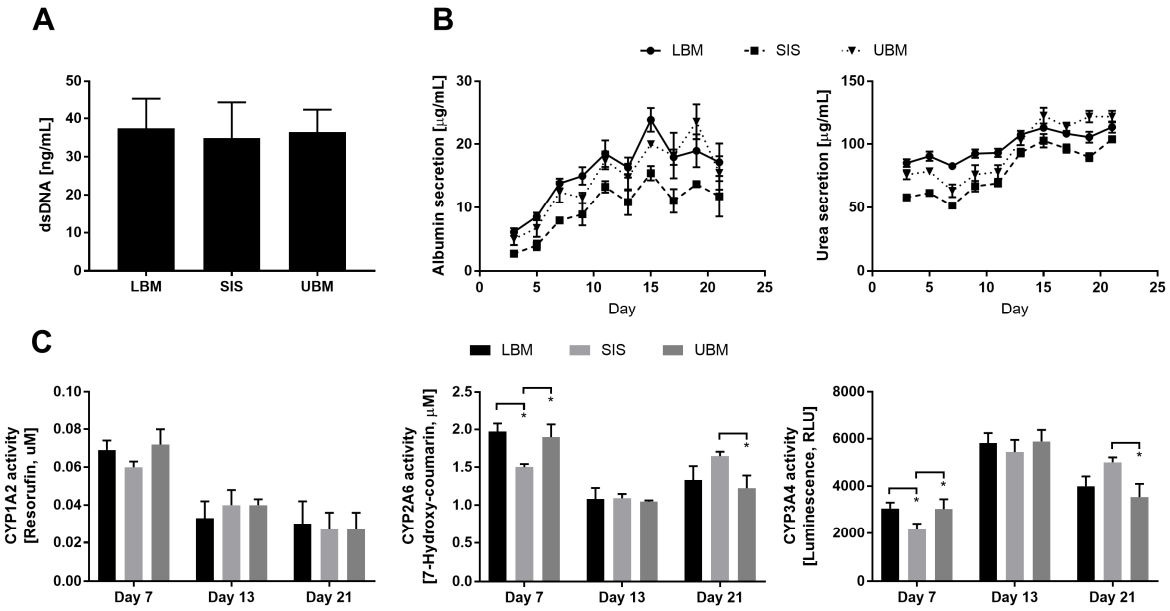

Figure 3.4 Comparison of MPCC functions on porcine-derived liver biomatrix (LBM), small intestinal submucosa (SIS), and urinary bladder matrix (UBM). **(A)** Double-stranded DNA (dsDNA) quantified 24 hours post hepatocyte seeding. **(B)** Albumin (left) and urea (right) secretion levels over 3 weeks. **(C)** CYP1A2 (left), CYP2A6 (middle), and CYP3A4 (right) activity levels were assessed in the same cultures used in panel A. *P≤0.05 (One-way ANOVA with post-hoc Tukey test). Error bars represent standard deviation.

3.3.3 Effects of solubilized LBM on MPCCs

To assess if upregulation of hepatic functions would be observed when MPCCs created using PHHs were dosed with solubilized human or porcine LBM, the LBM was separated into structural and soluble components via differential centrifugation. MPCCs were first established on 50 µg/mL of adsorbed human LBM and then dosed with 0, 25, 50, or 100 µg/mL of solubilized human LBM every other day via media changes starting on day 3 of culture. We observed that doses of soluble human LBM did not significantly affect either albumin or urea secretion levels (**Figure 3.5A**). In contrast, increasing doses of soluble human LBM resulted in higher CYP450 enzyme activity levels (**Figure 3.5B**). Similar trends were observed with another

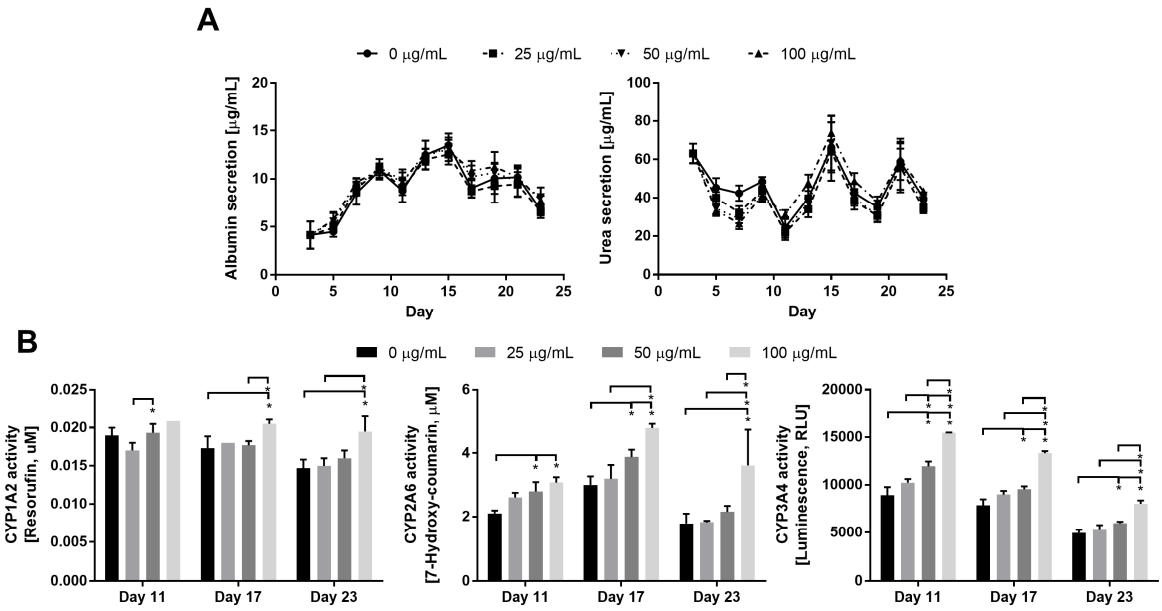

Figure 3.5 Modulation of MPCC functions by the presentation of solubilized human liver LBM via culture medium changes. MPCCs were established on 50 μg/mL of adsorbed human LBM. The cultures were dosed with 0, 25, 50, or 100 μg/mL of solubilized human LBM every other day with media changes starting on day 3. **(A)** Albumin (left) and urea (right) secretion levels over the course of ~3 weeks. **(B)** CYP1A2 (left), CYP2A6 (middle), and CYP3A4 (right) enzyme activity levels were assessed in the same cultures used in panel A. *P≤0.05 (One-way ANOVA with post-hoc Tukey test). Error bars represent standard deviation.

PHH donor, albeit statistical significance was not always reached at all time-points (**Supplemental Figure 3.5.2**).

MPCCs were also established on 50 μg/mL of adsorbed porcine LBM and dosed with 0, 20, or 40 μg/mL of solubilized porcine LBM every other day via media changes starting on day 3 of culture. Initially, MPCCs created using another PHH donor established on 50 μg/mL of adsorbed porcine LBM were dosed with 0, 25, and 50 μg/mL of solubilized porcine LBM, but a hydrogel overlay was observed in the condition dosed with 50 μg/mL, causing a significant downregulation of CYP450 activity levels (**Supplemental Figure 3.5.3**). Interestingly, albumin and urea secretion levels were not affected by the hydrogel overlay. Thus, the solubilized porcine LBM doses were decreased to 20 and 40 μg/mL. The solubilized porcine LBM did not affect

albumin and urea secretion levels significantly (**Figure 3.6A**), but unlike the solubilized human conditions, CYP450 activity levels were not upregulated with increasing concentrations of solubilized porcine LBM, except for CYP2A6 on day 7 of culture (**Figure 3.6B**).

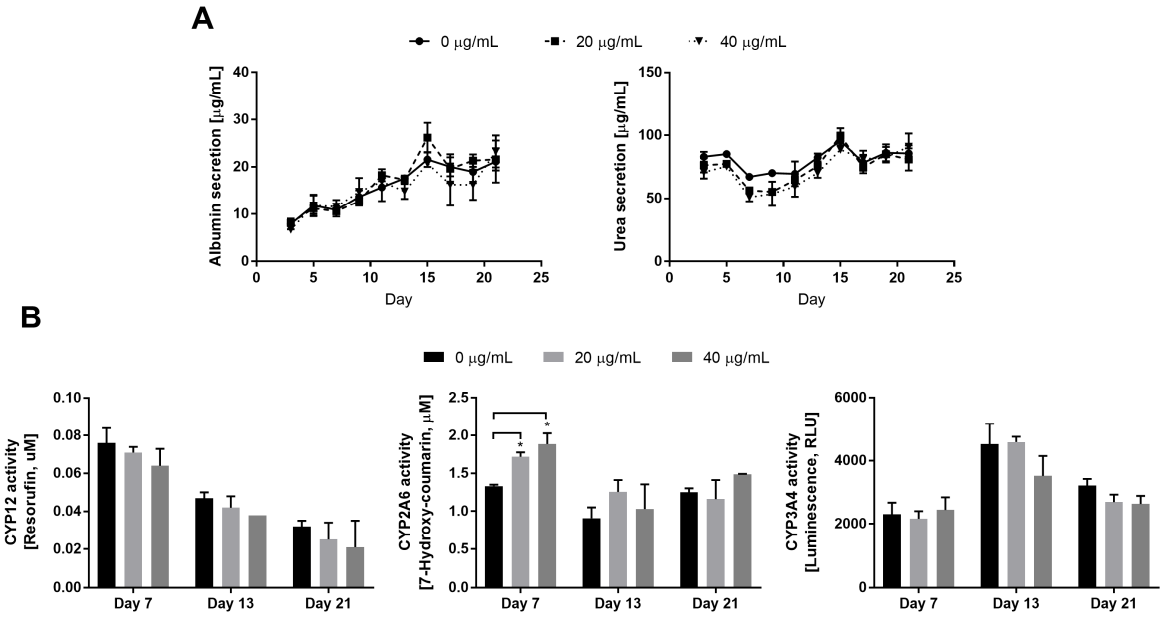

Figure 3.6 Modulation of MPCC functions by the presentation of solubilized porcine liver LBM via culture medium changes. MPCCs were established on 50 μg/mL of adsorbed porcine LBM. The cultures were dosed with 0, 20, or 40 μg/mL of solubilized porcine LBM every other day with media changes starting on day 3. **(A)** Albumin (left) and urea (right) secretion levels over the course of 3 weeks. **(B)** CYP1A2 (left), CYP2A6 (middle), and CYP3A4 (right) activity levels were assessed in the same cultures used in panel A. *P≤0.05 (One-way ANOVA with *post-hoc* Tukey test). Error bars represent standard deviation.

3.4 Discussion

In vitro liver models established using isolated PHHs are useful for many applications including drug screening, modeling human liver diseases, and creating cell-based therapies in the clinic. However, pure PHH monolayers are difficult to maintain in culture formats that rely exclusively on ECM derived from non-liver sources (i.e. rat tail collagen I), either adsorbed or in sandwich culture configurations where an ECM overlay is utilized[1,19]. Engineering techniques

such as micropatterning allow for control over the spatial organization of hepatocytes, which has been demonstrated to help maintain cell-cell interactions[29,30]. In this study, we evaluated the use of ECM derived from various organs and species as substrates for micropatterned hepatocytes either cultured alone or in a coculture with 3T3-J2 fibroblasts. The liver tissue utilized in this study was processed in such a way to preserve ECM proteins typically found in the liver[31,32]. Compared to rat tail collagen, these substrates consist of a variety of ECM proteins, including collagens, laminins, and fibronectins, as well as immobilized growth factors, which may be beneficial for *in vitro* hepatocyte culture[33]. For example, Lee et al have shown that human adipose-derived stem cells display upregulated hepatic gene expression when cultured on a rat liver ECM substrate as compared to collagen[13]. Additionally, the viability and functionality of primary rat hepatocytes were improved in a liver ECM hydrogel compared to a collagen hydrogel. We demonstrated that micropatterned PHHs cultured on adsorbed LBM show similar cell attachment densities as compared to collagen. Zeisberg et al previously found that PHHs adhered better to liver-derived basement membrane matrix compared to Matrigel or type I collagen, but gels were used rather than adsorbed proteins[34]. The authors also found that markers of hepatocyte dedifferentiation (vimentin and cytokeratin-18) were expressed at lower levels in PHHs on the liver ECM as compared to Matrigel and collagen, but liver-specific functions were not assessed. We found that although micropatterned pure hepatocytes on LBM display similar functional levels as compared to rat tail collagen, functions still decline.

In contrast to pure hepatocyte cultures, cocultures of hepatocytes with stromal cells have been shown to induce and stabilize primary hepatocyte functions[35]. Specifically, Khetani and Bhatia have demonstrated that 3T3-J2 fibroblasts secrete molecules that support hepatocytes *in vitro*[36,37] and that cocultures of PHHs and 3T3-J2 fibroblasts can be used for drug development

and disease modeling applications[1,38]. Thus, we established MPCCs on adsorbed ECM from porcine and human decellularized livers and found that both adsorbed human- and porcine-derived LBM supported hepatocyte adhesion and liver-specific functions similarly to rat tail collagen. Although Lin et al previously showed that primary rat hepatocytes secreted higher levels of albumin and urea on porcine liver-derived ECM as compared to adsorbed rat tail collagen, LBM membranes were utilized [8]. LBM membranes or scaffolds may retain some ultrastructure features of the ECM that upregulate hepatic functions better than adsorbed LBM solutions[15]; however, the latter approach is more amenable to creating higher-throughput culture platforms for drug screening. One such study that utilized a decellularized rat liver ECM scaffold and HepG2 cells as a hepatocellular carcinoma model showed that the cells cultured in the scaffold were less susceptible to lower concentrations of methotrexate as compared to 2D cultures and thus, cells in the ECM scaffold seem to respond to the drug in a more *in vivo*-relevant manner[16]. However, when drug studies are performed in more complex 3D models, there may be issues with penetration of the drugs, metabolites, and cytotoxicity markers through the scaffold that must be addressed prior to high-throughput drug screening[39]. Liver ECM scaffolds have also been used for coculture of HepG2, Sk-Hep-1, and LX-2 cells for transplantation applications[14]. However, there is a limited source of human liver ECM and Mattei et al found donor-to-donor variation when processing the scaffolds[40]. Variation in scaffolds may also arise when ECM from various locations in the liver are utilized. Thus, by digesting the decellularized liver ECM as we did prior to adsorption or gelation, a more homogenized sample is achieved. In addition to 3D scaffolds of decellularized matrix, recent studies have also shown that decellularized liver ECM can be used as a bioink for the precise deposition of ECM and spatial organization of multiple types of cells. For example, Lee et al

have shown that HepG2 albumin and urea secretion levels were upregulated in porcine liver bioink as compared to the porcine collagen bioink control[41]. By bioprinting combinations of cells and ECM in this manner, cocultures of multiple cell types encapsulated in various ECM can be achieved which is in contrast to our study where only the hepatocyte domains are in contact with the adsorbed ECM. In addition, the porcine liver bioink aided in the differentiation of human bone marrow-derived mesenchymal stem cells down the hepatic lineage. Other studies utilizing decellularized scaffolds have also demonstrated the differentiation and maintenance of stem cells down the hepatic lineage[10,11,42].

In this study, we also determined whether the organ source of the ECM modulated PHH functions *in vitro*. Since ECM composition varies depending on anatomic location with the ECM components reflecting the structural and functional requirements of the specific organ, it is conceivable that cells would perform optimally on the respective tissue-specific ECM[32]. Zhang et al found that ECM coatings from specific tissues were able to promote tissue-matched cellular proliferation and phenotype compared to tissue-mismatched cells[43]. Specifically, while there were no significant differences in cell attachment across adsorbed collagen, skin, muscle, or liver ECM, cells derived from specific organs proliferated and strongly expressed their specific cell markers on the tissue-matched ECM substrate. Additionally, it has been demonstrated that macrophages cultured on ECM derived from different organs display differential phenotypic responses[20,44]. In this study, we compared ECM from the liver to ECM from the small intestine and urinary bladder since acellular scaffolds derived from these organs are easy to obtain and thus, commonly used in regenerative medicine applications to induce tissue regeneration and remodeling[8,12]. Furthermore, it has previously been shown that liver sinusoidal endothelial cells maintain their differentiated phenotype the longest when cultured on liver ECM compared to SIS

or UBM[45]. We found that MPCCs established on LBM and UBM generally upregulated hepatic functions as compared to SIS. However, functions were stable on all 3 substrates suggesting that liver-specific components were not required to maintain hepatic functionality and thus, ECM from various organs can be utilized for *in vitro* tissue engineering applications. This is in agreement with other studies that have shown that although there were some differences in primary rat hepatocyte phenotype in decellularized liver and spleen ECM scaffolds, ECM from both organ sources were able to maintain cellular functionality and allow for the differentiation of bone marrow mesenchymal stem cells down the hepatic lineage, suggesting that ECM from multiple organs that have similar protein compositions can be utilized[46-48].

Finally, we tested the effects of solubilized liver ECM on hepatocyte phenotype over several weeks. The use of solubilized ECM as a media supplement can be utilized in both 2D and 3D *in vitro* liver systems. Fujita et al have demonstrated that the addition of proteoglycans and glycosaminoglycans to cell culture media induced the formation of gap junctions in primary rat hepatocytes, leading to improved cell-cell interactions[49]. We found that human hepatocytes supplemented with solubilized human, but not porcine liver ECM, displayed higher CYP450 activity levels. This suggests that homologous human solubilized ECM as a medium supplement is superior to xenogeneic heterologous porcine solubilized ECM for the culture of human hepatocytes. In contrast, Loneker et al found that cell culture medium supplementation of canine and porcine liver ECM supported primary rat hepatocytes *in vitro* better than rat or human ECM[50]. Interestingly, while there were few significant differences in hepatic functions between using adsorbed porcine and human LBM, presentation of solubilized human LBM, but not porcine LBM, resulted in a dose-dependent increase in CYP450 levels. The differences in CYP450 modulation between the adsorbed versus soluble human LBM presentation could be

attributed to the repeated doses of solubilized LBM replenishing growth factors in media over time versus the one-time adsorbed LBM delivery mode. We also found that using too high of a concentration of solubilized porcine LBM resulted in an LBM overlay over the course of a couple of days. Although Lin et al have suggested that an overlay may further increase liver-specific functions, we observed that while the overlay did not affect albumin or urea secretion levels, it caused a downregulation of CYP450 activity levels[8]. Lee-Montiel et al utilized a porcine LBM overlay in the Liver Acinus MicroPhysiology System (LAMPS) to mimic the space of Disse while also including a lower concentration of porcine LBM in their perfused media to help regulate hepatic functions[51]. However, complex platforms such as LAMPS, where multiple cell types are seeded into a microfluidic device, are more amenable to low-throughput studies where numerous biomarker readouts are required. While is not clear how the solubilized components of the liver ECM are interacting with the hepatocytes or adsorbed ECM, Nakamura et al have shown that it is also possible to immobilize specific growth factors to liver ECM films to modulate primary rat hepatocyte functionality *in vitro*[52].

Our findings suggest that LBM can serve as an alternative substrate to currently available substrates and can support the liver-specific functions of micropatterned cocultures of PHHs for tissue engineering applications. In the future, a comprehensive analysis of the components of LBM can be performed in order to assess how cell-ECM interactions via integrin signaling pathways may be modulating the cells. LBM from diseased patients can also be utilized as substrates to study the impact of diseases such as liver fibrosis and cirrhosis on the liver ECM and how the stiffness of the liver ECM can affect hepatocytes *in vitro*. In conclusion, we have successfully micropatterned PHHs on human- and porcine-derived ECM substrates. Although the LBM substrates were not sufficient to stabilize PHH phenotype in pure cultures, cocultures

displayed stable functions for at least 3 weeks. MPCCs could also be established on ECM derived from the urinary bladder and small intestine, although some hepatic functions were lower on SIS. Finally, the use of solubilized human ECM, but not porcine ECM, as a media supplement, upregulated CYP450 enzyme activity levels in a dose-dependent manner.

3.5 Supplemental Figures

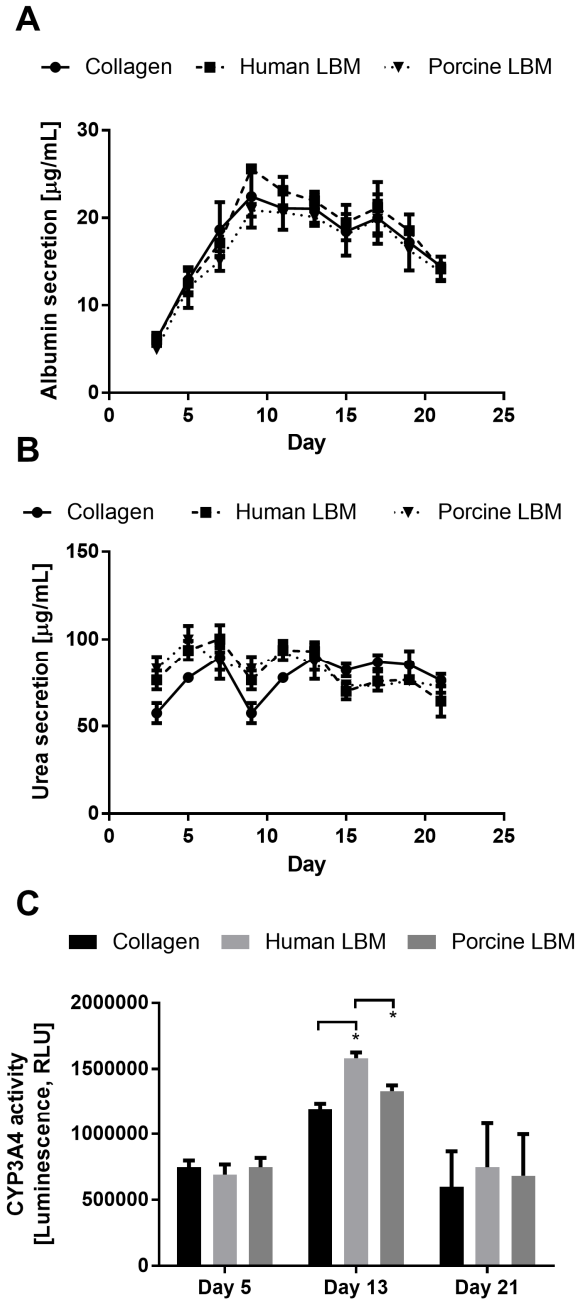

Figure 3.5.1 Comparison of MPCC functions on adsorbed collagen, human liver biomatrix (LBM), and porcine LBM substrates. Cultures were created using different a different primary human hepatocyte donor than the one featured in Figure 3.3.3. (A) Albumin and **(B)** urea secretion levels over 3 weeks. **(C)** CYP3A4 enzyme activity was assessed in the same cultures used in panels A and B. *P≤0.05 (One-way ANOVA with post-hoc Tukey test). Error bars represent standard deviation.

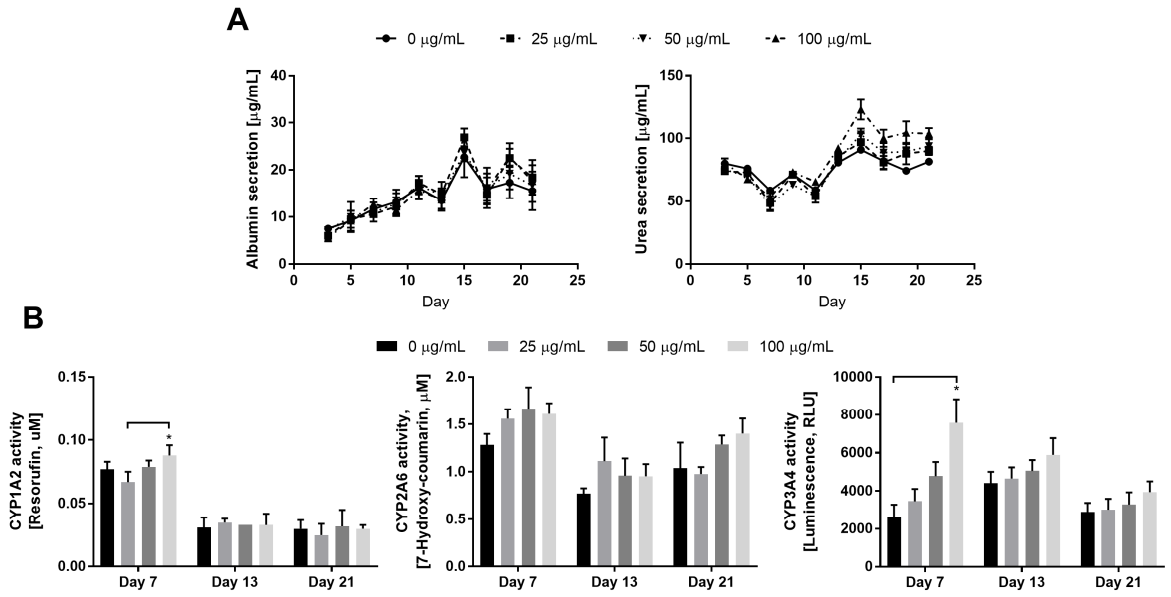

Figure 3.5.2 Modulation of MPCC functions by the presentation of solubilized human liver LBM via culture medium changes. Cultures were created using different a different primary human hepatocyte donor than the one featured in Figure 3.3.5. MPCCs were established on 50 μg/mL of adsorbed human LBM. The cultures were dosed with 0, 25, 50, or 100 μg/mL of solubilized human LBM every other day with media changes starting on day 3. **(A)** Albumin (left) and urea (right) secretion levels over the course of 3 weeks. **(B)** CYP1A2 (left), CYP2A6 (middle), and CYP3A4 (right) enzyme activity levels were assessed in the same cultures used in panel A. *P≤0.05 (One-way ANOVA with post-hoc Tukey test). Error bars represent standard deviation.

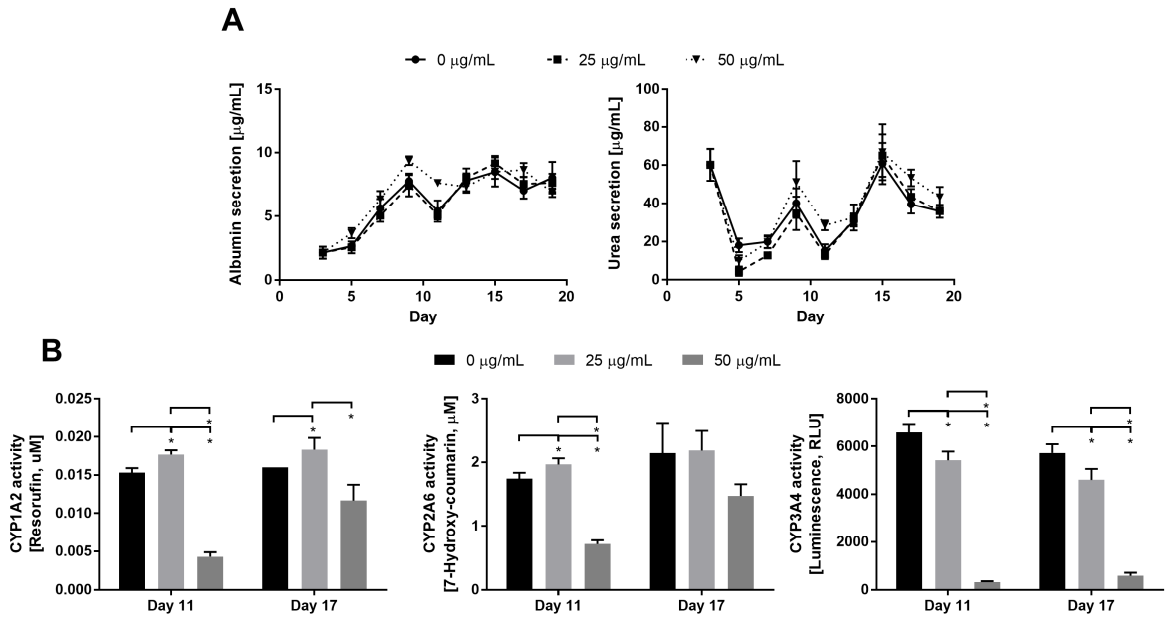

Figure 3.5.3 Modulation of MPCC functions by the presentation of solubilized porcine liver LBM via culture medium changes. Cultures were created using different a different primary human hepatocyte donor than the one featured in Figure 3.3.6. MPCCs were established on 50 μg/mL of adsorbed porcine LBM. The cultures were dosed with 0, 25, or 50 μg/mL of the porcine soluble fraction every other day with media changes starting on day 3. A thin hydrogel overlay was observed for the cultures that had been dosed with 50 μg/mL of porcine soluble fraction. **(A)** Albumin (left) and urea (right) secretion levels over the course of ~3 weeks. **(B)** CYP1A2 (left), CYP2A6 (middle), and CYP3A4 (right) activity levels were assessed in the same cultures used in panel A. *P≤0.05 (One-way ANOVA with *post-hoc* Tukey test). Error bars represent standard deviation.

References

1. Khetani SR, Berger DR, Ballinger KR, Davidson MD, Lin C, Ware BR. Microengineered liver tissues for drug testing. Journal of laboratory automation 2015;20(3):216-250.

2. Ben-Ze'ev A, Robinson GS, Bucher NL, Farmer SR. Cell-cell and cell-matrix interactions differentially regulate the expression of hepatic and cytoskeletal genes in primary cultures of rat hepatocytes. Proc Natl Acad Sci U S A 1988;85(7):2161-5.

3. Bhandari RN, Riccalton LA, Lewis AL, Fry JR, Hammond AH, Tendler SJ, Shakesheff KM. Liver tissue engineering: a role for co-culture systems in modifying hepatocyte function and viability. Tissue Eng 2001;7(3):345-57.

4. Kourouklis AP, Kaylan KB, Underhill GH. Substrate stiffness and matrix composition coordinately control the differentiation of liver progenitor cells. Biomaterials 2016;99:82-94.

5. Bhatia SN, Balis UJ, Yarmush ML, Toner M. Effect of cell-cell interactions in preservation of cellular phenotype: cocultivation of hepatocytes and nonparenchymal cells. FASEB J 1999;13(14):1883-900.

6. Nelson LJ, Treskes P, Howie AF, Walker SW, Hayes PC, Plevris JN. Profiling the impact of medium formulation on morphology and functionality of primary hepatocytes in vitro. Sci Rep 2013;3:2735.

7. Uygun BE, Yarmush ML, Uygun K. Application of whole-organ tissue engineering in hepatology. Nat Rev Gastroenterol Hepatol 2012;9(12):738-44.

8. Lin P, Chan WCW, Badylak SF, Bhatia SN. Assessing porcine liver-derived biomatrix for hepatic tissue engineering. Tissue engineering 2004;10(7-8):1046-1053.

9. Zhang X, Dong J. Direct comparison of different coating matrix on the hepatic differentiation from adipose-derived stem cells. Biochem Biophys Res Commun 2015;456(4):938-44.

10. Ji R, Zhang N, You N, Li Q, Liu W, Jiang N, Liu J, Zhang H, Wang D, Tao K and others. The differentiation of MSCs into functional hepatocyte-like cells in a liver biomatrix

scaffold and their transplantation into liver-fibrotic mice. Biomaterials 2012;33(35):8995-9008.

11. Bao J, Wu Q, Wang Y, Li Y, Li L, Chen F, Wu X, Xie M, Bu H. Enhanced hepatic differentiation of rat bone marrow-derived mesenchymal stem cells in spheroidal aggregate culture on a decellularized liver scaffold. Int J Mol Med 2016;38(2):457-65.

12. Badylak SF, Taylor D, Uygun K. Whole-organ tissue engineering: decellularization and recellularization of three-dimensional matrix scaffolds. Annual review of biomedical engineering 2011;13:27-53.

13. Lee JS, Shin J, Park HM, Kim YG, Kim BG, Oh JW, Cho SW. Liver extracellular matrix providing dual functions of two-dimensional substrate coating and three-dimensional injectable hydrogel platform for liver tissue engineering. Biomacromolecules 2014;15(1):206-18.

14. Mazza G, Rombouts K, Rennie Hall A, Urbani L, Vinh Luong T, Al-Akkad W, Longato L, Brown D, Maghsoudlou P, Dhillon AP and others. Decellularized human liver as a natural 3D-scaffold for liver bioengineering and transplantation. Sci Rep 2015;5:13079.

15. Takeda YS, Xu Q. Fabrication of 2D and 3D constructs from reconstituted decellularized tissue extracellular matrices. J Biomed Nanotechnol 2014;10(12):3631-7.

16. Hussein KH, Park KM, Ghim JH, Yang SR, Woo HM. Three dimensional culture of HepG2 liver cells on a rat decellularized liver matrix for pharmacological studies. J Biomed Mater Res B Appl Biomater 2016;104(2):263-73.

17. Sellaro TL, Ranade A, Faulk DM, McCabe GP, Dorko K, Badylak SF, Strom SC. Maintenance of human hepatocyte function in vitro by liver-derived extracellular matrix gels. Tissue Eng Part A 2010;16(3):1075-82.

18. Barakat O, Abbasi S, Rodriguez G, Rios J, Wood RP, Ozaki C, Holley LS, Gauthier PK. Use of decellularized porcine liver for engineering humanized liver organ. J Surg Res 2012;173(1):e11-25.

19. Khetani SR, Bhatia SN. Microscale culture of human liver cells for drug development. Nature biotechnology 2008;26(1):120-126.

20. Meng FW, Slivka PF, Dearth CL, Badylak SF. Solubilized extracellular matrix from brain and urinary bladder elicits distinct functional and phenotypic responses in macrophages. Biomaterials 2015;46:131-40.

21. Gilbert TW, Wognum S, Joyce EM, Freytes DO, Sacks MS, Badylak SF. Collagen fiber alignment and biaxial mechanical behavior of porcine urinary bladder derived extracellular matrix. Biomaterials 2008;29(36):4775-82.

22. Freytes DO, Martin J, Velankar SS, Lee AS, Badylak SF. Preparation and rheological characterization of a gel form of the porcine urinary bladder matrix. Biomaterials 2008;29(11):1630-7.

23. Record RD, Hillegonds D, Simmons C, Tullius R, Rickey FA, Elmore D, Badylak SF. In vivo degradation of 14C-labeled small intestinal submucosa (SIS) when used for urinary bladder repair. Biomaterials 2001;22(19):2653-9.

24. Lindberg K, Badylak SF. Porcine small intestinal submucosa (SIS): a bioscaffold supporting in vitro primary human epidermal cell differentiation and synthesis of basement membrane proteins. Burns 2001;27(3):254-66.

25. Freytes DO, Tullius RS, Badylak SF. Effect of storage upon material properties of lyophilized porcine extracellular matrix derived from the urinary bladder. J Biomed Mater Res B Appl Biomater 2006;78(2):327-33.

26. Khetani SR, Kanchagar C, Ukairo O, Krzyzewski S, Moore A, Shi J, Aoyama S, Aleo M, Will Y. Use of micropatterned cocultures to detect compounds that cause drug-induced liver injury in humans. Toxicological sciences : an official journal of the Society of Toxicology 2013;132(1):107-117.

27. Berger DR, Ware BR, Davidson MD, Allsup SR, Khetani SR. Enhancing the functional maturity of induced pluripotent stem cell-derived human hepatocytes by controlled presentation of cell-cell interactions in vitro. Hepatology (Baltimore, Md) 2015;61(4):1370-1381.

28. Lin C, Shi J, Moore A, Khetani SR. Prediction of Drug Clearance and Drug-Drug Interactions in Microscale Cultures of Human Hepatocytes. Drug metabolism and disposition: the biological fate of chemicals 2016;44(1):127-136.

29. Bhatia SN, Yarmush ML, Toner M. Controlling cell interactions by micropatterning in co-cultures: hepatocytes and 3T3 fibroblasts. Journal of biomedical materials research 1997;34(2):189-199.

30. Zinchenko YS, Schrum LW, Clemens M, Coger RN. Hepatocyte and kupffer cells co-cultured on micropatterned surfaces to optimize hepatocyte function. Tissue engineering 2006;12(4):751-761.

31. Faulk DM, Wildemann JD, Badylak SF. Decellularization and cell seeding of whole liver biologic scaffolds composed of extracellular matrix. J Clin Exp Hepatol 2015;5(1):69-80.

32. Brown BN, Barnes CA, Kasick RT, Michel R, Gilbert TW, Beer-Stolz D, Castner DG, Ratner BD, Badylak SF. Surface characterization of extracellular matrix scaffolds. Biomaterials 2010;31(3):428-37.

33. Naba A, Clauser KR, Whittaker CA, Carr SA, Tanabe KK, Hynes RO. Extracellular matrix signatures of human primary metastatic colon cancers and their metastases to liver. BMC Cancer 2014;14:518.

34. Zeisberg M, Kramer K, Sindhi N, Sarkar P, Upton M, Kalluri R. De-differentiation of primary human hepatocytes depends on the composition of specialized liver basement membrane. Mol Cell Biochem 2006;283(1-2):181-9.

35. Bhatia SN, Balis UJ, Yarmush ML, Toner M. Effect of cell-cell interactions in preservation of cellular phenotype: cocultivation of hepatocytes and nonparenchymal cells. The FASEB journal : official publication of the Federation of American Societies for Experimental Biology 1999;13(14):1883-1900.

36. Khetani SR, Szulgit G, Del Rio JA, Barlow C, Bhatia SN. Exploring interactions between rat hepatocytes and nonparenchymal cells using gene expression profiling. Hepatology (Baltimore, Md) 2004;40(3):545-554.

37. Khetani SR, Chen AA, Ranscht B, Bhatia SN. T-cadherin modulates hepatocyte functions in vitro. The FASEB journal : official publication of the Federation of American Societies for Experimental Biology 2008;22(11):3768-3775.

38. Ploss A, Khetani SR, Jones CT, Syder AJ, Trehan K, Gaysinskaya VA, Mu K, Ritola K, Rice CM, Bhatia SN. Persistent hepatitis C virus infection in microscale primary human hepatocyte cultures. Proceedings of the National Academy of Sciences 2010;107(7):3141-3145.

39. Jaroch K, Jaroch A, Bojko B. Cell cultures in drug discovery and development: The need of reliable in vitro-in vivo extrapolation for pharmacodynamics and pharmacokinetics assessment. J Pharm Biomed Anal 2018;147:297-312.

40. Mattei G, Magliaro C, Pirone A, Ahluwalia A. Decellularized Human Liver Is Too Heterogeneous for Designing a Generic Extracellular Matrix Mimic Hepatic Scaffold. Artif Organs 2017.

41. Lee H, Han W, Kim H, Ha DH, Jang J, Kim BS, Cho DW. Development of Liver Decellularized Extracellular Matrix Bioink for Three-Dimensional Cell Printing-Based Liver Tissue Engineering. Biomacromolecules 2017;18(4):1229-1237.

42. Hirata M, Yamaoka T. Hepatocytic differentiation of iPS cells on decellularized liver tissue. J Artif Organs 2017.

43. Zhang Y, He Y, Bharadwaj S, Hammam N, Carnagey K, Myers R, Atala A, Van Dyke M. Tissue-specific extracellular matrix coatings for the promotion of cell proliferation and maintenance of cell phenotype. Biomaterials 2009;30(23-24):4021-8.

44. Dziki JL, Wang DS, Pineda C, Sicari BM, Rausch T, Badylak SF. Solubilized extracellular matrix bioscaffolds derived from diverse source tissues differentially influence macrophage phenotype. J Biomed Mater Res A 2017;105(1):138-147.

45. Sellaro TL, Ravindra AK, Stolz DB, Badylak SF. Maintenance of hepatic sinusoidal endothelial cell phenotype in vitro using organ-specific extracellular matrix scaffolds. Tissue engineering 2007;13(9):2301-2310.

46. Zheng XL, Xiang JX, Wu WQ, Wang B, Liu WY, Gao R, Dong DH, Lv Y. Using a decellularized splenic matrix as a 3D scaffold for hepatocyte cultivation in vitro: a preliminary trial. Biomed Mater 2015;10(4):045023.

47. Gao R, Wu W, Xiang J, Lv Y, Zheng X, Chen Q, Wang H, Wang B, Liu Z, Ma F. Hepatocyte culture in autologous decellularized spleen matrix. Organogenesis 2015;11(1):16-29.

48. Xiang J, Zheng X, Liu P, Yang L, Dong D, Wu W, Liu X, Li J, Lv Y. Decellularized spleen matrix for reengineering functional hepatic-like tissue based on bone marrow mesenchymal stem cells. Organogenesis 2016;12(3):128-142.

49. Fujita M, Spray DC, Choi H, Saez J, Jefferson DM, Hertzberg E, Rosenberg LC, Reid LM. Extracellular matrix regulation of cell-cell communication and tissue-specific gene expression in primary liver cultures. Prog Clin Biol Res 1986;226:333-60.

50. Loneker AE, Faulk DM, Hussey GS, D'Amore A, Badylak SF. Solubilized liver extracellular matrix maintains primary rat hepatocyte phenotype in-vitro. J Biomed Mater Res A 2016;104(4):957-65.

51. Lee-Montiel FT, George SM, Gough AH, Sharma AD, Wu J, DeBiasio R, Vernetti LA, Taylor DL. Control of oxygen tension recapitulates zone-specific functions in human liver microphysiology systems. Exp Biol Med (Maywood) 2017:1535370217703978.

52. Nakamura S, Ijima H. Solubilized matrix derived from decellularized liver as a growth factor-immobilizable scaffold for hepatocyte culture. J Biosci Bioeng 2013;116(6):746-53.

Chapter 4

Prediction of drug clearance and drug-drug interactions in microscale cultures of human hepatocytes[4]

Summary

Accurate prediction of *in vivo* hepatic drug clearance using *in vitro* assays is important to properly estimate clinical dosing regimens. Clearance of low turnover compounds is especially difficult to predict using short-lived suspensions of un-pooled primary human hepatocytes (PHHs) and functionally declining PHH monolayers. Micropatterned co-cultures (MPCCs) of PHHs and 3T3-J2 fibroblasts have been previously shown to display major liver functions for several weeks *in vitro*. In this study, we first characterized long-term activities of major cytochrome P450 (CYP) enzymes in MPCCs created from un-pooled cryopreserved PHH donors. Then, MPCCs were utilized to predict the clearance of 26 drugs that exhibit a wide range of turnover rates *in vivo* (0.05-19.5 mL/min/kg). MPCCs predicted 73%, 92% and 96% of drug clearance values for all tested drugs within 2-fold, 3-fold and 4-fold of *in vivo* values, respectively. There was good correlation (R^2=0.94, slope=1.05) of predictions between the two PHH donors. On the other hand, suspension hepatocytes and conventional monolayers created from the same donor had significantly reduced predictive capacity (i.e. 30-50% clearance values

[4] This chapter has been adapted from Lin, C. et al. 2016. Prediction of drug clearance and drug-drug interactions in microscale cultures of human hepatocytes. Drug Metabolism and Disposition. 44 (1): 127-136. Reprinted with permission of the American Society for Pharmacology and Experimental Therapeutics.

within 4-fold of *in vivo*), and were not able to metabolize several drugs. Finally, we modulated drug clearance in MPCCs by inducing or inhibiting CYPs. Rifampin-mediated CYP3A4 induction increased midazolam clearance by 73%, while CYP3A4 inhibition with ritonavir decreased midazolam clearance by 79%. Similarly, quinidine-mediated CYP2D6 inhibition reduced clearance of dextromethorphan and desipramine by 71% and 22%, respectively. In conclusion, MPCCs created using cryopreserved un-pooled PHHs can be utilized for drug clearance prediction and to model drug-drug interactions.

4.1 Introduction

Metabolism by the liver accounts for the overall clearance of ~70% of marketed drugs[1]. Thus, accurate prediction of *in vivo* human hepatic clearance using preclinical models is important to set drug doses in the clinic[2]. Significant species-specific differences in liver pathways can lead to inaccuracies in the predictions of human drug clearance when using animals[3]. Therefore, *in vitro* human liver models are now increasingly utilized to predict human drug clearance[4]. While human liver microsomes are useful for evaluating cytochrome P450 (CYP)-mediated drug clearance in a high-throughput screening format, the lack of phase-II enzymes and membrane-bound transporters limits their utility for predicting clearances of different drug types. On the other hand, while retaining the complete architecture and cell types of the liver, liver slices are not amenable to high-throughput screening. Cancerous hepatic cell lines can be expanded cheaply and nearly indefinitely; however, they suffer from abnormal CYP levels and only represent single donors[5]. Thus, cryopreserved primary human hepatocytes (PHHs), which can be sourced from multiple donors, are ideal for on-demand assessment of drug disposition since they integrate all of the relevant metabolic pathways of the liver[6].

PHHs can be kept viable in suspension for 4-6h or plated in confluent monolayers on adsorbed collagen for a few days. For suspension PHHs, pooling can mitigate the large functional variability inherent across PHH donor lots. However, the limited incubation time using suspension hepatocytes often does not allow low turnover drugs to deplete sufficiently to predict *in vivo* clearance[2,7]. Low turnover drugs are increasingly being developed for one-pill-a-day dosing regimens, and often rank ordering of candidate compounds in a chemical series by clearance rates is necessary to progress with development. The relay method has addressed this limitation by transferring the drug-laden supernatant from 4h pooled PHH suspension incubations to freshly thawed PHHs to allow active enzymes to metabolize the drugs for prolonged times (~20h)[8]. However, this method requires at least 5-fold more PHHs (10+ pooled donors) than a single incubation, thereby depleting a limited lot faster and necessitating screening and large-scale banking of newer pooled lots. Additionally, suspension hepatocytes don't properly polarize with appropriate localization of transporters to the apical and basolateral domains, which is limiting for predicting clearance of drugs that are transporter substrates. While plated monolayers prolong PHH viability for a few days and show polarized phenotype when overlaid with an extracellular matrix gel[9], the CYP activities rapidly decline to <10% of levels observed in freshly isolated PHHs[10,11].

Organizing hepatocytes using engineering tools and co-culture with stromal cells can help maintain hepatic functions for prolonged times and at higher levels than possible with conventional monolayers, which has improved predictive capacities for drug studies[12]. Khetani and Bhatia developed a micropatterned co-culture (MPCC) model in which PHHs are organized onto collagen-coated domains of empirically-optimized dimensions and subsequently surrounded by 3T3-J2 murine embryonic fibroblasts[11]. Major hepatic functions (i.e. drug metabolism

enzymes, transporters) are stable in MPCCs for ~4 weeks. Due to the reduced number of PHHs (~10% of confluent monolayers), MPCCs can be incubated for up to 7d without a medium change, which led to detection of a greater number of clinically-relevant metabolites than was possible with suspension PHHs[13]. Chan *et al.* also used the 7d drug incubations in MPCCs to predict clearance of low turnover compounds[14]. However, drugs with high clearance rates were not tested, nor was MPCC performance compared against suspension hepatocytes and plated monolayers using the same donor. Furthermore, it remains unclear whether MPCCs created using cryopreserved PHHs from multiple donors can maintain high levels of major CYPs for several weeks, which could allow initiation of drug incubation at different culture ages. Therefore, here we sought to determine levels and longevity of major CYP enzymes in MPCCs created from cryopreserved PHH donors (un-pooled) in a 96-well plate format. We then utilized MPCCs to predict clearance rates of 26 drugs with a wide range of *in vivo* turnover rates, and compared results for a subset of these drugs across MPCCs, suspension PHHs and plated monolayers created from the same donor. Finally, we assessed the effects of drug-mediated CYP modulation on drug clearance rates in order to mimic drug-drug interaction (DDI) scenarios.

4.2 Materials and methods

4.2.1 Culture of primary human hepatocytes

Cryopreserved PHHs were purchased from vendors permitted to sell products derived from human organs procured in the United States by federally designated Organ Procurement Organizations (BioreclamationIVT, Baltimore, MD; Triangle Research Laboratories, Research Triangle Park, NC; Life Technologies, Carlsbad, CA). Information (lot classifier, age, sex, ethnicity, cause of death, available medical history) on the PHH lots is provided in **Supplemental Table 4.5.1**. PHH vials were thawed at 37°C for 120s and diluted with 25 mL of

pre-warmed KryoThaw I (SciKon, Chapel Hill, NC). The cell suspension was then spun at 50x*g* for 10 min, the supernatant was discarded, the cells were re-suspended in hepatocyte seeding medium, the formulation of which was described previously[15]. Hepatocyte viability was assessed using trypan blue exclusion (typically 80-95%). Liver-derived non-parenchymal cells were consistently found to be less than 1% of all the cells.

MPCCs were created as previously described[16]. Briefly, adsorbed collagen was lithographically patterned in each well of a multi-well plate to create 500 μm diameter circular domains spaced 1200 μm apart, center-to-center. Hepatocytes selectively attached to the collagen domains leaving ~4,500 attached hepatocytes on ~13 collagen-coated islands within each well of a 96-well plate. 3T3-J2 murine embryonic fibroblasts were seeded 18 to 24h later in each well to create MPCCs. Serum-supplemented culture medium, the formulation of which has been described previously[17], was replaced on cultures every 2d (~64 μL/well).

To create suspension cultures, $5.6x10^4$ hepatocytes were dispensed into each well (32 μL serum-free culture medium per well) of an uncoated 96-well plate. To create conventional confluent monolayers, $5.6x10^4$ hepatocytes were seeded into each well (64 μL serum-supplemented culture medium per well) of a 96-well plate coated with rat-tail collagen type I as described previously[11]. Serum-free culture medium for both suspension cultures and conventional monolayers was composed of William's E base (Sigma-Aldrich, St. Louis, MO), 15 mM HEPES buffer (Corning Cellgro, Manassas, VA), 1% vol/vol ITS+ supplement (Corning Life Sciences, Tewksbury, MA), 1% vol/vol penicillin-streptomycin (Corning Cellgro), 100 nM dexamethasone (Sigma-Aldrich), 0.2% vol/vol amphotericin B (Life Technologies), and 0.01% vol/vol gentamycin (Life Technologies). Fetal bovine serum (Life Technologies) was added at

10% vol/vol for seeding conventional monolayers for 24h and then cultures were switched to the serum-free formulation above for drug dosing studies.

4.2.2 Hepatocyte functionality assays

Urea concentration in supernatants was assayed using a colorimetric endpoint assay utilizing diacetyl monoxime with acid and heat (Stanbio Labs, Boerne, TX). Albumin levels were measured using an enzyme-linked immunosorbent assay (MP Biomedicals, Irvine, CA) with horseradish peroxidase detection and 3,3',5,5'-tetramethylbenzidine (TMB, Fitzgerald Industries, Concord, MA) as the substrate. CYP2C9 activity in cultures was measured using a luminescence-based assay (CYP2C9-glo, luciferin-H) by Promega (Madison, WI). Following incubation for 3h with the CYP2C9-glo substrate in serum-free dosing culture medium, culture supernatants were processed according to manufacturer instructions and luminescence was measured using a luminometer (BioTek, Winooski, VT). In addition, activities of major CYPs in MPCCs were assessed using substrates shown in **Supplemental Table 4.5.2**. Cultures were incubated with these substrates for 1h in serum-free dosing culture medium. Supernatants from cultures were frozen at -80°C prior to further analysis.

4.2.3 Drug dosing

MPCCs were allowed 7-9d to functionally stabilize and then dosed in serum-free culture medium with a set of 26 drugs (**Table 4.1**), ranging in known *in vivo* turnover rates between 0.05 mL/min/kg and 19.5 mL/min/kg. Conventional PHH monolayers were allowed 24h to acclimate before dosing in serum-free culture medium with a subset (10 total) of the drugs (**Table 4.2**). Suspension hepatocytes were dosed immediately after dispensing in wells with the same subset of drugs as those tested on conventional monolayers (**Table 4.3**). All drug solutions were

prepared in serum-free culture medium at 1 μM and placed on the cells (64 μL total volume per well). MPCCs were incubated with drug solutions for up to 7d without a medium change; conventional monolayers were dosed for up to 4d; and, suspension cultures were dosed for up to 4h. Supernatants (50 μL) from representative wells (single time-point per well of a 96-well plate) were collected at 6-7 time-points spread across the time series for each type of culture model. For MPCCs and conventional monolayers, removal of the supernatants was sufficient to stop the reaction with the cells. For suspension hepatocytes, however, mixing the cell suspension with 100 μL of acetonitrile was necessary to quench the reaction. All samples were immediately frozen at -80°C prior to further analysis.

For DDI studies, MPCCs stabilized for 7d were treated with serum-supplemented culture medium containing CYP inducer (12.5 μM rifampin for CYP3A4) for 3d or CYP inhibitor (0.5 μM ritonavir for CYP3A4 and 4 μM quinidine for CYP2D6) for 18h. Inducer and inhibitor concentrations were chosen based on preliminary experiments evaluating effects on the pertinent CYPs (data not shown). Then, cultures were dosed in serum-free culture medium with 1 μM of CYP substrates (midazolam for CYP3A4, and desipramine and dextromethorphan for CYP2D6) with or without CYP inducer/inhibitor. Control cultures were treated with dimethyl sulfoxide (DMSO, Corning Cellgro) alone (0.1% vol/vol) for the aforementioned time periods before dosing with CYP substrates. Sample collection was carried out as described above prior to further analysis.

4.2.4 Liquid chromatography-mass spectrometry (LC-MS) analysis

LC-MS analysis on culture supernatants (crashed with acetonitrile) was carried out by Integrated Analytical Solutions (IAS, Berkeley, CA). The amount of substrate metabolite or parent compound was measured using an Applied Biosystems/MDS Sciex API 3000 mass

spectrometer (Foster City, CA) coupled to a Shimadzu VP System (Shimadzu, Columbia, MD). The LC mobile phases consisted of: A) water containing 0.2% formic acid and B) methanol containing 0.2% formic acid. Samples were eluted through a Luna Mercury C8(2) column (2 x 30 mm; Phenomenex Inc., Torrance, CA), a Luna Mercury Hydro-RP column (2 x 3 mm), a Duragel G C18 column (2 x 10 mm; Peeke Scientific, Redwood City, CA), or a Titan 200 C18 column (2.1 x 30 mm; Sigma-Aldrich, St. Louis, MO). Solvent gradients from 0% (B) or 5% (B) to 95% (B) over the course of 1-2 minutes at flow rates of between 0.4 mL/min and 0.8 mL/min were used to elute the compounds from the columns. Injection volumes ranged from 2-100 μL for analysis.

4.2.5 Data analysis

The natural logarithm of the concentration of drug remaining in culture supernatants was first plotted against time of incubation. Further analysis of the data as described below was conducted only if the correlation coefficient of the linear fit to the natural log transformed data was greater than 0.8. If the correlation coefficient was less than 0.8, the data set was deemed not usable for prediction of clearance. The *in vitro* depletion half-lives of the drugs in culture supernatants were calculated by **equation 4.1**, where 'slope' was derived from the natural logarithm of the concentration of drug remaining plotted against time. For most of the compounds, the calculated half-life was within the maximal incubation time (i.e. no extrapolation) for both MPCCs and conventional monolayers, except for theophylline (both donors ~5 fold higher half-live than maximal incubation time), zolmatriptan (one of the two donors ~2 fold), and meloxicam (one of the two donors ~2 fold). For suspension hepatocytes, half-life needed to be extrapolated beyond the incubation time for 6 of 10 drugs (~2-3 fold).

$$t_{1/2} = \frac{0.693}{slope}$$ **Equation 4.1**

Next, the *in vitro* drug half-lives were used to calculate the intrinsic clearance (CL_{int}) using scaling factors (**equation 4.2**), where 21 g of liver weight per 1 kg of body weight, and 120 x 10^6 hepatocytes per 1 g of human liver were utilized as standard parameters[18]. PHH numbers per well were 4,500 for MPCCs and 56,000 for suspension and conventional monolayers. All cultures had incubation volumes of 64 μL.

$$CL_{int} = \frac{Ln(2)}{t_{1/2}} \times \frac{liver\ weight}{standard\ body\ weight} \times \frac{incubation\ volume\ (mL)}{hepatocytes\ /well} \times \frac{hepatocytes}{gram\ of\ liver}$$ **Equation 4.2**

The hepatic clearance (CL_h) was calculated from CL_{int} using the well-stirred model (**equation 4.3**) with liver blood flow (Q) being 21 mL/min/kg and protein binding (f_u) set to 1 if no protein binding correction was made or to its respective known *in vivo* value (**Table 1**).

$$CL_h = \frac{Q \times f_u \times CL_{int}}{Q + (f_u \times CL_{int})}$$ **Equation 4.3**

Error bars on graphs represent standard errors of the means. Microsoft Excel and GraphPad Prism 5.0 (La Jolla, CA) were used for data analysis, while GraphPad Prism 5.0 was used for plotting data.

4.3 Results

4.3.1 Long-term functional characterization of MPCCs

MPCCs were created in an industry-standard 96-well plate format using two cryopreserved PHH donors (lots: RTM and JNB). Prototypical hepatic morphology (polygonal shape, distinct nuclei and nucleoli, presence of bile canaliculi) was maintained for both donors in MPCCs for ~4 weeks (**Figure 4.1A and Supplemental Figure 4.5.1A**). As observed previously[11], albumin secretion in MPCCs took ~7-9d to reach higher steady-state levels than in the first few days of culture (**Figure 4.1B and Supplemental Figure 4.5.1B**). Urea secretion, on the other hand, either remained stable from the very beginning of the culture period or showed some down-regulation initially followed by stabilization for the remainder of the time-series (**Figure 4.1C and Supplemental Figure 4.5.1C**). Although donor dependent differences in albumin and urea secretion (as well as other functional markers as described below) were observed, overall trends were similar.

Activities of CYP1A2, 2C9, 2D6, and 3A4 were measured in both donors over time by quantifying metabolites of prototypical substrates, whereas the activities of CYP2A6, 2B6, 2C8, 2C19, and 2E1 were measured only in donor RTM (**Supplemental Table 4.5.2**) due to limitations in number of vials available for donor JNB. While enzyme activities were detected for ~4 weeks in both donors, there were differences in both the kinetics and magnitude of time-course for specific CYP activities (**Figure 4.2 and Supplemental Figure 4.5.1)**. CYP1A2 activities in RTM- and JNB-MPCCs at ~4 weeks of culture were 90% and 72% of week 1 activities, respectively (**Figure 4.2A and Supplemental Figure 4.5.1D**). CYP2C9 activities in RTM- and JNB-MPCCs at ~4 weeks were 176% and 91% of week 1 activities, respectively (**Figure 4.2C and Supplemental Figure 4.5.1D**). CYP2D6 activities in RTM- and JNB-MPCCs

at ~4 weeks were 73% and 85% of week 1 levels, respectively (**Figure 4.2D and Supplemental Figure 4.5.1E**). CYP3A4 activity in RTM at ~4 weeks was 131% of week 1 activity, while activity in JNB at 4 weeks had gradually declined to 58% of week 1 levels (**Figure 4.2E and Supplemental Figure 4.5.1E**). By ~4 weeks in RTM culture, CYP2A6 and CYP2B6 activities were down-regulated to 24% and 47% of week 1 levels, respectively. However, most of the decline occurred after 19d in culture (**Figures 4.2A-B**). CYP2C8 activity, on the other hand, was up-regulated by day 9 of culture to 658% of week 1 levels and then remained fairly stable until day 30 (**Figure 4.2B**). Use of CYP2C9-glo as a substrate showed similar relative stability as the measurement of 4-OH-tolbutamide in the same donor (**Figure 4.2C**). CYP2C19 activity was only stable for 15d followed by down-regulation to 22-33% of week 1 levels for the remainder of the time-series (**Figure 4.2D**). CYP2E1 activity at week 4 of culture declined to 12% of week 1 levels (**Figure 4.2E**). Nonetheless, activities of all major CYPs tested were detected out to at least 4 weeks in MPCCs created using both RTM and JNB donors. Lastly, we measured glucuronidation and sulfation (phase-II) activities in MPCCs created using both RTM and JNB donors (**Figure 4.2F and Supplemental Figure 4.5.1F**). By ~4 weeks in culture, RTM maintained phase-II activities to 90-116% of week 1 activities, while JNB at 4 weeks maintained activities to 77-105% of week 1 activities.

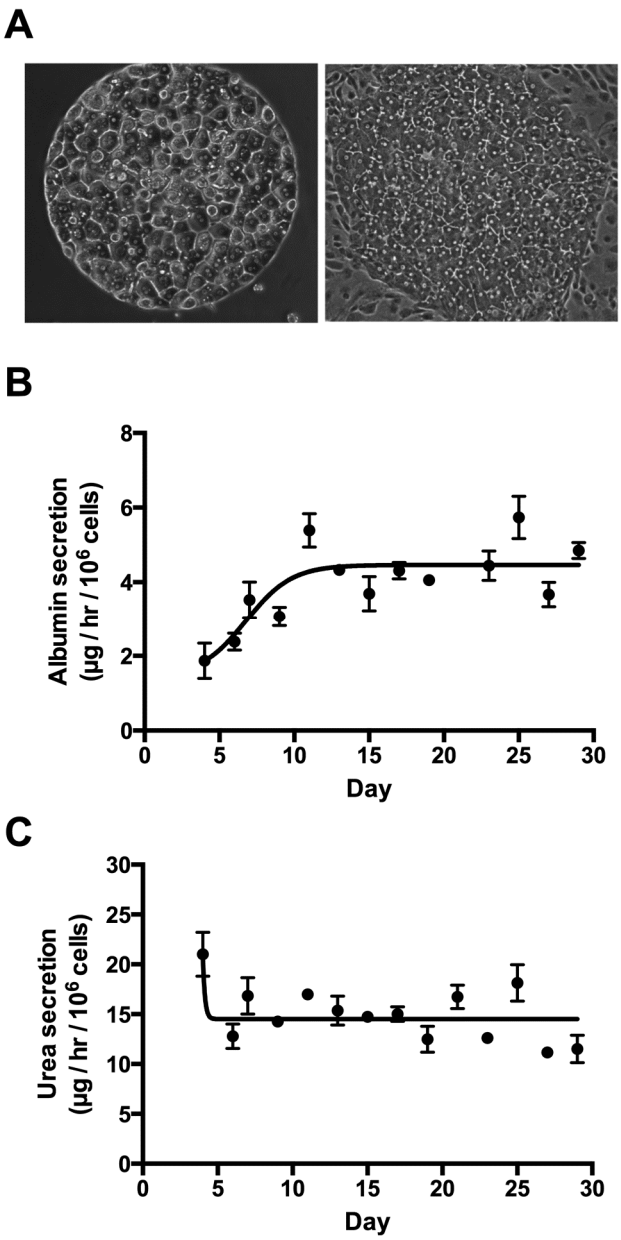

Figure 4.1 Morphology and functional characterization of MPCCs created using the RTM cryopreserved PHH donor. (A) Phase contrast micrographs of patterned PHHs prior to seeding of the 3T3-J2 murine embryonic fibroblasts (left) and 8 days in co-culture (right). Cultures showed similar hepatic morphology for at least 4 weeks (not shown). (B) Albumin secretion rates in MPCCs over time in culture. (C) Urea secretion rates in MPCCs over time in culture. Data in each graph was fit to a sigmoidal curve using GraphPad Prism software. Error bars represent standard errors of the means (n=3).

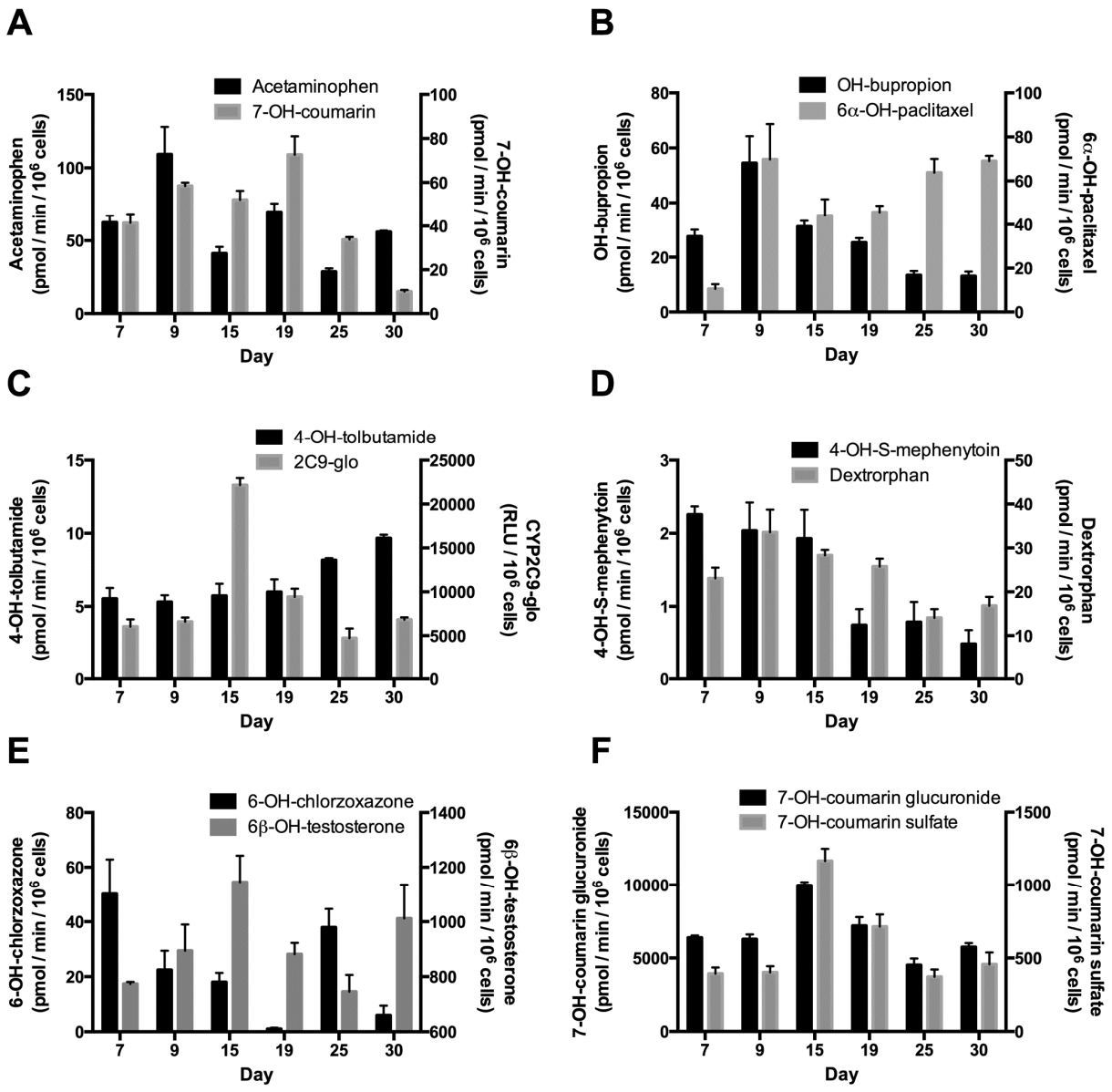

Figure 4.2 CYP activities in MPCCs created using the RTM cryopreserved PHH donor. Quantification of CYP-generated metabolites from MPCCs. *CYP, probe substrate, metabolite measured:* (A) 1A2, phenacetin, acetaminophen; 2A6, coumarin, 7-OH-coumarin; (B) 2B6, bupropion, OH-bupropion; 2C8, paclitaxel, 6α-OH-paclitaxel; (C) 2C9, tolbutamide, 4-OH-tolbutamide; 2C9, 2C9-glo, luciferin; (D) 2C19, S-mephenytoin, 4-OH-S-mephenytoin; 2D6, dextromethorphan, dextrorphan; (E) 2E1, chlorzoxazone, 6-OH-chlorzoxazone; 3A4, testosterone, 6β-OH-testosterone. (F) Production rates of glucuronide and sulfate metabolites of 7-hydroxycoumarin from MPCCs. Error bars represent standard errors of the means (n=3).

4.3.2 Drug clearance predictions in MPCCs

MPCCs were incubated for up to 7d with 26 drugs listed in **Table 4.1** (0.05-19.5 mL/min/kg *in vivo* clearance). Prototypical depletion of 3 drugs in MPCC supernatants is shown in **Supplemental Figure 4.5.2**. Drug clearance from *in vitro* MPCC data (and other models below) was predicted using the drug half-life, scaling parameters and well-stirred model as described in the 'methods' section. Predicted drug clearance rates in MPCCs with or without incorporation of protein binding into the analysis are shown in **Table 4.1**. Clearance data in 2 donors (JNB and RTM) was acquired for all drugs except timolol, imipramine and diclofenac, for which only a single donor was used due to PHH sourcing limitations. On average, with protein binding correction, MPCCs predicted 31%, 58% and 69% of the drug clearance values within 2-fold, 3-fold and 4-fold of *in vivo* clearance rates, respectively. When no protein binding correction was incorporated, MPCCs predicted on average 62%, 73% and 77% within 2-fold, 3-fold and 4-fold of *in vivo* clearance rates, respectively. We found that for compounds with *in vivo* reported clearance values less than or equal to ~1 mL/min/kg, correction for protein binding significantly improved MPCC predictive capacity, which is consistent with a previous study[14]. When utilizing a "mixed analysis" approach where correction for protein binding is only incorporated for compounds with reported clearance rates less than or equal to 1 mL/min/kg (low to very low turnover) and f_u=1 for all other compounds, MPCCs predicted 73%, 92% and 96% of the drug clearance values within 2-fold, 3-fold and 4-fold of *in vivo* clearance rates, respectively (**Table 4.1 and Figure 4.3**). Additionally, MPCCs were able to correctly rank order analog drugs based on predicted clearance rates (sumatriptan/zolmatriptan, methylprednisolone/prednisolone and lorazepam/diazepam). Lastly, the predicted drug clearance values in MPCCs created from two donors for drugs with clearance rates greater than 5 mL/min/kg (**Figure 4.4A**) and less than

5 mL/min/kg (**Figure 4.4B**) were compared against each other using linear regression analysis. Both donors provided similar predictions of drug clearance rates across all drugs (average R^2=0.94, slope=1.05) despite the functional differences observed in figures 4.1 and 4.2, and supplemental figure 4.5.1.

Table 4.1 Predicted clearance rates in MPCCs for 26 drugs. Donor 1 is the RTM lot. Asterisks next to compound names indicate that Donor 2 was Hu4163, rather than JNB. N/A indicates data are "not available" due to cell sourcing limitations. The *in vivo* PK parameters were compiled from several sources including: [7,14,19-23]

***In Vivo* Observed Pharmacokinetic Parameters**				**Predicted Clearance (mL/min/kg) in MPCCs**					
				f_u = reported literature values			**f_u = 1**		
Compound Name	**Known Routes of Metabolism**	***In Vivo* CL (mL/min/kg)**	**f_u**	**Donor 1**	**Donor 2**	**Average**	**Donor 1**	**Donor 2**	**Average**
Verapamil	CYP3A4, 2C9	19.5	0.10	6.79	6.86	6.83	17.36	17.41	17.39
Sumatriptan		19	0.83	12.36	13.74	13.05	13.29	14.60	13.95
Naloxone	UGT2B7	18	0.54	14.45	14.52	14.49	16.87	16.92	16.90
Propranolol	CYP2D6, 1A2	15.7	0.13	6.70	4.95	5.83	16.44	14.77	15.61
Metoprolol*	CYP2D6	13	0.88	3.80	5.76	4.78	4.29	5.37	4.83
Triprolidine*		13	0.50	3.30	7.78	5.54	5.70	11.35	8.52
Desipramine*	CYP2D6, 1A2; UGT	10.3	0.16	2.25	2.39	2.32	8.99	9.34	9.16
Timolol	CYP2D6	10.1	0.90	5.39	N/A	5.39	5.82	N/A	5.82
Dextromethorphan	CYP2D6, 3A4, 1A2, 2C19	8.6	0.50	10.66	11.39	11.03	14.14	14.77	14.46
Omeprazole	CYP2C19, 3A4	8.4	0.05	2.53	2.47	2.50	15.38	15.26	15.32
Imipramine*	CYP2D6, 1A2, 2C19, 3A4; UGT1A4	8	0.10	N/A	2.06	2.06	N/A	10.93	10.93
Diclofenac	CYP2C9	7.6	0.01	0.08	N/A	0.08	8.90	N/A	8.90
Zolmitriptan	CYP1A2	6.7	0.75	1.94	3.01	2.48	2.51	3.83	3.17
Methylprednisolone	CYP3A4	6.1	0.23	4.67	6.57	5.62	11.64	13.95	12.80
Erythromycin	CYP3A4	5.6	0.10	0.71	1.06	0.89	5.44	7.30	6.37
Ziprasidone	CYP3A4	5.1	0.00	0.10	0.10	0.10	16.66	16.63	16.65
Betaxolol*		4.8	0.40	0.83	0.21	0.52	4.20	3.15	3.67
Prednisolone*	CYP3A4	2.9	0.25	0.68	0.59	0.64	3.36	3.08	3.22
Furosemide*		1.7	0.01	0.03	0.04	0.04	2.51	2.74	2.63
Theophylline	CYP1A2	1.1	0.41	0.34	0.26	0.30	0.81	0.62	0.72
Lorazepam	UGT	1	0.09	0.46	0.43	0.45	4.15	3.97	4.06
Diazepam	CYP2C19, 1A2, 3A4	0.53	0.02	0.21	0.22	0.22	6.30	6.69	6.50

Tolbutamide	CYP2C9, 2C19	0.38	0.05	0.21	0.40	0.31	3.49	5.84	4.67
Naproxen	CYP2C9, 1A2	0.19	0.01	0.18	0.49	0.34	9.75	14.78	12.27
Meloxicam	CYP2C9, 3A4	0.12	0.01	0.01	0.03	0.02	1.38	3.98	2.68
Warfarin*	CYP2C9, 3A4	0.05	0.02	0.04	0.02	0.03	1.85	1.02	1.44
		Within 2-fold		32%	25%	31%	60%	63%	62%
		Within 3-fold		48%	58%	58%	68%	71%	73%
		Within 4-fold		64%	71%	69%	76%	79%	77%

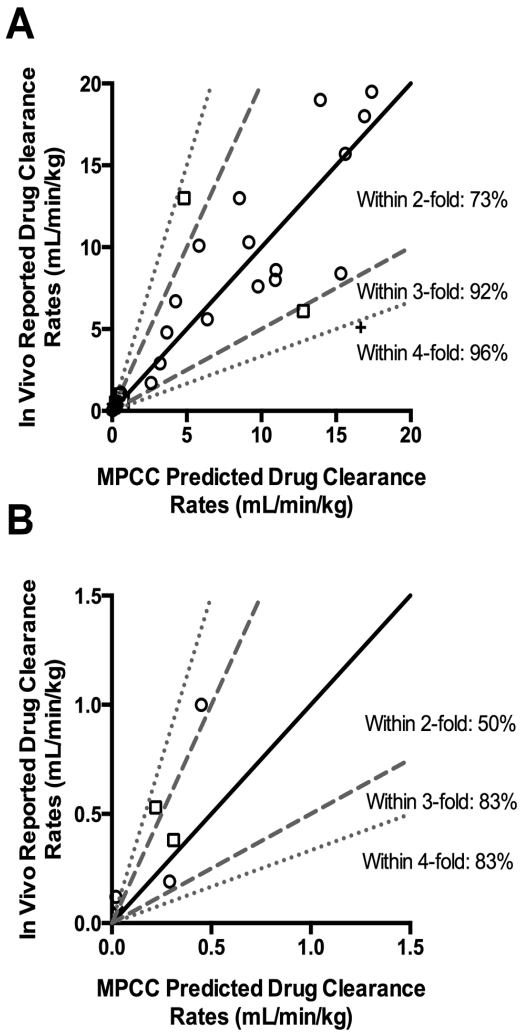

Figure 4.3 Correlation between drug clearance rates predicted in MPCCs and rates reported *in vivo*. The predicted clearance rates shown here are averaged from data obtained using two PHH donors in MPCCs for all drugs except timolol, imipramine and diclofenac, for which only a single donor was used (see table 4.1). Hepatocyte donors used were RTM (donor 1) and JNB or Hu4163 (donor 2). Open circles indicate predictions within 2-fold of *in vivo* levels (dashed lines); open squares indicate predictions within 3-fold (dotted lines); crosses indicate predictions within 4-fold; and X's indicate predictions greater than 4-fold (meloxicam). The solid line represents a perfect correlation. (A) Correlation analysis for all 26 compounds tested in this study. (B) Correlation analysis for a subset of compounds (*in vivo* reported clearance rates less than or equal to 1 mL/min/kg), for which data appears in the solid box marked in the

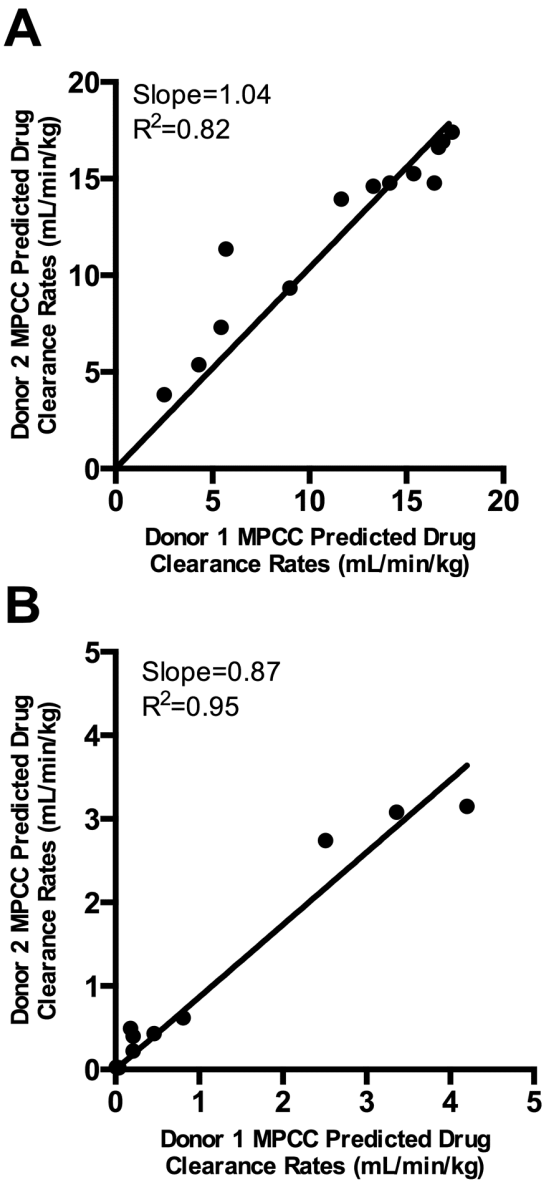

Figure 4.4 Correlation between drug clearance rates predicted in MPCCs created from two PHH donors. Hepatocyte donors used were RTM (donor 1) and JNB or Hu4163 (donor 2). (A) Comparison between two donors for compounds with reported *in vivo* clearance rates greater than 5 mL/min/kg. (B) Comparison between two donors for compounds with reported *in vivo* clearance rates less than 5 mL/min/kg.

4.3.3 Comparison of predicted drug clearance rates across different culture models

A subset of the drug set, 10 total drugs in particular across a wide range of *in vivo* turnover rates (0.19–19.5 mL/min/kg), were also tested in conventional PHH monolayers (**Table 4.2**) and suspension PHH cultures (**Table 4.3**) created from one of the PHH donors (RTM)

utilized for MPCCs in Table 4.1. Prototypical depletion of 3 drugs in supernatants of conventional monolayers and suspension cultures is shown in **Supplemental Figures 4.5.3 and 4.5.4**, respectively. Conventional monolayers were useful for predicting clearance rates for 9 of 10 compounds, except for naproxen, which did not metabolize sufficiently in the monolayers to make a clearance prediction. Without protein binding correction, monolayers predicted 50%, 60% and 80% and with protein binding correction, 10%, 20% and 20% within 2-fold, 3-fold and 4-fold of *in vivo* clearance rates, respectively. When utilizing the "mixed analysis" approach as described above, monolayers predicted 40%, 40% and 50% of the clearance rates within 2-fold, 3-fold and 4-fold of *in vivo* clearance rates, respectively, which was in contrast to the data obtained in MPCCs (80%, 100% and 100% within 2-fold, 3-fold and 4-fold, respectively). Most of the clearance rates obtained from monolayers were 12-86% lower than those predicted using MPCCs, with the exception of erythromycin (3% higher in monolayers relative to MPCCs) and theophylline (26% higher). For suspension cultures, 70% of the drugs with *in vivo* clearance rates of less than or equal to 6.1 mL/min/kg demonstrated little to no metabolism over the time course of 4h. For the 3 compounds that demonstrated metabolism in suspension cultures (verapamil, naloxone and timolol), clearance values were predicted within 3-fold of *in vivo* clearance values. Overall, 20%, 30% and 30% of the drug clearance were predicted within 2-fold, 3-fold and 4-fold of *in vivo* clearance rates, respectively, in suspension PHHs.

Table 4.2 Predicted drug clearance rates in MPCCs as compared to conventional confluent monolayers created using the same donor (RTM). MPCCs were stabilized for 7 days prior to dosing with drugs for up to 7 days, while conventional monolayers were stabilized for 1 day prior to dosing with drugs for up to 4 days. The '-' indicates that the drug did not turnover sufficiently in the model system to predict a clearance rate.

***In Vivo* Observed Pharmacokinetic Parameter Values**			**Predicted Clearance (mL/min/kg)**			
			f_u = reported literature values		**f_u = 1**	
Compound Name	***In Vivo* CL (mL/min/kg)**	**f_u**	**MPCCs**	**Conventional Monolayer**	**MPCCs**	**Conventional Monolayer**
Verapamil	19.5	0.10	6.79	0.8	17.36	5.98
Naloxone	18	0.54	14.45	11.98	16.87	14.93
Timolol	10.1	0.90	5.39	0.95	5.82	1.05
Methylprednisolone	6.1	0.23	4.67	0.91	11.64	3.46
Erythromycin	5.6	0.10	0.71	0.73	5.44	5.59
Theophylline	1.1	0.41	0.34	0.43	0.81	1.02
Lorazepam	1	0.09	0.46	0.11	4.15	1.13
Diazepam	0.53	0.02	0.21	0.03	6.3	1.27
Tolbutamide	0.38	0.05	0.21	0.06	3.49	1.19
Naproxen	0.19	0.01	0.18	-	9.75	-
Within 2-fold			50%	10%	60%	50%
Within 3-fold			80%	20%	60%	60%
Within 4-fold			90%	20%	60%	80%

Table 4.3 Predicted drug clearance rates in MPCCs as compared to suspension cultures created using the same donor (RTM). MPCCs were stabilized for 7 days prior to dosing with drugs for up to 7 days, while suspension hepatocytes were used immediately following thawing for up to 4 hours incubation with drugs. The '-' indicates that the drug did not turnover sufficiently in the model system to predict a clearance rate.

***In Vivo* Observed Pharmacokinetic Parameter Values**			**Predicted Clearance (mL/min/kg)**			
			f_u = reported literature values		**f_u = 1**	
Compound Name	***In Vivo* CL (mL/min/kg)**	**f_u**	**MPCCs**	**Suspension**	**MPCCs**	**Suspension**
Verapamil	19.5	0.10	6.79	1.23	17.36	8.03
Naloxone	18	0.54	14.45	11.12	16.87	14.19
Timolol	10.1	0.90	5.39	4.66	5.82	5.06
Methylprednisolone	6.1	0.23	4.67	-	11.64	-
Erythromycin	5.6	0.10	0.71	-	5.44	-
Theophylline	1.1	0.41	0.34	-	0.81	-
Lorazepam	1	0.09	0.46	-	4.15	-
Diazepam	0.53	0.02	0.21	-	6.3	-
Tolbutamide	0.38	0.05	0.21	-	3.49	-
Naproxen	0.19	0.01	0.18	-	9.75	-
Within 2-fold			50%	10%	60%	20%
Within 3-fold			80%	20%	60%	30%
Within 4-fold			90%	20%	60%	30%

4.3.4 Effects of drug-drug interactions (DDI) on drug clearance rates

CYP3A4 activity was induced ~4 fold relative to vehicle control in MPCCs by a 3d treatment with rifampin, or CYP3A4 was inhibited down to ~4% relative to vehicle controls by an 18h treatment with ritonavir (data not shown). Inducing CYP3A4 levels by ~4 fold led to significantly more turnover of midazolam (56.4% depletion in vehicle control vs. 99.8% depletion in rifampin-treated cultures) over 24h of incubation (**Figure 4.5A**). On the other hand, incubation with ritonavir significantly inhibited midazolam turnover (8.2% depletion) relative to vehicle controls. When the turnover of midazolam over time was converted to predicted

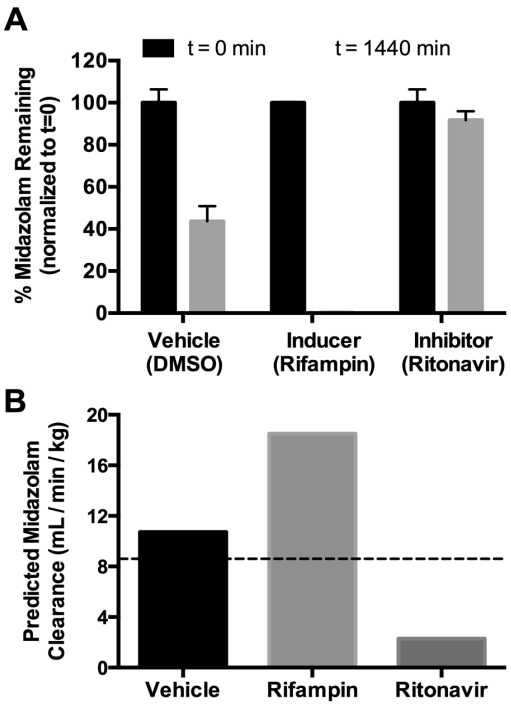

Figure 4.5 CYP3A4 drug-drug interaction studies in MPCCs. MPCCs created using donor lot Hum4011 were stabilized for 7 days prior to being treated with vehicle only (dimethyl sulfoxide), rifampin (3A4 inducer, 12.5 μM) for 3 days, or ritonavir (3A4 inhibitor, 0.5 μM) for 18 hours. The cultures were then dosed with 1 μM midazolam (3A4 substrate). (A) Midazolam depletion in the supernatants of cultures treated with the aforementioned compounds. (B) Predicted midazolam clearance rates from MPCCs treated with the aforementioned compounds. Dashed line indicates the reported *in vivo* midazolam clearance rate of 8.7 mL/min/kg. Similar trends were observed with a second donor, EJW (data not shown).

clearance rates, the vehicle control produced a rate within 2-fold of *in vivo* (vehicle control: 10.7 mL/min/kg, *in vivo*: 8.7 mL/min/kg), while rates in both induced and inhibited cultures were outside the 2-fold window (induced: 18.5 mL/min/kg, inhibited: 2.3 mL/min/kg), albeit in opposite directions as expected (**Figure 4.5B**).

When we inhibited CYP2D6 in MPCCs using quinidine, turnover of dextromethorphan over a 96h incubation was significantly inhibited relative to vehicle control cultures (85% turnover in vehicle controls vs. 13.5% turnover in inhibited cultures) (**Figure 4.6A**). Predicted dextromethorphan clearance from the turnover data was within 2-fold of *in vivo* rates in vehicle control cultures (vehicle control: 7.6 mL/min/kg, *in vivo*: 8.6 mL/min/kg), but outside 2-fold in inhibited cultures (2.2 mL/min/kg) (**Figure 4.6B**). On the other hand, effects of quinidine-mediated CYP2D6 inhibition were not as pronounced for desipramine turnover as for dextromethorphan (**Figure 4.6C-D**). In particular, 68% of desipramine was depleted over 48h in vehicle control cultures as opposed to 54% in inhibited cultures (**Figure 4.6C**). Such turnover corresponded to predicted desipramine clearance rates within 2-fold of *in vivo* values for both vehicle control and quinidine-inhibited cultures (vehicle control: 8.5 mL/min/kg, quinidine-inhibited: 6.6 mL/min/kg, *in vivo*: 10.3 mL/min/kg) (**Figure 4.6D**).

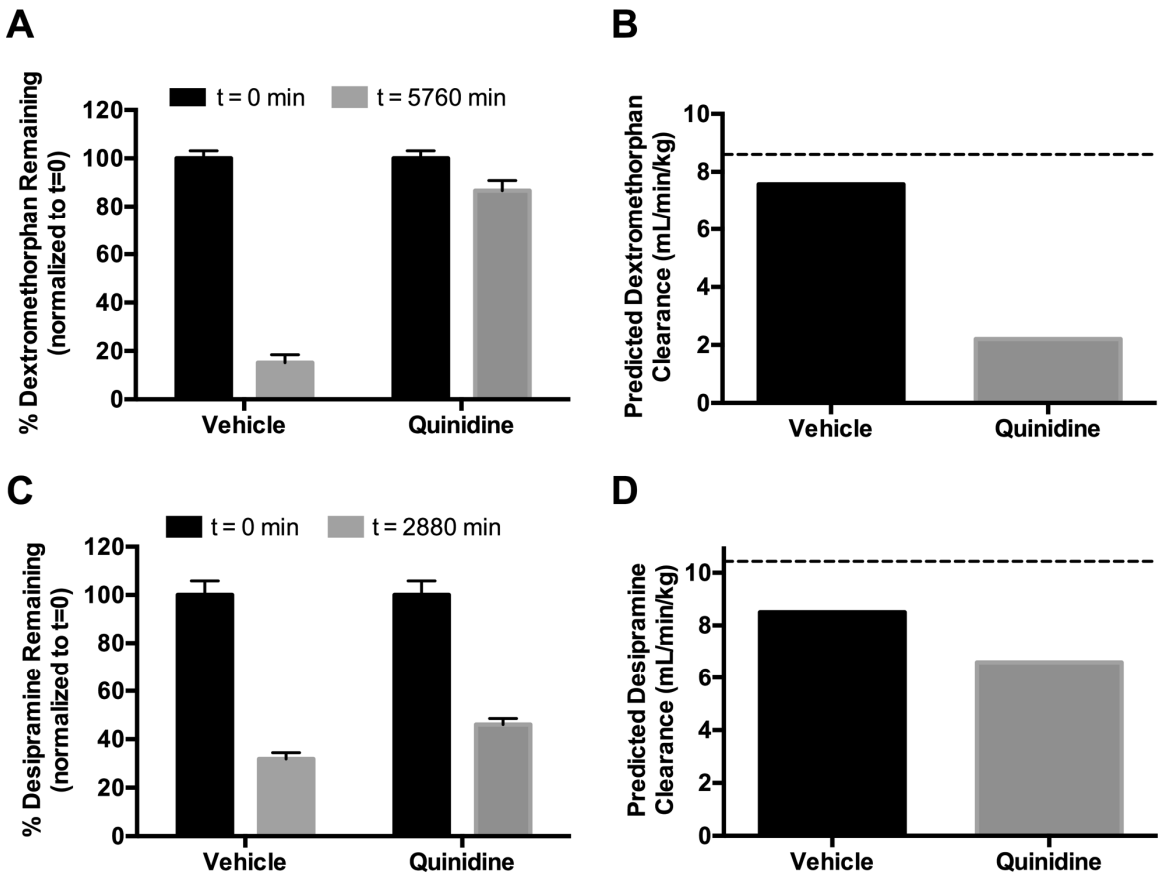

Figure 4.6 CYP2D6 drug-drug interaction studies in MPCCs. MPCCs created using donor lot Hum4011 were stabilized for 7 days prior to being treated with vehicle only (dimethyl sulfoxide) or quinidine (2D6 inhibitor, 4 μM) for 18 hours. The cultures were then dosed with 1 μM desipramine or dextromethorphan (2D6 substrates). (A) Dextromethorphan depletion in the supernatants of cultures treated with the aforementioned compounds. (B) Predicted dextromethorphan clearance rates from MPCCs treated with the aforementioned compounds. Dashed line indicates the reported *in vivo* dextromethorphan clearance rate of 8.6 mL/min/kg. (C) Desipramine depletion in the supernatants of cultures treated with the aforementioned compounds. (D) Predicted desipramine clearance rates from MPCCs treated with the aforementioned compounds. Dashed line indicates the reported *in vivo* despiramine clearance rate of 10.3 mL/min/kg. Similar trends were observed with a second donor, EJW (data not shown).

4.4 Discussion

Prediction of *in vivo* human drug clearance using *in vitro* hepatic clearance can help identify compounds with poor pharmacokinetic characteristics. An ideal hepatocyte culture platform for such purposes uses as few limited PHHs as possible in a reproducible/miniaturized

format; maintains high levels of drug metabolism enzymes (DMEs) with proper hepatocyte polarity to allow incubations with drugs that interact with multiple pathways; is compatible with multiple cryopreserved PHH donors for on-demand screening; and, can be used to predict clearance of compounds with a wide range of turnover rates, including slowly metabolized compounds. Additionally, the ability to interrogate effects of drug incubations on PHH enzyme levels and subsequently victim drug disposition is important for modeling clinical DDIs[12]. Towards approximating such features, we show that MPCCs created in a 96-well plate format display high levels of CYP and phase-II activities for ~4 weeks. Such activities coupled with the ability to dose drugs for 7d without a medium change led to better overall prediction of drug clearance rates than with suspension cultures or conventional monolayers created from the same donor. Finally, modulating CYP activities via perpetrator drugs altered the clearance of victim drugs in MPCCs.

We quantified albumin secretion, urea synthesis and enzyme activities over several weeks in MPCCs created from two cryopreserved PHH donors. The fibroblasts used in MPCCs do not metabolize drugs that primarily undergo hepatic metabolism[11,14]. Albumin and urea secretion rates in MPCCs were relatively stable across both donors for 3-4 weeks. CYP1A2, 2C9, 2D6, glucuronidation/sulfation activities were relatively stable between 1 and 4 weeks of culture across both donors; however, CYP3A4 declined by ~40% in one donor. We also measured the activities of CYP2A6, 2B6, 2C8, 2C19 and 2E1 in a single donor. CYP2A6 and 2B6 were relatively stable for ~3 weeks; 2C19 activity was relatively stable for ~2 weeks; and, CYP2E1 levels showed a decline between 1 and 4 weeks of culture. Nonetheless, activities of all major enzymes tested were detected for ~4 weeks in MPCCs with good stability for 2-3 weeks for most

CYPs. Culture medium formulations that can improve the stability of all major CYPs in MPCCs for at least 4 weeks should prove useful for drug dosing at later time points.

The 26 drugs chosen span a larger range of *in vivo* turnover rates (0.05-19.5 mL/min/kg) than previously tested in MPCCs[14]. These drugs can undergo metabolism via CYPs (i.e. tolbutamide, diclofenac) and phase II enzymes (naloxone, diazepam), while some are transporter substrates (i.e. triprolidine, desipramine)[21,24]. The well-stirred model was used to predict clearance from drug depletion in supernatants, an approach well suited for screening large numbers of compounds. Marginal differences have been observed across well-stirred, parallel-tube and dispersion models for clearance prediction, except for very high turnover compounds[25]. However, the well-stirred model produced good predictions for the high turnover compounds here. On average across two donors, MPCCs predicted 19 of 26 compounds (73%) within 2-fold of the known *in vivo* clearance rates, 24 of 26 compounds (92%) within 3-fold, and 25 of 26 compounds (96%) within 4-fold, with meloxicam's predicted clearance rate at a 6-fold deviation. In another study with MPCCs and in another engineered liver platform, meloxicam was under-predicted and its turnover was highly dependent on the donor[14,26].

The accuracy of predicted clearance rates for high and medium turnover compounds was improved when not incorporating plasma protein binding, as also observed previously[2,25]. On the other hand, MPCCs metabolized low turnover drugs (less than or equal to 1 mL/min/kg) significantly faster in the serum-free medium than *in vivo*, and thus use of reported f_u values significantly improved the accuracy of clearance predictions, as also observed previously[27,28]. While the mechanism is not known, others have speculated that since slowly metabolized compounds have more time to bind to proteins *in vivo* than higher turnover compounds, the unbound fraction available for metabolism for slowly metabolized compounds may be lower

than for higher turnover compounds[29]. Therefore, incorporation of protein binding correction in the analysis for low turnover compounds becomes important for more accurate clearance predictions. It is possible that inclusion of human albumin, alpha-1 acid glycoprotein and lipoproteins in culture medium at concentrations found in human blood may allow a consistent analysis scheme for the entire range of drug turnover rates[30].

The predicted drug clearance rates across two PHH donors used in MPCCs were strongly correlated (average R^2=0.94, slope=1.05) despite differences in CYP activities. Furthermore, in comparison to another study that tested 7 of the 26 compounds used here with the same two donors in MPCCs[14], we found good agreement with the rank ordering of drugs by their predicted clearance rates, thereby showing the reproducibility of the platform. With their use of individual PHH donors and ~40-50% fewer cells for seeding as compared to suspension and conventional confluent cultures, MPCCs can be used with limited donor lots for a larger number (~2-3 fold) of screening studies. Pooled plateable PHH lots could provide an "average" human response in plated culture formats; however, plating efficiencies need to be uniform across the various PHH donor lots to ensure that monolayers are composed of similar numbers of each donor's PHHs. Nonetheless, individual PHH lots with specific polymorphisms can provide useful information on population-specific differences in drug clearance.

Suspension PHHs, created from the same donor as that used in MPCCs, did not sufficiently deplete medium and low turnover drugs (7 of 10) within 4h to allow prediction of clearance rates, while clearance rates of higher turnover drugs were predicted within 2-3 fold of *in vivo* levels. Thus, while single donors can be used in MPCCs, carefully selected 10+ donor pooled lots along with the relay method are necessary to use suspension PHHs for prediction of medium and low turnover compounds[8]. On the other hand, conventional PHH monolayers

predicted the clearance rates for 9 of 10 drugs. Even though conventional monolayers display a rapid decline in functionality within the first 4-24 hours[12], continued metabolism of some low turnover compounds (i.e. diazepam) was observed over 4d . Naproxen, however, did not turnover in conventional monolayers even after 4d of incubation even though it was depleted within 3d in MPCCs, which contained ~10-fold fewer PHHs. Overall, conventional monolayers predicted 40%, 40% and 50% of the compounds within 2-, 3- and 4-fold of *in vivo* turnover rates, respectively, whereas MPCCs predicted 80% and 100% within 2- and 3-fold, respectively. Furthermore, conventional monolayers predicted lower clearance rates than in MPCCs for 8 of 10 drugs, likely due to the lower enzyme activity per cell in confluent monolayers[11].

The short lifetime (<7d) of conventional PHH monolayers coupled with a significant decline in CYP activities limits their utility in evaluating effects of CYP modulation on drug disposition, especially for those CYPs (i.e. 2D6) that are not as abundant as 3A4[12]. Here, we hypothesized that the greater longevity and higher functionality of MPCCs could help mitigate such a limitation. Inducing CYP3A4 in MPCCs via rifampin for 3d led to a ~73% increase in subsequent midazolam clearance, while inhibiting CYP3A4 via ritonavir for 18h led to a ~79% decrease in midazolam clearance relative to vehicle controls. The ~1.7 fold increase in midazolam clearance in MPCCs with rifampin pre-treatment is in line with ~2 fold increase observed in the clinic, albeit patients in the clinic were pre-treated with rifampin for 7d[31]. Furthermore, our use of serum with inducers in MPCC culture medium coupled with higher baseline CYP activities typically leads to lower fold induction values (2-8 fold) than can be observed with declining conventional monolayers incubated with inducers in serum-free medium (up to 80-100 fold)[32-34]. Inhibition of CYP2D6 via quinidine led to ~71% and ~22% reduction in clearance of dextromethorphan and desipramine, respectively, relative to controls. Such a

difference across the compounds highlights the need for evaluating effects of DDI on drug clearance *in vitro*.

Incorporation of liver stromal cells in MPCCs may allow prediction of drug clearance rates under disease perturbations such as fibrosis and inflammation[35]. Furthermore, miniaturization into a 384-well format should enable higher-throughput screening in MPCCs. In conclusion, we show that MPCCs with cryopreserved PHHs can predict the clearance rates of drugs with a wide range of *in vivo* turnover rates, including slowly metabolized drugs. The accuracy of drug clearance prediction in MPCCs was significantly better than that observed in suspension and conventional monolayers created from the same donor. Furthermore, the longevity of MPCCs allowed evaluation of the effects of DDI on drug clearance, which should prove useful for better modeling clinical scenarios.

4.5 Supplemental Figures

Table 4.5.1 Demographics and available medical histories of the primary human hepatocyte donor lots used for *in vitro* experiments.

Lot (Vendor)	Age	Ethnicity	Sex	Cause of Death	Medical History
JNB (BioreclamationIVT)	19	Caucasian	F	IC Bleed; Secondary to ICH/Stroke	No alcohol, tobacco or drug use; Lupus
Hum4011 (Triangle Research Labs)	26	Caucasian	M	Cardiovascular	No alcohol, tobacco or drug use
EJW (BioreclamationIVT)	29	Caucasian	F	Cardiovascular; 2nd to Natural Causes	Alcohol, tobacco and drug use; Borderline HTN, Type I Diabetes, UTI
Hu4163 (Life Technologies)	57	Caucasian	F	Anoxia	Tobacco use; Clonipine and synthroid use
RTM (BioreclamationIVT)	61	Caucasian	F	Anoxia; Secondary to Cardiovascular	No alcohol, tobacco or drug use; Cardiac arrest, C1-C2 fracture, Diverticulitis, GIRD, Hypothyroidism

Table 4.5.2 Compounds used for *in vitro* CYP450 profiling studies. All substrates were reconstituted in dimethyl sulfoxide (DMSO) and incubated on RTM and/or JNB cultures at indicated concentrations for 1h except for CYP2C9-glo, which was incubated for 3h. The supernatants were then collected and stored at -80°C prior to LC-MS/MS or luminescence analysis.

Enzyme	Concentration (μM)	Substrate	Metabolites
1A2	100	Phenacetin	Acetaminophen
2A6	50	Coumarin	7-OH-coumarin
2B6	500	Bupropion	OH-bupropion
2C8	30	Paclitaxel	6α-OH-paclitaxel
2C9	50	Tolbutamide	4-OH-tolbutamide
2C9	100	Diclofenac	4-OH-diclofenac
2C9	100	CYP2C9-glo	Luciferin
2C19	100	S-mephenytoin	4-OH-S-mephenytoin
2D6	16	Dextromethorphan	Dextrorphan
2E1	300	Chlorzoxazone	6-OH-chlorzoxazone
3A4	200	Testosterone	6β-OH-testosterone
Phase II Metabolism	50	7-OH-coumarin	7-OH-coumarin glucuronide and 7-OH-coumarin sulfate

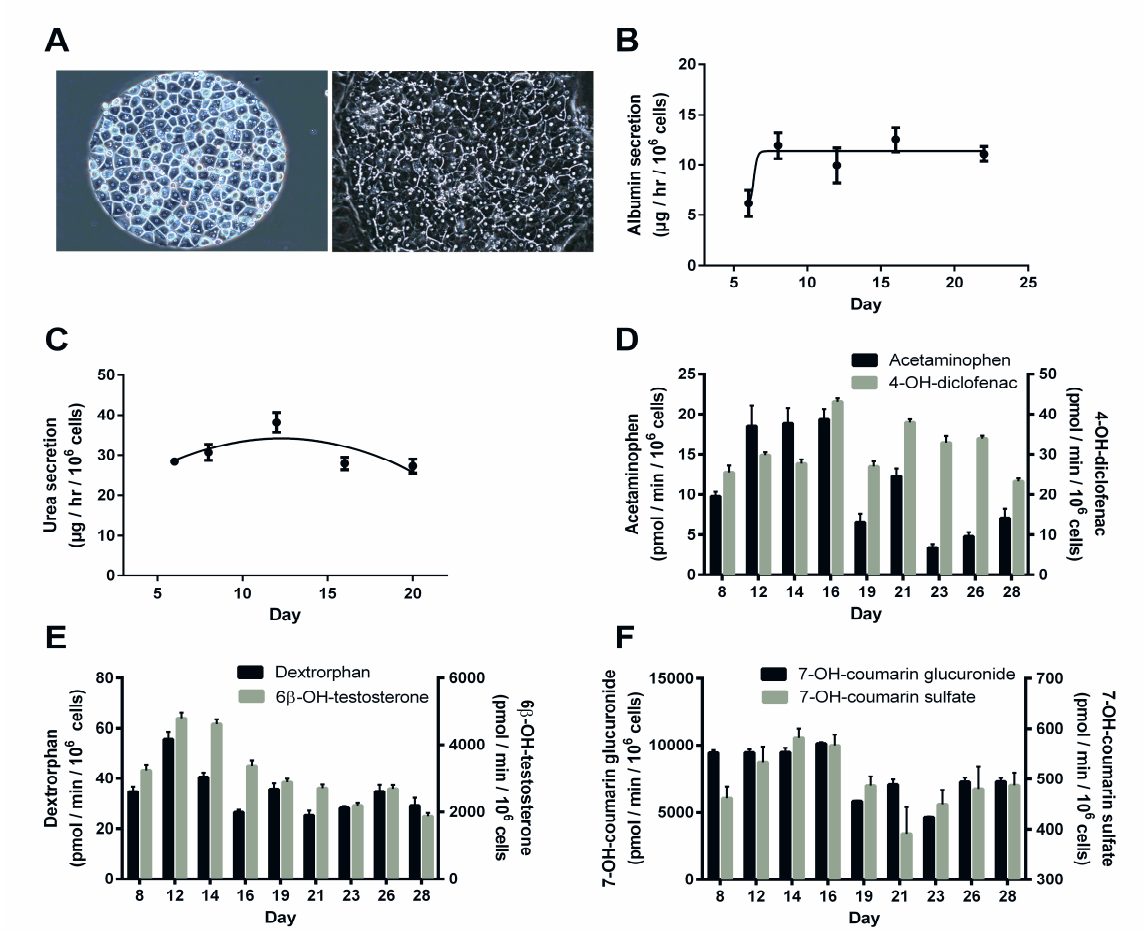

Figure 4.5.1 Functional characterization of MPCCs created using the JNB cryopreserved PHH donor. (A) Phase contrast micrographs of patterned PHHs on the day of seeding prior to seeding of the 3T3-J2 murine embryonic fibroblasts (left) and 10d in co-culture (right). Cultures showed similar hepatic morphology for at least 4 weeks (not shown). (B-C) Albumin and urea secretion rates in MPCCs over time in culture. (D-E) Quantification of CYP-generated metabolites from MPCCs. *CYP, probe substrate, metabolite measured:* 1A2, phenacetin, acetaminophen; 2C9, diclofenac; 4-OH-diclofenac; 2D6, dextromethorphan, dextrorphan; 3A4, testosterone, 6b-OH-testosterone. (F) Production rates of glucuronide and sulfate metabolites of 7-hydroxycoumarin from MPCCs. Error bars represent standard errors of the means (n=3).

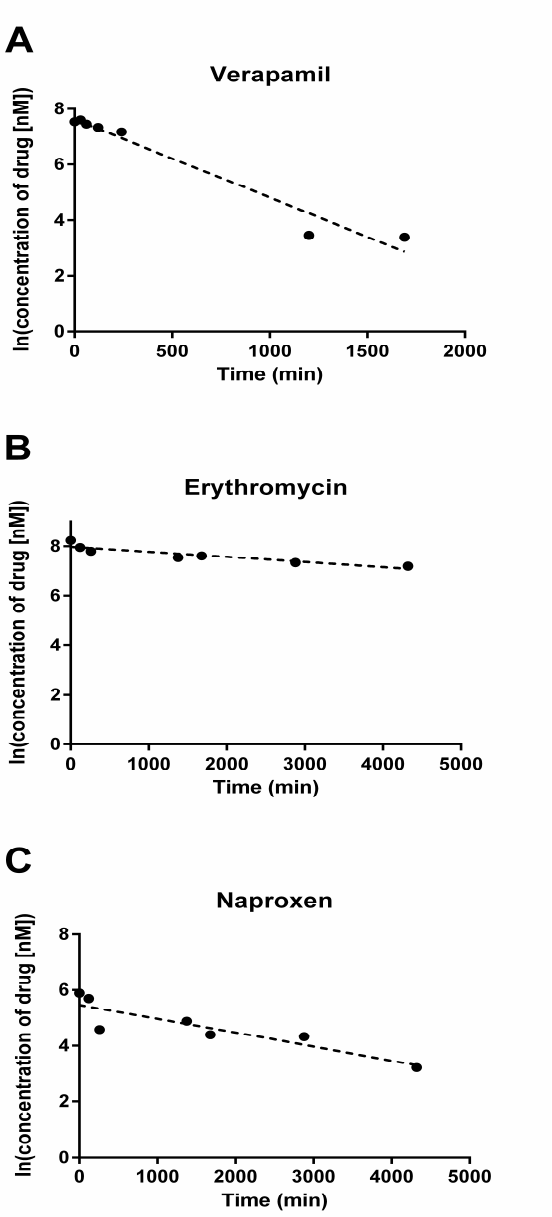

Figure 4.5.2 Substrate depletion in MPCCs created using the RTM cryopreserved PHH donor. (A) Verapamil (high-turnover), (B) erythromycin (medium-turnover), and (C) naproxen (low-turnover) depletion in MPCCs.

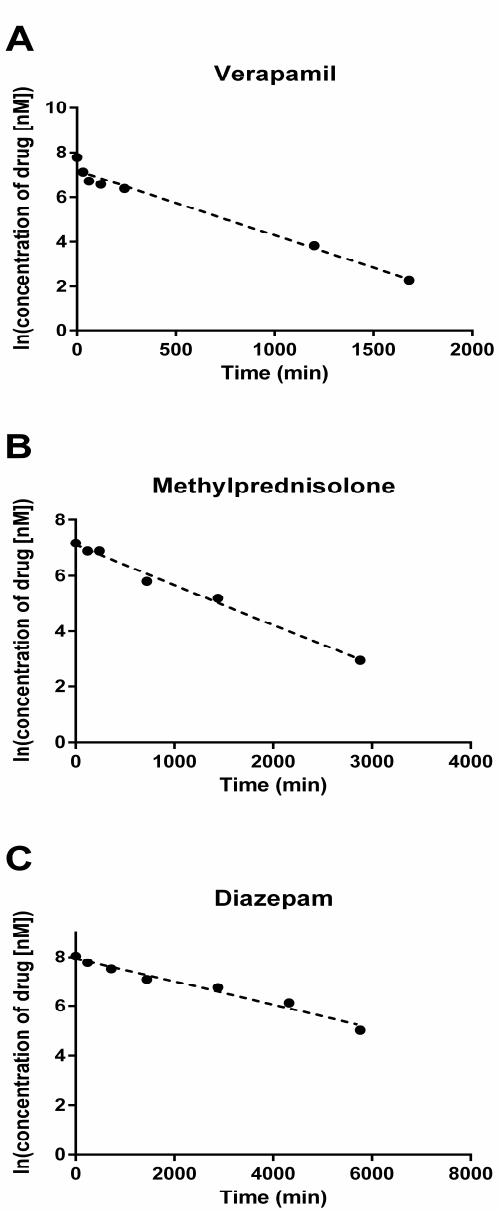

Figure 4.5.3 Substrate depletion in conventional monolayers created using the RTM cryopreserved PHH donor. (A) Verapamil (high-turnover), (B) methylprednisolone (medium-turnover), and (C) diazepam (low-turnover) depletion in conventional monolayers.

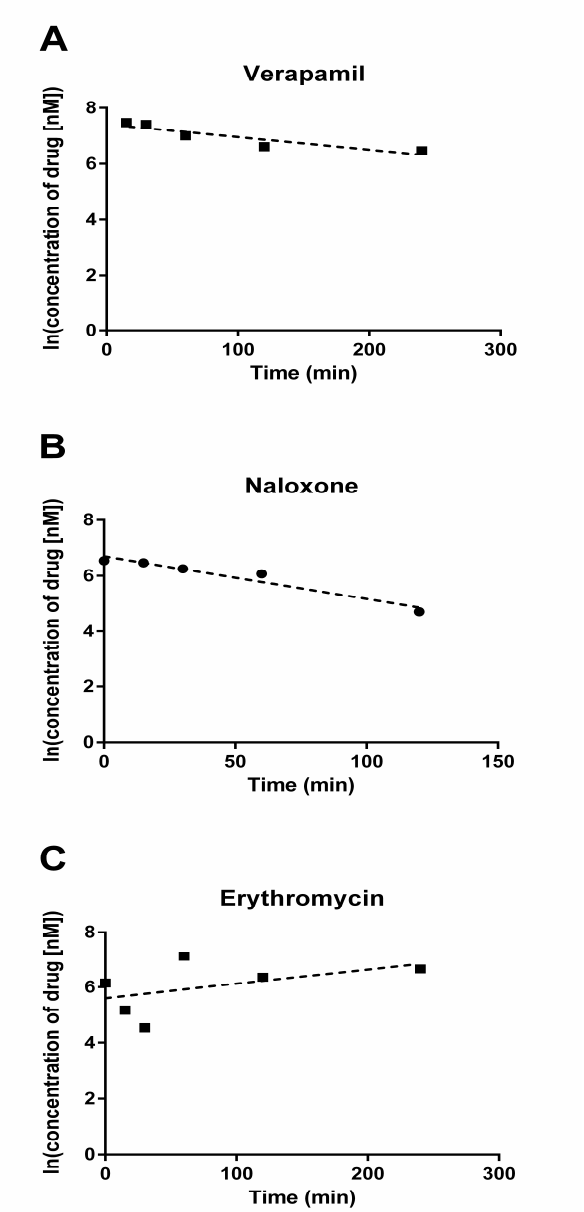

Figure 4.5.4 Substrate depletion in suspension cultures created using the RTM cryopreserved PHH donor. (A) Verapamil (B) naloxone (high-turnover) depletion in suspension cultures. (C) Erythromycin (medium-turnover) did not demonstrate metabolism in suspension cultures.

References

1. Wienkers LC, Heath TG. Predicting in vivo drug interactions from in vitro drug discovery data. Nat Rev Drug Discov 2005;4(10):825-33.

2. Ring BJ, Chien JY, Adkison KK, Jones HM, Rowland M, Jones RD, Yates JWT, Ku MS, Gibson CR, He H and others. PhRMA CPCDC initiative on predictive models of human pharmacokinetics, part 3: comparative assessement of prediction methods of human clearance. Journal of pharmaceutical sciences 2011;100(10):4090-4110.

3. Shih H, Pickwell GV, Guenette DK, Bilir B, Quattrochi LC. Species differences in hepatocyte induction of CYP1A1 and CYP1A2 by omeprazole. 1999;18(2):95-105.

4. Di L, Obach RS. Addressing the challenges of low clearance in drug research. The AAPS journal 2015;17(2):352-357.

5. Wilkening S, Stahl F, Bader A. Comparison of primary human hepatocytes and hepatoma cell line Hepg2 with regard to their biotransformation properties. Drug Metabolism and Disposition 2003;31(8):1035-1042.

6. Godoy P, Hewitt NJ, Albrecht U, Andersen ME, Ansari N, Bhattacharya S, Bode JG, Bolleyn J, Borner C, Böttger J and others. Recent advances in 2D and 3D in vitro systems using primary hepatocytes, alternative hepatocyte sources and non-parenchymal liver cells and their use in investigating mechanisms of hepatotoxicity, cell signaling and ADME. Archives of toxicology 2013;87(8):1315-1530.

7. Brown HS, Griffin M, Houston JB. Evaluation of cryopreserved human hepatocytes as an alternative in vitro system to microsomes for the prediction of metabolic clearance. Drug Metabolism and Disposition 2007;35(2):293-301.

8. Di L, Hsu IC, Trapa P, Tokiwa T, Obach RS, Bennett W, Atkinson K, Metcalf RA, Bi Y-A, Welsh JA and others. A novel relay method for determining low-clearance values. Drug metabolism and disposition: the biological fate of chemicals 2012;40(9):1860-1865.

9. Bi YA, Kazolias D, Duignan DB. Use of cryopreserved human hepatocytes in sandwich culture to measure hepatobiliary transport. Drug Metab Dispos 2006;34(9):1658-65.

10. Lecluyse EL. Human hepatocyte culture systems for the in vitro evaluation of cytochrome P450 expression and regulation. European journal of pharmaceutical sciences : official journal of the European Federation for Pharmaceutical Sciences 2001;13(4):343-368.

11. Khetani SR, Bhatia SN. Microscale culture of human liver cells for drug development. Nature biotechnology 2008;26(1):120-126.

12. Khetani SR, Berger DR, Ballinger KR, Davidson MD, Lin C, Ware BR. Microengineered liver tissues for drug testing. Journal of laboratory automation 2015;20(3):216-250.

13. Wang WW, Khetani SR, Krzyzewski S, Duignan DB, Obach RS. Assessment of a Micropatterned Hepatocyte Coculture System to Generate Major Human Excretory and Circulating Drug Metabolites. Drug metabolism and disposition: the biological fate of chemicals 2010;38(10):1900-1905.

14. Chan TS, Yu H, Moore A, Khetani SR, Tweedie D. Meeting the challenge of predicting hepatic clearance of compounds slowly metabolized by cytochrome P450 using a novel hepatocyte model, HepatoPac. Drug Metab Dispos 2013;41(12):2024-32.

15. Khetani SR, Kanchagar C, Ukairo O, Krzyzewski S, Moore A, Shi J, Aoyama S, Aleo M, Will Y. Use of micropatterned cocultures to detect compounds that cause drug-induced liver injury in humans. Toxicological sciences : an official journal of the Society of Toxicology 2013;132(1):107-117.

16. Berger DR, Ware BR, Davidson MD, Allsup SR, Khetani SR. Enhancing the functional maturity of induced pluripotent stem cell-derived human hepatocytes by controlled presentation of cell-cell interactions in vitro. Hepatology (Baltimore, Md) 2015;61(4):1370-1381.

17. Ramsden D, Tweedie DJ, Chan TS, Tracy TS. Altered CYP2C9 activity following modulation of CYP3A4 levels in human hepatocytes: an example of protein-protein interactions. Drug metabolism and disposition: the biological fate of chemicals 2014;42(11):1940-1946.

18. Obach RS, Baxter JG, Liston TE, Silber BM, Jones BC, MacIntyre F, Rance DJ, Wastall P. The prediction of human pharmacokinetic parameters from preclinical and in vitro metabolism data. The Journal of pharmacology and experimental therapeutics 1997;283(1):46-58.

19. Obach RS. Prediction of human clearance of twenty-nine drugs from hepatic microsomal intrinsic clearance data: An examination of in vitro half-life approach and nonspecific binding to microsomes. Drug Metabolism and Disposition 1999;27(11):1350-1359.

20. Lau YY, Sapidou E, Cui X, White RE, Cheng KC. Development of a novel in vitro model to predict hepatic clearance using fresh, cryopreserved, and sandwich-cultured hepatocytes. Drug Metabolism and Disposition 2002;30(12):1446-1454.

21. McGinnity DF, Soars MG, Urbanowicz RA, Riley RJ. Evaluation of fresh and cryopreserved hepatocytes as in vitro drug metabolism tools for the prediction of metabolic clearance. Drug Metabolism and Disposition 2004;32(11):1247-1253.

22. Obach RS, Lombardo F, Waters NJ. Trend Analysis of a Database of Intravenous Pharmacokinetic Parameters in Humans for 670 Drug Compounds. Drug Metabolism and Disposition 2008;36(7):1385-1405.

23. Brunton L, Chabner B, Knollman B. Goodman and Gilman's The Pharmacological Basis of Therapeutics, Twelfth Edition: McGraw-Hill Professional; 2011. 1808 p.

24. Koepsell H, Lips K, Volk C. Polyspecific organic cation transporters: structure, function, physiological roles, and biopharmaceutical implications. Pharmaceutical research 2007;24(7):1227-1251.

25. Hallifax D, Foster JA, Houston JB. Prediction of human metabolic clearance from in vitro systems: retrospective analysis and prospective view. Pharmaceutical research 2010;27(10):2150-2161.

26. Dash A, Inman W, Hoffmaster K, Sevidal S, Kelly J, Obach RS, Griffith LG, Tannenbaum SR. Liver tissue engineering in the evaluation of drug safety. Expert opinion on drug metabolism & toxicology 2009;5(10):1159-1174.

27. Blanchard N, Alexandre E, Abadie C, Lavé T, Heyd B, Mantion G, Jaeck D, Richert L, Coassolo P. Comparison of clearance predictions using primary cultures and suspensions of human hepatocytes. Xenobiotica; the fate of foreign compounds in biological systems 2005;35(1):1-15.

28. Smith CM, Nolan CK, Edwards MA, Hatfield JB, Stewart TW, Ferguson SS, LeCluyse EL, Sahi J. A comprehensive evaluation of metabolic activity and intrinsic clearance in suspensions and monolayer cultures of cryopreserved primary human hepatocytes. Journal of pharmaceutical sciences 2012;101(10):3989-4002.

29. Atkinson AJ, Kushner W. Clinical pharmacokinetics. Annual review of pharmacology and toxicology 1979;19:105-127.

30. Chao P, Barminko J, Novik E, Han Y, Maguire T, Cheng KC. Prediction of human hepatic clearance using an in vitro plated hepatocyte clearance model. Drug metabolism letters 2009;3(4):296-307.

31. Gorski JC, Vannaprasaht S, Hamman MA, Ambrosius WT, Bruce MA, Haehner-Daniels B, Hall SD. The effect of age, sex, and rifampin administration on intestinal and hepatic cytochrome P450 3A activity. Clinical pharmacology and therapeutics 2003;74(3):275-287.

32. Rae JM, Johnson MD, Lippman ME, Flockhart DA. Rifampin is a selective, pleiotropic inducer of drug metabolism genes in human hepatocytes: studies with cDNA and oligonucleotide expression arrays. The Journal of pharmacology and experimental therapeutics 2001;299(3):849-857.

33. Hariparsad N, Nallani SC, Sane RS, Buckley DJ, Buckley AR, Desai PB. Induction of CYP3A4 by efavirenz in primary human hepatocytes: comparison with rifampin and phenobarbital. Journal of clinical pharmacology 2004;44(11):1273-1281.

34. Williamson B, Dooley KE, Zhang Y, Back DJ, Owen A. Induction of influx and efflux transporters and cytochrome P450 3A4 in primary human hepatocytes by rifampin, rifabutin, and rifapentine. Antimicrobial agents and chemotherapy 2013;57(12):6366-6369.

35. Nguyen TV, Ukairo O, Khetani SR, McVay M, Kanchagar C, Seghezzi W, Ayanoglu G, Irrechukwu O, Evers R. Establishment of a hepatocyte-kupffer cell coculture model for assessment of proinflammatory cytokine effects on metabolizing enzymes and drug transporters. Drug Metab Dispos 2015;43(5):774-85.

Chapter 5

Microengineered co-cultures of primary human hepatocytes and Kupffer cells for investigating drug-induced liver injury[5]

Summary

Drug-induced liver injury (DILI) is the leading cause of drug attrition and acute liver failures in the US. Given species-specific differences in liver pathways, *in vitro* models of primary human hepatocytes (PHHs) are the gold standard for evaluating drug disposition. However, PHH monolayers display a rapid decline in hepatic functions and lack Kupffer cells (KCs) that are known to modulate hepatocyte responses to drugs. Thus, we established and characterized an *in vitro* platform that can keep both cryopreserved PHHs and KCs highly functional for several weeks, allowing modeling of inflammation effects on drug toxicity. Human KCs were seeded at physiologically-relevant ratios into micropatterned co-cultures (MPCC) containing PHHs and 3T3-J2 murine embryonic fibroblasts. While the addition of unstimulated KCs to MPCCs did not cause significant changes in hepatic functions, stimulation with bacterial lipopolysaccharide (LPS) for ~24 hours caused an upregulation of pro-inflammatory cytokines. These effects were verified in cultures where PHHs and KCs were obtained from the same human donor and from different donors. Modulation of hepatic functionality by a panel of 23 drugs was evaluated in MPCCs with a low KC density (normal) or a high KC density stimulated with LPS (inflamed). For 35% of the toxins, the inflamed model

[5] A manuscript similar to the work described in this chapter is in preparation and will be submitted for publication shortly.

demonstrated a more pronounced decrease in hepatic functionality compared to the normal model while differences between the two models were insignificant for non-toxins. Therefore, we have established an *in vitro* liver model with both PHHs and KCs that can be used for evaluating the effects of inflammatory stimuli on drug exposure.

5.1 Introduction

Drug-induced liver injury (DILI) is a leading cause of drug attrition and acute liver failures in the US[1]. Although some incidences of DILI can be assessed in preclinical animal studies or early clinical trials, other DILI reactions are termed idiosyncratic because they occur in a small percentage of the population and are not dose-dependent and thus, are less predictable. There are multiple reasons that an individual will react poorly to a drug. One hypothesized cause is that inflammation can sensitize the liver tissue, thus reducing the threshold for liver injury[1-3]. Additionally, elevated levels of pro-inflammatory cytokines, such as interleukin 6 (IL-6) and tumor necrosis factor α (TNF-α), can modulate drug metabolism enzymes in the liver (i.e. cytochrome P450s or CYP450s), thereby leading to altered drug disposition in disease-drug interactions[4]. Although the effects of individual cytokines on some CYP450 enzymes and transporters is well documented[5], the complete mechanisms of how inflammation affects drug disposition are not well defined. Some compounds may also disturb the redox balance and induce generation of reactive oxygen species (ROS), leading to oxidative stress, while other compounds can form metabolites that can react with proteins to form haptens, which can be identified by immune cells, causing sensitizing reactions[6]. Other factors that may be implicated in idiosyncratic DILI include metabolic polymorphisms, physiochemical properties of the drug, immunogenicity, environmental factors, and genetics. The incomplete molecular understanding of idiosyncratic DILI is partly due to a lack of models in which to study idiosyncratic DILI early

in the drug development process. Understanding the mechanisms underlying idiosyncratic DILI is important because hepatic injury can develop quickly and become life-threatening prior to the appearance of any physical symptoms[5,7].

Kupffer cells (KCs) are the primary macrophage population in the liver and play important roles in maintaining liver function by acting as scavenger cells to clear cell debris, macromolecules, and proteins from the circulating blood[6]. Exposure to high concentrations of such factors can lead to KC activation and the subsequent induction of inflammatory mediators such as cytokines, prostaglandins, leukotrienes, ROS, platelet activating factors, and nitric oxide, which can lead to enhanced liver sensitivity and affect a variety of hepatic functions. Thus, to study the mechanisms of how inflammatory mediators affect hepatocellular injury during idiosyncratic DILI, it is important to incorporate KCs into *in vitro* liver models for drug testing. Most protocols for KC isolation require sophisticated equipment and techniques so it has only been recently that cryopreserved KCs have been commercially available and thus, drug studies that utilize co-cultures of primary human hepatocytes (PHHs) and KCs are limited[8,9].

One such study established PHH and KC co-cultures in the micropatterned co-culture (MPCC) format to assess the impact of cytokines and cytokine modulators on co-cultures and hepatocyte-only control cultures[10]. MPCCs of PHHs and supportive murine embryonic 3T3-J2 fibroblasts have been previously demonstrated to keep PHHs functioning at high levels for multiple weeks, allowing for long-term drug studies[11,12]. Nguyen et al. showed that cytokines that are used as therapeutic proteins can alter the expression levels of CYP450s, transporters, and acute-phase proteins in hepatocytes. Although PHHs and KCs were co-cultured allowing for direct cell-to-cell contact, cells from mismatched human donors were utilized, it is unclear if 3T3-J2s were necessary to support PHH-KC co-cultures, and the model was not validated using

a panel of drugs that have demonstrated clinical evidence of increased hepatotoxicity in the presence of an inflamed liver. In a study by Cosgrove et al, synergistic effects between drugs and cytokines were observed for 19% of the hepatotoxins tested in human hepatocyte cultures without the use of KCs[13]. While this platform is useful to initially screen for candidate idiosyncratic drugs, it is unclear whether such a model would allow for mechanistic insights into the cause for toxicity as it lacks KCs and drug dosing was limited to 48 hours. Furthermore, clinical drug and cytokine exposure can be cyclical *in vivo*, which is difficult to recapitulate in such a short-term model.

Thus, to investigate the role primary human KCs play in idiosyncratic DILI, we utilized the MPCC-KC model that Nguyen et al used since this model kept both PHHs and KCs highly functional for several weeks *in vitro*[10]. First, we assessed whether co-culturing with 3T3-J2 fibroblasts was required to stabilize PHH-KC co-cultures or if KCs alone could stabilize PHHs. We then characterized both PHHs and KCs in the MPCC platform to determine whether utilizing PHHs and KCs from mismatched human donors resulted in significant functional differences of either cell type compared to using cells from matched donors. Next, we evaluated the effects lipopolysaccharide (LPS)-activated KCs had on hepatic functionality and toxicity over a dosing period of 6-8 days using a panel of 23 drugs. Finally, we took a subset of 7 drugs: 4 drugs for which inflammation exacerbated hepatotoxicity (chlorpromazine, clozapine, mexiletine, and trovafloxacin) and 3 non-toxins (aspirin, buspirone, and levofloxacin), to assess whether dosing with exogenous pro-inflammatory cytokines as Cosgrove et al demonstrated resulted in similar drug responses compared to activated KCs in the model[13].

5.2 Materials and methods

5.2.1 Cell processing

Cryopreserved PHHs were purchased from vendors permitted to sell products derived from human organs procured in the United States by federally designated Organ Procurement Organizations (BioreclamationIVT, Baltimore, MD; Triangle Research Laboratories, Research Triangle Park, NC). Information (lot classifier, age, sex, ethnicity, cause of death, available medical history) on the PHH lots utilized in this paper is provided in **Table 5.1**. PHHs were processed as previously described[12]. Briefly, the cells were thawed at 37°C for 120 seconds and transferred into pre-warmed cell seeding medium, the formulation of which has been described previously[12]. The cells were then spun at 50x*g* for 10 minutes, the supernatant was discarded, and the cells were re-suspended in hepatocyte seeding medium prior to assessment of viability using trypan blue exclusion (typically 80-95%). Liver-derived non-parenchymal cells were consistently found to be less than 1% of all the cells.

Cryopreserved KCs were obtained from BioreclamationIVT (Baltimore, MD). Donor information is provided in **Table 5.1** where available. KCs were thawed at 37°C for 120 seconds and transferred into cell seeding medium at ~23°C without glucocorticosteroids, as glucocorticosteroids can inhibit LPS-induced responses[14]. The cells were then spun at 800x*g* for 5 minutes, the supernatant discarded, and the cells were re-suspended in seeding medium prior to the assessment of viability using trypan blue exclusion (typically 80-95%).

Table 5.1 Demographics and available medical histories of the primary human hepatocyte and Kupffer cell donor lots used for the *in vitro* experiments. NA indicates that data is not available.

Lot Identifier (Vendor)	Cell Type	Age	Ethnicity	Sex	Cause of Death	Medical History	Abbreviation in Paper
IQV	Kupffer cell	NA	NA	M	NA	NA	
SSX	Kupffer cell	NA	NA	M	NA	NA	
LCU	Kupffer cell	80 yr	C	F	Cardiovascular arrest	No ETOH, tobacco, or drug use; Hysterectomy, prolapsed uterus x 5yrs; anxiety; arthritis in neck, legs, ankles; broken femur w/pins; hypertension; depression; COPD; stroke; Toxo IgG+; EBV-positive; Meds: Natural supplements, cayenne pepper, chia seeds, vitamin B injection, anxiety meds, Lotrel, Atenolol, Lorazepam, Paxil	KC1
THM	Hepatocyte						PHH1
HSS	Kupffer cell	10 mo	AA	M	Anoxia	No ETOH, tobacco, or drug use; No medical history	KC2
JLP	Hepatocyte						PHH2
Hum 4055A	Hepatocyte	54 yr	C	F	Stroke	1 wine/day; No drug or tobacco use; CMV+, EBV+	
Hum 4016	Hepatocyte	46 yr	C	M	Anoxia	No drug, alcohol or tobacco use	

5.2.2 Creation of micropatterned cultures

Micropatterned hepatocytes (MPHs) were created as previously described[15]. Briefly, type I rat-tail collagen at a concentration of 25 μg/mL in ddH_2O was adsorbed to industry-standard 24-well or 96-well tissue culture-treated polystyrene (TCPS) plates and lithographically-patterned using a polydimethylsiloxane mask to create 500-μm diameter circular domains with a center-to-center spacing of 1200-μm. PHHs that were processed as described above selectively attached to the collagen domains, leaving ~5,000 or ~30,000 attached PHHs within each well of a 96-well plate or 24-well plate, respectively. To create micropatterned hepatocytes with Kupffer cells (MPH-KCs), KCs were processed as described above and seeded at a density of 200,000 cells per well in a 24-well plate format 18 to 24 hours after seeding the PHHs.

To create MPCCs, 3T3-J2 murine embryonic fibroblasts were seeded at ~15,000 and ~90,000 cells per well in 96-well and 24-well formats, respectively, 18 to 24 hours after seeding of the PHHs[11]. To create MPCCs with KCs (MPCC-KCs), MPCCs were stabilized for ~1 week prior to KC seeding. KCs were seeded at physiologically-relevant ratios of 10 PHHs:1 KC (normal state) or 10 PHHs:4 KCs (inflamed state)[10,16]. To activate the KCs in the inflamed conditions, 50 ng/mL or 1 μg/mL of LPS was added to the cultures for 24 hours for characterization studies or continuously for drug dosing studies, respectively. To assess whether culturing PHHs and KCs from the same donor resulted in variable functionality of either cell type compared to culturing donor-mismatched cells, PHHs and KCs from the same donor or different donors (as indicated in **Table 5.1**) were obtained and seeded as described above prior to the assessment of functionality with and without 50 ng/mL of LPS stimulation. Serum-supplemented culture medium, the formulation of which has been described previously, was replaced on the cultures every 2 days[17].

5.2.3 Drug and cytokine treatments

MPCCs were stabilized for approximately 1 week prior to KC seeding as described above. MPCC-KCs were stabilized for an additional 2 days prior to drug dosing. A panel of 23 drugs consisting of 20 known hepatotoxins (herein referred to as toxins) and 3 non-liver-toxins (herein referred to a non-toxins) were incubated on cultures at a single concentration between 10 and 100xCmax (**Table 5.2**)[18]. All drugs were purchased from Sigma-Aldrich (St. Louis, MO), reconstituted in dimethyl sulfoxide (DMSO), and further diluted in serum-free culture medium comprising of Dulbecco's Modified Eagle's Medium (DMEM, Sigma-Aldrich), 15 mM HEPES buffer (Corning Cellgro, Manassas, VA), 1% vol/vol ITS+ supplement (Corning Life Sciences, Tewksbury, MA), 1% vol/vol penicillin-streptomycin (Corning Cellgro), and 100 nM glucagon (Sigma-Aldrich). Although glucocorticosteroids such as hydrocortisone and dexamethasone are commonly used for *in vitro* hepatocyte maintenance, they were omitted from the medium formulation since they can suppress LPS-induced activation of the KCs[14]. The normal cultures with a low KC density (10 PHHs:1 KC) were treated with the 23 drugs or the DMSO-only controls without LPS stimulation in the serum-free dosing medium. The inflamed MPCC-KC cultures with a high KC density (10 PHHs:4 KCs) were concurrently treated with 1 μg/mL LPS and each of the 23 drugs or the DMSO control with LPS in the serum-free dosing medium. Culture medium, drug, and LPS (in the inflamed cultures) were replaced every other day for 6-8 days. The DMSO concentration that the cultures were exposed to was kept between 0.1% and 0.5% (vol/vol) relative to the culture medium for all compounds and control cultures were treated with DMSO at corresponding concentrations. Cell culture supernatant was collected every other day for the assessment of alanine aminotransferase (ALT), lactate dehydrogenase (LDH), albumin, and urea secretion levels.

To assess if the presence of activated KCs could be recapitulated with the treatment of cultures with recombinant cytokines known to be secreted by KCs, MPCCs without KCs were simultaneously treated with a subset of 7 drugs and 10 μg/mL LPS, 100 ng/mL IFNγ, 20 ng/mL IL-1α, 20 ng/mL IL-6, and 100 ng/mL TNF-α; however, such a cytokine cocktail at the specified doses caused overt toxicity in the hepatocytes[13] (data not shown). Thus, the experiment was repeated and instead, cultures were treated with a subset of cytokines at lower doses chosen based on previously-obtained empirical data: 1 μg/mL LPS, 10 pg/mL TNF-α, and 600 pg/mL IL-6. MPCCs were treated every other day simultaneously with both the drug of interest and the cytokine mixture.

Table 5.2 Drugs used for toxicity experiments. The Cmax, Cmax used to treat the cultures, and percentage of DMSO used for each drug are specified.

Drug	Cmax [uM]	Concentration [xCmax]	% DMSO used
Diclofenac	8.032	25	0.1
Nortriptyline	0.122	50	0.1
Mebendazole	0.126	50	0.1
Nefazodone	0.859	25	0.1
Tamoxifen	0.162	25	0.1
Riluzole	1.652	50	0.1
Sulindac	31.986	50	0.2
Troglitazone	6.387	10	0.1
Ranitidine	1.425	50	0.1
Acetaminophen	151.177	25	0.1
Amiodarone	0.806	25	0.1
Trazodone	5.065	50	0.1
Bromfenac	16.4	50	0.2
Quinine	9.254	10	1
Phenacetin	13.401	75	1
Clarithromycin	3.34	50	0.2
Chlorpromazine	0.844	25	0.1
Clozapine	0.951	50	0.1
Mexiletine	3.18	50	0.1
Trovafloxacin	4.078	25	1
Aspirin	5.526	50	0.1
Buspirone	0.005	50	0.1
Levofloxacin	15.773	50	1

5.2.4 Hepatocyte functionality and toxicity assays

Cell viability was assessed using PrestoBlue (Life Technologies, Carlsbad, CA) following the manufacturer's protocol. Alanine aminotransferase (ALT) levels in the supernatant were assessed using a commercially-available colorimetric assay (Biovision, Milpitas, CA). Briefly, supernatant was collected and immediately processed according to the manufacturer's protocols and absorbance was obtained after 10 minutes and 1 hour of incubation. The difference in absorbance values was plotted against the standard curve to determine the amount of ALT activity. Secreted lactate dehydrogenase (LDH) was assessed using a colorimetric assay from

Pierce Biotechnology (Rockford, IL). Albumin levels were measured using an enzyme-linked immunosorbent assay (MP Biomedicals, Irvine, CA) with horseradish peroxidase detection and 3,3',5,5'-tetramethylbenzidine (TMB, Fitzgerald Industries, Concord, MA) as the substrate. Urea concentration in supernatants was assessed using a colorimetric endpoint assay utilizing diacetyl monoxime with acid and heat (Stanbio Labs, Boerne, TX). CYP3A4 activity in the cultures was measured using a luminescence-based assay by Promega (Madison, WI). Following incubation for 1 hour with the CYP3A4-glo substrate, luciferin-IPA, culture supernatants were processed according to manufacturer instructions and luminescence was measured. Absorbance and luminescence readings for the above-mentioned assays were obtained using a luminometer (BioTek, Winooski, VT).

5.2.5 Kupffer cell functionality assays

After stimulation of KC-only or MPCC-KC cultures with 50 ng/mL of LPS for 18-24 hours, IL-6 and TNF-α levels in supernatants were assessed using commercially-available ELISA kits (R&D Systems, Minneapolis, MN) (Saad *et al.*, 1995). Bioparticle uptake was utilized to assess the presence, location, and phagocytic ability of the KCs. PHrodo red *S. aureus* bioparticles (Life Technologies, Eugene, OR) were added to the wells at 1 mg/mL, incubated at 37˚C for 30 minutes, rinsed 3 times with 1X phosphate buffered saline (PBS), and imaged using a red fluorescent protein (RFP) light cube (excitation/emission: 560/585 nm) on an EVOS FL Imaging System (Life Technologies).

5.2.6 Data analysis

Each experiment was carried out twice with at least duplicate wells for each condition. Multiple PHH and KC donor lots (**Table 5.1**) were used to confirm trends. Data from

representative experiments are presented, whereas similar trends were observed in repeat experiments. Microsoft Excel and GraphPad Prism 7.0 (La Jolla, CA) were used for data analysis and graphing. For the drug dosing studies, albumin and urea data were normalized to the appropriate DMSO control. Error bars on graphs represent standard errors of the means. Statistical significance of the data was determined using Student's *t*-test or one-way ANOVA coupled with Tukey's post-hoc analysis ($p \leq 0.05$).

5.3 Results

5.3.1 Engineering a culture platform to stabilize both PHHs and KCs

Micropatterned hepatocytes (MPHs) were established without KCs or with 200,000 KCs per well (MPH+KCs) to assess if KCs alone could help stabilize hepatocyte morphology and functionality as compared to micropatterned co-cultures of hepatocytes and 3T3-J2 fibroblasts (MPCCs). Culture supernatant was collected every other day for the assessment of albumin and urea secretion levels while CYP3A4 activity was assessed on days 7 and 15. MPH+KCs did not help sustain albumin (**Figure 5.1A**) or urea (**Figure 5.1B**) secretion levels relative to MPH controls. Albumin levels for both MPHs and MPH+KCs were consistently at less than 7% of levels observed in MPCCs, whereas urea levels were initially similar to MPCCs, but declined quickly by day 5 of culture to less than 50% of the levels observed in MPCCs. CYP3A4 activity on both days 7 and 15 in MPH+KCs were lower than those in MPHs alone, while activity in both MPH+KCs and MPHs was lower than in MPCCs (**Figure 5.1C**). On day 7, CYP3A4 activities in MPHs and MPH+KCs were ~50% and ~7% of activity in MPCCs, respectively. By day 15, CYP3A4 activity increased in MPCCs and activity in MPHs dropped to ~14% of MPCCs while activity in MPH-KCs remained at ~7% of MPCCs. Phase contrast images of MPHs, MPH+KCs,

and MPCCs on day 8 of culture are shown in **Figure 5.1D**. Unlike the 3T3-J2s in MPCCs, KCs do not fill in around the hepatocyte islands and thus, do not facilitate controlled homotypic and heterotypic cell-cell interactions.

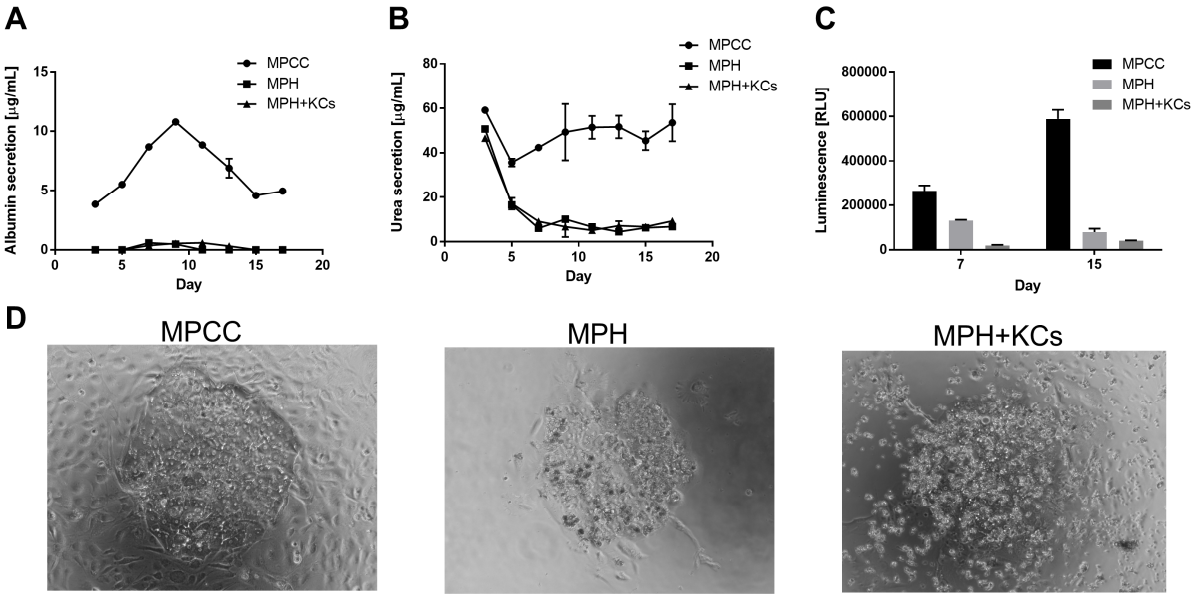

Figure 5.1 Kupffer cells (KCs) alone cannot help sustain the phenotype of micropatterned hepatocytes (MPHs). (A) Albumin secretion and (B) urea secretion levels in micropatterned co-cultures (MPCCs) of hepatocytes and 3T3-J2s. (C) CYP3A4 activity levels for the 3 conditions were assessed on days 7 and 15. (D) Phase contrast images of the 3 model types on day 8 of culture are shown.

5.3.2 Non-activated KCs do not negatively impact hepatocyte functionality in MPCCs

To verify that KCs do not affect hepatic functionality, MPCC-KCs were established at a ratio of 10 PHH:4 KCs and functions were compared to those measured in MPCC controls. The schematic in **Figure 5.2A** depicts an overview for creating MPCC-KCs. Phase contrast images from day 9 of culture are shown in **Figure 5.2B** with MPCC-only cultures on the left and MPCC-KC cultures on the right. Additionally, a bioparticle uptake assay was performed in

MPCC-only controls (left) and MPCC-KCs (right) on day 20 to confirm the presence, location, and phagocytic ability of KCs (**Figure 5.2C**).

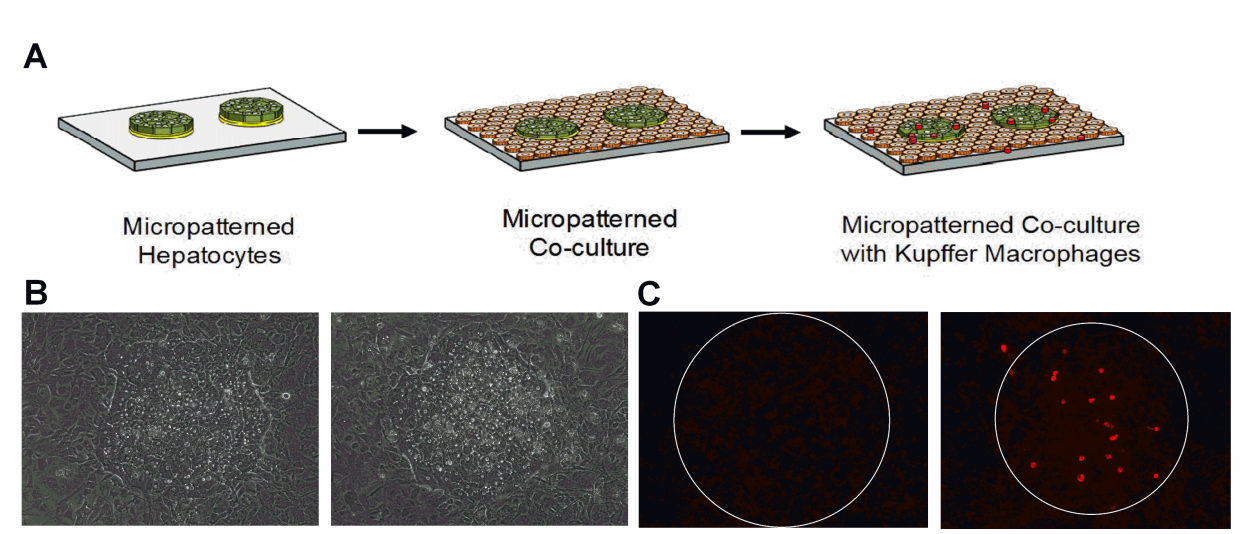

Figure 5.2 Micropatterned co-cultures with Kupffer cells (MPCC-KCs). (A) The creation of MPCC-KCs starts with collagen coating and patterning industry-standard tissue culture plates. Primary human hepatocytes (PHHs) attach to the collagen domains while 3T3-J2 fibroblasts seeded 18-24 hours post hepatocyte seeding attach to the areas surrounding the PHH islands. MPCCs are then stabilized for approximately 1 week prior to KC seeding. (B) Phase contrast images of MPCCs (left) and MPCC-KCs (right) on day 9 of culture are shown. (C) The bioparticle uptake assay performed on day 20 of culture demonstrates that KCs are present and functioning.

Culture supernatant was collected every other day for 19 days for the assessment of albumin and urea secretion levels. The secretion of albumin and urea between non LPS-stimulated MPCC-only cultures and MPCC-KCs were similar as shown in **Figures 5.3A and 5.3B**. TNF-α (**Figure 5.3C**) and IL-6 (**Figure 5.3D**) secretion levels in the supernatant were assessed on days 9, 12, 17, and 20 after MPCCs and MPCC-KCs were stimulated with 50 ng/mL of LPS on days 8, 11, 16, and 19 for 24 hours. MPCC-only cultures did not secrete TNF-α and showed low levels (≤50 pg/mL) of IL-6, whereas MPCC-KC cultures displayed ~6 to 20-fold higher levels of both TNF-α (~0-10 pg/mL) and IL-6 (~50-350 pg/mL). KC endotoxin tolerance

was observed where the LPS stimulations on days 11 and 19 resulted in decreased secretion of TNF-α and IL-6 as compared to the day 8 and 16 stimulations.

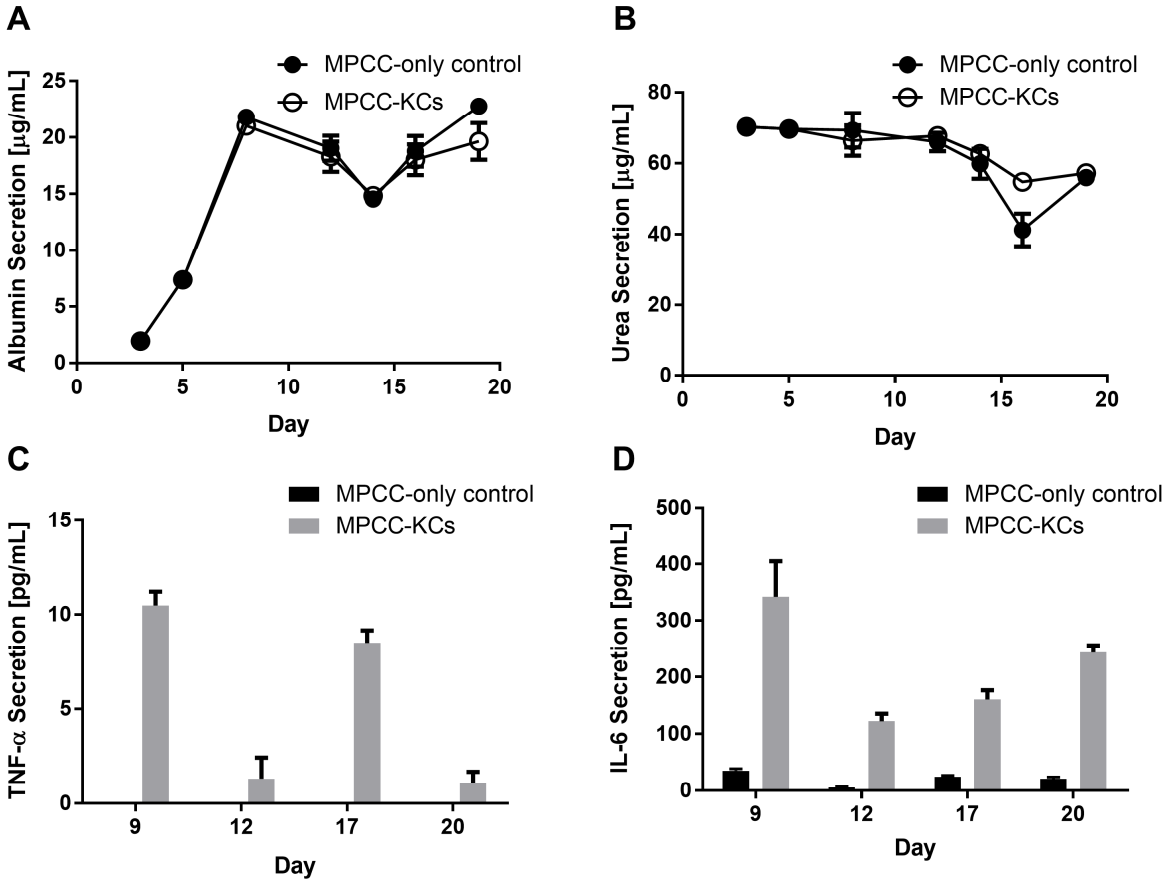

Figure 5.3 Kupffer cells (KCs) do not significantly down-regulate hepatic functions in micropatterned co-cultures (MPCCs). (A) Albumin and (B) urea secretion levels in MPCC-only controls and MPCC-KCs are shown over the course of 19 days with KCs seeded on day 5. (C) TNF-α and (D) IL-6 secretion levels in MPCC-only and MPCC-KC cultures after 50 ng/mL LPS stimulation on days 8, 11, 16, and 19 for 24 hours.

5.3.3 Comparing donor matched and mismatched PHHs and KCs

MPCC-KCs were created using PHHs (donor 1 lot: THM and donor 2 lot: JLP) and KCs (donor 1 lot: LCU and donor 2 lot: HSS) from the same donor (THM-LCU and JLP-HSS) and from different donors (THM-HSS and JLP-LCU) (**Table 5.1**) to assess differences in hepatic and macrophage functional levels between the two conditions. KCs were seeded at a ratio of 10

PHHs:4 KCs after MPCCs had been established for 5 days. MPCC-only and KC-only controls were also established as controls. Results from day 12 of culture are shown in **Figure 5.4** with similar trends observed throughout the time-series. No significant differences were observed in albumin (**Figure 5.4A**) or urea (**Figure 5.4B**) secretion levels across MPCC-only controls, MPCCs created using matched donors, and MPCCs created using mismatched donors. For PHH donor 1, there was a significant difference in CYP3A4 activity between the matched and mismatched-donor conditions. Additionally, both conditions were significantly different from the MPCC-only control with the matched donor condition at ~82% and the mismatched condition at ~57% of the MPCC-only control. On the other hand, PHH donor 2 did not show a significant difference between the matched and mismatched donor conditions, but both were significantly different than the MPCC-only control with the matched donor condition at ~74% and the mismatched condition at ~70% of the MPCC-only control (**Figure 5.4C**). When KC-only cultures and MPCC-KC cultures created using matched and mismatched donors were stimulated on day 11 with 50 ng/mL of LPS for 24 hours, IL-6 secretion levels on day 12, as shown in **Figure 5.4D**, demonstrated that for both donors, there were no significant differences observed between the matched and mismatched donor conditions. However, both of the matched and mismatched donor conditions were significantly different than the KC-only controls, suggesting that KCs respond more robustly to LPS stimulation when they are co-cultured with stabilized PHHs in MPCCs. TNF-α secretion showed similar trends to IL-6 secretion (data not shown). Overall, using mismatched PHH and KC donors results in similar functions as the matched donors for both cell types across multiple donors.

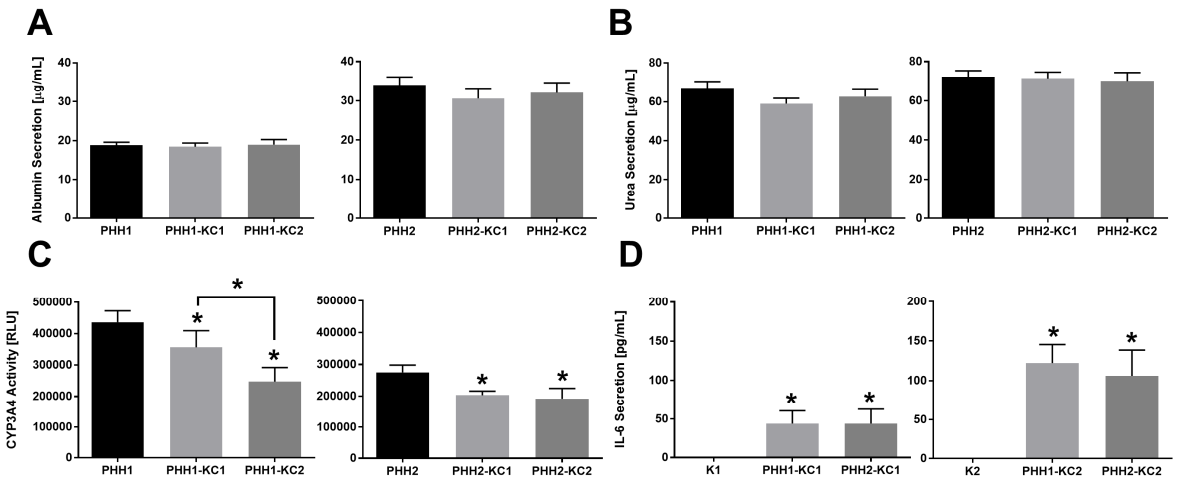

Figure 5.4 Micropatterned co-cultures (MPCCs) created using primary human hepatocytes (PHHs) and Kupffer cells (KCs) from the same versus different donors does not significantly affect hepatocyte or macrophage functionality. (A) Albumin and (B) urea secretion in MPCC-only and MPCC with matched donor KCs and mismatched donor KCs are shown for 2 different donors (1 and 2) on day 12 of culture. No significant differences were observed. (C) CYP3A4 activity was assessed on day 12 after 50 ng/mL LPS stimulation on day 11 for 24 hours. Asterisks on individual bars indicate significant differences from the MPCC control (black bar), whereas the asterisk on the bracket indicates that the 2 indicated bars are significantly different from each other. (D) IL-6 secretion levels were assessed on day 12 after 50 ng/mL LPS on day 11 for 24 hours. Asterisks on the individual bars indicate statistically-significant differences as compared to the KC-only controls. *$p \leq 0.05$.

5.3.4 Comparing hepatic functionality and toxicity using levofloxacin and trovafloxacin as a case study

Normal and inflamed MPCC-KC cultures were established as described earlier. Briefly, MPCCs were seeded and stabilized prior to KC seeding on day 7 with a PHH:KC ratio of 10:1 for normal cultures and 10:4 for inflamed cultures. Starting on day 9, the inflamed cultures were simultaneously stimulated with 1 µg/mL LPS and treated with the two drugs while the normal cultures were treated with the drugs only. Freshly-prepared levofloxacin at 50xCmax or trovafloxacin at 25xCmax with or without LPS was added to the cultures every other day for 6 days. ALT was assessed on day 15 (**Figure 5.5A**) and demonstrated similar levels in both the normal and inflamed cultures treated with levofloxacin and normal cultures treated with

trovafloxacin. In contrast, the inflamed cultures treated with trovafloxacin showed a 2.3-fold increase in ALT compared to the normal cultures treated with trovafloxacin. LDH was measured on day 13 with significant differences between the normal and inflamed cultures treated with both levofloxacin and trovafloxacin (**Figure 5.5B**). Cell viability was assessed on day 15 with significant differences between the normal and inflamed cultures treated with both levofloxacin and trovafloxacin (**Figure 5.5C**). Specifically, cell viability increased by 30% when the inflamed model was treated with levofloxacin, whereas viability decreased by 51% in the trovafloxacin-treated inflamed cultures compared to the normal cultures treated with the respective drugs. Albumin (**Figure 5.5D**) and urea (**Figure 5.5E**) levels were evaluated on day 17 and normalized to the control cultures without drugs. While there were no significant differences between the normal and inflamed cultures when they were treated with levofloxacin, toxicity was observed when the cultures were treated with trovafloxacin. Specifically, trovafloxacin caused a 94% reduction in albumin secretion levels and a 67% reduction in urea secretion levels in the inflamed cultures as compared to the normal cultures treated with the respective drugs. Downregulation of hepatic functionality precedes upregulation in hepatic toxicity markers and thus, albumin and urea secretion levels were measured for the other 21 drugs that were assessed in this study.

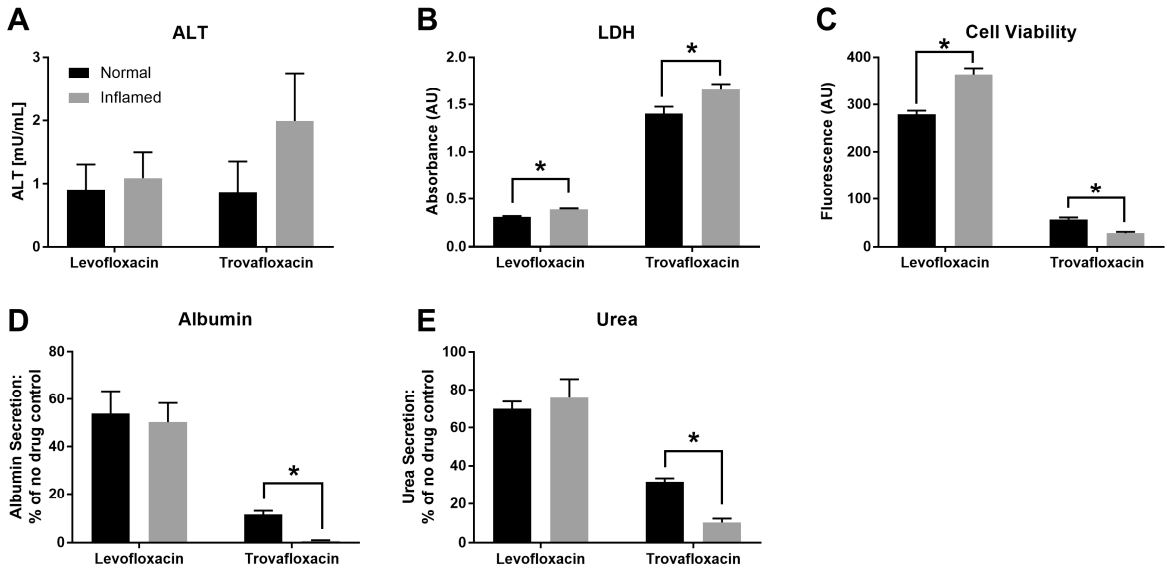

Figure 5.5 Hepatotoxicity and functionality endpoints after dosing with 50xCmax levofloxacin and 25xCmax trovafloxacin in the normal and inflamed cultures. (A) Alanine aminotransferase (ALT) levels 6 days post dosing, (B) lactate dehydrogenase (LDH) levels 4 days post dosing, and (C) cell viability 6 days post dosing are shown. (D) Albumin and (E) urea secretion levels after 8 days of dosing indicate no significant differences for levofloxacin between the normal and inflamed models, but a significant decrease in function for trovafloxacin in the inflamed model compared to the normal model. Asterisks on the brackets indicate that the 2 indicated bars are significantly different from each other. *$p \leq 0.05$.

5.3.5 Drug modulation of hepatic functionality in the normal versus inflamed MPCC-KC models

Normal and inflamed MPCC-KC cultures were established as described earlier. Freshly-prepared drug solution with or without 1 μg/mL LPS was added every other day for 6 days. A panel of 23 drugs was chosen with 20 prototypical hepatotoxins and 3 non-liver-toxins (aspirin, buspirone, and levofloxacin). One concentration between 10 and 100xCmax was chosen for each drug to ensure no overt toxicity was seen (**Table 5.2**). Albumin and urea secretion levels were assessed as markers of toxicity and normalized to the appropriate DMSO control without LPS for the normal cultures and with LPS for the inflamed cultures. Out of the 20 toxins tested, 7 demonstrated increased drug-induced downregulation of albumin and urea in the inflamed model

compared to the normal model (**Figure 5.6**). After normalizing to the respective controls, there was a 29%, 38%, 25%, 37%, 49%, 91%, and 22% difference in albumin secretion levels and a 39%, 31%, 23%, 20%, 44%, 39%, and 10% difference in urea secretion levels between the normal and the inflamed cultures dosed with chlorpromazine, clozapine, mexiletine, trovafloxacin, nefazodone, acetaminophen, and bromfenac, respectively. On the other hand, there were no significant decreases in functional levels between the normal and inflamed cultures when treated with the 3 non-toxins (aspirin, buspirone, and levofloxacin). Additionally, albumin and urea secretion levels were above the 50% toxicity cut-off for the non-toxic compounds, demonstrating the specificity of this test[18,19].

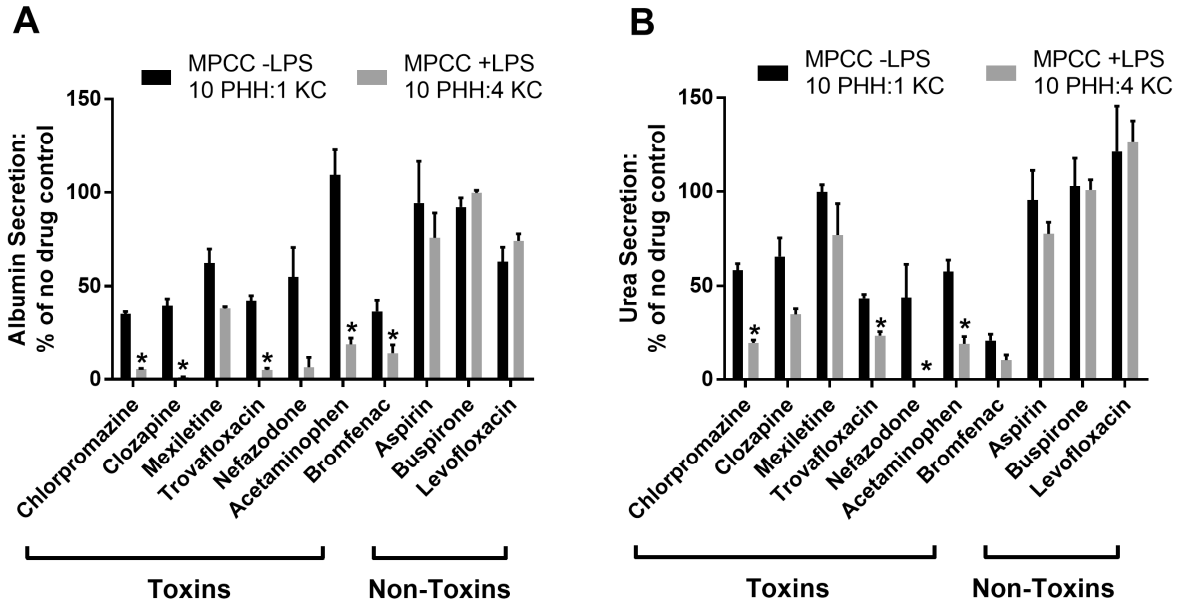

Figure 5.6 A panel of 23 drugs (20 toxins and 3 non-toxins) were incubated on normal (10 PHH:1 KC, no LPS) and inflamed (10 PHH:4 KC, 1 µg/mL LPS) cultures. Out of the 20 toxins, 7 demonstrated differences in albumin and urea secretion levels between the normal and inflamed models. (A) Albumin and (B) urea secretion levels were assessed and normalized to the appropriate DMSO controls. Asterisks indicate significant differences between the normal and inflamed cultures. *$p \leq 0.05$.

5.3.6 Exogenous cytokines can mimic the toxicity seen in MPCC-KCs

To assess if a mixture of cytokines could be used in lieu of cryopreserved KCs for the assessment of inflammation-mediated adverse drug effects, we treated MPCCs (without KCs) simultaneously with a mixture of cytokines at concentrations cryopreserved KCs secrete and a subset of 7 drugs (4 toxins: chlorpromazine, clozapine, mexiletine, and trovafloxacin; 3 non-toxins: aspirin, buspirone, and levofloxacin); the toxicity in these cytokine-treated MPCCs was compared to the results obtained using MPCC-KC cultures. A cytokine mixture (10 μg/mL LPS, 100 ng/mL IFNγ, 20 ng/mL Il-1α, 20 ng/mL IL-6, and 100 ng/mL TNF-α) based off of a previous study was used initially but caused significant toxicity (data not shown) so the cytokine components and concentrations were altered[13]. MPCCs were instead, treated with fresh 1 μg/mL LPS, 10 pg/mL TNF-α, and 600 pg/mL IL-6, and the panel of 7 drugs every other day for 6 days. Clozapine, mexiletine, aspirin, buspirone, and levofloxacin were at 50xCmax, whereas chlorpromazine and trovafloxacin were at 25xCmax due to significant toxicity observed at 50xCmax in preliminary experiments. An MPCC model without cytokines but dosed with the same panel of 7 drugs was utilized as the control. As shown in **Figure 5.7**, similar trends as the inflamed MPCC-KCs were observed such that increased toxin-induced downregulation of hepatic functionality occurred in the conditions with the added cytokines as compared to the conditions without the cytokines. For the non-toxins, there were no significant decreases in albumin and urea secretion between the conditions with cytokines and the conditions without cytokines.

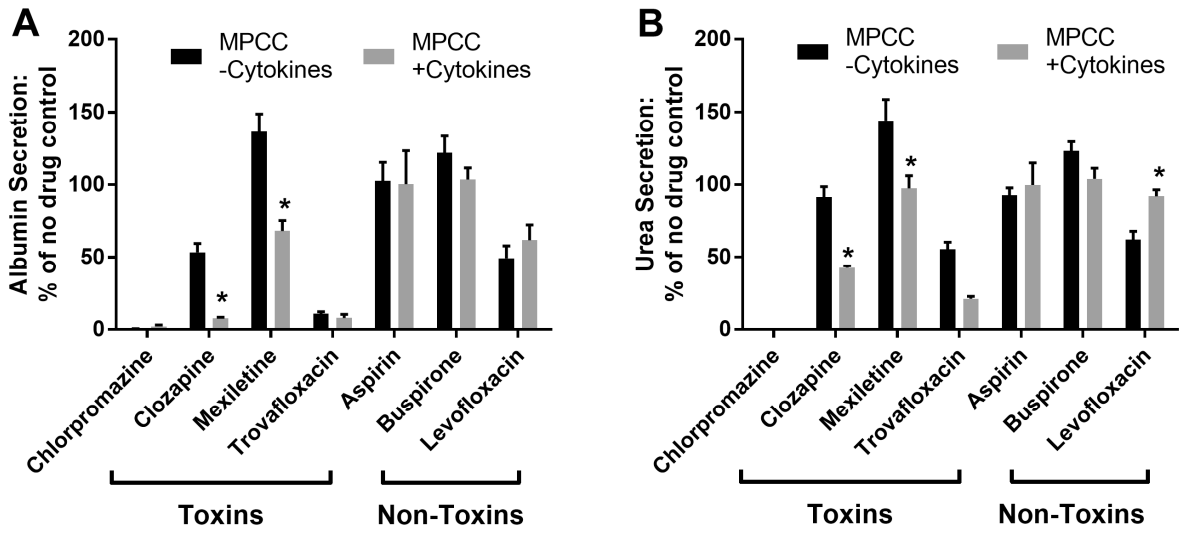

Figure 5.7 A panel of 7 drugs (4 toxins and 3 non-toxins) were dosed in MPCC-only cultures with and without simultaneous treatment with a mixture of exogenous cytokines: 1 µg/mL LPS, 10 pg/mL TNF-α, and 600 pg/mL IL-6. (A) Albumin and (B) urea secretion levels were assessed and normalized to the appropriate DMSO controls. Asterisks indicate significant differences between the models with and without cytokines. *$p \leq 0.05$.

5.4 Discussion

DILI is a leading cause of acute liver failure and drug withdrawal[1]. Although there are models available for the assessment of hepatotoxicity, there are some compounds that do not get flagged during *in vitro* screening, but can cause adverse reactions in select patients during clinical trials. This may be due to idiosyncratic DILI being caused by the interactions of liver parenchymal and non-parenchymal cells (NPCs), such as KCs. As the primary macrophages of the liver, KCs are responsible for systemic blood clearance through phagocytosis of cell debris, macromolecules, and endogenous and foreign entities. KCs can also present antigens to other cell types in the liver and secrete cytokines to communicate with the immune system during inflammation. Inflammation-mediated toxicity involving the innate and adaptive immune response is believed to be an important factor in idiosyncratic DILI but is not trivial to assess *in vitro* due to intra- and extrahepatic signaling as well as genetic factors[20,21]. Therefore, *in vitro*

models in which we can study the role of KC-mediated inflammation in idiosyncratic DILI are necessary.

Most hepatocyte-KC studies have utilized immortalized monocytic/macrophage cell lines, such as THP1[22,23] or U937[24-27], but it is unclear how comparable these cell lines are to primary macrophages. Schildberger et al found that upon LPS stimulation, THP-1 cells had a different cytokine release profile as compared to peripheral blood mononuclear cells (PBMCs), monocytes, or whole blood[28]. Additionally, although THP-1 and whole blood both secreted equal amounts of TNF-α after stimulation, conditioned media from the two conditions resulted in differing levels of subsequent human umbilical vein endothelial cell activation. Other groups have used freshly-isolated KCs from animals[29-33]. For example, one of the first studies in which porcine hepatocytes and KCs were co-cultured for the study of drug hepatotoxicity was by Hoebe et al. where hepatocyte-only and hepatocyte-KC cultures seeded at a 1:1 ratio were dosed with tiamulin and chlorpromazine[32]. While chlorpromazine caused higher toxicity in co-cultures as measured by mitochondrial activity due to increased secretion of TNF-α, IL-6, and ROS, there were no significant differences in toxicity between the hepatocyte-only culture and the hepatocyte-KC cultures for tiamulin[34]. In another study using porcine cells, co-cultures of hepatocytes and KCs were used to study the effects of anti-inflammatory substances[35] and how mycotoxins and LPS interact to affect cytokine levels[36,37].

Rodent and murine animal models[38-41], rat liver slices[42], and rat cells have also been utilized to study LPS-induced inflammatory responses and how it affects drug toxicity. For example, rats have been used to study the effects the TNF-α on LPS- and ranitidine-induced inflammatory liver injury[43]. Zinchenko and Coger was one of the first groups to micropattern rat hepatocytes and KCs to control cell-cell interactions[44]. Billiar et al showed that co-cultures of rat

hepatocytes and activated KCs may result in hepatocellular dysfunction[45,46]. Co-cultures of rat hepatocytes and KCs have been used to study downregulation of CYP1A2[47], drug-inflammation interactions[48], and the role of IL-6 in regulating insulin-like growth factors[49]. Rose et al developed and utilized a donor-matched rat co-culture model to assess hepatotoxicity in a panel of 6 drugs[50]. However, since there are significant differences between humans and animals in drug metabolism pathways, human-relevant models are required to assess drug disposition[51,52]. Additionally, it is difficult to assess complex cellular interactions that take place either simultaneously or sequentially in whole animal studies[53]. Thus, *in vitro* cultures of PHHs and KCs are ideal for the evaluation of human-relevant DILI outcomes and their interactions with inflammatory stimuli[51].

While most human-relevant models for drug toxicity screening include only hepatocytes[20], some groups have developed platforms that include KCs for drug screening applications. In one example, Long et al co-cultured PHHs and KCs in the LiverChip bioreactor platform and demonstrated that IL-6 was able to modulate CYP3A4 activity and C-reactive protein (CRP) secretion over 2 weeks[54]. Tocilizumab, an anti-IL-6R antibody, showed an effect on IL-6 signaling by de-suppressing CYP3A4 activity and decreasing CRP levels. The half-life of simvastatin hydroxy acid, a CYP3A4 substrate, was subsequently decreased. However, these PHH-KC co-cultures were stimulated with exogenous IL-6 rather than activating the KCs for endogenous IL-6 secretion, and no hepatocyte-only controls were assessed so it is uncertain what effects KCs alone would have on hepatic response to the stimulants. In another study by Kegel et al, PHHs and KCs were cultured separately[6]. The authors found that KCs treated directly with the hepatotoxins, acetaminophen and diclofenac, did not demonstrate significant activation based on reactive oxygen intermediate (ROI) production, but cytokine secretion was not assessed.

However, KCs treated with the supernatants of hepatocyte cultures that had been treated with acetaminophen and diclofenac were activated as assessed by ROI production and cytokine secretion. Cultures of hepatocytes and KCs were carried out separately and KCs were only able to be cultured for up to 5 days. Thus, cell-to-cell contact and signaling as it would occur *in vivo* could not be mimicked and the concentrations of the parent compound, metabolites, and other factors in the supernatants that would affect KCs is unknown. Cell-to-cell contact is important because co-cultures may demonstrate increased sensitivity to cytokine stimulation compared to hepatocyte- or KC-only cultures, augmenting hepatic injury[10,32]. Therefore, *in vitro* models that include both PHHs and KCs where KCs can be activated and secrete cytokines that may further sensitize hepatocytes to potential toxins is necessary to screen for drugs that may be toxic in a sub-population of patients. In this study, we developed and validated a model that incorporated both PHHs and KCs towards the screening of compounds for which inflammatory stimuli can exacerbate hepatocellular injury.

We first characterized the MPCC-KC model that had been utilized by Nguyen et al previously and confirmed that 3T3-J2s are required to stabilize hepatic functions[10]. For characterization studies, MPCCs were stabilized for approximately 1 week prior to KC seeding. Albumin and urea were assessed as biomarkers of hepatic functionality and found to be stable throughout the study[12]. IL-6 and TNF-α secretion levels were assessed for KC functionality since they have been shown to be two of the most important cytokines in the regulation of acute phase protein synthesis during inflammation[4,55]. Although stimulation with 50 ng/mL LPS in MPCC-only controls showed little to no secretion of IL-6 and TNF-α, MPCC-KCs displayed higher levels of IL-6 and TNF-α secretion. However, TNF-α concentration was frequently too low to be assessed. Other *in vitro* studies have shown that TNF-α levels peak quickly within the first

couple of hours and then decrease after 24-48 hours, which we have also confirmed (data not shown)[53]. We also observed that repeated exposure to LPS resulted in endotoxin tolerance where KCs secrete lower amounts of pro-inflammatory cytokines over time, which has been demonstrated in other studies[56,57]. In our study, the 4-day period between days 12 and 16 where the cells were not treated with LPS allowed the KCs to recover from tolerance and respond robustly to LPS stimulation again on day 16. This correlates with previous studies in which KC tolerance against LPS-stimulation was observed[58]. The extent to which IL-6 downregulated CYP3A4 activity in our MPCC-KC cultures compared to MPCC-only cultures (57%-82%) is comparable to other studies, indicating that the platform is responding to cytokines as expected[10,59].

Since other studies have indicated that there may be immune reactions due to incompatibility between using PHHs and KCs from 2 separate donors[6], we wanted to verify that using cells from different human donors didn't result in differential functions compared to using cells from the same donor. We did not observe significant differences in hepatic or macrophage functions when matched-donor or mismatched-donor cells were used. Donor differences with respect to cytokine secretion levels after KCs have been stimulated with LPS may be attributed to differences in the intestinal flora of the donors prior to cell isolation[60]. We also observed that KC-only cultures demonstrated lower and more inconsistent responses to LPS stimulation compared to MPCC-KC cultures, suggesting that hepatocytes, 3T3-J2s, or the combination of both cell types may help to stabilize KCs *in vitro*.

After characterization of cell functions, we demonstrated that the MPCC-KC platform could be used to assess hepatocellular toxicity in the presence or absence of LPS-stimulated KCs and recombinant cytokines known to be secreted by KCs. Toxicity (ALT, LDH, cell viability)

and functionality (albumin, urea) markers were first assessed using trovafloxacin and levofloxacin. We observed both significant downregulation of functionality as well as differences in toxicity. Thus, albumin and urea were assessed for an additional 21 drugs. However, changes in toxicity markers are also important as increasing levels of enzymes like aspartate transaminase (AST), ALT, and LDH are utilized clinically to diagnose various liver diseases. MPCC-KCs were treated with 20 toxins and 3 non-toxins and in the inflamed conditions, stimulated with 1 μg/mL of LPS 2 days post KC seeding[53]. For 35% of the toxins (7 out of 20), we observed a more drastic downregulation in hepatic functionality in the inflamed model as compared to the normal model, suggesting that KC-mediated inflammation can exacerbate hepatocellular injury. For the other 65% of the toxins, the inflamed model did not demonstrate increased toxicity compared to the normal model, suggesting that there are other mechanisms of toxicity causing idiosyncratic injury. Cosgrove et al had previously demonstrated that for a panel of 90 drugs that were dosed in PHH cultures with cytokines for up to 48 hours, 19% of the toxins and 3% of the non-toxins showed synergistic drug-cytokine hepatotoxicity[13]. The lower percentage of drugs that demonstrated synergistic effects may be due to the shorter drug treatment period as compared to our study and the use of exogenous cytokines rather than activated KCs. We also assessed drug-cytokine synergy by treating MPCCs (without KCs) with 4 toxins (chlorpromazine, clozapine, mexiletine, trovafloxacin) and 3 non-toxins (aspirin, buspirone, levofloxacin) in the presence of a mixture of recombinant cytokines that are known to be secreted by KCs. We found that treatment with recombinant cytokines was sufficient to mimic drug toxicity effects observed in MPCC-KC inflamed cultures. Nonetheless, the presence of live KCs may be important when one wants to study intercellular interactions, the actual concentration of many signals and factors that are released by KCs, the time sequence, and

resulting type of cellular damage. For example, activated KCs secrete a multitude of cytokines and treating PHHs with all of these recombinant cytokines to mimic *in vivo* temporal patterns that would be impractical[61]. The presence of KCs is also required for LPS-induced hepatic lipid accumulation which may be important for nutritional studies[57].

Our study and previous studies have demonstrated that activated KCs in co-culture with hepatocytes can affect drug disposition through various mechanisms. Drug exposure can directly stimulate the release of KC-derived factors, hepatocytes can metabolize drugs into intermediates which can then stimulate KCs, or drugs can cause hepatocellular injury which is then enhanced after exposure to KC-derived factors[5,53]. In this study, we have demonstrated the utility of the MPCC-KC model for the study of increased hepatocellular injury caused by activated KCs. Because this platform has the capability to mimic an inflammatory response by enabling cellular cross-talk, it is more physiologically-relevant than hepatocyte-only models. In the future, this model can be used in combination with high content imaging to identify the mechanistic pathways (mitochondrial injury, inflammation, and endoplasmic reticulum stress) that lead to increased DILI susceptibility in patients with concurrent or pre-existing liver inflammation[62]. By identifying how inflammatory stimuli can affect drug disposition, drug doses can then be adjusted, and biomarkers can be developed and validated for predicting the effects inflammation will have on drug disposition for a particular sub-population. This model can also be used in the screening of biologics in which a biologic targeting an inflammatory cytokine could result in increased CYP450 activity, increased drug clearance, reduced exposure, and diminished drug efficacy. In addition to drug screening, we anticipate that such a model can be used to study PHH-KC interactions in diseases such as liver steatosis, fibrosis, alcoholic liver disease, and hepatitis since studies have shown that such diseases can affect plasma endotoxin levels, which

may then affect drug disposition[63], and toxins that cause upregulation of cytokine secretion from KCs can affect downstream lipid metabolism[30]. Additionally, the platform can be combined with other liver NPC types or gut cells in a microfluidic device platform since the interactions amongst all of these cell types is important in modeling inflammation-mediated drug disposition[64]. Therefore, the model establishment and characterization presented in this study sets the stage for many future augmentations and lines of inquiry.

References

1. Kaplowitz N. Idiosyncratic drug hepatotoxicity. Nature reviews Drug discovery 2005;4(6):489-499.

2. Deng X, Lu J, Lehman-McKeeman LD, Malle E, Crandall DL, Ganey PE, Roth RA. p38 mitogen-activated protein kinase-dependent tumor necrosis factor-alpha-converting enzyme is important for liver injury in hepatotoxic interaction between lipopolysaccharide and ranitidine. J Pharmacol Exp Ther 2008;326(1):144-52.

3. Roth RA, Luyendyk JP, Maddox JF, Ganey PE. Inflammation and drug idiosyncrasy--is there a connection? J Pharmacol Exp Ther 2003;307(1):1-8.

4. Morgan ET. Impact of infectious and inflammatory disease on cytochrome P450-mediated drug metabolism and pharmacokinetics. Clin Pharmacol Ther 2009;85(4):434-8.

5. Aitken AE, Richardson TA, Morgan ET. Regulation of drug-metabolizing enzymes and transporters in inflammation. Annu Rev Pharmacol Toxicol 2006;46:123-49.

6. Kegel V, Pfeiffer E, Burkhardt B, Liu JL, Zeilinger K, Nussler AK, Seehofer D, Damm G. Subtoxic Concentrations of Hepatotoxic Drugs Lead to Kupffer Cell Activation in a Human In Vitro Liver Model: An Approach to Study DILI. Mediators Inflamm 2015;2015:640631.

7. Will Y, McDuffie JE, Olaharski AJ, Jeffy BD. Drug Discovery Toxicology: From Target Assessment to Translational Biomarkers. Hoboken, New Jersey: John Wiley & Sons; 2016.

8. Kitani H, Takenouchi T, Sato M, Yoshioka M, Yamanaka N. A simple and efficient method to isolate macrophages from mixed primary cultures of adult liver cells. J Vis Exp 2011(51).

9. Smedsrod B, Pertoft H, Eggertsen G, Sundstrom C. Functional and morphological characterization of cultures of Kupffer cells and liver endothelial cells prepared by means of density separation in Percoll, and selective substrate adherence. Cell Tissue Res 1985;241(3):639-49.

10. Nguyen TV, Ukairo O, Khetani SR, McVay M, Kanchagar C, Seghezzi W, Ayanoglu G, Irrechukwu O, Evers R. Establishment of a hepatocyte-kupffer cell coculture model for assessment of proinflammatory cytokine effects on metabolizing enzymes and drug transporters. Drug Metab Dispos 2015;43(5):774-85.

11. Khetani SR, Bhatia SN. Microscale culture of human liver cells for drug development. Nature biotechnology 2008;26(1):120-126.

12. Khetani SR, Kanchagar C, Ukairo O, Krzyzewski S, Moore A, Shi J, Aoyama S, Aleo M, Will Y. Use of micropatterned cocultures to detect compounds that cause drug-induced liver injury in humans. Toxicological sciences : an official journal of the Society of Toxicology 2013;132(1):107-117.

13. Cosgrove BD, King BM, Hasan MA, Alexopoulos LG, Farazi PA, Hendriks BS, Griffith LG, Sorger PK, Tidor B, Xu JJ and others. Synergistic drug-cytokine induction of hepatocellular death as an in vitro approach for the study of inflammation-associated idiosyncratic drug hepatotoxicity. Toxicol Appl Pharmacol 2009;237(3):317-30.

14. Wei SD, Li JZ, Liu ZJ, Chen Q, Chen Y, Chen M, Gong JP. Dexamethasone attenuates lipopolysaccharide-induced liver injury by downregulating glucocorticoid-induced tumor necrosis factor receptor ligand in Kupffer cells. Hepatol Res 2011;41(10):989-99.

15. Berger DR, Ware BR, Davidson MD, Allsup SR, Khetani SR. Enhancing the functional maturity of induced pluripotent stem cell-derived human hepatocytes by controlled presentation of cell-cell interactions in vitro. Hepatology (Baltimore, Md) 2015;61(4):1370-1381.

16. Sunman JA, Hawke RL, LeCluyse EL, Kashuba AD. Kupffer cell-mediated IL-2 suppression of CYP3A activity in human hepatocytes. Drug Metab Dispos 2004;32(3):359-63.

17. Lin C, Shi J, Moore A, Khetani SR. Prediction of Drug Clearance and Drug-Drug Interactions in Microscale Cultures of Human Hepatocytes. Drug metabolism and disposition: the biological fate of chemicals 2016;44(1):127-136.

18. Xu JJ, Henstock PV, Dunn MC, Smith AR, Chabot JR, de Graaf D. Cellular Imaging Predictions of Clinical Drug-Induced Liver Injury. Toxicological sciences : an official journal of the Society of Toxicology 2008;105(1):97-105.

19. Ware BR, Berger DR, Khetani SR. Prediction of Drug-Induced Liver Injury in Micropatterned Co-cultures Containing iPSC-Derived Human Hepatocytes. Toxicological sciences : an official journal of the Society of Toxicology 2015;145(2):252-262.

20. Atienzar FA, Blomme EA, Chen M, Hewitt P, Kenna JG, Labbe G, Moulin F, Pognan F, Roth AB, Suter-Dick L and others. Key Challenges and Opportunities Associated with the Use of In Vitro Models to Detect Human DILI: Integrated Risk Assessment and Mitigation Plans. Biomed Res Int 2016;2016:9737920.

21. Roth RA, Ganey PE. Intrinsic versus idiosyncratic drug-induced hepatotoxicity--two villains or one? J Pharmacol Exp Ther 2010;332(3):692-7.

22. Momen-Heravi F, Bala S, Kodys K, Szabo G. Exosomes derived from alcohol-treated hepatocytes horizontally transfer liver specific miRNA-122 and sensitize monocytes to LPS. Sci Rep 2015;5:9991.

23. Andriopoulos B, Pantopoulos K. Hepcidin generated by hepatoma cells inhibits iron export from co-cultured THP1 monocytes. J Hepatol 2006;44(6):1125-31.

24. Vernetti LA, Senutovitch N, Boltz R, Debiasio R, Shun TY, Gough A, Taylor DL. A human liver microphysiology platform for investigating physiology, drug safety, and disease models. Experimental biology and medicine (Maywood, N.J.) 2016;241(1):101-114.

25. Kenny O, O'Callaghan Y, O'Connell NM, McCarthy FO, Maguire AR, O'Brien NM. Oxidized derivatives of dihydrobrassicasterol: cytotoxic and apoptotic potential in U937 and HepG2 cells. J Agric Food Chem 2012;60(23):5952-61.

26. Costa S, Schwaiger S, Cervellati R, Stuppner H, Speroni E, Guerra MC. In vitro evaluation of the chemoprotective action mechanisms of leontopodic acid against aflatoxin B1 and deoxynivalenol-induced cell damage. J Appl Toxicol 2009;29(1):7-14.

27. O'Callaghan YC, Woods JA, O'Brien NM. Characteristics of 7 beta-hydroxycholesterol-induced cell death in a human monocytic blood cell line, U937, and a human hepatoma cell line, HepG2. Toxicol In Vitro 2002;16(3):245-51.

28. Schildberger A, Rossmanith E, Eichhorn T, Strassl K, Weber V. Monocytes, peripheral blood mononuclear cells, and THP-1 cells exhibit different cytokine expression patterns following stimulation with lipopolysaccharide. Mediators Inflamm 2013;2013:697972.

29. Hamada E, Nishida T, Uchiyama Y, Nakamura J, Isahara K, Kazuo H, Huang TP, Momoi T, Ito T, Matsuda H. Activation of Kupffer cells and caspase-3 involved in rat hepatocyte apoptosis induced by endotoxin. J Hepatol 1999;30(5):807-18.

30. Fang X, Gao G, Xue H, Zhang X, Wang H. In vitro and in vivo studies of the toxic effects of perfluorononanoic acid on rat hepatocytes and Kupffer cells. Environ Toxicol Pharmacol 2012;34(2):484-94.

31. Milosevic N, Maier P. Lead stimulates intercellular signalling between hepatocytes and Kupffer cells. Eur J Pharmacol 2000;401(3):317-28.

32. Hoebe KH, Witkamp RF, Fink-Gremmels J, Van Miert AS, Monshouwer M. Direct cell-to-cell contact between Kupffer cells and hepatocytes augments endotoxin-induced hepatic injury. Am J Physiol Gastrointest Liver Physiol 2001;280(4):G720-8.

33. Batai-Konczos A, Veres Z, Szabo M, Ioja E, Laszlo G, Torok G, Homolya L, Jemnitz K. Comparative study of CYP2B1/2 induction and the transport of bilirubin and taurocholate in rat hepatocyte-mono- and hepatocyte-Kupffer cell co-cultures. J Pharmacol Toxicol Methods 2016;82:1-8.

34. Hoebe KH, Monshouwer M, Witkamp RF, Fink-Gremmels J, van Miert AS. Cocultures of porcine hepatocytes and Kupffer cells as an improved in vitro model for the study of hepatotoxic compounds. Vet Q 2000;22(1):21-5.

35. Matis G, Kulcsar A, Petrilla J, Talapka P, Neogrady Z. Porcine hepatocyte-Kupffer cell co-culture as an in vitro model for testing the efficacy of anti-inflammatory substances. J Anim Physiol Anim Nutr (Berl) 2017;101(2):201-207.

36. Doll S, Schrickx JA, Danicke S, Fink-Gremmels J. Interactions of deoxynivalenol and lipopolysaccharides on cytokine excretion and mRNA expression in porcine hepatocytes and Kupffer cell enriched hepatocyte cultures. Toxicol Lett 2009;190(1):96-105.

37. Doll S, Schrickx JA, Valenta H, Danicke S, Fink-Gremmels J. Interactions of deoxynivalenol and lipopolysaccharides on cytotoxicity protein synthesis and metabolism of DON in porcine hepatocytes and Kupffer cell enriched hepatocyte cultures. Toxicol Lett 2009;189(2):121-9.

38. Poulsen KL, Olivero-Verbel J, Beggs KM, Ganey PE, Roth RA. Trovafloxacin enhances lipopolysaccharide-stimulated production of tumor necrosis factor-alpha by

macrophages: role of the DNA damage response. J Pharmacol Exp Ther 2014;350(1):164-70.

39. Zou W, Roth RA, Younis HS, Malle E, Ganey PE. Neutrophil-cytokine interactions in a rat model of sulindac-induced idiosyncratic liver injury. Toxicology 2011;290(2-3):278-85.

40. Lu J, Jones AD, Harkema JR, Roth RA, Ganey PE. Amiodarone exposure during modest inflammation induces idiosyncrasy-like liver injury in rats: role of tumor necrosis factor-alpha. Toxicological sciences : an official journal of the Society of Toxicology 2012;125(1):126-133.

41. Deng X, Stachlewitz RF, Liguori MJ, Blomme EA, Waring JF, Luyendyk JP, Maddox JF, Ganey PE, Roth RA. Modest inflammation enhances diclofenac hepatotoxicity in rats: role of neutrophils and bacterial translocation. J Pharmacol Exp Ther 2006;319(3):1191-9.

42. Olinga P, Merema MT, de Jager MH, Derks F, Melgert BN, Moshage H, Slooff MJ, Meijer DK, Poelstra K, Groothuis GM. Rat liver slices as a tool to study LPS-induced inflammatory response in the liver. J Hepatol 2001;35(2):187-94.

43. Tukov FF, Luyendyk JP, Ganey PE, Roth RA. The role of tumor necrosis factor alpha in lipopolysaccharide/ranitidine-induced inflammatory liver injury. Toxicol Sci 2007;100(1):267-80.

44. Zinchenko YS, Coger RN. Engineering micropatterned surfaces for the coculture of hepatocytes and Kupffer cells. Journal of biomedical materials research. Part A 2005;75(1):242-248.

45. Billiar TR, Curran RD, West MA, Hofmann K, Simmons RL. Kupffer cell cytotoxicity to hepatocytes in coculture requires L-arginine. Arch Surg 1989;124(12):1416-20; discussion 1420-1.

46. Billiar TR, Curran RD, Stuehr DJ, West MA, Bentz BG, Simmons RL. An L-arginine-dependent mechanism mediates Kupffer cell inhibition of hepatocyte protein synthesis in vitro. J Exp Med 1989;169(4):1467-72.

47. Wu R, Cui X, Dong W, Zhou M, Simms HH, Wang P. Suppression of hepatocyte CYP1A2 expression by Kupffer cells via AhR pathway: the central role of proinflammatory cytokines. Int J Mol Med 2006;18(2):339-46.

48. Tukov FF, Maddox JF, Amacher DE, Bobrowski WF, Roth RA, Ganey PE. Modeling inflammation-drug interactions in vitro: a rat Kupffer cell-hepatocyte coculture system. Toxicol In Vitro 2006;20(8):1488-99.

49. Lelbach A, Scharf JG, Ramadori G. Regulation of insulin-like growth factor-I and of insulin-like growth factor binding protein-1, -3 and -4 in cocultures of rat hepatocytes and Kupffer cells by interleukin-6. J Hepatol 2001;35(5):558-67.

50. Rose KA, Holman NS, Green AM, Andersen ME, LeCluyse EL. Co-culture of Hepatocytes and Kupffer Cells as an In Vitro Model of Inflammation and Drug-Induced Hepatotoxicity. Journal of Pharmaceutical Sciences 2016;105(2):950-964.

51. Olson H, Betton G, Robinson D, Thomas K, Monro A, Kolaja G, Lilly P, Sanders J, Sipes G, Bracken W and others. Concordance of the toxicity of pharmaceuticals in humans and in animals. Regulatory toxicology and pharmacology : RTP 2000;32(1):56-67.

52. Hamano T, Tong V, Mutai M, Hayashi M, Tanaka E. Kupffer cell-mediated cytotoxicity induced by lipopolysaccharide0111:B4 is greater in dogs than in rats and monkeys. J Toxicol Sci 2002;27(1):1-9.

53. Milosevic N, Schawalder H, Maier P. Kupffer cell-mediated differential down-regulation of cytochrome P450 metabolism in rat hepatocytes. European journal of pharmacology 1999;368(1):75-87.

54. Long TJ, Cosgrove PA, Dunn RT, 2nd, Stolz DB, Hamadeh H, Afshari C, McBride H, Griffith LG. Modeling Therapeutic Antibody-Small Molecule Drug-Drug Interactions Using a Three-Dimensional Perfusable Human Liver Coculture Platform. Drug Metab Dispos 2016;44(12):1940-1948.

55. Bieghs V, Trautwein C. The innate immune response during liver inflammation and metabolic disease. Trends Immunol 2013;34(9):446-52.

56. West MA, Manthei R, Bubrick MP. Autoregulation of hepatic macrophage activation in sepsis. J Trauma 1993;34(4):473-9; discussion 479-80.

57. Dembek A, Laggai S, Kessler SM, Czepukojc B, Simon Y, Kiemer AK, Hoppstadter J. Hepatic interleukin-6 production is maintained during endotoxin tolerance and facilitates lipid accumulation. Immunobiology 2017;222(6):786-796.

58. Hafenrichter DG, Roland CR, Mangino MJ, Flye MW. The Kupffer cell in endotoxin tolerance: mechanisms of protection against lethal endotoxemia. Shock 1994;2(4):251-6.

59. Dickmann LJ, Patel SK, Rock DA, Wienkers LC, Slatter JG. Effects of interleukin-6 (IL-6) and an anti-IL-6 monoclonal antibody on drug-metabolizing enzymes in human hepatocyte culture. Drug Metab Dispos 2011;39(8):1415-22.

60. Billiar TR, Maddaus MA, West MA, Dunn DL, Simmons RL. The role of intestinal flora on the interactions between nonparenchymal cells and hepatocytes in coculture. J Surg Res 1988;44(4):397-403.

61. Sarkar U, Ravindra KC, Large E, Young CL, Rivera-Burgos D, Yu J, Cirit M, Hughes DJ, Wishnok JS, Lauffenburger DA and others. Integrated assessment of diclofenac biotransformation, pharmacokinetics, and omics-based toxicity in a 3D human liver-immunocompetent co-culture system. Drug Metab Dispos 2017.

62. Laifenfeld D, Qiu L, Swiss R, Park J, Macoritto M, Will Y, Younis HS, Lawton M. Utilization of causal reasoning of hepatic gene expression in rats to identify molecular pathways of idiosyncratic drug-induced liver injury. Toxicol Sci 2014;137(1):234-48.

63. Ghanim H, Abuaysheh S, Sia CL, Korzeniewski K, Chaudhuri A, Fernandez-Real JM, Dandona P. Increase in plasma endotoxin concentrations and the expression of Toll-like receptors and suppressor of cytokine signaling-3 in mononuclear cells after a high-fat, high-carbohydrate meal: implications for insulin resistance. Diabetes Care 2009;32(12):2281-7.

64. Chen WLK, Edington C, Suter E, Yu J, Velazquez JJ, Velazquez JG, Shockley M, Large EM, Venkataramanan R, Hughes DJ and others. Integrated gut/liver microphysiological systems elucidates inflammatory inter-tissue crosstalk. Biotechnol Bioeng 2017;114(11):2648-2659.

Chapter 6

Hepatitis B and C infection in micropatterned co-cultures of induced pluripotent stem cell-derived human hepatocytes[6]

Summary

Hepatitis C virus (HCV) and hepatitis B virus (HBV) affect ~130-170 million and >250 million people worldwide, respectively, and chronic infection can lead to advanced liver diseases. Because preventative and therapeutic options are limited and costly, human liver models are essential for studying host-pathogen interactions to better understand disease and patient-specific pathogenesis towards developing better HCV and HBV therapies. While primary human hepatocytes (PHHs) are the gold standard for *in vitro* studies given differences between animals and humans in drug metabolism pathways and abnormal liver functions in immortalized cell lines, PHHs are a limited and expensive resource. Induced pluripotent stem cell-derived human hepatocyte-like cells (iPSC-HHs or iHeps) can mitigate the aforementioned limitations of existing liver cell sources, as well as provide an avenue to investigate inter-individual differences in viral disease progression and drug susceptibilities. Therefore, we have developed a functionally mature and stable micropatterned iPSC-HH coculture model that can be infected with both HCV and HBV, recapitulate the viral lifecycle, demonstrate a robust antiviral response, and has utility in drug development.

[6] A manuscript similar to the work described in this chapter is in preparation and will be submitted for publication shortly.

6.1 Introduction

Hepatotropic viruses are a worldwide problem with hepatitis C virus (HCV) affecting ~130-170 million people and hepatitis B virus (HBV) affecting >250 million people globally[1,2]. Chronic infection can lead to advanced liver diseases such as fibrosis, cirrhosis, and hepatocellular carcinoma[3]. Viral suppression can lead to decreased rates of liver complications and thus, effective treatments that improve liver histology are required. There are currently no vaccines available for HCV and the cost of existing HCV treatments is prohibitively high (~$1000/pill), which necessitates continued discovery of novel drugs that are more accessible to the developing world[4]. Additionally, these direct-acting antivirals (DAAs) are not pan-genotypic and how patients respond to the treatment regimens will depend on both host factors and viral genotype[5]. While prophylactic vaccines and nucleotide/nucleoside analog therapies are available for HBV, treatments are usually lifelong and do not fully cure chronically-infected patients due to the persistence and stability of covalently closed circular DNA (cccDNA)[6]. Thus, the presence of the suppressed virus leads to chronic liver inflammation that can still progress towards end-stage liver diseases[7].

HBV and HCV exhibit distinct life cycles, but both demonstrate narrow host and tissue tropism so human-relevant models are required for the study and identification of therapeutic targets. While animal models such as chimpanzees and tree shrews (*Tupaia belangeri*) have been utilized for the study of hepatitis, it is difficult to manipulate and analyze these large models for human relevance[8,9]. Specifically, real-time analysis of cellular parameters to gain insight into specific signaling pathways is impossible. There are also differences between animals and humans in drug metabolism pathways[10]. Thus, *in vitro* liver models are more commonly used for the study of hepatotropic viruses as the complexity of the model can be easily manipulated to

assess specific virological and cellular endpoints. Many *in vitro* studies utilize cancerous/immortalized cell lines, but cell lines display abnormal liver functions and do not always mount a physiologically-relevant antiviral response, which is important to study why some individuals demonstrate a sustained virologic response (SVR) to available viral therapies while other patients are non-responders[11,12]. Therefore, primary human hepatocytes (PHHs) are ideal for studying the viral lifecycle and virus-host interactions since their functions are closest to what is found *in vivo*. However, PHHs in conventional culture formats decline quickly in phenotype, losing their susceptibility to viral infection, and are a limited and expensive resource for high-throughput drug screening[13].

Induced pluripotent stem cell-derived human hepatocyte-like cells (iPSC-HHs or iHeps) can mitigate the aforementioned limitations of existing liver cell sources and potentially be used to investigate inter-individual differences in viral disease progression and drug susceptibilities[14,15]. However, hepatic functional levels in conventionally-differentiated iPSC-HHs are typically <10% of those observed in stable PHH cultures[16]. Towards addressing such a shortcoming, we have previously microengineered a more functionally mature and stable iPSC-HH culture model[16] and demonstrated its utility for drug screening[17]. We found that by controlling the homotypic and heterotypic cell-cell interactions between iPSC-HHs and 3T3-J2 murine embryonic fibroblasts, iPSC-HH functionality could be significantly enhanced and prolonged such that these micropatterned cocultures (iMPCCs) became highly sensitive for drug toxicity detection[17]. Maintenance of cellular polarity, host factors, and innate immunity may allow for viruses to better replicate its lifecycle as it occurs *in vivo*[18]. In this study, we sought to demonstrate infection of iPSC-HHs with both HBV and HCV in various formats in comparison to PHHs, show that a robust antiviral response can be obtained when iMPCCs were infected with

HCV, and that HCV-infected iMPCCs can be utilized to test clinically-relevant HCV drugs. We anticipate that in the future, this model can be utilized to study the pathogenesis of these hepatotropic diseases towards the development of vaccines. Additionally, panels of multiple iPSC-HH donors with various genetic polymorphisms can be used to investigate inter-individual responses to HBV and HCV drugs and thus, allow for the discovery and screening of novel compounds which can alleviate these global burdens.

6.2 Materials and methods

6.2.1 Cell processing

Cryopreserved vials of iPSC-HH/iHeps (commercially available as iCell and myCell hepatocytes) were obtained from Cellular Dynamics International (CDI, Madison, WI) and processed following CDI's protocols. Briefly, the vials were thawed at 37°C for 3 minutes and diluted with 10 mL of pre-warmed iHep thawing medium. The cell suspension was spun at 200x*g* for 3 minutes, the supernatant was discarded, the cells were re-suspended in iHep plating medium, and viability was assessed using trypan blue exclusion (typically 75–95%).

Cryopreserved PHHs were obtained from a vendor permitted to sell products derived from human organs procured in the United States by federally designated Organ Procurement Organizations (Triangle Research Laboratories, Research Triangle Park, NC). PHHs were processed as previously described[19]. The cells were first thawed at 37°C for 2 minutes and transferred into pre-warmed hepatocyte seeding medium. The cells were then spun at 50x*g* for 10 minutes, the supernatant was discarded, and the cells were resuspended in hepatocyte seeding medium prior to the assessment of viability using trypan blue exclusion (typically 80-95%). Liver-derived non-parenchymal cells were consistently found to be less than 1% of all the cells.

6.2.2 Establishing cell models

Standard 24-well tissue culture polystyrene (TCPS) plates were coated with 25 μg/mL of rat tail type 1 collagen for 2 hours at 37°C and rinsed twice with water. To create confluent conventional cultures of iHeps (iCCs) or PHHs (CCs), cells were processed as described above and seeded at ~500,000-600,000 cells per well. Random co-cultures of iHeps (iRCCs) or PHHs (RCCs) and 3T3-J2 murine embryonic fibroblasts were established by seeding either 30,000 (30k) or 100,000 (100k) hepatocytes per well in the collagen-coated TCPS plates and left overnight to attach. Within the next 1-5 days, 3T3-J2s were seeded at a density of 90,000 cells per well. To establish micropatterned iHeps (iMPHs) or PHHs (MPHs), the collagen-coated TCPS plates were lithographically patterned using a polydimethylsiloxane mask to create 500-μm diameter circular domains with a center-to-center spacing of 1200-μm as has been previously described[16]. The iHeps or PHHs selectively attached to the adsorbed collagen domains leaving ~30,000 attached cells within each well. To create micropatterned co-cultures of iHeps (iMPCCs) or PHHs (MPCCs), 90,000 3T3-J2 fibroblasts were seeded 5 days or 1 day later, respectively.

PHH and iHep cultures were maintained in culture medium as has previously been described[16]. In some cases, FPH2 (Sigma Aldrich, St. Louis, MO), a small molecule (SM), was included in the cell culture medium to help maintain the phenotype of the iHeps, as has been previously described[20]. CCs were infected on day 1 while RCCs and MPCCs were maintained for ~7 days prior to viral infection to allow for stabilization of functions. Unless otherwise indicated, iCCs and iMPHs were maintained for 5 days and iRCCs and iMPCCs were maintained for 11 days prior to viral infection due to the rapid decline in iHep phenotype in iCC and iMPH formats.

6.2.3 HBV infection of cultures

Cell culture-derived HBV at $1.4x10^{11}$ viral particles/mL was obtained from Dr. Jisu Li at Brown University. For 24-well format plates, 3 μL of the HBV stock was diluted in hepatocyte maintenance medium with 4% PEG-8000 to a total volume of 300 μL per well. For some conditions, a Janus kinase (JAK)-inhibitor (EMD Millipore, Burlington, MA) at 1 or 0.5 μM was added to the medium 24 hours prior to infection and during infection (pulse) or prior to infection through the end of the experiment (continuous)[14]. For all conditions, the virus was removed 24 hours after infection, the cultures were rinsed 3 times with medium, and fresh hepatocyte maintenance medium was added. Media was changed every other day and collected at 1 and 2 weeks post infection to quantify HBV e antigen (HBeAg) and surface antigen (HBsAg) using commercially-available ELISA kits (Cell Biolabs, San Diego, CA). Cultures were fixed at 2 weeks post infection for immunofluorescent staining of HBV core antigen (HBcAg)[21].

6.2.4 HCV infection of cultures

Cell culture-derived HCV (JFH-1 and Jc1 clones[22]) were obtained from Dr. Hugo Rosen at the University of Colorado at Denver and Dr. Raymond Chung at Massachusetts General Hospital and was propagated in Huh7.5.1 cells. The TCID50 of the Jc1 stock was $2.51\text{-}3.16x10^{-4}$ (TCID50/mL=31623-39811). The stock viral material was filtered through a 0.45-μm filter to remove cell debris prior to use. Cultures were infected with undiluted HCV inoculum for 24 hours before the virus was removed, the cultures rinsed 3 times with medium, and fresh medium added. Media was changed every other day and cultures were typically lysed 5-21 days post infection for assessment of intrahepatic HCV gene expression via quantitative PCR.

6.2.5 HCV drug studies

Interferon α-2A (IFNα-2A) and ribavirin were obtained from Sigma Aldrich (St. Louis, MO), daclatasvir and danoprevir were obtained from ApexBio (Houston, TX), and sofosbuvir was obtained from Santa Cruz Biotechnology (Dallas, TX). All drugs were reconstituted in dimethyl sulfoxide (DMSO) and the concentration of DMSO in the dosing culture media was kept at 0.1% (vol/vol). iMPCCs were established, infected with HCV (Jc1) on day 11, and rinsed on day 12 as described in the previous section. The cultures were then dosed with the 5 HCV drugs on days 14 and 16 at concentrations ranging from 0.00001 μM to 100 μM. Viability of the cells was assessed on days 16 and 18 using PrestoBlue reagent (Themo Fisher, Waltham, MA) to ensure that the drugs were not causing hepatotoxicity. The cultures were lysed on day 18 for quantification of HCV expression via qPCR.

6.2.6 Gene expression profiling

To quantify intrahepatic HCV gene expression, cultures were lysed for RNA isolation. RNA was prepared using the GeneJET RNA Purification Kit (Thermo Fisher Scientific), treated with recombinant DNase I (New England Biolabs, Ipswich, Massachusetts), and reverse transcribed into cDNA. qPCR was performed on a MasterCycler RealPlex-2 machine (Eppendorf, Hamburg, Germany) using probe-primer gene expression assays. The HCV primer sequences utilized were: CGACACTCCGCCATGAATCACT (forward), CACTCGCAAGCGCCCTATCA (reverse), and FAM-AGGCCTTTCGCAACCCAACGCTACT-TAMRA (probe). Expression levels were normalized to glyceraldehyde-3-phosphate dehydrogenase (GAPDH) and calculated using the delta-delta C_T method relative to the indicated controls. Global gene expression profiling was also performed on freshly-isolated primary human hepatocytes from 2 separate donors and day 21 iMPCCs

using an Affymetrix whole genome human microarray and data was quantified using previously published protocols[19].

6.2.7 Data analysis

Experiments were repeated 2 times with triplicate samples for each condition. Data from representative experiments are presented, whereas similar trends were seen in both experiments. Error bars on graphs represent standard deviations. Microsoft Excel and GraphPad Prism 7.0 (La Jolla, CA) were used for data analysis and graphing.

6.3 Results

6.3.1 Characterization of iHeps

Conventional cultures (iCCs), random cocultures (iRCCs), micropatterned iHeps (iMPHs) and micropatterned cocultures (iMPCCs) were established as described in the methods section. Schematics and phase contrast images from days 9 and 19 of culture for each of these models are depicted in **Figures 6.1A and 6.1B**, respectively. iHeps in both iCC and iRCC formats detached over time as demonstrated by the lower cell density at later timepoints while those in iMPHs spread out and dedifferentiated. While iHep domains in iMPCCs also spread out over time, cell morphology was better maintained compared to the other model formats over several weeks in culture. Our previous publications have demonstrated that albumin and urea production by iMPCCs reach steady-state levels of 5-6 μg/hr/million cells in ~1 week and remained stable for 3 more weeks[16]. Additionally, activity levels for several CYP450 enzymes were maintained in iMPCCs for 27 days[16].

We identified 71 HCV host factors from global gene profiling. 45 of these host factors were present in freshly isolated hepatocytes obtained from 2 human donors. Out of these 45

HCV host factors present in fresh PHHs, 43 (95.6%) were also present in iMPCCs on day 21 of culture. Compared to the average expression levels from the 2 freshly isolated primary human hepatocytes, 12 of the HCV host factors were downregulated, 22 were similar, and 9 were upregulated in iMPCCs from day 21. Downregulation and upregulation of gene expression were defined as greater than a 2-fold difference. All of the identified HCV host factors and fold differences are shown in **Table 6.1**.

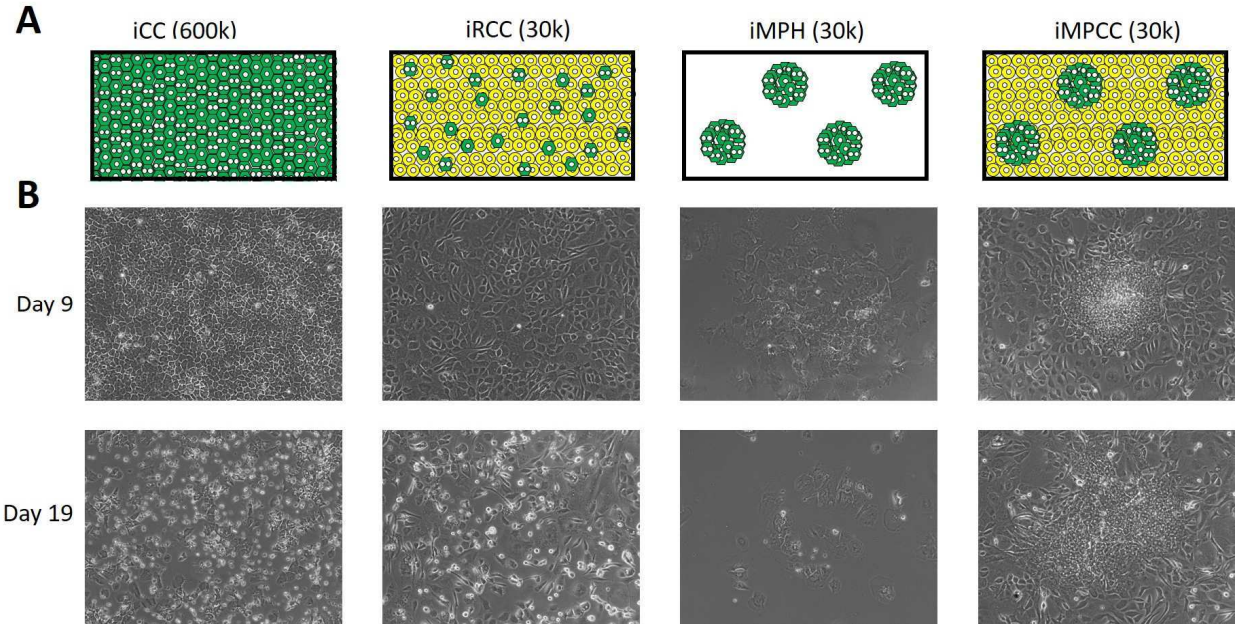

Figure 6.1 Culture of iHeps in various model configurations. (A) Schematics for iHep conventional cultures (iCC), random cocultures (iRCCs), micropatterned hepatocytes (iMPHs), and micropatterned cocultures (iMPCCs) with the number of iHeps per well indicated in parentheses. **(B)** Phase contrast images of each of model are shown from days 9 and 19 of culture.

Table 6.1 Fold change of HCV host factor expression in iMPCCs from day 21 of culture are compared against the average of two freshly-isolated human hepatocyte donors.

HCV Host Factor	Fold change in Day 21 of iMPCC relative to fresh primary human hepatocytes (average of 2 donors)
PPIL4 /// ZC3H12D: peptidylprolyl isomerase (cyclophilin)-like 4 /// zinc finger CCCH-type containing 12D	NA
PPIL6: peptidylprolyl isomerase (cyclophilin)-like 6	NA
FKBP11: FK506 binding protein 11, 19 kDa	0.065
HS3ST3B1: heparan sulfate (glucosamine) 3-O-sulfotransferase 3B1	0.185
PPID: Peptidylprolyl isomerase D	0.194
CLK1 /// PPIL3: CDC-like kinase 1 /// peptidylprolyl isomerase (cyclophilin)-like 3	0.236
LDLR: low density lipoprotein receptor	0.237
HSP90AA1: heat shock protein 90kDa alpha (cytosolic), class A member 1	0.261
PPIL1: peptidylprolyl isomerase (cyclophilin)-like 1	0.263
CIDEB: cell death-inducing DFFA-like effector b	0.314
FKBP2: FK506 binding protein 2, 13kDa	0.355
FKBP5: FK506 binding protein 5	0.362
EGFR: epidermal growth factor receptor (erythroblastic leukemia viral (v-erb-b) oncogene homolog, avian)	0.384
OCLN: occludin	0.488
MTFR1: mitochondrial fission regulator 1	0.555
PPIF: peptidylprolyl isomerase F	0.583
PPIL4: peptidylprolyl isomerase (cyclophilin)-like 4	0.641
CD81: CD81 molecule	0.665
FKBPL: FK506 binding protein like	0.790
HSP90B1: heat shock protein 90kDa beta (Grp94), member 1	0.810
SCARB1: scavenger receptor class B, member 1	0.964
FKBP4: FK506 binding protein 4, 59kDa	0.972
FKBP3: FK506 binding protein 3, 25kDa	0.992
FKBP1B /// MFSD2B: FK506 binding protein 1B, 12.6 kDa /// major facilitator superfamily domain-containing protein 2b	1.024
PPIB: peptidylprolyl isomerase B (cyclophilin B)	1.044
HSP90AB1: heat shock protein 90kDa alpha (cytosolic), class B member 1	1.073
DPP4: dipeptidyl-peptidase 4	1.079
PPIG: peptidylprolyl isomerase G (cyclophilin G)	1.093
NPC1L1: NPC1 (Niemann-Pick disease, type C1, gene)-like 1	1.178

FKBP15: FK506 binding protein 15, 133kDa	1.238
LTB: lymphotoxin beta (TNF superfamily, member 3)	1.463
PPIE: peptidylprolyl isomerase E (cyclophilin E)	1.464
FKBP14: FK506 binding protein 14, 22 kDa	1.526
FKBP1A: FK506 binding protein 1A, 12kDa	1.607
CLDN1: claudin 1	1.704
PPIL5: peptidylprolyl isomerase (cyclophilin)-like 5	1.783
PPIC: peptidylprolyl isomerase C (cyclophilin C)	2.239
TNIK: TRAF2 and NCK interacting kinase	2.263
PPIL3: peptidylprolyl isomerase (cyclophilin)-like 3	2.431
HS6ST1: heparan sulfate 6-O-sulfotransferase 1	2.705
HRAS: v-Ha-ras Harvey rat sarcoma viral oncogene homolog	3.089
PPIA: peptidylprolyl isomerase A (cyclophilin A)	3.188
FKBP7: FK506 binding protein 7	3.688
FKBP9: FK506 binding protein 9, 63 kDa	5.960
FKBP1B: FK506 binding protein 1B, 12.6 kDa	8.879

6.3.2 HBV infection of iHeps

Conventional cultures (iCCs) with 600,000 iHeps and random cocultures (iRCCs), micropatterned iHeps (iMPHs), and micropatterned cocultures (iMPCCs) with 30,000 iHeps, were established as described in the methods section. iCCs and iMPHs were infected on day 5 and iRCCs and iMPCCs, on day 11. Culture supernatant was collected approximately 1 and 2 weeks post infection for quantification of HBeAg and HBsAg. iCCs, iRCCs, and iMPHs did not show detectable levels of HBeAg (**Figure 6.2A**) or HBsAg (**Figure 6.2B**). On the other hand, iMPCCs, either without or with the small molecule (SM), FPH2, and without/with JAK inhibitor (JAKi), showed sustained levels of both HBeAg and HBsAg for 2 weeks post infection. We found that HBV antigen levels were similar between treating the cultures with 1 μM JAKi for 24 hours prior to and during infection (pulse) or with 0.5 μM JAKi starting 24 hours prior to infection through the end of the experiment (continuous). The addition of 1 μM JAKi continuously led to hepatotoxicity (data not shown). While antigen levels were lower for iMPCCs without JAKi, they are still stable for at least 2 weeks post infection. These trends were confirmed via immunofluorescent staining for HBcAg 2 weeks post infection (**Supplemental Figure 6.5.1**). We also confirmed that 3T3-J2 fibroblasts alone do not retain or secrete HBV antigens (data not shown).

6.3.3 HCV infection of iHeps

Conventional cultures (iCCs) with 600k iHeps, random cocultures (iRCCs) with 30k and 100k iHeps, micropatterned iHeps (iMPHs) with 30k iHeps, and micropatterned cocultures (iMPCCs) with 30k iHeps were established as described in the methods section. iCCs were infected on day 5 and iRCCs, iMPHs and iMPCCs, on day 11. Cultures were lysed 5 days post infection and RNA processed for relative quantification of HCV using qPCR (**Figure 6.2C**). We

observed the highest levels of HCV in iCCs. HCV expression levels in iMPHs and iMPCCs were at approximately 60% of iCCs. iRCCs with 100k iHeps showed an expression level at approximately 30% of iCCs while iRCCs with 30k iHeps had almost undetectable HCV.

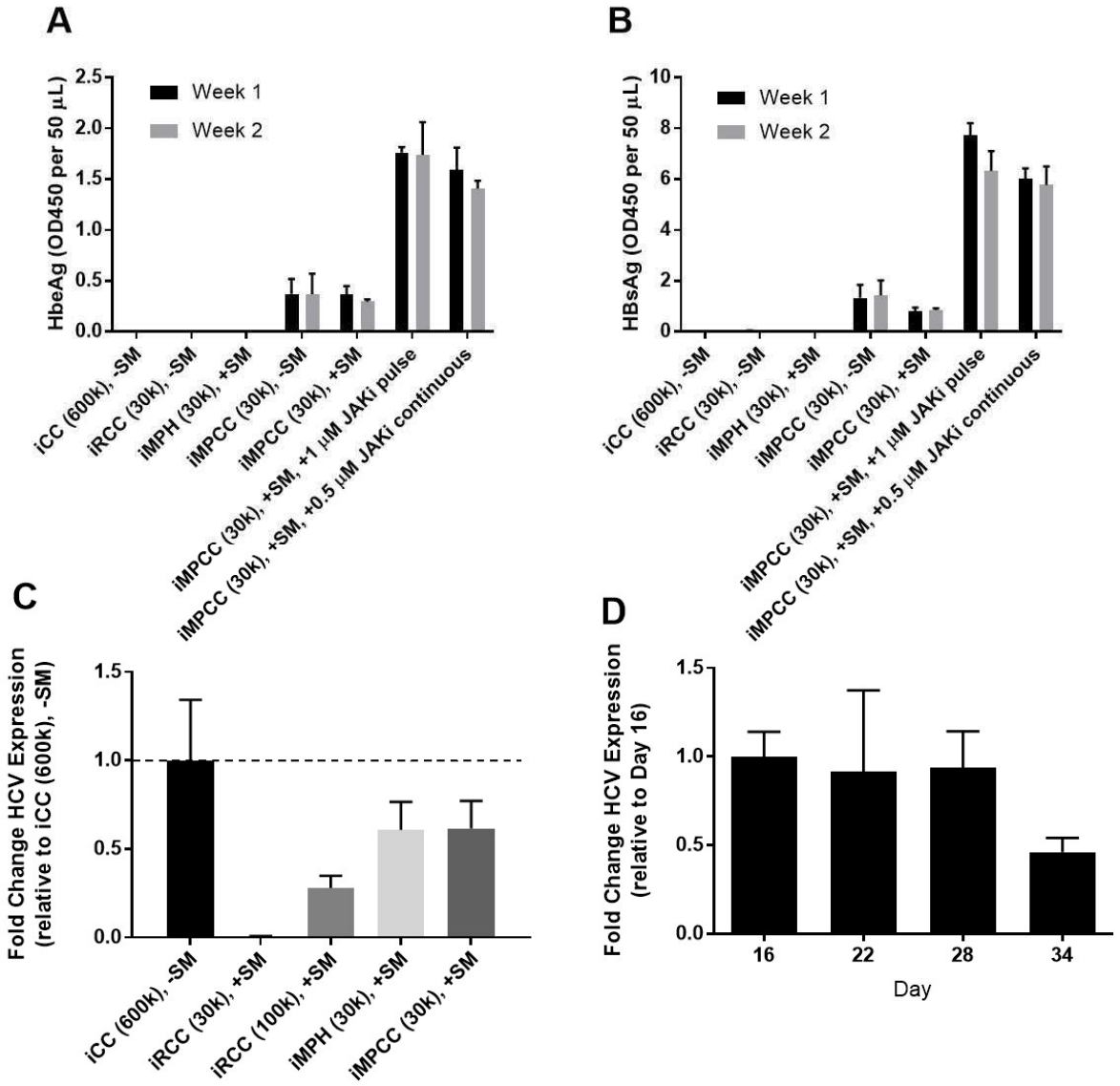

Figure 6.2 HBV and HCV infection of iHeps. (A) The various iHep models were infected with HBV and HBV envelope antigen (HBeAg) was assessed 1 and 2 weeks post infection. **(B)** The same cultures from panel A were assessed for HBV surface antigen (HBsAg). **(C)** The various iHep models were infected with HCV, and HCV expression levels were assessed 5 days post infection. **(D)** iMPCCs were infected with HCV, and HCV expression assessed at multiple timepoints.

We also assessed the longevity of HCV expression in iMPCCs. iMPCCs were infected on day 11 and cell lysate was collected on days 16, 22, 28, and 34 for quantification of HCV expression. As shown in **Figure 6.2D**, HCV expression was stable until day 28 and showed an approximately 50% decrease on day 34. Additionally, to assess *de novo* generation of HCV infectious particles, supernatant from HCV-infected iMPCCs were collected on days 14, 18, 22, and 26, and added to naïve iMPCCs on day 11 of culture for 24 hours. The cells were lysed 4 days later (on day 16) for quantification of HCV expression. As shown in **Supplemental Figure 6.5.2**, supernatant from all 4 days were infectious with supernatant from day 22 of culture showing the highest levels of infectivity.

6.3.4 HBV infection of PHHs

CCs (510,000 PHHs), RCCs (30,000 or 100,000 PHHs), and MPCCs (30,000 PHHs) were also established for comparison against iHep cultures. Phase contrast images from days 5, 10, and 15 of culture for these models are shown in **Figure 6.3**. CCs were infected on day 1 while RCCs and MPCCs were infected on day 7 with quantification of HBeAg (**Figure 6.4A**) and HBsAg (**Figure 6.4B**) 1 and 2 weeks post infection. Unlike iCCs, CCs showed high levels of HBeAg with levels increasing by ~3.8-fold from 1 to 2 weeks post infection. RCCs also demonstrated HBV permissivity with the 100k hepatocyte condition showing a ~35% reduction in HBeAg from 1 to 2 weeks. RCCs with 30k hepatocytes showed lower levels of infection (~9% of 100k) 1 week post infection as compared to the 100k condition. By week 2, HBeAg levels had dropped by 60% compared to week 1. MPCCs showed more stable infection with a ~13% drop in HBeAg from 1 to 2 weeks post infection. HBsAg showed similar trends as HBeAg. Overall, HBV infection levels appear to be higher in MPCCs created using PHHs compared to iHeps. We also observed HBcAg in MPCCs 2 weeks post infection via immunofluorescent staining

(**Supplemental Figure 6.5.3**). Additionally, the addition of 1 μM JAKi 24 hours prior to and during infection (pulse) did not increase HBeAg or HBsAg levels as it did in iMPCCs (**Supplemental Figure 6.5.4**).

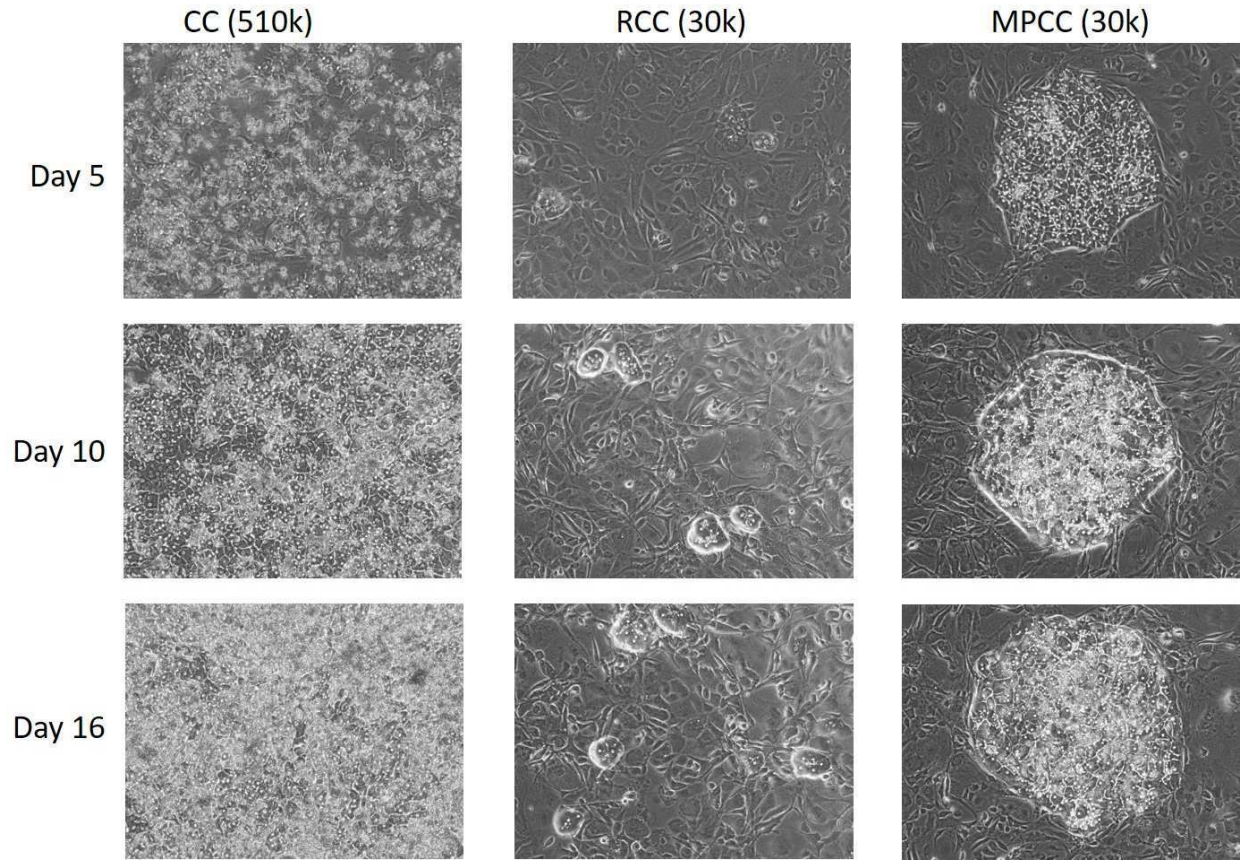

Figure 6.3 Culture of PHHs in various model configurations. Phase contrast images of PHHs cultured in conventional cultures (CCs), random cocultures (RCCs), and micropatterned cocultures (MPCCs) from days 5, 10, and 16 of culture.

In order to compare our models against conventional platforms, we attempted to infect HepG2 and HepaRG cultures with HBV as shown in **Supplemental Figure 6.5.5.** HepG2 cells, either in conventional confluent monolayers (CC) or in the MPCC format, did not show any detectable HBeAg. On the other hand, confluent monolayers of HepaRG with the addition of 2% DMSO showed stable HBeAg levels for at least 2 weeks post infection.

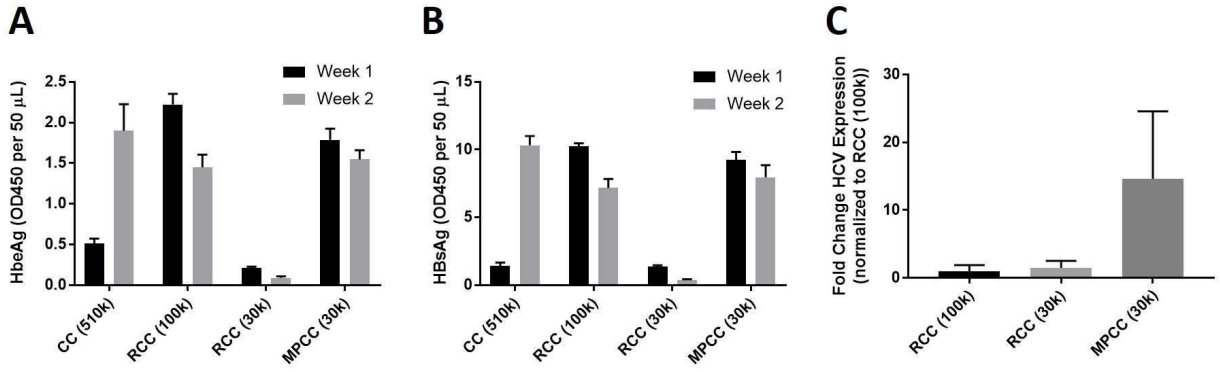

Figure 6.4 HBV and HCV infection of PHHs. (A) The various PHH models were infected with HBV, and HBV envelope antigen (HBeAg) was assessed 1 and 2 weeks post infection. **(B)** The same cultures from panel A were assessed for HBV surface antigen (HBsAg). **(C)** The various PHH models were infected with HCV, and HCV expression levels were assessed 5 days post infection.

6.3.5 HCV infection of PHHs

RCCs with 30,000 and 100,000 hepatocytes and MPCCs with 30,000 hepatocytes were established using PHHs for comparison against HCV infection in iHeps. Cultures were infected on day 7 and RNA collected 9 days post infection (day 16) for the assessment of HCV expression. HCV expression was higher in MPCCs as compared to RCCs with 30k or 100k hepatocytes as shown in **Figure 6.4C**.

6.3.6 Attenuation of HCV in iMPCCs using existing DAAs

iMPCCs were established as previously described in the methods section and infected with HCV on day 11. Cultures were treated with a panel of 5 drugs at various concentrations on days 14 and 16. Viability of the cultures was assessed on days 16 and 18. Cultures were lysed for RNA on day 18 to assess HCV expression levels as compared to the infected vehicle (DMSO)-treated control. All 5 drugs demonstrated a dose-dependent attenuation of HCV expression (**Figure 6.5**) with no significant loss of viability in the cultures (**Supplemental Figure 6.5.6**).

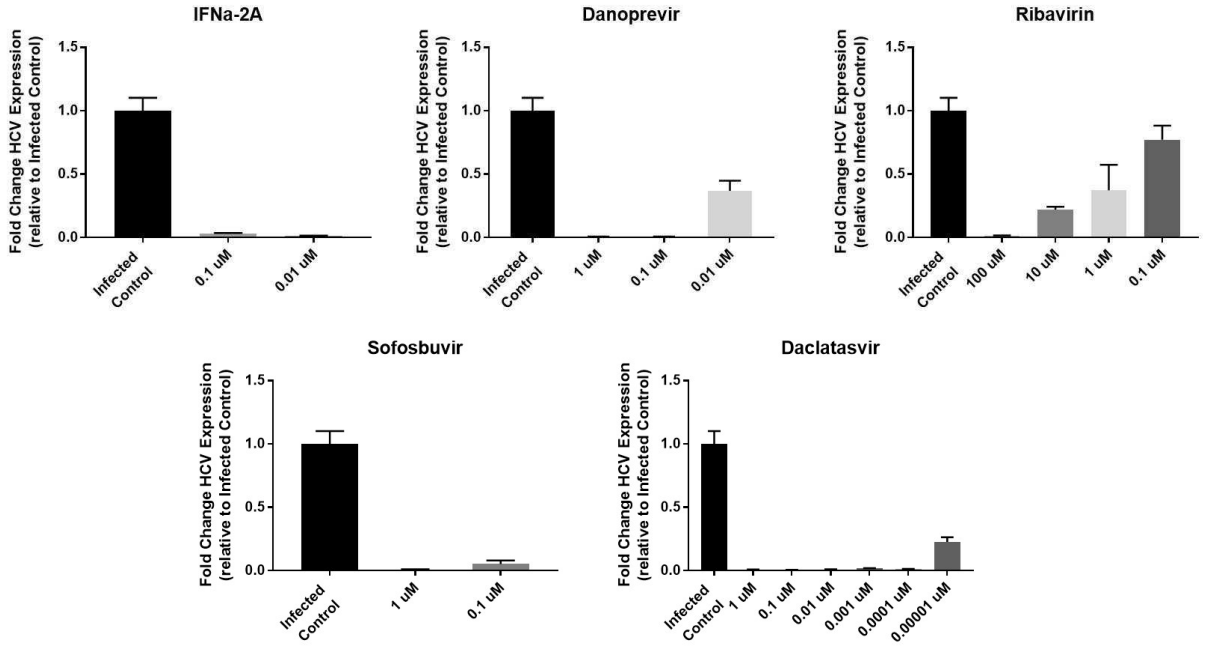

Figure 6.5 Drug attenuation of HCV in iMPCCs. Dose-dependent attenuation of HCV expression was observed in HCV-infected iMPCCs treated with a panel of 5 HCV drugs as compared to infected iMPCC treated with the vehicle control.

6.4 Discussion

The study of hepatitis B and C has been difficult due to the narrow host and tissue tropism of these viruses and subsequent lack of relevant experimental models. Robust models of HBV and HCV infection are necessary for the study of viral-host interactions towards the creation of better prophylactic therapies and treatment regimens. While *in vivo* models of hepatitis have offered valuable insight into the mechanisms of infection, the use of large animals, such as chimpanzees, tree shrews, ducks, and woodchucks, for drug screening is impractical due to cost and differences in drug metabolism pathways between human and animal livers[9]. Recently, humanized murine models have allowed for completion of the entire viral life cycle, but there are issues with robust engraftment of human hepatocytes, low breeding efficiency, and high mortality[23]. Thus, *in vitro* liver models are more commonly used[24]. Ideally, these models

should exhibit expression of viral entry factors, host factors that support virus replication and longevity of the virus, maintenance of hepatocyte functionality such that the cells can mount an antiviral response, and scalability/reproducibility for drug screening applications.

While there have been multiple cell culture systems that support HCV replication such as the Huh 7.5 cell line or HepG2 ectopically expressing miR-122 and CD81[9], systems that are physiologically-relevant are required. Primary hepatocytes have been infected with HCV through the use of serum-derived virions and HCV-like particles[25]. More recently, the replicon system has been instrumental in the study of HCV replication and virus-host cell interactions[25]. For example, the genotype 2a replicon (JFH-1) can replicate efficiently, produce infectious viral particles, and can be passaged *in vitro*[26]. Chimeric constructs with the J6 genotype 2a clone (Jc1) improved the infectivity of the system[27,28]. Thus, we utilized these replicons for HCV infection of our iPSC-HH platform. Although iPSC-HHs have been utilized by several groups for various drug screening[29-32] and disease modeling[33-35] applications, the maturity and functionality of these cells are far from those found in primary human hepatocytes. In this study and previous studies, we have shown that through co-culturing and controlling cell-cell interactions between iPSC-HHs and 3T3-J2 fibroblasts through micropatterning techniques, iPSC-HH functions are significantly enhanced and stabilized such that these iMPCCs become highly sensitive to drug toxicity detection[16,17]. This platform also allows for maintenance of cell polarity, which is important for defining accurate entry mechanisms since disruption of cell junctions (claudin-1 and occludin) may lead to disrupted viral entry[36]. Through global gene expression analysis, we were able to demonstrate that the majority of HCV host factors that appear in fresh PHHs are also expressed in day 21 iMPCC cultures. We found that although iCCs, iRCCs, iMPHs, and iMPCCs could all be infected with HCV with iCCs and iMPHs showing similar intrahepatic

HCV expression levels as iMPCCs, iMPCCs constitute a more robust model for drug screening due to functional stability and higher expression of CYP450 enzymes that are critical for drug metabolism[16,17]. HCV infection of PHHs in MPCC format has previously been demonstrated by Ploss et al[37] and we determined that the level of HCV expression in iMPCCs was higher than those in MPCCs based on PCR cycle numbers (data not shown). For both iHeps and PHHs, the higher levels of HCV expression in MPCCs compared to RCCs at 30k (density-matched to MPCCs) and 100k cells may be due to the maintenance of cell polarity over time and higher expression of host factors since MPCCs allow cells to function better than RCCs as has been shown previously[19].

Although therapeutics are available for HCV, they are still cost-prohibitive and patients respond to various drugs and drugs concentration differently. iPSC technology allows for the study of inter-individualistic responses to infection and drugs since the limited availability of PHH lots does not allow for adequate modeling of genetic diversity in patients. To establish proof-of-concept, iMPCCs were dosed with a panel of 5 drugs that attenuate HCV through different targets. IFNα-2A has multiple mechanisms of action, including immunomodulatory and antiproliferative effects, but its use is limited due to severe side effects[6]. The mechanisms of ribavirin, which is a guanosine analogue, are also not well understood, but it may inhibit HCV polymerase. DAAs, such as danoprevir (protease inhibitor), 2'CMA and sofosbuvir (NS5B polymerase inhibitors), and daclatasvir (NS5A inhibitor) were also assessed. Attenuation of viral expression in the iMPCC model showed similar trends compared to MPCCs treated with some of the same HCV drugs[37]. This model can also be used to assess drug-drug interactions by dosing with combinations of these drugs as they are prescribed to patients in the clinic. We anticipate

that lower concentrations of individual drugs may be utilized when used in combination with other drugs.

We also demonstrated the utility of iPSC-HHs for HBV infection. While cell lines such as HepG2[38,39] and HepaRG[40] have allowed for insight into viral entry mechanisms, they require additional manipulation to maintain a more polarized or differentiated state[39]. Indeed, although our DMSO-differentiated HepaRG cells were permissive to HBV, our HepG2 cells were not, possibly due to the lack of ectopically-expressed NTCP, which has been identified as an important receptor for HBV[41,42]. Cell lines also do not fully mimic physiological responses due to numerous morphological and functional abnormalities and defective innate immune signaling. Thus, the use of PHHs and iPSC-HHs is preferred for the study of HBV pathophysiology and screening of drugs for efficacy and toxicity. Due to issues with low viral permissivity and donor dependence in PHHs, groups have utilized integrated HBV genomes, transfection of HBV DNA into cells, or the addition of factors such as DMSO, PEG[43], and immunosuppressants[44]. PEG has been shown to increase cell susceptibility to HBV so we included it in our studies, but found that even with the addition of PEG, HBV was only permissive to iMPCCs and not iCCs, iRCCs, or iMPHs, which is in contrast to what we observed with HCV. This highlights the importance of maintaining iHep polarity through controlled homotypic cell interactions for HBV infection. Additionally, Shlomai et al found that the addition of a JAK inhibitor was necessary for robust infection with various PHH donors[14]. However, since HBV does not induce a strong antiviral response, suppressing antiviral signaling should not be necessary for robust infection[45,46]. We found that while suppressing the JAK signaling pathway in iMPCCs resulted in higher levels of HBV, infection was still observed in multiple donors when JAK signaling was not inhibited. Overall, HBV infection seems to be only slightly lower (<35% decrease) in iMPCCs with JAKi

compared to MPCCs based on quantification of secreted HBsAg and HBeAg and immunofluorescent staining of HBcAg. Unlike iHeps, PHHs in CC and RCC formats also showed robust HBV infection for at least 2 weeks, which Winer et al have demonstrated[21]. These differences may be due to the lower functional maturity of iHeps, especially in the CC and RCC formats. This lack of maturity may result in lack of viral entry and replication factors. Thus, in the future, iHeps in the iMPCC format can be utilized for the identification and screening of HBV therapeutics.

In conclusion, we have demonstrated that iHeps in the iMPCC platform are permissive to cell culture-derived HBV and HCV isolates. In the future, this model can be augmented for the study of host-pathogen interactions through the inclusion of other cell types that are also involved in infection *in vivo*. For example, virions have been shown to bind to liver sinusoidal endothelial cells, which affect downstream infection in hepatocytes through the secretion of cytokines and exosomes[47]. Furthermore, the activation of Kupffer and hepatic stellate cells by HCV induces an immune response that can affect patients' responses to therapy and progression towards advanced liver diseases[48]. While the HCV strains we used in this study are of genotype 2a derived from a Japanese patient with fulminant hepatitis C, *in vitro* infection with other genotypes are important to study differences in genotypic responses to therapies[49]. Besides cell culture-derived virus, other sources of virus such as patient isolate-derived HBV and HCV can be used to infect these cultures. Through the utilization and augmentation of the iMPCC model, we anticipate that panels of multiple iPSC-HH donors can eventually be used to investigate inter-individual susceptibility to both HBV and HCV drugs and thus allow discovery and screening of novel compounds which can alleviate these global diseases.

6.5 Supplemental Figures

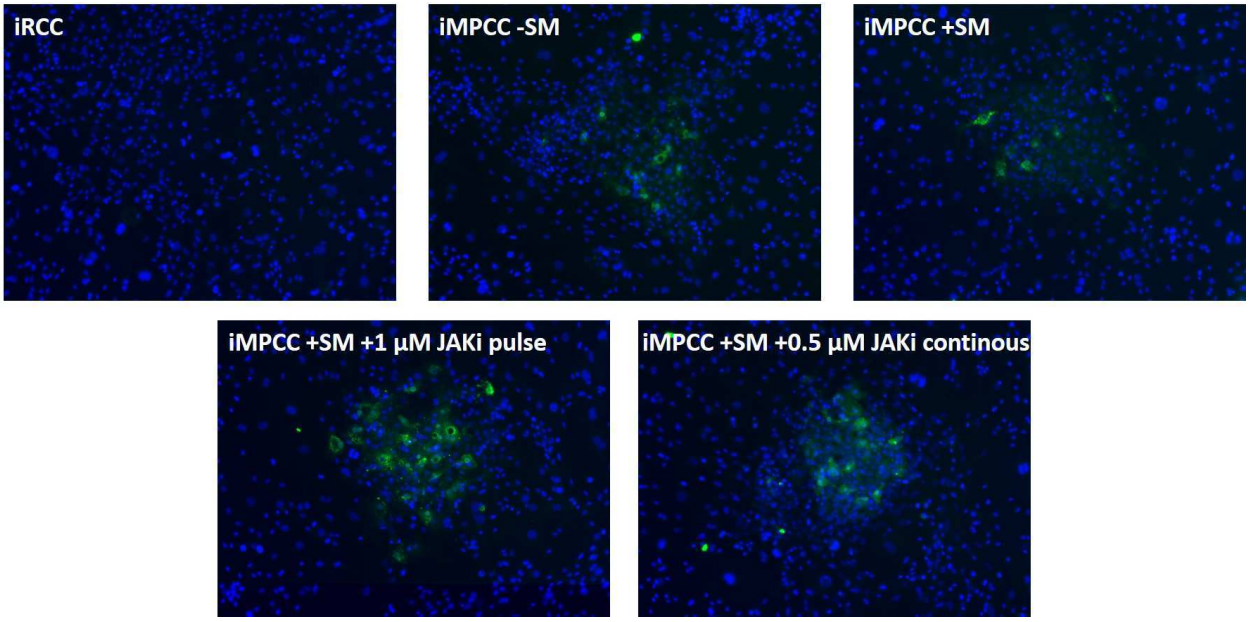

Figure 6.5.1 Immunofluorescent staining of HBV-infected iHep cultures in various model configurations. Each model type was infected with HBV on day 11 and fixed for staining of HBcAg (green) and DAPI (blue) 2 weeks post infection.

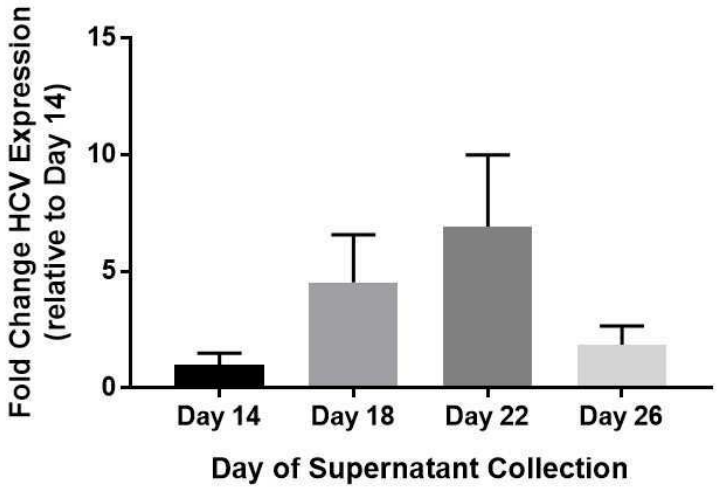

Figure 6.5.2 iMPCCs demonstrate *de novo* production of infectious HCV particles. Supernatant from HCV-infected iMPCCs was collected on days 14, 18, 22, and 26, and added to naïve iMPCCs on day 11 of culture for 24 hours. The cells were rinsed after 24 hours, media was changed 2 days post infection, and the cells were lysed 4 days post infection (on day 16) for quantification of HCV expression.

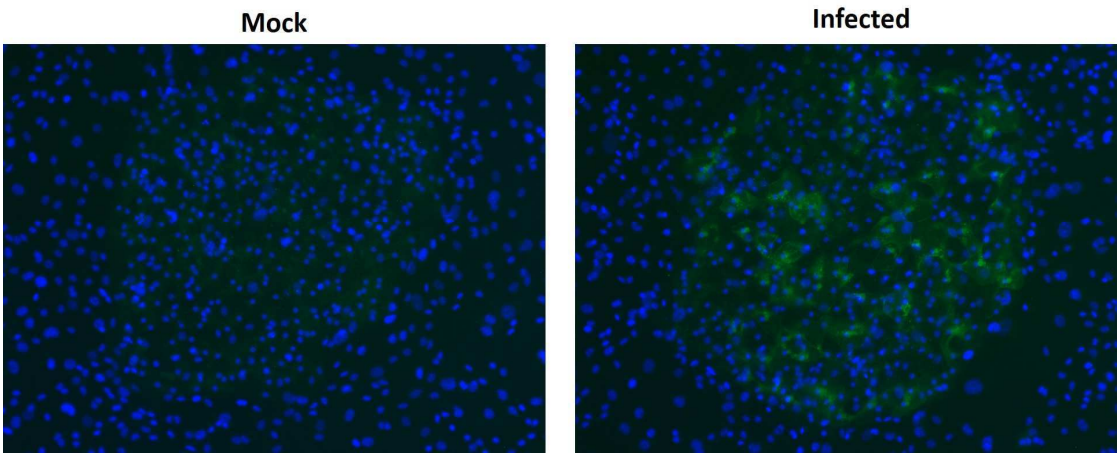

Figure 6.5.3 Immunofluorescent staining of mock and HCV-infected MPCCs. MPCCs created using primary human hepatocytes were infected with HCV or mock media on day 7 and fixed for staining of HBcAg (green) and DAPI (blue) 2 weeks post infection.

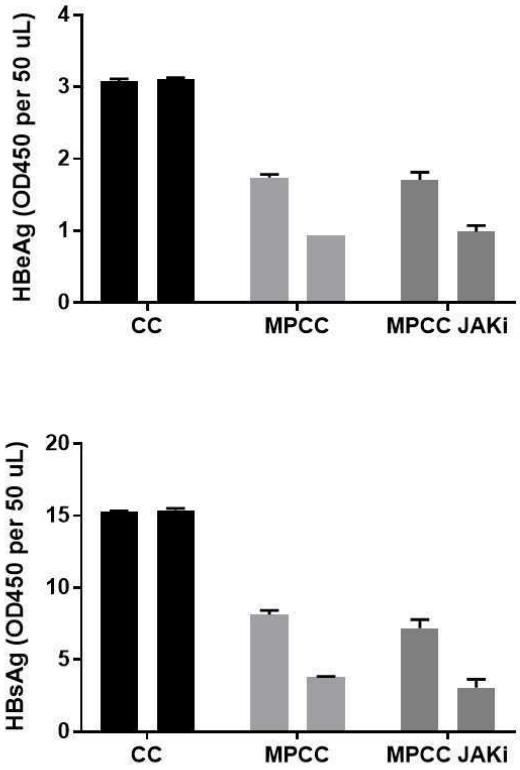

Figure 6.5.4 Primary human hepatocytes of a different donor compared to the one shown in Figure 6.4 were infected with HBV, and HBeAg and HBsAg were measured 1 week (1st bar) and 2 weeks (2nd bar) post infection. MPCCs treated with 1 μM of JAKi 24 hours prior to and during HBV inoculation (pulse) showed similar HBeAg and HBsAg secretion levels as compared to non-JAKi-treated MPCC controls.

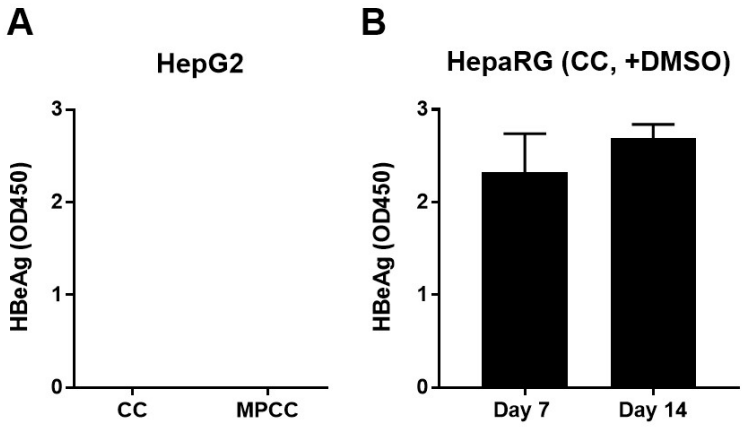

Figure 6.5.5 Cell lines were infected with HBV and secreted HBeAg was measured 1 and 2 weeks post infection. HepG2 cells, either in conventional confluent monolayers (CC) or in the MPCC format, had undetectable levels of HBeAg. Confluent monolayers of HepaRG with the addition of 2% DMSO showed stable HBeAg levels for at least 2 weeks post infection.

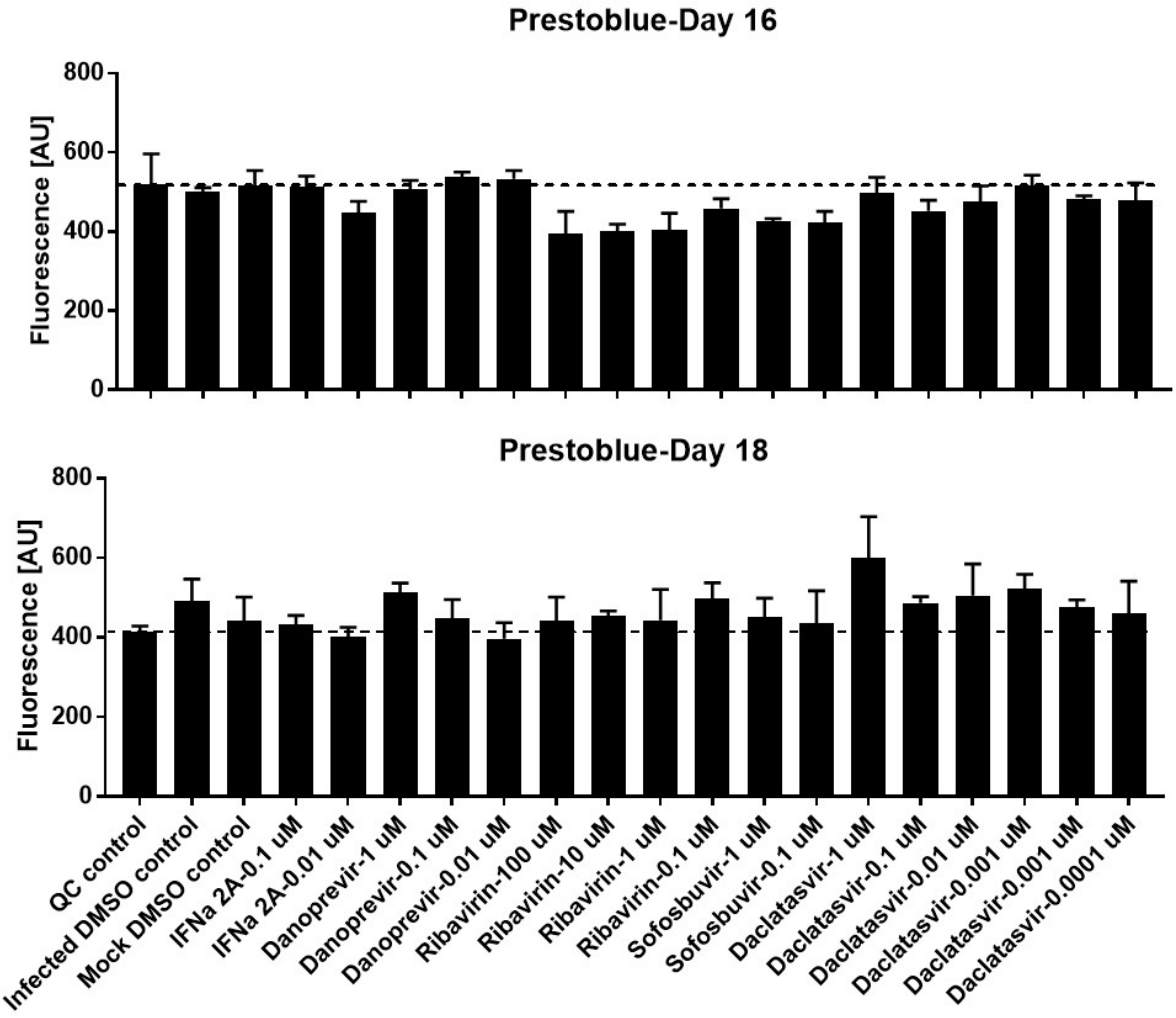

Figure 6.5.6 Viability was assessed in HCV-infected iMPCCs treated with HCV drugs as compared to the non-infected and non-treated QC (quality control), and vehicle (DMSO)-treated mock and infected iMPCCs. iMPCCs were infected with HCV on day 11, treated with the drugs on days 14 and 16, and assessed for viability on days 16 (top) and 18 (bottom).

References

1. Gonzalez-Grande R, Jimenez-Perez M, Gonzalez Arjona C, Mostazo Torres J. New approaches in the treatment of hepatitis C. World J Gastroenterol 2016;22(4):1421-32.

2. Zou ZQ, Wang L, Wang K, Yu JG. Innate immune targets of hepatitis B virus infection. World J Hepatol 2016;8(17):716-25.

3. El-Serag HB. CURRENT CONCEPTS Hepatocellular Carcinoma. New England Journal of Medicine 2011;365(12):1118-1127.

4. Wei L, Lok AS. Impact of new hepatitis C treatments in different regions of the world. Gastroenterology 2014;146(5):1145-50 e1-4.

5. Bagaglio S, Uberti-Foppa C, Morsica G. Resistance Mechanisms in Hepatitis C Virus: implications for Direct-Acting Antiviral Use. Drugs 2017;77(10):1043-1055.

6. Alaluf MB, Shlomai A. New therapies for chronic hepatitis B. Liver International 2016;36(6):775-782.

7. Morikawa K, Shimazaki T, Takeda R, Izumi T, Umumura M, Sakamoto N. Hepatitis B: progress in understanding chronicity, the innate immune response, and cccDNA protection. Annals of Translational Medicine 2016;4(18).

8. Allweiss L, Dandri M. Experimental in vitro and in vivo models for the study of human hepatitis B virus infection. J Hepatol 2016;64(1 Suppl):S17-S31.

9. Schinazi RF, Ilan E, Black PL, Yao XJ, Dagan S. Cell-based and animal models for hepatitis B and C viruses. Antiviral Chemistry & Chemotherapy 1999;10(3):99-114.

10. Olson H, Betton G, Robinson D, Thomas K, Monro A, Kolaja G, Lilly P, Sanders J, Sipes G, Bracken W and others. Concordance of the toxicity of pharmaceuticals in humans and in animals. Regulatory toxicology and pharmacology : RTP 2000;32(1):56-67.

11. Gerets HHJ, Tilmant K, Gerin B, Chanteux H, Depelchin BO, Dhalluin S, Atienzar FA. Characterization of primary human hepatocytes, HepG2 cells, and HepaRG cells at the

mRNA level and CYP activity in response to inducers and their predictivity for the detection of human hepatotoxins. Cell biology and toxicology 2012;28(2):69-87.

12. Wilkening S, Stahl F, Bader A. Comparison of primary human hepatocytes and hepatoma cell line Hepg2 with regard to their biotransformation properties. Drug Metabolism and Disposition 2003;31(8):1035-1042.

13. Bhatia SN, Balis UJ, Yarmush ML, Toner M. Effect of cell-cell interactions in preservation of cellular phenotype: cocultivation of hepatocytes and nonparenchymal cells. The FASEB journal : official publication of the Federation of American Societies for Experimental Biology 1999;13(14):1883-1900.

14. Shlomai A, Schwartz RE, Ramanan V, Bhatta A, de Jong YP, Bhatia SN, Rice CM. Modeling host interactions with hepatitis B virus using primary and induced pluripotent stem cell-derived hepatocellular systems. Proc Natl Acad Sci U S A 2014;111(33):12193-8.

15. Schwartz RE, Trehan K, Andrus L, Sheahan TP, Ploss A, Duncan SA, Rice CM, Bhatia SN. Modeling hepatitis C virus infection using human induced pluripotent stem cells. Proceedings of the National Academy of Sciences of the United States of America 2012;109(7):2544-2548.

16. Berger DR, Ware BR, Davidson MD, Allsup SR, Khetani SR. Enhancing the functional maturity of induced pluripotent stem cell-derived human hepatocytes by controlled presentation of cell-cell interactions in vitro. Hepatology (Baltimore, Md) 2015;61(4):1370-1381.

17. Ware BR, Berger DR, Khetani SR. Prediction of Drug-Induced Liver Injury in Micropatterned Co-cultures Containing iPSC-Derived Human Hepatocytes. Toxicological sciences : an official journal of the Society of Toxicology 2015;145(2):252-262.

18. Ramanan V, Scull MA, Sheahan TP, Rice CM, Bhatia SN. New Methods in Tissue Engineering: Improved Models for Viral Infection. Annual Review of Virology 2014;1(1):475-499.

19. Khetani SR, Bhatia SN. Microscale culture of human liver cells for drug development. Nature biotechnology 2008;26(1):120-126.

20. Shan J, Schwartz RE, Ross NT, Logan DJ, Thomas D, Duncan SA, North TE, Goessling W, Carpenter AE, Bhatia SN. Identification of small molecules for human hepatocyte expansion and iPS differentiation. Nature chemical biology 2013;9(8):514-520.

21. Winer BY, Huang TS, Pludwinski E, Heller B, Wojcik F, Lipkowitz GE, Parekh A, Cho C, Shrirao A, Muir TW and others. Long-term hepatitis B infection in a scalable hepatic co-culture system. Nat Commun 2017;8(1):125.

22. Jones CT, Catanese MT, Law LM, Khetani SR, Syder AJ, Ploss A, Oh TS, Schoggins JW, MacDonald MR, Bhatia SN and others. Real-time imaging of hepatitis C virus infection using a fluorescent cell-based reporter system. Nat Biotechnol 2010;28(2):167-71.

23. Mercer DF, Schiller DE, Elliott JF, Douglas DN, Hao C, Rinfret A, Addison WR, Fischer KP, Churchill TA, Lakey JR and others. Hepatitis C virus replication in mice with chimeric human livers. Nature medicine 2001;7(8):927-933.

24. Davidson MD, Ware BR, Khetani SR. Stem cell-derived liver cells for drug testing and disease modeling. Discovery medicine 2015;19(106):349-358.

25. Brass V, Moradpour D, Blum HE. Hepatitis C virus infection: in vivo and in vitro models. Journal of viral hepatitis 2007;14(s1):64-67.

26. Kato T, Date T, Miyamoto M, Furusaka A, Tokushige K, Mizokami M, Wakita T. Efficient replication of the genotype 2a hepatitis C virus subgenomic replicon. Gastroenterology 2003;125(6):1808-17.

27. Lindenbach BD, Evans MJ, Syder AJ, Wolk B, Tellinghuisen TL, Liu CC, Maruyama T, Hynes RO, Burton DR, McKeating JA and others. Complete replication of hepatitis C virus in cell culture. Science 2005;309(5734):623-6.

28. Pietschmann T, Kaul A, Koutsoudakis G, Shavinskaya A, Kallis S, Steinmann E, Abid K, Negro F, Dreux M, Cosset FL and others. Construction and characterization of infectious intragenotypic and intergenotypic hepatitis C virus chimeras. Proc Natl Acad Sci U S A 2006;103(19):7408-13.

29. Ulvestad M, Nordell P, Asplund A, Rehnström M, Jacobsson S, Holmgren G, Davidson L, Brolén G, Edsbagge J, Björquist P and others. Drug metabolizing enzyme and transporter protein profiles of hepatocytes derived from human embryonic and induced pluripotent stem cells. Biochemical pharmacology 2013;86(5):691-702.

30. Medine CN, Lucendo-Villarin B, Storck C, Wang F, Szkolnicka D, Khan F, Pernagallo S, Black JR, Marriage HM, Ross JA and others. Developing high-fidelity hepatotoxicity models from pluripotent stem cells. Stem cells translational medicine 2013;2(7):505-509.

31. Sjogren A-KM, Liljevald M, Glinghammar B, Sagemark J, Li X-Q, Jonebring A, Cotgreave I, Brolén G, Andersson TB. Critical differences in toxicity mechanisms in induced pluripotent stem cell-derived hepatocytes, hepatic cell lines and primary hepatocytes. Archives of toxicology 2014;88(7):1427-1437.

32. Sirenko O, Hesley J, Rusyn I, Cromwell EF. High-Content Assays for Hepatotoxicity Using Induced Pluripotent Stem Cell–Derived Cells. Assay and drug development technologies 2014;12(1):43-54.

33. Rashid ST, Corbineau S, Hannan N, Marciniak SJ, Miranda E, Alexander G, Huang-Doran I, Griffin J, Ahrlund-Richter L, Skepper J and others. Modeling inherited metabolic disorders of the liver using human induced pluripotent stem cells. J Clin Invest 2010;120(9):3127-36.

34. Tafaleng EN, Chakraborty S, Han B, Hale P, Wu W, Soto-Gutierrez A, Feghali-Bostwick CA, Wilson AA, Kotton DN, Nagaya M and others. Induced pluripotent stem cells model personalized variations in liver disease due to α1 -antitrypsin deficiency. Hepatology (Baltimore, Md) 2015.

35. Ng S, Schwartz RE, March S, Galstian A, Gural N, Shan J, Prabhu M, Mota MM, Bhatia SN. Human iPSC-Derived Hepatocyte-like Cells Support Plasmodium Liver-Stage Infection In Vitro. Stem cell reports 2015;4(3):348-359.

36. Harris HJ, Farquhar MJ, Mee CJ, Davis C, Reynolds GM, Jennings A, Hu K, Yuan F, Deng H, Hubscher SG and others. CD81 and Claudin 1 Coreceptor Association: Role in Hepatitis C Virus Entry. Journal of virology 2008;82(10):5007-5020.

37. Ploss A, Khetani SR, Jones CT, Syder AJ, Trehan K, Gaysinskaya VA, Mu K, Ritola K, Rice CM, Bhatia SN. Persistent hepatitis C virus infection in microscale primary human hepatocyte cultures. Proc Natl Acad Sci U S A 2010;107(7):3141-5.

38. Sells MA, Chen ML, Acs G. Production of hepatitis B virus particles in Hep G2 cells transfected with cloned hepatitis B virus DNA. Proc Natl Acad Sci U S A 1987;84(4):1005-9.

39. Paran N, Geiger B, Shaul Y. HBV infection of cell culture: evidence for multivalent and cooperative attachment. EMBO J 2001;20(16):4443-53.

40. Gripon P, Rumin S, Urban S, Le Seyec J, Glaise D, Cannie I, Guyomard C, Lucas J, Trepo C, Guguen-Guillouzo C. Infection of a human hepatoma cell line by hepatitis B virus. Proc Natl Acad Sci U S A 2002;99(24):15655-60.

41. Yan H, Zhong GC, Xu GW, He WH, Jing ZY, Gao ZC, Huang Y, Qi YH, Peng B, Wang HM and others. Sodium taurocholate cotransporting polypeptide is a functional receptor for human hepatitis B and D virus. Elife 2012;1.

42. Ni Y, Lempp FA, Mehrle S, Nkongolo S, Kaufman C, Falth M, Stindt J, Koniger C, Nassal M, Kubitz R and others. Hepatitis B and D Viruses Exploit Sodium Taurocholate Co-transporting Polypeptide for Species-Specific Entry into Hepatocytes. Gastroenterology 2014;146(4):1070-U301.

43. Gripon P, Diot C, Thézé N, Fourel I, Loreal O, Brechot C, Guguen-Guillouzo C. Hepatitis B virus infection of adult human hepatocytes cultured in the presence of dimethyl sulfoxide. Journal of virology 1988;62(11):4136-4143.

44. Shlomai A, Schwartz RE, Ramanan V, Bhatta A, de Jong YP, Bhatia SN, Rice CM. Modeling host interactions with hepatitis B virus using primary and induced pluripotent stem cell-derived hepatocellular systems. Proceedings of the National Academy of Sciences 2014;111(33):12193-12198.

45. Ortega-Prieto AM, Dorner M. Immune Evasion Strategies during Chronic Hepatitis B and C Virus Infection. Vaccines (Basel) 2017;5(3).

46. Dandri M, Burda MR, E T, Pollok JM, Iwanska A, Sommer G, Rogiers X, Rogler CE, Gupta S, Will H and others. Repopulation of mouse liver with human hepatocytes and in vivo infection with hepatitis B virus. Hepatology (Baltimore, Md) 2001;33(4):981-988.

47. Giugliano S, Kriss M, Golden-Mason L, Dobrinskikh E, Stone AE, Soto-Gutierrez A, Mitchell A, Khetani SR, Yamane D, Stoddard M and others. Hepatitis C virus infection induces autocrine interferon signaling by human liver endothelial cells and release of exosomes, which inhibits viral replication. Gastroenterology 2015;148(2):392-402 e13.

48. Affo S, Bataller R. RANTES antagonism: a promising approach to treat chronic liver diseases. J Hepatol 2011;55(4):936-8.

49. Gottwein JM, Bukh J. Cutting the gordian knot-development and biological relevance of hepatitis C virus cell culture systems. Adv Virus Res 2008;71:51-133.

Chapter 7

Conclusions and future work[7]

7.1 Conclusions

Liver diseases such as DILI and hepatitis are major global health burdens and it is clear that animal studies are not sufficient to fully predict and understand human-relevant outcomes[1]. While the development of human liver models was initiated many decades ago with the isolation and culture of PHHs on ECM, the rapid functional decline of these cells outside of their native liver microenvironment limits the prediction of clinical DILI outcomes[2,3]. Over the last few years, engineers have developed tools that now allow for more precise control over the microenvironment of PHHs such that functions can be stabilized for several weeks to months. This dissertation sought to improve upon existing *in vitro* liver models for drug screening and disease modeling applications. This was accomplished first by utilizing more physiologically-relevant biomaterials. Specifically, polyelectrolyte multilayers were used to present growth factors to liver cultures in a more physiologic manner and liver ECM was also utilized as a complex cell culture substrate that's more similar to what hepatocytes experience *in vivo*. In addition to assessment of substrates, we sought to augment the micropatterned coculture (MPCC) model with Kupffer cells. While many studies have validated the MPCC model for drug

[7] Sections of this chapter have been adapted from: Lin, C. and Khetani, S.R. Advances in engineered liver models for investigating drug-induced liver injury. BioMed Research International: 1829148 (2016) and Lin, C. et al, The application of engineered liver tissues for novel drug discovery. Expert Opinion on Drug Discovery 10(5):519-540 (2015).
With permission from Hindawi Publishing Corporation (open access) and the Taylor & Francis Group.

disposition and disease modeling applications, the addition of non-parenchymal cell types of the liver is necessary to gain a more complete picture of pathophysiological states. For example, the incorporation of Kupffer cells has allowed for us to screen for drugs which may induce idiosyncratic toxicity. We believe that this platform will be invaluable towards the discovery of better therapeutics since many hepatic disease states will induce an inflammatory response by the Kupffer cells. One such disease is hepatitis viral infection. In this dissertation, we have demonstrated that the MPCC model with either PHHs or iHeps can be infected with hepatitis B and C and responds to current HCV therapeutics as expected. The genetic variability that iHep technology offers can allow for the study of antiviral responses and personalized medicine. Overall, the work described here has set the foundation for future studies into human diseases.

7.2 Future work

7.2.1 Comprehensive *in vitro* liver models

Over many years of research, the field of engineered liver models has come to realize some important considerations in the design of such models, including the addition of multiple liver cell types at physiologic ratios *in vitro* and control over homotypic and heterotypic cell-cell interactions. These liver NPCs play vital roles in liver homeostasis and diseases states through heterotypic cell-cell communication. For instance, activation of Kupffer cells into a more inflamed state can downregulate certain CYP450s in PHHs, which can modulate the toxicity of drugs that are metabolized by those enzymes[4]. Additionally, drugs can activate hepatic stellate cells into becoming myofibroblasts that deposit excessive amounts of ECM and secrete cytokines which affect hepatocyte functions due to the changing microenvironment[5]. While in this dissertation, we have augmented the MPCC model with Kupffer cells, hepatic stellate cells, liver

sinusoidal endothelial cells, and cholangiocytes should also be included in the model to gain a more comprehensive insight into cell-cell interactions during pathophysiology.

Additionally, human liver models are now being coupled with models of other organs/tissues to better predict and understand how drug metabolism in the liver affects toxicity in other tissue types and how other organs can modulate liver functionality. Such integration is being done *in vitro* using microfluidic perfusion through biochip platforms. As candidate drugs progress through the drug development pipeline, such organs-on-a-chip platforms could be used to determine how different tissue types interact to produce toxicity in one or more tissue types[6]. Additionally, these chips are useful for modeling the pharmacokinetics and pharmacodynamics of drugs in a single device through the creation of gradients of molecular factors such as those that occur *in vivo* (zonation). There is always a chance that a candidate drug is flagged as toxic only when the most complex/complete culture system such as an organs-on-a-chip is utilized.

7.2.2. LBM and PEMs substrates for the delivery of growth factors to iHeps

Although LBM and PEMs were only utilized for the culture of PHHs in this dissertation, it is conceivable that such substrates may be used for iHep maturation. These biomaterials can be used to present important microenvironmental factors that are critical for the maturation of iHeps, such as oncostatin M (OsM). In pilot studies, we observed that OsM adsorbed to PEMs induced 40-65% more albumin secretion in iMPCCs compared to the soluble OsM control delivered via media changes over the course of 2 weeks (i.e. 25.6 μg/mL vs 16.8 μg/mL). The same trends were seen for urea production (20% higher concentrations in PEM-adsorbed conditions) and CYP450 activities. The iMPCC model also stabilized the effects of OsM on iHeps since in conventional pure cultures, the adsorbed OsM conditions functionally crashed

after 1 week while the soluble OsM conditions were able to survive for at least 2 weeks, presumably due to fresh OsM delivery every 2 days. In the future, PEMs could be used to deliver multiple growth factors to iMPCCs in a spatiotemporally-controlled manner. Additionally, decellularized LBM may contain several factors that may aid in iHep maturation. It would be interesting to see if LBM could be used to present growth factors to iHeps to mimic maturation pathways as they occur in vivo.

7.2.3 Utilization of KCs for insight into mechanisms of other liver diseases

Although in this dissertation, KCs were only utilized as a drug screening platform to identify drugs that may show increased toxicity in the background of an inflamed liver, the MPCC-KC model may also be used for the study of other diseases, such as hepatitis and diseases related to over-nutrition, including steatosis, non-alcoholic fatty liver disease (NAFLD), and NASH (non-alcoholic steatohepatitis).

In vivo, liver NPCs are thought to be involved in the presentation of HCV to hepatocytes, spreading of HCV infection, and inflammation. However, the specific roles and pathways that liver NPCs such as KCs are involved in and the downstream effects they have on HCV infection are still unknown. During infection, HCV induces IFN within hepatocytes and liver stromal cells. IFN-mediated activation of the immune system, including upregulation of ISGs, may lead to divergent outcomes in HCV infection. It has been demonstrated that HCV interacts with host factors such as IFN-γ and LPS to activate KCs, which may favor chronic inflammation in HCV patients[7]. KC activation assessed using the CD163 activation marker has recently been associated with inflammation and fibrosis in chronic HCV infection. After successful treatment with antivirals, serum CD163 levels dropped significantly *in vivo*[8]. KCs themselves are also a

source of IFN and based on basal IFN and subsequent ISG expression levels, patients will either respond or not respond to interferon therapy[9]. High IFN baseline production by KCs can lead to innate immune tolerance, lack of ISG expression, and lack of response to IFN therapy[7]. KCs have also been shown to bind and phagocytose HCV *in vivo*[10,11]. However, another study stated that although KCs phagocytose HCV particles, they do not serve as a reservoir for the virus and cytokine secretions by KCs are not induced[12]. Additionally, Jilg et al showed that by treating hepatocytes with IFN-α or IL28B, different kinetics of ISG induction were achieved and substantially altered by HCV infection[13]. Finally, HCV can evade the innate immune response by cleaving and inactivating signaling molecules that react to HCV PAMPs that induce IFNs. Despite these escape mechanisms, ISGs are still induced in chronically-infected patients. However, these patients do not respond well to IFN therapy[14]. Thus, in the future, we would like to assess how the presence of quiescent and TLR-ligand-activated KCs modulate HCV uptake and progression through IFN signaling pathways in MPCCs. We hypothesize that by incorporating activated KCS, upregulation of IFNs and ISGs will occur post infection. Additionally, we postulate that activation of KCs via TLR ligands may lead to the increased secretion of inflammatory cytokines, such as IL-6 and TNF-α, which has been demonstrated *in vivo*[7].

Liver NPCs, such as KCs and hepatic stellate cells are also believed to play important roles in over-nutritional diseases. A liver is considered fatty when lipids account for more than 5% of the liver's weight[15]. Triglycerides are stored in the hepatocyte cytoplasm, which leads to micro- and macro-vesicular steatosis. Steatosis can result from alcohol consumption resulting in alcoholic fatty liver disease, or a high-fat diet leading to NAFLD and NASH. NAFLD has been implicated in causing insulin resistance in hepatocytes and may contribute to the pathogenesis of

liver fibrosis, cirrhosis, hepatocellular carcinoma, and type 2 diabetes[16,17]. Cell-based liver models can also be used to better understand how fat accumulation affects the liver on a cellular level, which can aid in the development of novel therapeutics. In a human-relevant study, cultures of PHHs and HepG2 were incubated with both saturated and unsaturated long-chain free fatty acids (FFAs), and while both types of fats caused lipid accumulation, saturated FFAs led to more lipotoxicity and subsequent apoptosis[18]. Additionally, steatosis led to a down-regulation of CYP enzymes, which may affect the metabolism of administered drugs[19]. Ultimately, how NAFLD leads to fibrosis, which can then ultimately lead to cirrhosis and hepatocellular carcinoma are complex questions that will require multicellular, human-relevant, and long-term culture models to be able to properly answer to a degree that accurately mimics human liver biology.

7.2.4 Hepatitis mechanistic studies utilizing iHeps

While pilot studies of iHep infection with hepatitis were conducted in this dissertation, the potential of utilizing panels of iHep donors for the study of interindividual differences in response to viruses and drugs were not assessed. We anticipate that iHep models will eventually allow for the study of inter-individual differences in HCV infection and progression. HCV persists in 85% of those who are infected and standard therapies of pegylated-interferon and ribavirin or direct-acting antivirals (DAAs) such as boceprevir and telaprevir will cure 50-80% of infected patients[20]. The differences in responses to HCV therapeutics can be partially attributed to the different genotypes of HCV. Genetic polymorphisms may also affect how an individual will respond to HCV therapy. For example, patients with IL28B polymorphisms will respond better to interferon therapy when infected with certain HCV genotypes[21]. This may be due to an initially lower level of KC activation in these patients as IFN lowers the KC activation

marker, CD163, after successful treatment[8]. The outcome of infection will depend on the HCV genotype as well as the specific patient. For example, HCV genotype 3a leads to significant lipid accumulation, which can be associated with fibrosis progression[22]. Some patients will start out with varying levels of IFN and ISGs, which can then affect response to therapeutics. For instance, patients with high pretreatment levels of ISG expression may not respond to therapeutics[9]. Additionally, certain HCV genotypes may lead to more pronounced induction of inflammatory pathways[23].

With current *in vitro* liver models, it is not possible to predict how specific individuals will progress through infection and which of these individuals will adapt to drug-induced cell stress and which individuals will experience severe DILI. Creation of hundreds and thousands of iPSC lines from different individuals may ultimately be necessary to fully understand interindividual variations in antiviral response and treatment outcomes due to genetic makeup. However, iPSC-HH functions need to be further improved to be similar to PHHs before their potential for investigating DILI can be fully realized. In this dissertation and previous studies, we have shown that engineering tools have shown great promise in improving iPSC-HH functions. However, more progress needs to be made with further functional maturation and the use of standardized endpoints for appraising such maturity before this model can be used to study inter-individual differences in HCV infection, progression, and response to therapeutics.

References

1. Olson H, Betton G, Robinson D, Thomas K, Monro A, Kolaja G, Lilly P, Sanders J, Sipes G, Bracken W and others. Concordance of the toxicity of pharmaceuticals in humans and in animals. Regulatory toxicology and pharmacology : RTP 2000;32(1):56-67.

2. Xu JJ, Henstock PV, Dunn MC, Smith AR, Chabot JR, de Graaf D. Cellular Imaging Predictions of Clinical Drug-Induced Liver Injury. Toxicological sciences : an official journal of the Society of Toxicology 2008;105(1):97-105.

3. Khetani SR, Bhatia SN. Microscale culture of human liver cells for drug development. Nature biotechnology 2008;26(1):120-126.

4. Nguyen TV, Ukairo O, Khetani SR, McVay M, Kanchagar C, Seghezzi W, Ayanoglu G, Irrechukwu O, Evers R. Establishment of a hepatocyte-kupffer cell coculture model for assessment of proinflammatory cytokine effects on metabolizing enzymes and drug transporters. Drug Metab Dispos 2015;43(5):774-85.

5. Vernetti LA, Senutovitch N, Boltz R, Debiasio R, Shun TY, Gough A, Taylor DL. A human liver microphysiology platform for investigating physiology, drug safety, and disease models. Experimental biology and medicine (Maywood, N.J.) 2016;241(1):101-114.

6. Esch MB, King TL, Shuler ML. The Role of Body-on-a-Chip Devices in Drug and Toxicity Studies. Annual review of biomedical engineering 2011;13(1):55-72.

7. Dolganiuc A, Dolganiuc A, Norkina O, Norkina O, Kodys K, Kodys K, Catalano D, Catalano D, Bakis G, Bakis G and others. Viral and host factors induce macrophage activation and loss of toll-like receptor tolerance in chronic HCV infection. Gastroenterology 2007;133(5):1627-1636.

8. Dultz G, Gerber L, Zeuzem S, Sarrazin C, Waidmann O. The macrophage activation marker CD163 is associated with IL28B genotype and hepatic inflammation in chronic hepatitis C virus infected patients. Journal of Viral Hepatitis 2016;23(4):267-273.

9. Lau DT, Negash A, Chen J, Crochet N, Sinha M, Zhang Y, Guedj J, Holder S, Saito T, Lemon SM and others. Innate immune tolerance and the role of kupffer cells in

differential responses to interferon therapy among patients with HCV genotype 1 infection. Gastroenterology 2013;144(2):402-413 e12.

10. Burgio VL, Ballardini G, Artini M, Caratozzolo M, Bianchi FB, Levrero M. Expression of co-stimulatory molecules by Kupffer cells in chronic hepatitis of hepatitis C virus etiology. Hepatology (Baltimore, Md) 1998;27(6):1600-1606.

11. Falcon V, Acosta-Rivero N, Shibayama M, Chinea G, Gavilondo JV, de la Rosa MC, Menendez I, Gra B, Duenas-Carrera S, Vina A and others. HCV core protein localizes in the nuclei of nonparenchymal liver cells from chronically HCV-infected patients. Biochemical and Biophysical Research Communications 2005;329(4):1320-1328.

12. Royer C, Steffan AM, Navas MC, Fuchs A, Jaeck D, Stoll-Keller F. A study of susceptibility of primary human Kupffer cells to hepatitis C virus. Journal of Hepatology 2003;38(3):250-256.

13. Jilg N, Lin WY, Hong J, Schaefer EA, Wolski D, Meixong J, Goto K, Brisac C, Chusri P, Fusco DN and others. Kinetic Differences in the Induction of Interferon Stimulated Genes by Interferon-alpha and Interleukin 28B Are Altered by Infection With Hepatitis C Virus. Hepatology 2014;59(4):1250-1261.

14. Heim MH, Thimme R. Innate and adaptive immune responses in HCV infections. J Hepatol 2014;61(1 Suppl):S14-25.

15. Kleiner DE, Brunt EM, Van Natta M, Behling C, Contos MJ, Cummings OW, Ferrell LD, Liu Y-C, Torbenson MS, Unalp-Arida A and others. Design and validation of a histological scoring system for nonalcoholic fatty liver disease. Hepatology (Baltimore, Md) 2005;41(6):1313-1321.

16. Collison KS, Saleh SM, Bakheet RH, Al-Rabiah RK, Inglis AL, Makhoul NJ, Maqbool ZM, Zaidi MZ, Al-Johi MA, Al-Mohanna FA. Diabetes of the liver: the link between nonalcoholic fatty liver disease and HFCS-55. Obesity (Silver Spring, Md.) 2009;17(11):2003-2013.

17. Ali R, Cusi K. New diagnostic and treatment approaches in non-alcoholic fatty liver disease (NAFLD). Annals of medicine 2009;41(4):265-278.

18. Gómez-Lechón MJ, Donato MT, Martínez-Romero A, Jiménez N, Castell JV, O'Connor JE. A human hepatocellular in vitro model to investigate steatosis. Chemico-biological interactions 2007;165(2):106-116.

19. Donato MT, Jiménez N, Serralta A, Mir J, Castell JV, Gómez-Lechón MJ. Effects of steatosis on drug-metabolizing capability of primary human hepatocytes. Toxicology in Vitro 2007;21(2):271-276.

20. Yang DR, Zhu HZ. Hepatitis C virus and antiviral innate immunity: who wins at tug-of-war? World J Gastroenterol 2015;21(13):3786-800.

21. Antaki N, Bibert S, Kebbewar K, Asaad F, Baroudi O, Alideeb S, Hadad M, Abboud D, Sabah H, Bochud PY and others. IL28B polymorphisms predict response to therapy among chronic hepatitis C patients with HCV genotype 4. Journal of Viral Hepatitis 2013;20(1):59-64.

22. Abid K, Pazienza V, de Gottardi A, Rubbia-Brandt L, Conne B, Pugnale P, Rossi C, Mangia A, Negro F. An in vitro model of hepatitis C virus genotype 3a-associated triglycerides accumulation. Journal of Hepatology 2005;42(5):744-751.

23. Mitchell AM, Stone AE, Cheng L, Ballinger K, Edwards MG, Stoddard M, Li H, Golden-Mason L, Shaw GM, Khetani S and others. Transmitted/founder hepatitis C viruses induce cell-type- and genotype-specific differences in innate signaling within the liver. MBio 2015;6(2):e02510.